AN INVESTIGATION OF NOVEL REACTIVITY AND BONDING IN RARE EARTH METAL COMPLEXES

KEVIN ROSS DAVID JOHNSON
Bachelor of Science, University of Victoria, 2007

A Dissertation
Submitted to the School of Graduate Studies
of the University of Lethbridge
in Partial Fulfilment of the
Requirements for the Degree

DOCTOR OF PHILOSOPHY

Department of Chemistry and Biochemistry
University of Lethbridge
LETHBRIDGE, ALBERTA, CANADA

Knowledge speaks, but wisdom listens

—Jimi Hendrix

Abstract

The synthesis, structure and reactivity of organolanthanide complexes supported by a family of novel bis(phosphinimine)carbazole and bis(phosphinimine)pyrrole pincer ligands is presented. Through the systematic development of the ligand frameworks, rare earth metal species with unique structure and reactivity were encountered. A variety of complexes that exhibited unusual bonding modes were prepared and characterized by single-crystal X-ray diffraction and multinuclear NMR spectroscopy.

Modulation of the ligand frameworks allowed for rational manipulation of the steric and electronic environment imparted to the metal. Incorporation of a variety of *N*-aryl rings (mesityl, phenyl, *para*-isopropylphenyl and 2-pyrimidine) and PR_2 moieties (PPh_2, $PO_2C_2H_4$ and PMe_2) into the ligand design led to rare earth complexes that revealed diverse reaction behaviour. In particular, C–H bond activation, sigmatropic alkyl migration and ring opening insertion reactivity were observed. Kinetic and deuterium labeling studies are discussed with respect to the unique reaction mechanisms encountered during the study of these highly reactive organometallic rare earth complexes.

Acknowledgement

I would like to thank my supervisor, Dr. Paul Hayes for everything he has done for me over the past five years as a supervisor, mentor, and friend. As a researcher in his group, I have acquired a broad knowledge base and a variety of practical skills. For the active role he has played in my professional development, I am genuinely appreciative.

I have learned a great deal from fellow graduate students at the University of Lethbridge and the members of the Hayes research group. I would especially like to thank Dr. Craig Wheaton, Dr. Jamie Ritch, Dr. Hudson Sun, Dr. Delphine Julienne, Ben Ireland, Alex Borisov, Matt Hannon, Joline Utri, Dave Franz and Evan Mercier for their intellectual support and friendship over the years. A special thanks to the members of my rock band *The City We Live In* for being awesome.

I am grateful to the Faculty and supporting staff at the University of Lethbridge. In particular, the members of my Ph.D. research committee, Dr. René Boeré, Dr. Michael Gerken and Dr. Ken Vos, as well as the external examiner Dr. Michael Fryzuk. I would also like to thank Dr. Dave Berg for introducing me to the field of synthetic lanthanide chemistry, Dr. Adrien Côté for his collaboration and expertise in crystallography and Dr. Marc Roussel for useful discussions regarding kinetic data modeling.

I would like to thank my parents, Vance Johnson and Debbie Gaunt; my sisters, Heather Johnson and Lisa Alexander; my stepfather David Gaunt; and also Sheryl and Denny Kamenz for providing a tremendous amount of support over the years. Finally, I would like to thank Breanne Kamenz for always believing in me and providing constant love, support and encouragement.

Table of Contents

List of Tables

List of Figures

List of Schemes

List of Charts

List of New Compounds

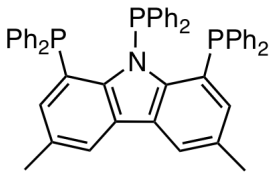

1

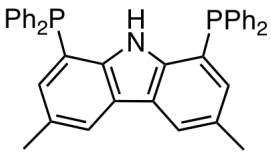

2

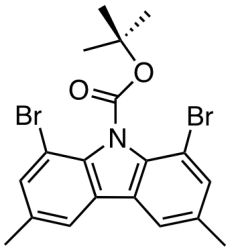

3

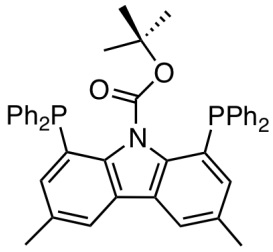

4

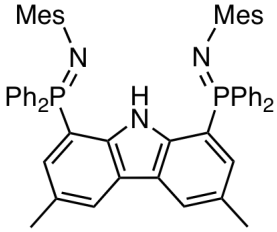

5

HL_A^{Mes}

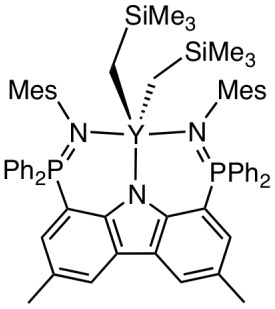

6

$(L_A^{Mes}\text{-}\kappa^3N)Y(CH_2SiMe_3)_2$

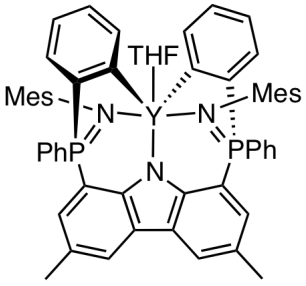

7

$(L_A^{Mes}\text{-}\kappa^3N,\kappa^2C^{P\text{-}Ph})Y(THF)$

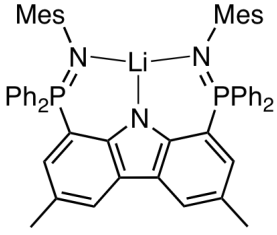

8

$(L_A^{Mes}\text{-}\kappa^3N)Li$

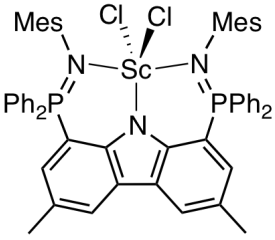

9

$(L_A^{Mes}\text{-}\kappa^3N)ScCl_2$

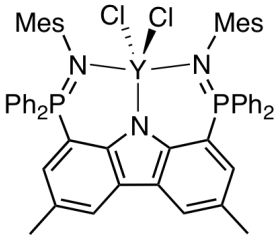

10

$(\mathbf{L}_{\mathbf{A}}^{\mathbf{Mes}}\text{-}\kappa^3N)YCl_2$

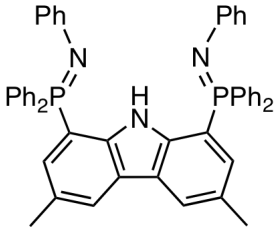

11

$H\mathbf{L}_{\mathbf{A}}^{\mathbf{Ph}}$

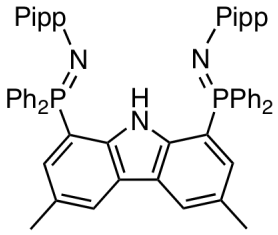

12

$H\mathbf{L}_{\mathbf{A}}^{\mathbf{Pipp}}$

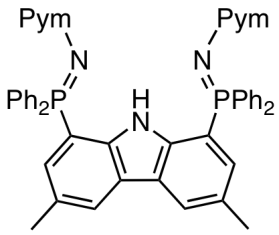

13

$H\mathbf{L}_{\mathbf{A}}^{\mathbf{Pym}}$

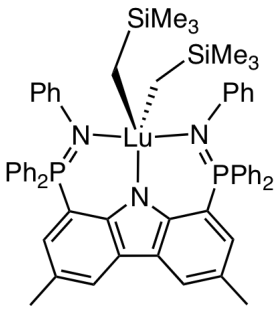

14

$(\mathbf{L}_{\mathbf{A}}^{\mathbf{Ph}}\text{-}\kappa^3N)Lu(CH_2SiMe_3)_2$

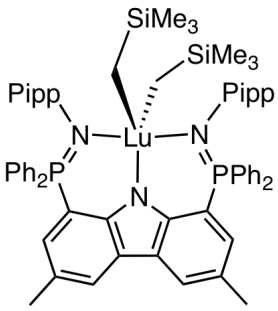

15

$(\mathbf{L}_{\mathbf{A}}^{\mathbf{Pipp}}\text{-}\kappa^3N)Lu(CH_2SiMe_3)_2$

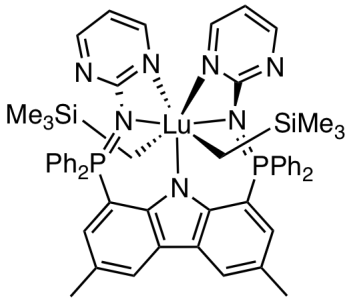

16

$(\mathbf{L}_{\mathbf{A}}^{\mathbf{Pym}}\text{-}\kappa^5N)Lu(CH_2SiMe_3)_2$

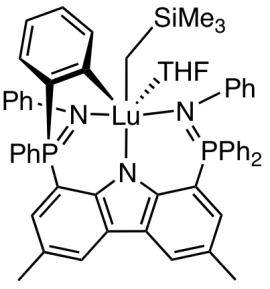

17

$(\mathbf{L}_{\mathbf{A}}^{\mathbf{Ph}}\text{-}\kappa^3N,\kappa C^{P\text{-}Ph})LuR(THF)$

$R = CH_2SiMe_3$

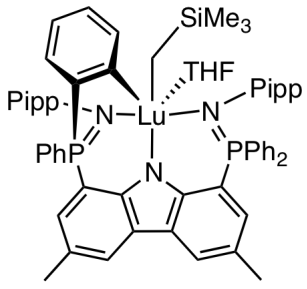

18

$(\mathbf{L}_{\mathbf{A}}^{\mathbf{Pipp}}\text{-}\kappa^3N,\kappa C^{P\text{-}Ph})LuR(THF)$

$R = CH_2SiMe_3$

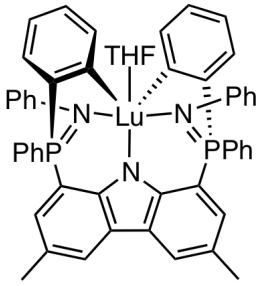

19

($\mathbf{L}_{\mathbf{A}}^{\mathbf{Ph}}$-κ^3*N*,κ^2*C*$^{P\text{-Ph}}$)Lu(THF)

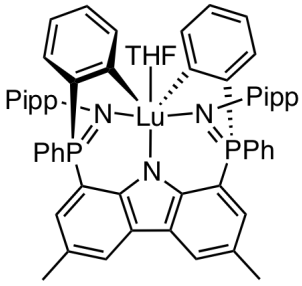

20

($\mathbf{L}_{\mathbf{A}}^{\mathbf{Pipp}}$-κ^3*N*,κ^2*C*$^{P\text{-Ph}}$)Lu(THF)

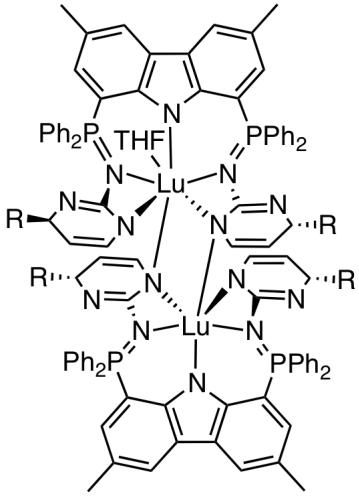

21

[($\mathbf{L}_{\mathbf{A}}^{\mathbf{Pym*}}$-κ^5*N*)Lu]$_2$(THF)

R = CH_2SiMe_3

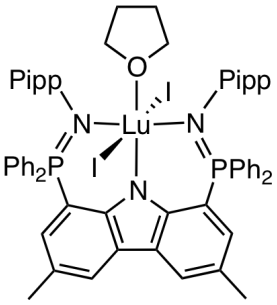

22

($\mathbf{L}_{\mathbf{A}}^{\mathbf{Pipp}}$-κ^3*N*)LuI$_2$(THF)

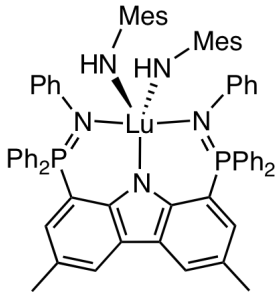

23

($\mathbf{L}_{\mathbf{A}}^{\mathbf{Ph}}$-κ^3*N*)Lu(NHMes)$_2$

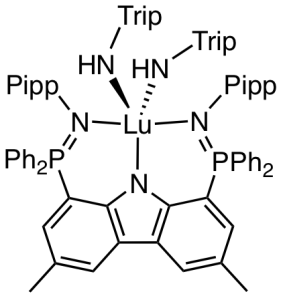

24

($\mathbf{L}_{\mathbf{A}}^{\mathbf{Pipp}}$-κ^3*N*)Lu(NHTrip)$_2$

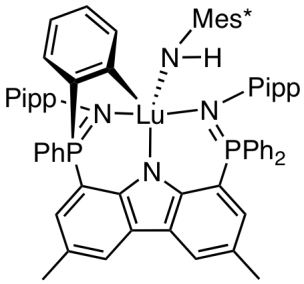

25

($\mathbf{L}_{\mathbf{A}}^{\mathbf{Pipp}}$-κ^3*N*,κ*C*$^{P\text{-Ph}}$)Lu(NHMes*)

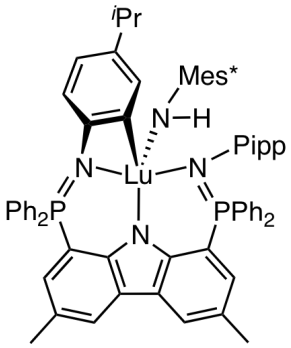

26

($\mathbf{L}_{\mathbf{A}}^{\mathbf{Pipp}}$-κ^3*N*,κ*C*$^{N\text{-Pipp}}$)Lu(NHMes*)

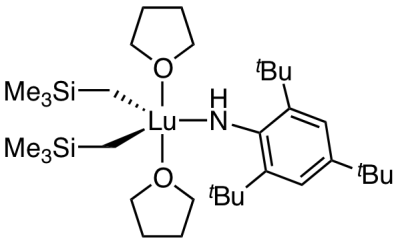

27

Lu(CH_2SiMe_3)$_2$NHMes*(THF)$_2$

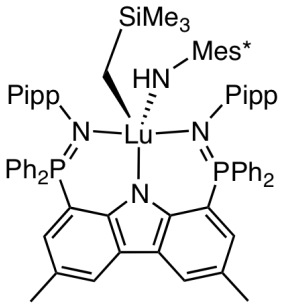

28

($\mathbf{L}_{\mathbf{A}}^{\mathbf{Pipp}}$-κ^3*N*)Lu(R)NHMes*

R = CH_2SiMe_3

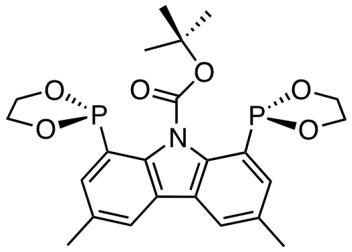

29

BOC(ONO)

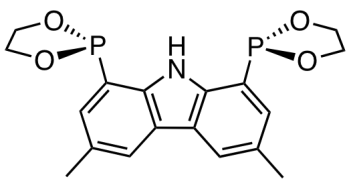

30

H(ONO)

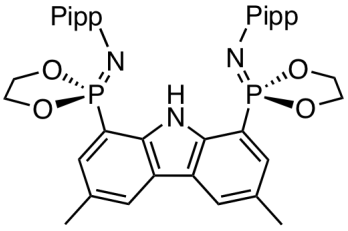

31

$H\mathbf{L}_{\mathbf{B}}^{\mathbf{Pipp}}$

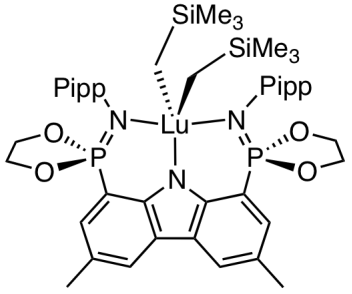

32

($\mathbf{L}_{\mathbf{B}}^{\mathbf{Pipp}}$-κ^3*N*)Lu($CH_2SiMe_3$)$_2$

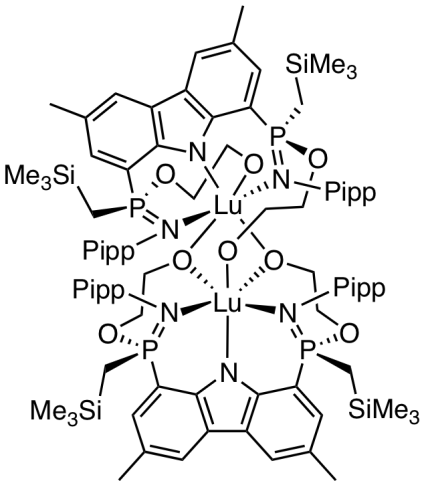

33

[($\mathbf{L}_{\mathbf{B}}^{\mathbf{Pipp}}$-κ^3*N*,κ^2*O*)Lu]$_2$

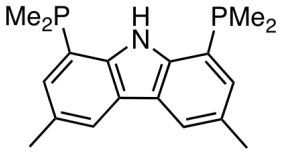

34

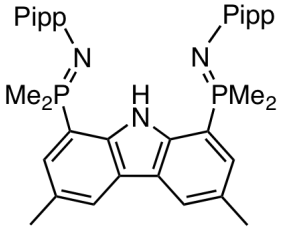

35

$H\mathbf{L}_{\mathbf{C}}^{\mathbf{Pipp}}$

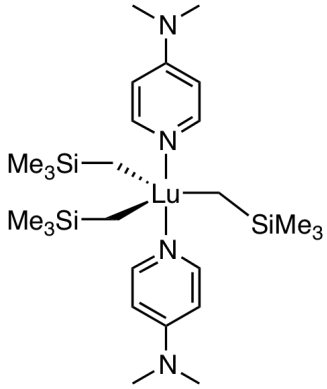

36

$Lu(CH_2SiMe_3)_3(DMAP)_2$

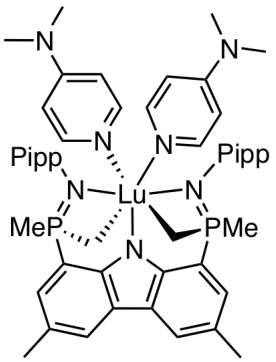

37

($\mathbf{L}_{\mathbf{C}}^{\mathbf{Pipp}}$-κ^3*N*,κ^2*C*)Lu(DMAP)$_2$

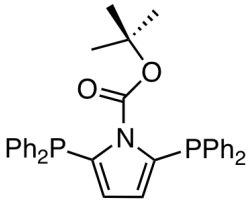

38

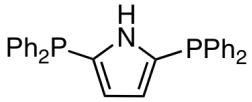

39

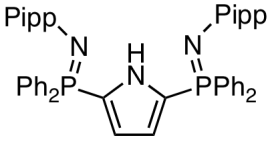

40

H$\mathbf{L}_{\mathbf{D}}^{\mathbf{Pipp}}$

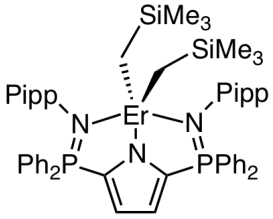

41

($\mathbf{L}_{\mathbf{D}}^{\mathbf{Pipp}}$-κ^3*N*)Er(CH$_2$SiMe$_3$)$_2$

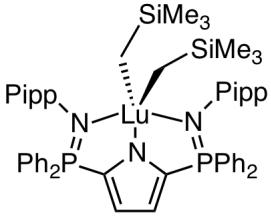

42

($\mathbf{L}_{\mathbf{D}}^{\mathbf{Pipp}}$-κ^3*N*)Lu(CH$_2$SiMe$_3$)$_2$

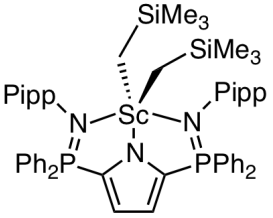

43

($\mathbf{L}_{\mathbf{D}}^{\mathbf{Pipp}}$-κ^3*N*)Sc(CH$_2$SiMe$_3$)$_2$

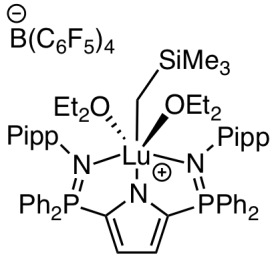

44

[($\mathbf{L}_{\mathbf{D}}^{\mathbf{Pipp}}$-κ^3*N*)Lu(CH$_2$SiMe$_3$)(OEt$_2$)$_2$]
[B(C$_6$F$_5$)$_4$]

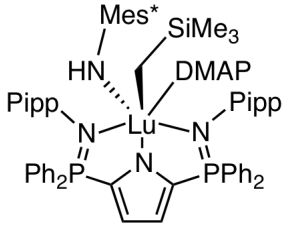

45

($\mathbf{L}_{\mathbf{D}}^{\mathbf{Pipp}}$-κ^3*N*)Lu(R)NHMes*(DMAP)
R = CH$_2$SiMe$_3$

List of Symbols and Abbreviations

a, b, c, α, β, γ	crystallographic unit cell parameters
Å	angstrom, 10^{-10} metres
Anal. Calcd.	analysis calculated
Ar	aryl group
ATR	attenuated total reflectance
BOC	*tert*-butoxycarbonyl
br	broad
C	Celsius
cm^{-1}	reciprocal centimetres
Cp	η^5-cyclopentadienyl (C_5H_5)
Cp*	η^5-pentamethylcyclopentadienyl (C_5Me_5)
Cy	cyclohexyl
Cz	carbazole
d	doublet
D_{calc}	calculated density
DCM	dichloromethane
dd	doublet of doublets
DEPT	distortionless enhancement by polarization transfer
Dipp	2,6-diisopropylphenyl
DMAP	4-dimethylaminopyridine
dmpe	1,2-bis(dimethylphosphino)ethane
dt	doublet of triplets
E	element
Et	ethyl
F_c	calculated structure factor
F_o	observed structure factor
FW	formula weight
g	gram(s)
GoF	goodness of fit
h	hour(s) or Planck's constant
Hz	hertz
I	nuclear spin quantum number or intensity
IMes	1,3-bis(2,4,6-trimethylphenyl)imidazol-2-ylidene
IPr	1,3-bis(2,6-diisopropylphenyl)imidazol-2-ylidene
^{i}Pr	isopropyl
^{i}Pr-trisox	1,1,1-tris[(*S*)-4-isopropyloxazolinyl]ethane
IR	infrared
J	Joules
k	rate constant
K	Kelvin
kJ	kilojoules
L	ligand or litre

Ln	lanthanide or group 3 metal
m	multiplet (NMR) or medium (IR)
m-	*meta*
mL	millilitre
M	metal or molar
Me	methyl
Mes	2,4,6-trimethylphenyl
Mes*	2,4,6-tri-*tert*-butylphenyl
mg	milligram(s)
MHz	megahertz
min	minute(s)
mmol	millimole(s)
N	number of measured reflections
NBS	*N*-bromosuccinimide
n-Bu	normal butyl
N_{ind}	number of independent reflections
NHC	*N*-heterocyclic carbene
$^{n}J_{AB}$	coupling constant between nuclei A and B, separated by n bonds
NMR	nuclear magnetic resonance
o-	*ortho*
ov	overlapping
p-	*para*
Ph	phenyl
Pipp	*para*-isopropylphenyl
PNP	$(2\text{-}^{i}Pr_2P\text{-}4\text{-}Me\text{-}C_6H_3)_2N^-$
ppm	parts per million
py	pyridine
Pym	pyrimidine
R	alkyl group
R_1	conventional agreement index
R^2	coefficient of determination for a linear regression
RT	room temperature
s	second(s), singlet (NMR) or strong (IR)
sp	septet
t	time or triplet (NMR)
T	temperature
T_1	spin lattice relaxation time
$t_{1/2}$	half-life
t- or *tert*-	tertiary
t-Bu	*tert*-butyl
t-Bu_2bpy	4,4″-di-*tert*-butyl-2,2″-bipyridyl
TACN	1,4,7-triazacyclononane
terpy	2,2′:6′,2″-terpyridine
THF	tetrahydrofuran
TMEDA	*N*,*N*,*N*′,*N*′-tetramethylethylenediamine
Tp	tris(pyrazolyl)borate

Trip	2,4,6-triisopropylphenyl
vw	very weak (IR)
w	weak (IR)
wR_2	weighted agreement index
Z	number of formula units per unit cell
12-crown-4	1,4,7,10-tetraoxacyclododecane
$\{^1H\}$	proton decoupled
$\{^{31}P\}$	phosphorus decoupled
°	degree(s)
δ	chemical shift relative to the reference signal
Δ	heat
$\Delta H^{\ddagger}$	enthalpy of activation
$\Delta S^{\ddagger}$	entropy of activation
$\Delta\rho_{max}$ and $\Delta\rho_{min}$	largest difference map peak and hole in terms of electron density
η^n	hapticity of order n
κ^n	denticity of order n
λ	wavelength
μ	absorption coefficient or bridging
μL	microlitre
ν	frequency
$\nu_{1/2}$	peak width at half height
σ	standard uncertainty

Chapter 1

Introduction and Literature Review

1.1 Introduction to Rare Earth Organometallic Chemistry

Organometallic chemistry of the rare earth metals* began over 50 years ago with the synthesis of tris(cyclopentadienyl)lanthanide derivatives.[1] The compounds Cp_3Ln, (Ln = Sc, Y, La, Ce, Pr, Nd, Sm, Gd, Dy, Er, Yb) were initially prepared by Wilkinson and Birmingham via the salt metathesis reaction of sodium pentadienide with anhydrous lanthanide chlorides in THF (Scheme 1.1).[2,3]

$$LnCl_3 + 3\ NaCp \xrightarrow{THF} LnCp_3 + 3\ NaCl$$

Scheme 1.1 Synthesis tris(cyclopentadienyl)lanthanide derivatives

The tris(cyclopentadienyl) lanthanide derivatives exhibited highly ionic character and similar reaction chemistry was observed for all complexes despite the variable

* In the context of this thesis, the rare earth metals are considered to be a grouping of elements that include the lanthanide and group 3 metals

electron configurations. For these reasons, the rare earth metals were labeled as "trivalent analogues" to the alkali and alkaline earth metals.[2,3]

Early research involving rare earth ions revealed that the +3 oxidation state predominated and few examples of lanthanide metals were known at the time to possess stable divalent or tetravalent states.[†] This lack in variety of oxidation states restricted access to two-electron transformations common in transition metal chemistry such as oxidative addition and reductive elimination. Furthermore, chemistry of the lanthanides in the zero oxidation state appeared to be hindered due to the limited radial extension of the 4f orbitals, thus restricting the ability of these orbitals to participate in back-bonding in a manner analogous to the d-orbitals in transition metal complexes.[‡] As a result, reagents of common interest to transition metal organometallic chemists, such as CO, olefins and phosphines were not found to be particularly well suited for use in lanthanide chemistry. Moreover, lanthanide metal ions are synthetically far more difficult to handle than their transition metal counterparts. Due to the extreme oxophilicity and hydrolytic instability of almost all organolanthanide compounds, manipulations involving these species must involve the rigorous exclusion of air and moisture. Accordingly, the options available for convenient isolation and purification of organolanthanide compounds are relatively limited.

[†] In addition to the ubiquitous +3 oxidation state accessible by all rare earth ions, stable molecular species of Ce^{4+}, La^{2+}, Nd^{2+}, Sm^{2+}, Eu^{2+}, Dy^{2+}, Yb^{2+}, Tm^{2+}, Sc^{2+} and Sc^{1+} have since been reported in the literature.[4-10]

[‡] Examples of well-defined rare earth complexes in the zero oxidation state have been documented; however, they generally require exotic synthetic methodologies such as metal-vapour synthesis.[6,11]

Until the late 1970's, very little organolanthanide research was performed. This may have been due to an erroneous assumption that organometallic chemistry of the rare earths was a limited field of research; in addition, it was hindered by a lack of modern preparative and analytical techniques.[1] However, over the past 30 years, interest in the organometallic chemistry of the rare earth metals has steadily increased; the field of f-element organometallic chemistry has been witness to a plethora of discoveries including the development of highly active catalysts, novel reagents for organic synthesis and a greater fundamental understanding of the unique bonding and reactivity of these metals.

A variety of principles regarding organolanthanide chemistry have been established and can often be used to predict reactivity patterns and characteristics of lanthanide complexes:

1. The highly contracted 4f valence orbitals lead to predominately ionic bonding and minimal orbital effects. As a result of this:
    i. Reactivity is not strongly dependent on the $4f^n$ electron configuration.
    ii. Coordination geometries are strongly influenced by ligand steric factors.
    iii. Ligands can be quite labile and can give rise to fluxional behaviour or facile ligand exchange processes.
2. Lanthanide metal ions have large ionic radii and often exhibit high coordination numbers. As a consequence:
    i. Sterically unsaturated complexes will tend to dimerize or oligomerize in order to sterically saturate the metal coordination sphere.
    ii. Salts are often retained in the coordination sphere resulting in "ate complex" formation.

3. Trivalent rare earth ions are hard and Lewis acidic.

   i. Ligands with hard donor atoms (*e.g.* N, O, Cl) are preferred.

   ii. Lewis basic solvents (*e.g.* THF, Et_2O) are easily coordinated and retained.

1.2 Rare Earth Metal Complexation Strategies

Various routes have been developed in support of rare earth organometallic chemistry for attaching a ligand to a trivalent metal ion. Salt metathesis is a commonly utilized approach and involves the reaction of a lanthanide trihalide with the metal salt of a ligand (Scheme 1.2). The elimination of salt is the driving force of the reaction and yields a lanthanide dihalide complex of the ligand. From a synthetic perspective, salt metathesis routes are a convenient method to draw upon because lanthanide halide precursors are commercially available at reasonable cost, and the lanthanide dihalide product can be readily derivatized by further salt metathesis reactions. Problems often encountered with this approach, however, include the low solubility of the lanthanide trihalide reagents in organic solvents, and retention of the salt byproduct in the coordination sphere of the product in the form an "ate" complex. Coordinating solvents such as Et_2O or THF are often utilized in response to the low solubility of the rare earth trihalide precursors; however, this often leads to retention of the solvent as a Lewis base by the lanthanide metal. Alternatively, THF adducts of the lanthanide halides can be readily prepared and reacted in weakly-coordinating solvents (*e.g.* toluene or benzene) due to their enhanced solubility.

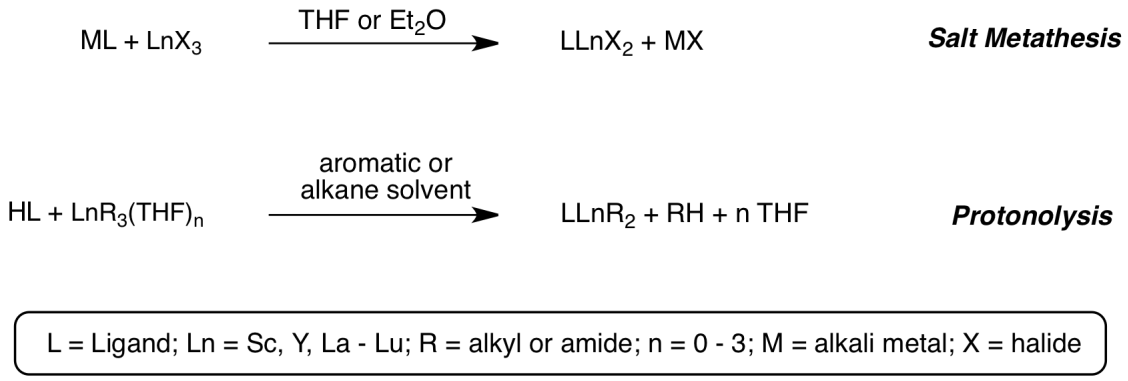

Scheme 1.2 Salt metathesis and protonolysis reactions

To mitigate the "ate complex" problem commonly encountered with salt metathesis, protonolysis methods have been developed as alternative metal complexation strategies (Scheme 1.2). For example, the alkane elimination reaction of a protic ligand with a highly reactive metal precursor such as $Ln(CH_2SiMe_3)_3(THF)_2$,[12,13] or $Ln(CH_2Ph)_3(THF)_3$,[14-16] can lead to facile ligand chelation with the direct formation of organometallic species. Problems associated with such reactions are that lanthanide alkyl complexes are often highly thermally sensitive, leading to difficulty in handling and isolation. Additionally, the trialkyl lanthanide precursors are not commercially available and must be synthesized prior to use. Alternatively, silylamido lanthanide complexes can be readily obtained via the silylamide route using $Ln[N(SiMe_3)_2]_3$ reagents as precursors.[17-19] Products of such amine elimination reactions are often both thermally stable and volatile, allowing for easy purification by sublimation. Unfortunately, the sterically demanding bis(trimethylsilyl)amido groups are often too bulky for facile amine elimination.

1.3 Literature Review

In the rapidly developing field of rare earth organometallic chemistry, the use of ancillary ligands is key in the stabilization of highly reactive metal complexes. Typically, sterically bulky ligands are utilized in organometallic complexes of these metals for the purpose of sterically saturating the large coordination sphere of the metal. The development of sterically crowded f-element complexes has led to the formation of remarkably stable compounds, and also new forms of reactivity, such as sterically induced reduction.[8] In other cases, however, steric crowding in lanthanide complexes is a contributing factor of ligand cyclometalative C–H bond activation reactions.

This literature review will discuss the major factors leading to ligand cyclometalation in rare earth complexes, including kinetic and mechanistic considerations. The reactivity discussed should be of broad interest for reasons such as the development of new types of catalysts for the activation of hydrocarbons or fundamental interest from a perspective of studying unique bonding and reactivity patterns.

1.3.1 Cyclometalative C–H Bond Activation

Cyclometalative C–H bond activation is a process that is encountered relatively frequently in the field of organometallic chemistry. It is defined as a reaction whereby a ligand undergoes an intramolecular metalation to afford a chelate ring containing a new M–C bond (Scheme 1.3)

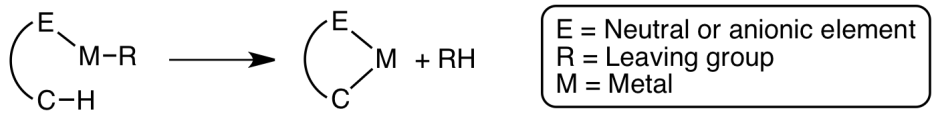

Scheme 1.3 Ligand cyclometalation

This form of reactivity has been observed in ligands coordinated to a multitude of metals across the periodic table. Cyclometalation reactions involving main group,[20] late transition,[21-24] and early transition[25] metal complexes have been previously reviewed and for this reason will not be discussed. The focus of this literature review will describe cyclometalation reactions involving rare earth metal complexes. It is not intended to be fully comprehensive, but rather to highlight some interesting and representative examples of cyclometalative reactivity in group 3 and lanthanide complexes.

Ligand cyclometalation has a propensity to occur in highly reactive alkyl or hydrido rare earth complexes. It typically occurs via a σ-bond metathesis reaction involving a four-centre [2s + 2s] transition state. The process is entropically driven (*vide infra*) and steric factors can also significantly influence ligand metalation.[24]

With regard to thermodynamics of the cyclometalation reaction, the process is typically slightly endothermic in nature, *i.e.*, exhibits a positive ΔH. However, as the reaction involves the formation of a metalated chelate ring and loss of alkane or hydrogen as a byproduct, it gains entropy, and hence, the reaction has a large positive ΔS. With sufficient temperature, the free energy change in the reaction according to Equation 1.1 becomes negative and thermodynamically favoured.[26] In general terms, a complex of form L_nMR is entropically susceptible towards a metalative alkane elimination reaction to form a cyclometalated complex and RH as a byproduct.

$$\Delta G = \Delta H - T\Delta S \qquad \text{Equation 1.1}$$

1.3.2 Carbocyclic Ligand Cyclometalation

1.3.2.1 Tuck-in and Tuck-over Complexes

As one of the most commonly encountered ligands in organolanthanide chemistry, Cp* (Cp* = η^5-C_5Me_5) has been utilized to stabilize a wide range of rare earth complexes.[27] Compared to other common carbocyclic ligands such as η^5-C_5H_5, Cp* has proven popular for use in lanthanide chemistry due to its large size and enhanced solubilizing ability. To a considerable extent, the C–H bonds of the Cp* ligand are resilient to cyclometalative C–H bond activation; however, cyclometalation of the ligand has been found to occur in some highly reactive alkyl and hydrido lanthanide complexes. In the case of cyclometalation occurring within the Cp* ligand, the C–H bond activation of a methyl group results in a species containing a tetramethylfulvene moiety, and are commonly referred to as "tuck-in" complexes. Various resonance structures for tetramethylfulvene can be drawn whereby the ligand can coordinate to a metal π-η^5:σ-η^1 with a formal charge of −2 (i, Chart 1.1) or π-η^6 with a formal charge of 0 (ii, Chart 1.1). The relative resonance contribution of these two forms has been previously discussed with regard to high and low valent transition metal tuck-in complexes.[28-31] In terms of f-element tuck-in complexes, the π-η^6 mode is not considered likely due to the limited oxidation states available, and the ligand is generally believed to coordinate in the π-η^5:σ-η^1 mode.[32]

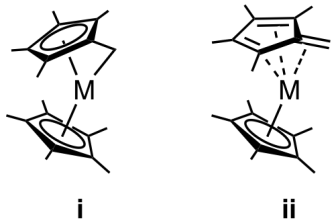

Chart 1.1 Tetramethylfulvene

Rare earth tuck-in complexes were first proposed in the early 1980's. For example, an investigation by Watson regarding the activation of methane and benzene by a methyllutetium complex $[(\eta^5\text{-}C_5Me_5)_2LuCH_3]_n$ (**1.1**, n = 1 or 2) implicated the formation of a tucked-in lutetium intermediate $(\eta^5\text{-}C_5Me_5)Lu\{\eta^5\text{:}\eta^1\text{-}C_5Me_4(CH_2)\}$ (**1.2**) (Scheme 1.4).[33]

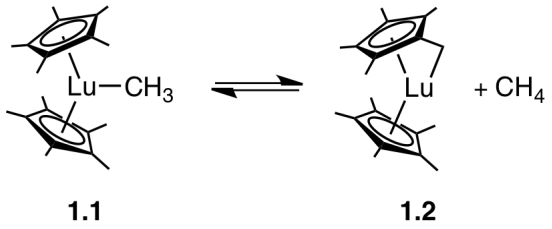

Scheme 1.4 Postulated lutetium tuck-in complex

A related scandium complex was developed by Bercaw and co-workers,[34] whereby $(\eta^5\text{-}C_5Me_5)_2ScCH_3$ (**1.3**) was heated in cyclohexane at 80 ºC for several days to afford $[(\eta^5\text{-}C_5Me_5)Sc\{\eta^5\text{:}\eta^1\text{-}C_5Me_4(CH_2)\}]_2$ (**1.4**) and methane. The proposed structure of one $\eta^5\text{-}C_5Me_5$ ring and one cyclometalated $\eta^5\text{:}\eta^1\text{-}C_5Me_4(CH_2)$ ring per scandium centre was supported by the ^{1}H NMR spectrum (benzene-d_6) of **1.4** whereby a singlet at δ 1.96 with an integration of 15H, and three singlets at δ 2.08, 1.54 and 1.39 with relative integrations of 6:6:2 were observed. Early studies initially assigned **1.4** as a dimeric complex with bridging methylene groups based on its low solubility.[35] The solid-state

structure was later obtained, corroborating the structure of **1.4** as a dimer.[36] The fully deuterated analogue of **1.4** can be prepared by the thermolysis reaction of perdeuterated complex (Cp*-d_{15})$_2$ScCH$_3$ (**1.3**-d_{30}) in cyclohexane at 80 ºC with loss of CH$_3$D. A measurable kinetic isotope effect in this reaction (k_H/k_D = 1.6(2)) was supportive of the fact that ligand cyclometalation was the rate limiting step.

It was found that complex **1.4** would react cleanly with either H$_2$ (1 atm) or benzene-d_6 to afford (η^5-C$_5$Me$_5$)$_2$ScH (**1.5**) or (η^5-C$_5$Me$_5$)(η^5-C$_5$Me$_4$CH$_2$D)Sc(C$_6$D$_5$) (**1.6**-d_6), respectively as the sole products (Scheme 1.5).

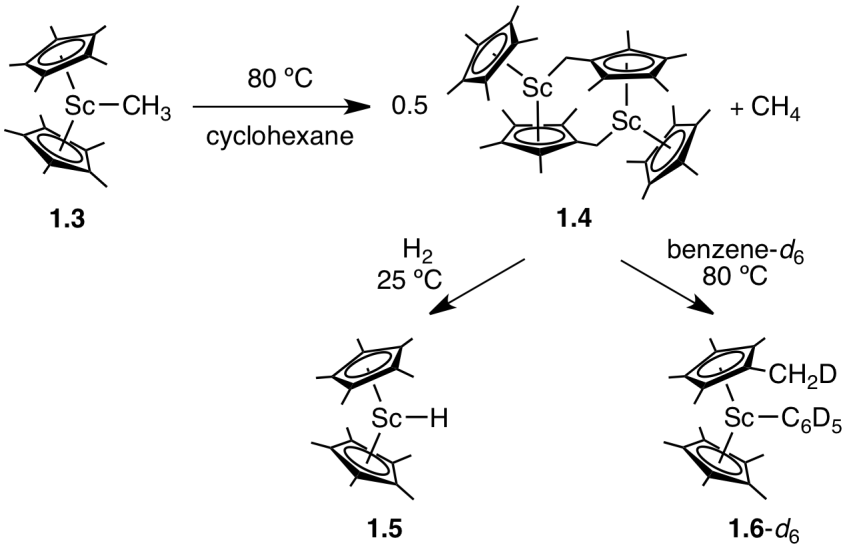

Scheme 1.5 Scandium complex reactivity

Interestingly, if complex **1.3** was reacted with benzene-d_6 at elevated temperature a competitive process was observed, involving (i) the bimolecular reaction of **1.3** with benzene-d_6 to afford **1.6**-d_5 and CH$_3$D; and (ii) the unimolecular cyclometalation reaction to **1.4** with loss of CH$_4$, followed by reaction with benzene-d_6 to afford **1.6**-d_6 (Scheme 1.6). The bimolecular pathway was favoured at low temperature (60 ºC) relative to the

unimolecular metalation by a ratio of 76:24. However, at elevated temperature (125 ºC) equal (50:50) preference for both pathways was reported.

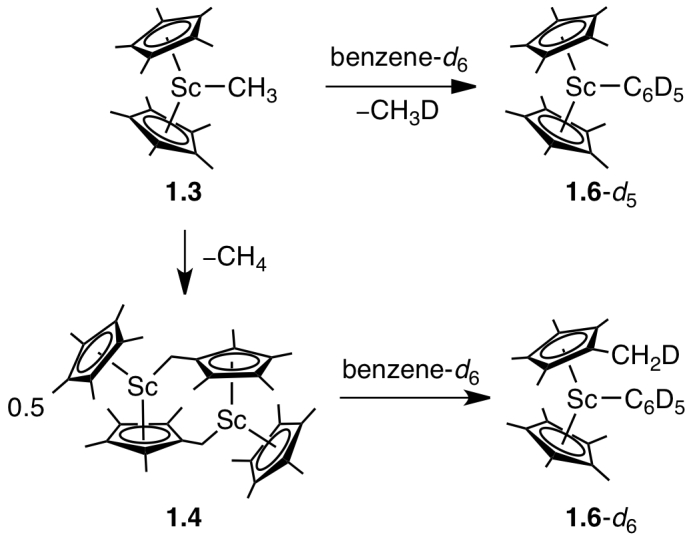

Scheme 1.6 Competitive reactivity in complex **1.3**

For comparison in reactivity of the scandium methyl complex **1.3**, the scandium neopentyl derivative was prepared. This complex could be used to activate hydrocarbons, but notably, was not susceptible to the intramolecular ligand cyclometalation pathway. Rather, hydrocarbon C–H bond activation was favoured via the intermolecular pathway.[37]

The term "tuck-over" complex is commonly used to describe the class of Cp* metalated species that are formed by an intermolecular metalative C–H bond activation pathway. Thus, the dimeric scandium complex **1.4** discussed above can be referred to as a tuck-over complex. An array of other rare earth tuck-over variants has also been outlined in the lanthanide literature. For example, thermolysis of lanthanide hydride complexes $[(\eta^5\text{-}C_5Me_5)_2LnH]_n$ resulted in intermolecular C–H bond activation of a Cp* methyl group to afford complexes of form $[(\eta^5\text{-}C_5Me_5)Ln(\mu\text{-}\eta^5\text{:}\eta^1\text{-}C_5Me_4CH_2)(\mu\text{-}H)Ln(\eta^5\text{-}C_5Me_5)_2]$ (Ln = Y, **1.7**;[38,39] Lu, **1.8**;[40] Sm, **1.9**;[41] La, **1.10**[42]) with concomitant generation

of hydrogen gas (Scheme 1.7). The final products of this transformation were binuclear species with bridging hydride and tetramethylfulvene ligands. The reaction itself is reversible in closed systems; accordingly, formation of the tuck-over complexes can be inhibited by an atmosphere of hydrogen.[41] The structures of lanthanide tuck-over complexes have been unambiguously established by single-crystal X-ray diffraction for Ln = Y,[38] Lu,[40] Sm,[41] La[42]. Additional characterization of the complexes was performed by NMR spectroscopy, IR spectroscopy and elemental analysis, and in the case of **1.9**, magnetic susceptibly measurements. Furthermore, Toepler pump collection of the gases liberated during the formation of **1.9** revealed 1 mol of H_2 was released, rather than 2 mols. This analysis was consistent with the expected bimetallic structure containing one hydride ligand.

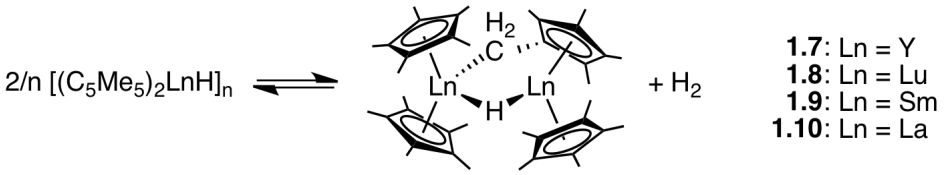

Scheme 1.7 Preparation of a lanthanide tuck-over complex via hydrogen abstraction from a Cp* ligand

Intermolecular double metalation of a Cp* ligand was reported in cerium[43] lanthanum[43] and samarium[44] alkyl complexes. In cyclohexane or methylcyclohexane solutions, complexes of form $(\eta^5\text{-}C_5Me_5)_2LnR$ (Ln = Ce, R = $CH(SiMe_3)_2$; Ln = La, R = $CH(SiMe_3)_2$; Ln = Sm, R = CH_2SiMe_3 or CH_3) underwent ligand metalation with loss of alkane to afford the polymetallic cluster compounds $(\eta^5\text{-}C_5Me_5)_6Ln_4(\mu_3\text{-}\eta^5\text{:}\eta^1\text{:}\eta^1\text{-}C_5Me_3(CH_2)_2)_2$ (Scheme 1.8). The products of these thermolysis reactions contained two trianionic $[C_5Me_3(CH_2)_2]^{3-}$ ligands whereby two methyl groups of the Cp* ring had

undergone C–H bond activation. The cerium and samarium complexes were characterized by X-ray diffraction; however, the crystal structures were not isomorphous due to the fact that the cerium derivative contained cyclohexane in the lattice, while the samarium complex was unsolvated.

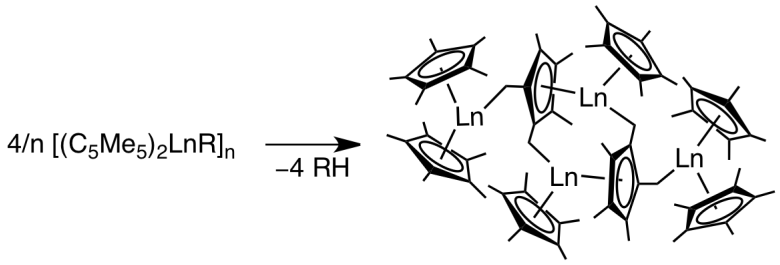

1.11: Ln = Ce, R = $CH(SiMe_3)_2$
1.12: Ln = La, R = $CH(SiMe_3)_2$
1.13: Ln = Sm, R = CH_2SiMe_3 or CH_3

Scheme 1.8 Double metalation of Cp* ligands

Related reactivity involving the thermolysis of $(\eta^5\text{-}C_5Me_5)_2LnCH(SiMe_3)_2$ (Ln = Ce, La) in toluene solution rather than cyclohexane afforded the benzyl derivative $(\eta^5\text{-}C_5Me_5)_2LnCH_2Ph$. When this reaction was performed in toluene-d_8 and followed *in situ*, formation of a deuterated benzyl complex ensued with initial generation of only $CH_2(SiMe_3)_2$ and no $CHD(SiMe_3)_2$. This result implicated that the reaction proceeded via the metalated derivatives **1.11** and **1.12** rather than by direct σ-bond metathesis of $(\eta^5\text{-}C_5Me_5)_2LnCH(SiMe_3)_2$ with toluene. The mechanism was ascertained by thermolysis of **1.11** in toluene-d_8 at 80 ºC, whereby $(\eta^5\text{-}C_5Me_5)(\eta^5\text{-}C_5Me_4CH_2D)CeCD_2C_6D_5$ was obtained as the product (Scheme 1.9). Interestingly, the reaction is reversible and scrambling of deuterium atoms into the Cp* rings was observed.

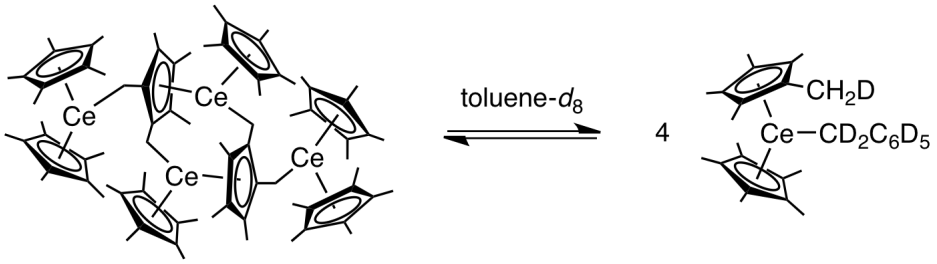

Scheme 1.9 Activation of toluene

The doubly metalated Ce, La and Sm complexes act as complementary C–H bond activation products to the tuck-in and tuck-over complexes discussed above. Clearly, the Cp* ligand is not fully resistant to metalative C–H bond activation and a diverse collection of products can be generated as a result of this process.

1.3.3 Non-carbocyclic Ligand Cyclometalation

The cyclopentadienyl ligand (Cp) and its derivatives have been extremely influential as ancillaries in the development of organolanthanide chemistry; much of the early work involving these metals utilized a carbocyclic ligand scaffold.[1,8,27] Unfortunately, limitations exist in the extent to which carbocyclic ligands can be electronically or sterically tuned.[45-55] Consequently, significant attention has recently been devoted to the exploration of non-carbocyclic ancillaries for supporting rare earth metals.

A surge in the development of non-carbocyclic ligand scaffolds for supporting highly reactive rare earth metal species has occurred over the past decade.[56-58] The novel ancillary ligands that have arisen throughout this "post-metallocene" era have often been shown to be attractive scaffolds for supporting rare bonding modes, in addition to various

catalytic transformations due to their high degrees of tunability. This is a property inherent to most non-carbocyclic ancillary ligands that allows for rational and convenient adjustment of the steric or electronic properties to control metal reactivity.

The modular nature of non-carbocyclic ligands allows for the incorporation of large or bulky groups onto ancillary frameworks. In many cases, the presence of sterically demanding moieties will stabilize highly reactive metal fragments or species that display unique bonding modes.[59] Excessive steric bulk has also, however, been implicated as a major contributing factor to ligand cyclometalation reactions in rare earth alkyl and hydrido complexes.

1.3.3.1 γ-Metalation of Silylamido Ligands

The bis(trimethylsilyl)amide ligand has proven to be popular for use in rare earth chemistry. The ligand lacks β-hydrogens, provides steric protection and is commercially available as the amine or a variety of salts. The bis(trimethylsilyl)amide ligand is capable of interacting with metals via $NSiCH_3\cdots M$ agostic interactions; this interaction can help to stabilize what may otherwise be coordinatively unsaturated and electron deficient metal complexes. While the ligand has been employed to stabilize a wide array of metal complexes, reactivity occasionally encountered involves deprotonation of the γ-methyl C–H group. The deprotonation and subsequent functionalization of this carbon atom in lanthanide complexes of the bis(trimethylsilyl)amide ligand has been demonstrated by Deacon and co-workers.[60,61]

Cyclometalation has been documented in some lanthanide complexes as a result of γ-methyl deprotonation of the bis(trimethylsilyl)amide ligand by a strong base. For example, reaction of tris(trimethylsilyl)amide lanthanide complexes (Ln = Sc, Lu, Yb) with $NaN(SiMe_3)_2$ resulted in deprotonation of the γ-carbon and formation of cyclometalated ate complexes (Scheme 1.10). Structural analysis of complexes **1.14** and **1.16** revealed planar four-membered metallacycles with Ln–C bond lengths of 2.271(5) Å and 2.386(11) Å for **1.14** and **1.16**, respectively. The Ln–C bonds in **1.16** were found to be highly reactive towards insertion of 2,6-dimethylbenzoisonitrile.[62]

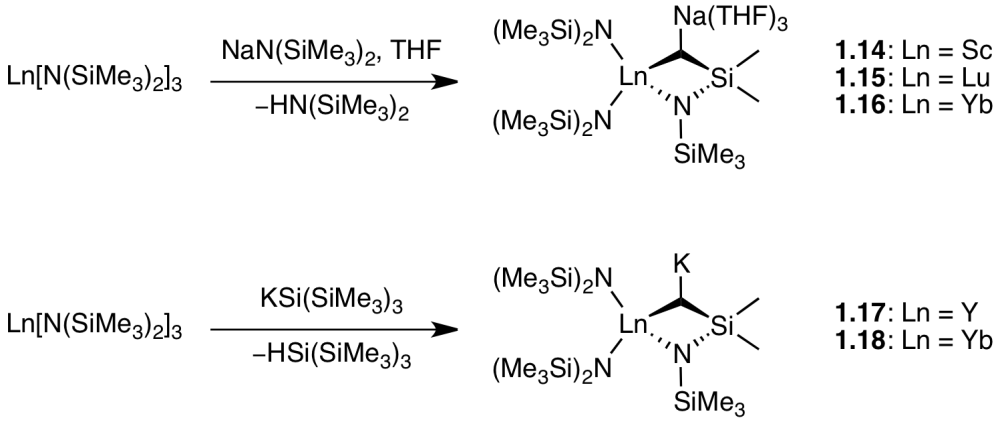

Scheme 1.10 γ-Deprotonation of the bis(trimethylsilyl)amide ligand

Niemeyer reported the reaction of $Ln[N(SiMe_3)_2]_3$ (Ln = Y, Yb) with hypersilyl potassium ($KSi(SiMe_3)_3$) to afford σ-donor-free ate complexes with the composition $[N(SiMe_3)_2]_2LnN(SiMe_3)SiMe_2(CH_2)K$ (Ln = Y, **1.17**; Ln = Yb, **1.18**).[63] Recrystallization of **1.17** from a mixture of *n*-heptane and benzene (20:1) at −60 °C gave the corresponding benzene solvate $[N(SiMe_3)_2]_2YN(SiMe_3)SiMe_2(CH_2)K(C_6H_6)_2$, which was structurally characterized by X-ray crystallography. It has been demonstrated that the $[N(SiMe_3)_2]_2YN(SiMe_3)SiMe_2(CH_2)^-$ anion can be generated through various other means. For example, reaction of $Y[N(SiMe_3)_2]_3$ with *n*-BuLi in the presence of TMEDA

afforded $[N(SiMe_3)_2]_2YN(SiMe_3)SiMe_2(CH_2)Li(TMEDA)$ in good yield.[63] Alternatively, $[N(SiMe_3)_2]_2YN(SiMe_3)SiMe_2(CH_2)K(THF)_2$ and $[N(SiMe_3)_2]_2YN(SiMe_3)SiMe_2(CH_2)]$-[K(18-crown-6)(THF)(toluene)] were obtained from a $Y[N(SiMe_3)_2]_3/KC_8/N_2$ reaction mixture in the presence of either THF or a combination of 18-crown-6, THF and toluene, respectively.[64] Interestingly two equivalents of complex **1.17** can be reacted with $YbI_2(THF)_2$ to generate the neutral dimer $[N(SiMe_3)_2YN(SiMe_3)SiMe_2(CH_2)(THF)]_2$, **1.19**, with loss of $Yb[N(SiMe_3)_2]_2(THF)_2$ and KI (Scheme 1.11).[63] Product **1.19** is notable as a cyclometalated rare earth compound of the bis(trimethylsilyl)amide ligand because it is not an ate complex like derivatives **1.14** – **1.18**. To this degree, it much more resembles the corresponding cyclometalated transition metal[65-71] and actinide[72-74] complexes of the bis(trimethylsilyl)amide ligand.

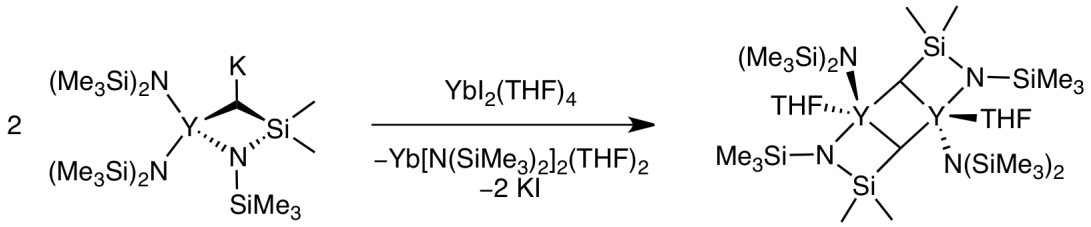

1.19

Scheme 1.11 Synthesis of a neutral γ-cyclometalated yttrium dimer

Reactivity involving γ-methyl deprotonation was also observed in a samarium bis(trimethylsilyl)amido complex of a *trans*-difuranyl substituted porphyrinogen ligand. Reaction with $NaN(SiMe_3)_2$ in THF, followed by recrystallization in toluene resulted in formation of the γ-cyclometalated derivative **1.20**, whereby one Na ion was retained in the product. In **1.20**, the Sm(III) metal centre was bound to the cyclometalated γ-alkylamide moiety and to the porphyrinogen ligand in a $\eta^5:\eta^1:\eta^5:\eta^1$-bonding mode. The sodium cation was coordinated η^6 by a molecule of toluene and $\eta^5:\eta^1:\eta^5:\eta^1$ by the

porphyrinogen ligand. The four-membered metallacycle in **1.20** exhibited similar metrical parameters to the cyclometalated silylamido ligand in complexes **1.14** and **1.16** (Table 1.1).

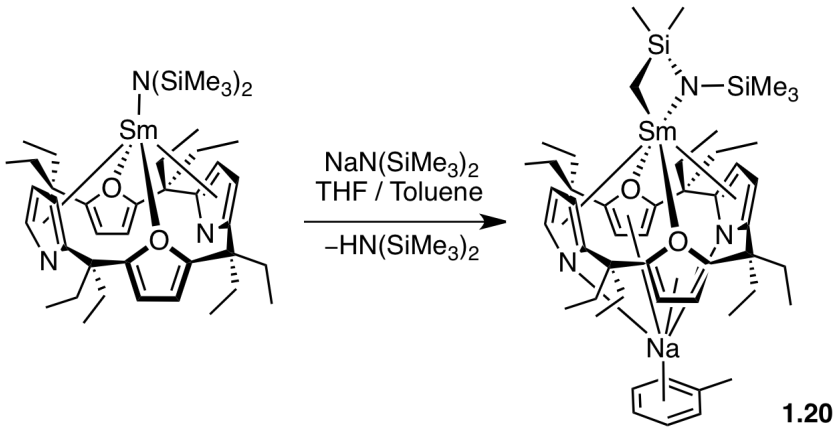

Scheme 1.12 γ-Cyclometalation in a samarium porphyrinogen complex

Many of the γ-cyclometalated rare earth complexes described above have been structurally characterized by X-ray crystallography. Similar structural features and metrical parameters of the Ln–C–Si–N metallacycles were reported in all cases. To illustrate this point, the metical parameters defining the geometry of the Ln–C–Si–N metallacycle are listed in Table 1.1 for selected compounds.

Table 1.1 Bond distances /Å and angles /º for selected Ln–C–Si–N metallacycles formed by cyclometalation of a bis(trimethylsilyl)amide ligand

	1.14	**1.16**	**1.17·$(C_6H_6)_2$**	**1.19**	**1.20**
Ln–C	2.271(5)	2.386(11)	3.000(4)	2.589(6)	2.464(4)
C–Si	1.819(6)	1.82(2)	1.835(4)	1.881(6)	1.825(4)
Si–N	1.727(4)	1.721(6)	1.721(3)	1.711(4)	1.733(3)
Ln–N	2.077(4)	2.199(8)	2.222(3)	2.254(4)	2.292(2)
C–Ln–N	77.9(2)	74.3(4)	73.17(12)	70.84(16)	71.77(10)
N–Si–C	101.0(2)	102.9(5)	103.32(16)	103.3(2)	103.30(15)
Ln–N–Si	94.9(2)	95.7(3)	96.39(14)	100.59(19)	96.43(11)
Ln–C–Si	86.1(2)	86.9(4)	86.07(14)	85.2(2)	88.4(1)

Related to the bis(trimethylsilyl)amido ligand is the chelating amido-diphosphine framework $[N(SiMe_2CH_2PMe_2)_2]^-$, developed by Fryzuk. This ancillary, which possesses a hard anionic nitrogen and two pendant phosphines as soft donors, has been proven as a highly versatile ligand in late and early transition metal chemistry.[75] In group 3 and lanthanide chemistry, reaction of metal chloride complexes of the ligand, $LnCl[N(SiMe_2CH_2PMe_2)_2]_2$ (Ln = Y, Lu), with phenyllithium or benzyl potassium afforded the organometallic derivatives $LnR[N(SiMe_2CH_2PMe_2)_2]_2$ (Ln = Y, R = Ph, CH_2Ph; Ln = Lu, R = Ph). Intramolecular thermal decomposition of the phenyl and benzyl complexes resulted in cyclometalation of the ligand methylene carbon with loss of hydrocarbon (**1.21**, Ln = Y; **1.22**, Ln = Lu). Reaction of the lanthanum chloride complex with phenyllithium resulted only in the cyclometalated product (**1.23**); while the phenyl complex was not observed, it is likely that it existed as a transient highly reactive intermediate (Scheme 1.13). The site of ligand cyclometalation in these complexes at the methylene C–H bond was inferred from $^{13}C\{^1H\}$ NMR spectroscopy and also confirmed by an X-ray crystal structure of **1.21**.[76]

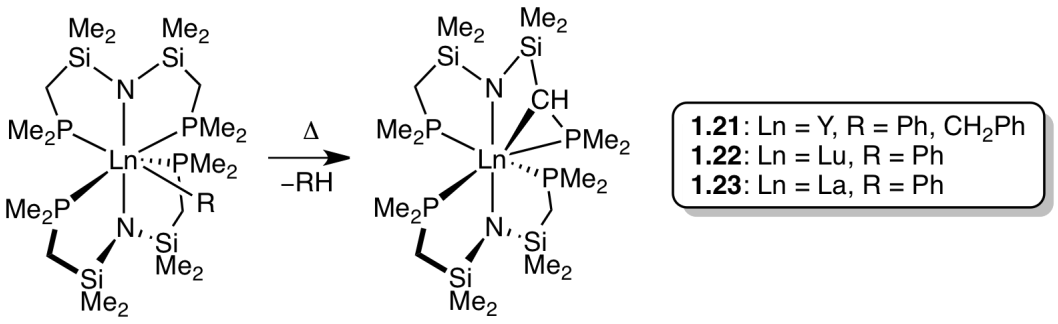

Scheme 1.13 Cyclometalation of a hybrid amido-diphosphine ligand

Kinetic analysis of the cyclometalation reaction to form **1.21** revealed a first order process across a broad range of temperatures. From an Eyring analysis, the activation parameters involving loss of benzene ($\Delta H^{\ddagger}$ = 85.8 ± 4 kJ·mol^{-1} and $\Delta S^{\ddagger}$ = −17 ± 10 J·mol^{-1}·K^{-1}) and toluene ($\Delta H^{\ddagger}$ = 86.2 ± 4 kJ·mol^{-1} and $\Delta S^{\ddagger}$ = −14 ± 10 J·mol^{-1}·K^{-1} were highly comparable. Typically, a large negative $\Delta S^{\ddagger}$ value is expected due to the formation of a highly ordered four-centre transition state; however, the small negative $\Delta S^{\ddagger}$ value observed experimentally for this particular system was attributed to a transition state with a dissociated phosphine. The rate of cyclometalation at 73 ºC was one order of magnitude faster in the yttrium phenyl complex (k = 1.65 × 10^{-3} s^{-1}, half-life = 7.0 min) compared to the lutetium phenyl complex (k = 1.88 × 10^{-4} s^{-1}, half-life = 61.3 min). The difference in rate was attributed to the larger size of yttrium versus lutetium, whereby the strained four-centre transition state was more difficult to access in a smaller metal. This notion was consistent with the fact that the lanthanum phenyl complex could not be isolated due to the larger size of the metal, and thus, higher reactivity.[76]

1.3.3.2 Cyclometalation of β-Diketiminato Ligands

The β-diketiminato (nacnac) framework is a popular scaffold for use in rare earth metal chemistry.[77] It is commonly substituted at the *N*-aryl positions with bulky 2,6-diisopropylphenyl rings and a variety of organolanthanide complexes have been stabilized with this ligand.[77,78] In some highly reactive complexes, however, the sterically demanding nature of the ligand has also resulted in cyclometalation reactivity. Well-defined examples of this process were documented in four coordinate scandium dialkyl

complexes of the 2,6-diisopropylphenyl-substituted nacnac ligand. In these complexes, a thermally induced cyclometalative reaction involving the methyl C–H bond of a 2,6-diisopropylphenyl group transpired with extrusion of alkane (Scheme 1.14).[79] It was found that the less bulky nacnac derivatives (R = Me) resulted in initial cyclometalation with loss of alkane, but subsequent reaction progress led to ill-defined products. Incorporation of bulkier *tert*-butyl groups at the R site on the nacnac backbone allowed for clean formation of the cyclometalated products.

The NMR spectra of cyclometalated complexes of non-Cp ligands are often quite complex due to the low symmetry of the resultant products. The ^{1}H NMR spectrum of cyclometalated compound **1.31**, for example, exhibited seven doublets for the isopropyl methyl groups and four multiplets for the methine hydrogen atoms. The cyclometalation process also resulted in diastereotopic methylene protons in the Sc–CH_2 groups.

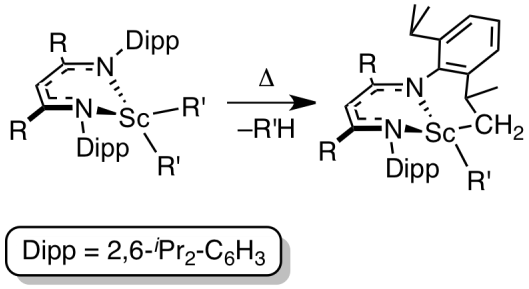

R	R'	Compound
^{t}Bu	CH_3	**1.24**
^{t}Bu	CH_2CH_3	**1.25**
CH_3	CH_2Ph	**1.26**
^{t}Bu	CH_2Ph	**1.27**
CH_3	CH_2CMe_3	**1.28**
^{t}Bu	CH_2CMe_3	**1.29**
CH_3	CH_2SiMe_3	**1.30**
^{t}Bu	CH_2SiMe_3	**1.31**

Scheme 1.14 Cyclometalation of a β-diketiminato framework

Kinetic analysis of the metalation process to generate **1.31**, revealed a first order reaction, as expected, across a broad temperature range from 30 ºC to 70 ºC. Activation parameters of $\Delta H^{\ddagger} = 82.4 \pm 3$ kJ·mol^{-1} and $\Delta S^{\ddagger} = -71 \pm 8$ J·mol^{-1}·K^{-1} were obtained

from an Eyring analysis. The rate of cyclometalation in the formation of compounds **1.24** – **1.31**, was found to be influenced by steric factors; the bulkier derivatives experienced a faster rate of cyclometalation. An accelerated rate of ligand cyclometalation was also observed in cationic scandium nacnac complexes compared to the neutral analogues.[80]

1.3.3.3 Cyclometalation in Phosphinimine Ligands

Dialkyl rare earth complexes of anilido-phosphinimine ligands have previously been shown to be prone to cyclometalation reactivity. For example, in *P*-phenyl substituted derivatives, *ortho*-metalation of a phosphinimine phenyl ring occurred with concomitant loss of alkane (Scheme 1.15). This transformation resulted in the formation of cyclometalated mixed aryl/alkyl rare earth products (Ln = Y, **1.32**; Ln = Lu, **1.33**).

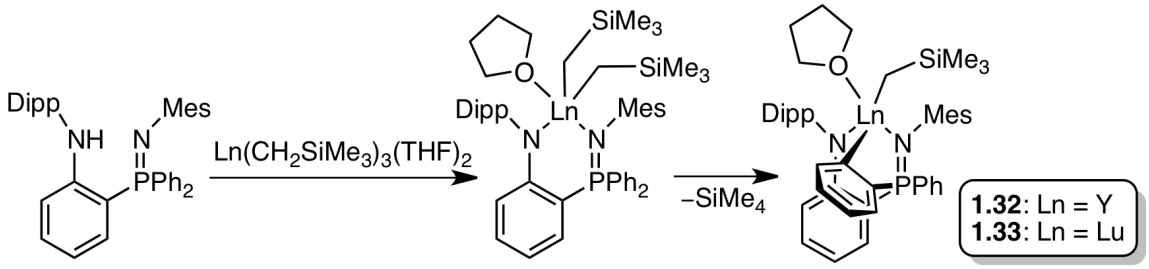

Scheme 1.15 *Ortho*-metalation of a *P*-phenyl substituted anilido-phosphinimine ligand

Some interesting reactivity has been achieved from these species through reaction with various small molecules. Protonolysis reactivity of **1.32** with two equivalents of 2,6-diisopropylaniline resulted in alkane elimination and metallacycle ring opening to afford the bis(anilide) complex (**1.34**).[81] Additionally, similar protonolysis chemistry resulted

from the reaction of **1.33** with phenylacetylene, thereby generating a bis(alkynyl) lutetium complex (Scheme 1.16).[82]

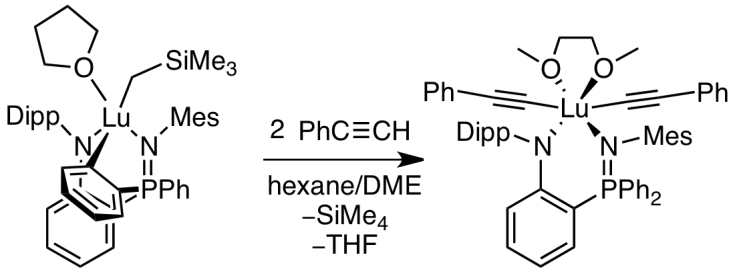

1.33 **1.35**

Scheme 1.16 Synthesis of a bis(alkynyl) lutetium complex

Precedent for cyclometalation has also been demonstrated in a less sterically demanding *P*-methyl substituted derivative of the anilido-phosphinimine ligand. Reaction of a scandium chloride complex of the ligand with two equivalents of methyllithium resulted in a cyclometalated scandium methyl dimer (**1.36**) with loss of methane. It was speculated that the reaction proceeded through a transient scandium dimethyl complex that was thermally susceptible to a cyclometalative alkane elimination reaction (Scheme 1.17).[83]

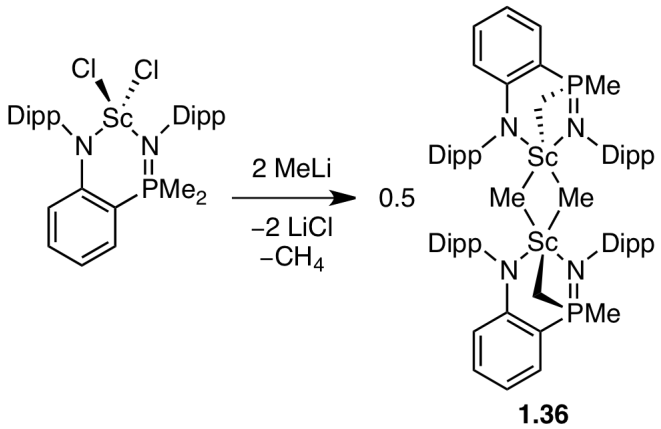

1.36

Scheme 1.17 Cyclometalation of a *P*-methyl substituted anilido-phosphinimine ligand

1.3.3.4 Other Ligand Types

A variety of other ligand scaffolds have been shown to undergo cyclometalation reactions in rare earth alkyl complexes. For example an yttrium dialkyl complex of a triamino-amide ligand was found to quantitatively cyclometalate via an NMe group at ambient temperature (Scheme 1.18). In aromatic solvent (benzene-d_6), full conversion to the cyclometalated product **1.37** occurred over 8 h. However, in Lewis basic solvent (THF-d_8), the transformation required substantially more time (2 days), implying a stabilizing effect of the dialkyl complex by the coordinating solvent.[84] The cyclometalated yttrium complex was determined to be monomeric by $^{13}C\{^1H\}$ NMR spectroscopy, whereby the NCH_2Y and $SiCH_2Y$ carbon resonances exhibited coupling to a single ^{89}Y nucleus. In comparison, a cyclometalated lanthanum complex of a related TACN-amide ligand, $\{[(\mu\text{-}CH_2)Me(TACN)SiMe_2N(^tBu)]La(CH_2SiMe_3)\}_2$ (**1.38**, TACN = 1,4,7-triazacyclononane), was observed to be a dimeric species, likely due to the larger ionic radius of lanthanum.[85]

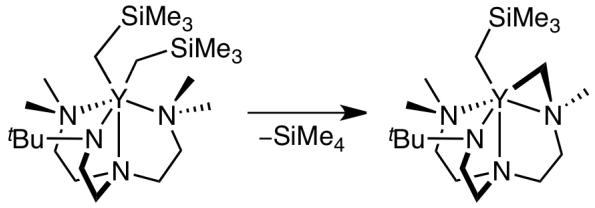

1.37

Scheme 1.18 Cyclometalation in an yttrium dialkyl complex of a triamino-amide ligand

The synthesis of *N*-heterocyclic carbene (NHC) complexes of rare earth metals was recently investigated by Okuda and co-workers. Reaction of 1,3-bis(2,6-diisopropylphenyl)imidazol-2-ylidene (IPr) with $Ln(CH_2SiMe_3)_3(THF)_2$, Ln = Y, Lu,

resulted in formation of thermally robust trialkyl NHC complexes (Ln = Y, **1.39**; Ln = Lu, **1.40**, Scheme 1.19).

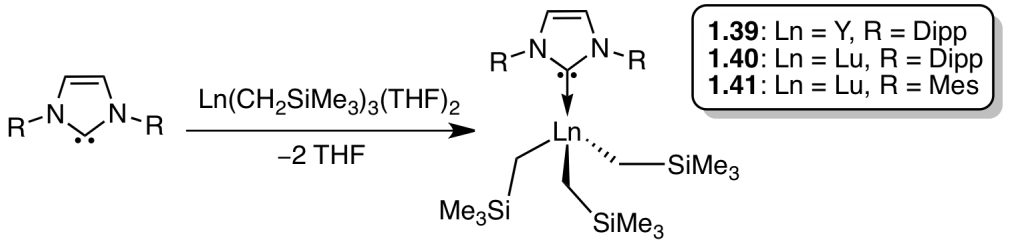

Scheme 1.19 Synthesis of NHC rare earth complexes

When the analogous reaction was performed using the slightly less bulky NHC 1,3-bis(2,4,6-trimethylphenyl)imidazol-2-ylidene (IMes), only the lutetium derivative, (IMes)Lu(CH_2SiMe_3)$_3$ could be isolated (**1.41**, Scheme 1.19). The corresponding reaction between IMes and Y(CH_2SiMe_3)$_3$(THF)$_2$, resulted in a cyclometalated dialkyl product **1.42**. Complex **1.42** arose through a C–H activation one of the *ortho*-methyl groups of the mesityl ring with elimination of tetramethylsilane (Scheme 1.20).[86]

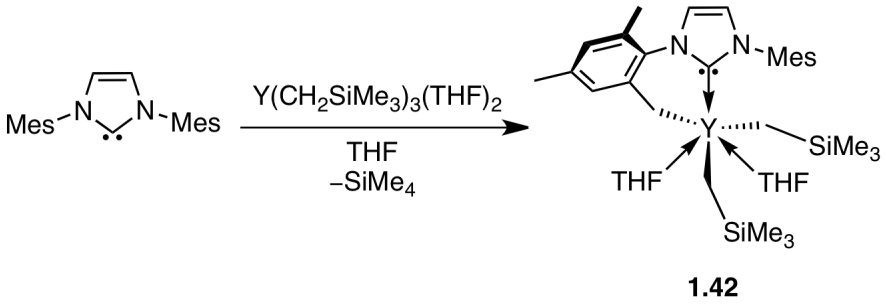

1.42

Scheme 1.20 Cyclometalation of IMes

1.3.3.5 Cylcometalation of *N*-heterocycles

Heterocycles such as pyridine are commonly encountered in rare earth chemistry. It has been well-documented that *N*-heterocycles are capable of cyclometalative C–H

bond reactions involving transition, lanthanide and actinide metals.[87] Notably, the cyclometalated species have proven useful from a perspective of (a) generating functionalized heterocyclic derivatives by insertion of unsaturated substrates into the M–C bond; and (b) the synthesis of metal element multiple bonds via metallacycle ring opening.

An early example of heterocycle metalation in rare earth chemistry involved the reaction of $(\eta^5\text{-}C_5Me_5)_2LuR$ (R = CH_3 or H) with pyridine. Coordination of pyridine to lutetium initially gave the pyridine adduct (**1.43**); however, subsequent C–H bond activation of the heterocycle at the 2-position led to cyclometalation and formation of **1.44** with loss of either methane or hydrogen gas (Scheme 1.21). Kinetic analysis revealed that the cyclometalation reaction was first order in **1.43** with no dependence on the excess of pyridine used, thus suggesting an intramolecular reaction. Notably, the metalated carbon atom in **1.44** exhibited a downfield shift in its ^{13}C NMR spectrum at δ 234.26 (cyclohexane-d_{12}), which is often diagnostic of a Ln–C_{aryl} bond in diamagnetic lanthanide complexes.[88]

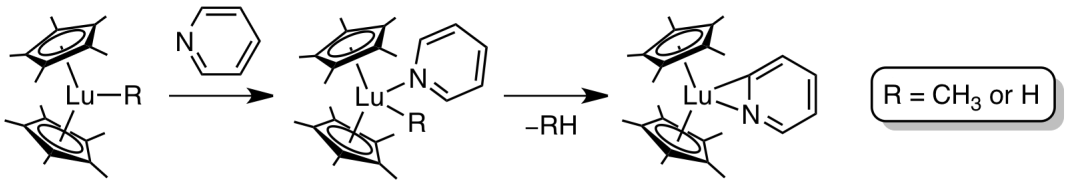

1.43 **1.44**

Scheme 1.21 Pyridine activation in a lutetium metallocene complex

A similar pyridine activation process was observed in the half-metallocene complex $(\eta^5\text{-}C_5Me_5)Lu(CH_2SiMe_3)_2(THF)$. Reaction with two equivalents of pyridine in toluene solution generated the double adduct, **1.45**. Subsequent C–H bond activation of

the pyridine ring in the 2-position led to formation of (η^5-C_5Me_5)Lu[(η^2-(*N,C*)-NC_5H_4](CH_2SiMe_3)(NC_5H_5), **1.46** (Scheme 1.22).[89]

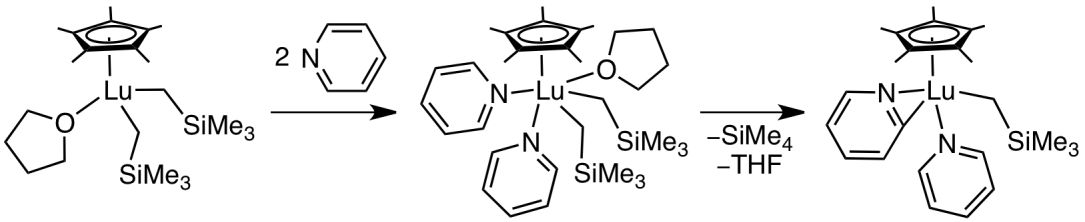

1.45 **1.46**

Scheme 1.22 Pyridine activation in a lutetium half-metallocene complex

Okuda reported reaction of the dicationic yttrium complex $[YMe(THF)_6]^{2+}[BPh_4]_2^-$ with excess pyridine, which resulted in rapid exchange of THF ligands for pyridine donors to afford $[YMe(py)_6]^{2+}[BPh_4]_2^-$. When left in a 2:1 solution of pyridine and pentane at ambient temperature over the course of 5 days, conversion to a cyclometalated complex, $[Y(\eta^2\text{-}(N,C)\text{-}NC_5H_4)(NC_5H_5)_6]^{2+}[BPh_4]_2^-$, **1.47**, occurred.[90]

A cyclometalated pyridine ligand was instrumental in the development of scandium imido chemistry by Mindiola and co-workers. It was found that the mixed alkyl/anilide complex (PNP)Sc(CH_3)NHDipp, where PNP = (2-^{i}Pr$_2$P-4-Me-C_6H_4)$_2$N$^-$, reacts with pyridine to form a cyclometalated product (PNP)Sc(η^2-(*C,N*)-NC_5H_4)NHDipp (**1.49**) with loss of methane. Various mechanisms were considered for this transformation, including (i) direct cyclometalation of pyridine with loss of methane; and (ii) α-NH abstraction to form a transient scandium imide and methane, followed by 1,2-addition of pyridine across the double bond. Deuterium labeling studies using pyridine-d_5 revealed the formation of (PNP)Sc(η^2-(*C,N*)-NC_5D_4)NDDipp (**1.49**-d_5), suggesting that α-hydrogen abstraction and loss of methane occurred prior to *ortho*-metalation of pyridine. Furthermore, loss of CH_4 rather than CH_3D and no deuterium incorporation into

the anilide ring or PNP framework was observed. Accordingly, the deuterium labeling study supported a mechanism that involved the formation of a transient scandium imide complex (**1.48**) and subsequent 1,2-C–H bond addition across the reactive Sc=NAr bond (Scheme 1.23).[91] This work was notable in that it provided the first reactivity evidence to demonstrate the existence of a terminal scandium imide. Shortly thereafter, a terminal scandium imide was in fact isolated and structurally characterized by Chen and co-workers.[92]

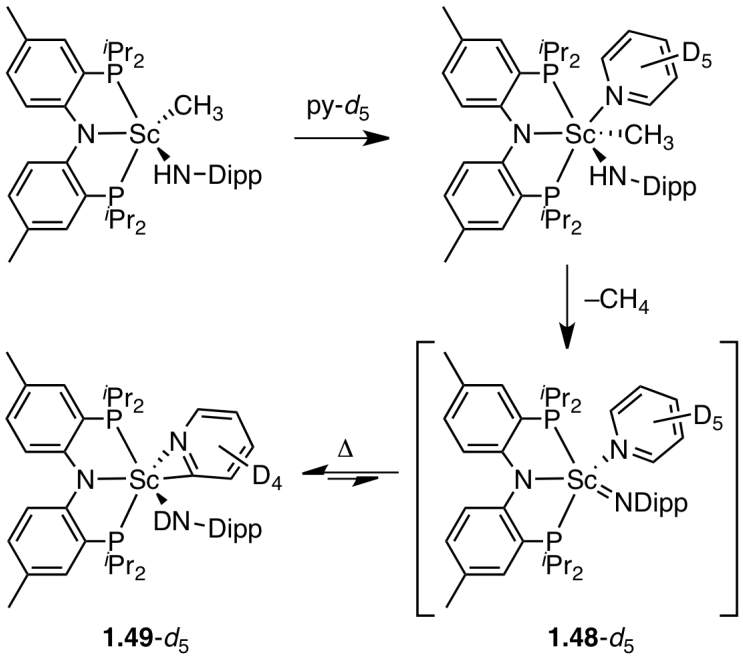

Scheme 1.23 *Ortho*-metalation of pyridine via 1,2 addition across a transient Sc=N double bond

1.4 Scope of the Project

Over the past 30 years, research into the rare earth elements has resulted in a diverse array of rich organometallic and coordination chemistry. Rapid expansion in the development of both fundamental and application-based research has occurred over this

time. As a result, two distinct, but integrally correlated fields of research have surfaced, being, (i) the fundamental study of bonding and reactivity in rare earth complexes; and (ii) the development of lanthanide complexes to be applied in a specific catalytic activity. In both fields, a common theme typically encountered is the requirement for control of reactivity at the metal centre; to a large degree, this can be accomplished through manipulation of its steric and electronic environment. Accordingly, the majority of research in rare earth metal chemistry involves a metal bound to one or more ancillary ligands for the purpose of controlling its steric and electronic properties.

As outlined in the literature review in this chapter, cyclometalative C–H bond activation is a process that is highly prevalent in rare earth chemistry. It occurs, in part, due to a lack of control in reactivity at the metal centre. To this end, the goal of this thesis was to develop strategies for controlling reactivity in organometallic lanthanide complexes. For this purpose, several families of novel bis(phosphinimine) pincer ligands based on rigid carbazole and pyrrole frameworks (Chart 1.2) were designed and synthesized. Rare earth complexes of the developed ligands were prepared and the ability of the ligands to stabilize highly reactive metal complexes was evaluated. An integral component of this objective included the synthesis of well-defined alkyl complexes that exhibited resistance to intramolecular cyclometalative reactivity. This is a significant objective to strive for from a practical perspective because this work serves to develop model systems of reactivity that may lead to industrial advances. For example, reactivity encountered in this project has the potential to be applied in the mechanism-based design of new catalysts for small-molecule transformations. Additionally, with adequate

stabilization of the metal centre by an ancillary ligand, it is anticipated that the development of rare bonding modes and reactivity should also be possible.

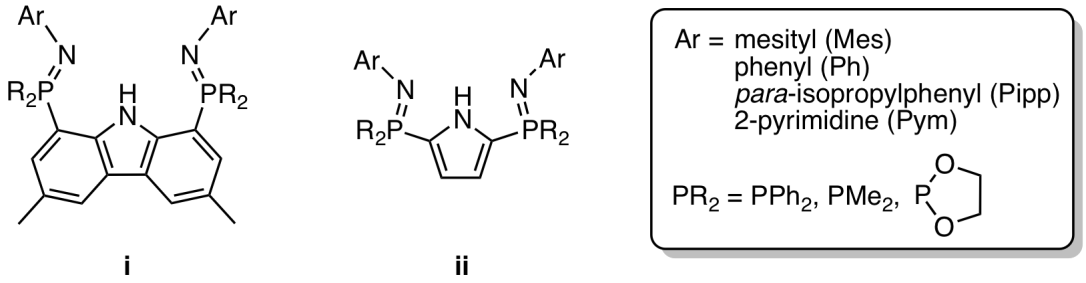

Chart 1.2 Developed bis(phosphinimine) pincer ligands

The work herein discusses the design and synthesis of novel non-Cp ligands for use in stabilizing dialkyl complexes of rare earth metals (Sc, Y, Lu and Er). The modular nature of the ancillary frameworks was intended so as to allow for development of rare earth complexes with variable steric and electronic properties. Accordingly, with a family of ligands that exhibit a wide range of properties, comparisons in the structure and reactivity of resultant complexes is possible. It should be noted that the reactivity studies performed in this thesis are not exhaustive and it is expected that much organometallic chemistry can be further harvested from many of the presented complexes.

Chapter 2

Rare Earth Complexes of a Novel Bis(phosphinimine)carbazole Ligand

2.1 Overview

Over the past decade, there has been a surge in the development of non-carbocyclic ligands for use in supporting highly reactive rare earth complexes.[56-58] This "post-metallocene era" has witnessed a diverse array of new ligand scaffolds that can support metal ions and provide a wide variety of different steric and electronic environments. As a result, unique coordination modes have often been encountered in lanthanide complexes supported by non-Cp ligands, a trend unparalleled to that observed with traditional carbocyclic ligands. To this end, a novel bis(phosphinimine) ligand based on an aromatic carbazole framework has been developed for use in stabilizing rare earth metal ions. The ancillary ligand was designed to impart a unique coordination environment on metal complexes and thus act as a platform for obtaining unique bonding modes and reaction behaviour. Herein, the design, synthesis and rare earth complexation

of the novel bis(phosphinimine)carbazole ligand is reported. Over the course of this development, some intriguing reactivity patterns of the ancillary ligand with rare earth metals have been discovered.

2.2 Phosphinimine Chemistry

The phosphinimine functional group has received significant interest recently in organometallic chemistry. It has proven to be an effective donor ligand in rare earth,[81-83,93-107] main group,[108-112] actinide,[113,114] early[115-120] and late[121-123] transition metal chemistry. In particular, bis(phosphinimine)methane ligands (i, Chart 2.1) have received a large degree of attention in the lanthanide literature due to their unique ability, when doubly deprotonated, to support rare earth carbene complexes.[124-129] For example, the first example of a lanthanide complex containing a Ln=C bond was synthesized by the reaction of a bis(phosphinimine)methane ligand with samarium tris(dicyclohexylamide). This carbene complex formed through double deprotonation of the ligand methylene with loss of dicyclohexylamine (Scheme 2.1).[124] Other phosphinimine-based ligand scaffolds have also recently surfaced in rare earth chemistry, such as amine-phosphinimine (ii)[100,101] and aniline-phosphinimine (iii)[81-83] frameworks.

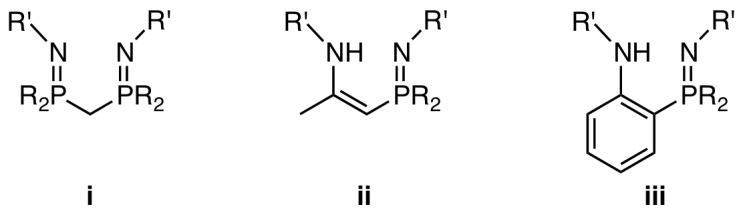

Chart 2.1 Selected phosphinimine ligands

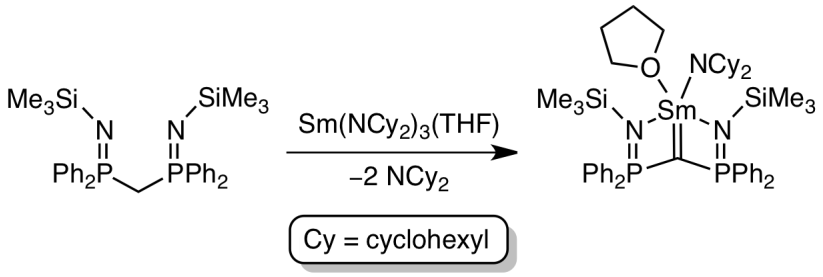

Scheme 2.1 Synthesis of a samarium carbene complex

In terms of electronic properties, phosphinimine subunits are highly polar and can act as strong σ-donors (Scheme 2.2). A recent computational study has revealed that phosphinimines exhibit comparable σ-donor ability to that of organic imines (C=N); however, they were shown to be much poorer π-acceptors.[130] For a lanthanide complex, a deficit of π-acceptor ability in a ligand is not of significant concern as the limited radial extension of 4f atomic orbitals generally restricts any π-back-bonding interactions with the metal centre. The strong σ-donor ability of the phosphinimine functionality does, however, make it an ideal candidate for incorporation into a ligand for use with lanthanide metals. Since the rare earth metals are highly electropositive, a ligand with a strong electron donating capacity is expected to provide an electronically stabilizing effect.

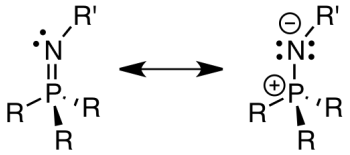

Scheme 2.2 Phosphinimine resonance contributors

The phosphinimine functionality can be synthesized via the Staudinger reaction,[131] whereby an appropriate phosphine is reacted with an aryl or alkyl azide to generate a phosphazide intermediate. From this intermediate, loss of dinitrogen liberates

the phosphinimine functionality. Under anhydrous conditions, the phosphinimine functionality is quite stable (even at temperatures >140 ºC) and can be readily isolated. Phosphinimines are also quite robust compared to other functional groups such as the organic imine, which is susceptible to nucleophilic attack at the imine carbon.[132,133] From a synthetic and mechanistic standpoint, the presence of a phosphorus nucleus expedites the identification and characterization of metal phosphinimine complexes by NMR spectroscopy (^{31}P = 100% abundant, I = ½). A final feature of the phosphinimine functionality is its high degree of synthetic modularity at the phosphorus and nitrogen atoms. For example, judicious choice of phosphine and azide affords a product with variable steric and electronic properties at these sites. For these reasons, the phosphinimine functionality is desirable for use as a donor group in an ancillary ligand for rare earth metals.

2.3 Ligand Design

When designing an ancillary ligand for use with rare earth metals, a variety of attributes is desired. In particular, a monoanionic ligand is ideal so that it would be capable of binding tightly to a rare earth ion in the +3 oxidation state, while retaining two valences for further reactivity at the metal. A tridentate pincer geometry promotes coordinative saturation of the metal ion and incorporation of bulky groups may help to block Lewis bases such as THF from binding to the metal. The presence of bulky groups can also reduce the potential for dimerization; however, the degree of incorporated steric bulk must be somewhat limited so as to not completely inhibit reactivity at the metal

centre. In rare earth organometallic chemistry, tridentate pincer ligand designs have been quite successful in the study of unique reaction behaviour and the stabilization of rare bonding modes. For example, pincer geometries were implemented in the preparation of lanthanide carbene complexes via a bis(phosphinimine)methanediide ligand[124] and the synthesis of a terminal scandium imide supported by a tridentate β-diketiminate-amino ligand.[92]

As depicted in Figure 2.1, a rigid 3,6-dimethylcarbazole framework was chosen as the backbone of the targeted ancillary ligand with two phosphinimine donors installed at the 1 and 8 positions. The rigid aromatic backbone was expected to prevent fluxional ligand behaviour.[76,134,135] As mentioned previously, the incorporation of highly polar phosphinimine subunits was desirable because of strong donor properties and thermal robustness. Furthermore, the phosphinimine functionality allows for a high degree of steric and electronic tunability through adjustment of R groups attached at the phosphorus or nitrogen atoms.

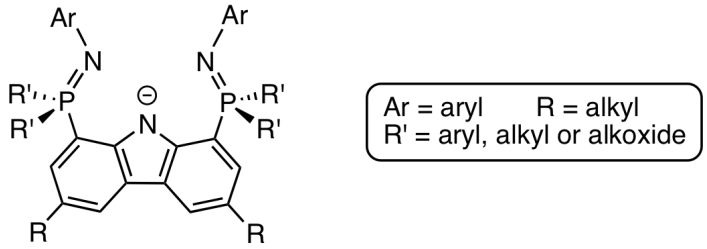

Figure 2.1 Generic bis(phosphinimine)carbazole ligand design

2.4 Ligand Synthesis

2.4.1 Synthetic Approach

Synthesis of the target bis(phosphinimine)carbazole ligand requires multiple steps and a variety of synthetic approaches can be envisioned. The protocol developed in this work involved (i) preparation of a suitable carbazole-based framework, (ii) halogenation of the aromatic backbone and *N*-protection, (iii) installation of two phosphine moieties at the 1 and 8 carbazole sites followed by deprotection and (iv) reaction of the diphosphine with two equivalents of an aryl azide to give the final desired ligand (Scheme 2.3). This approach is described in full detail in the following sections.

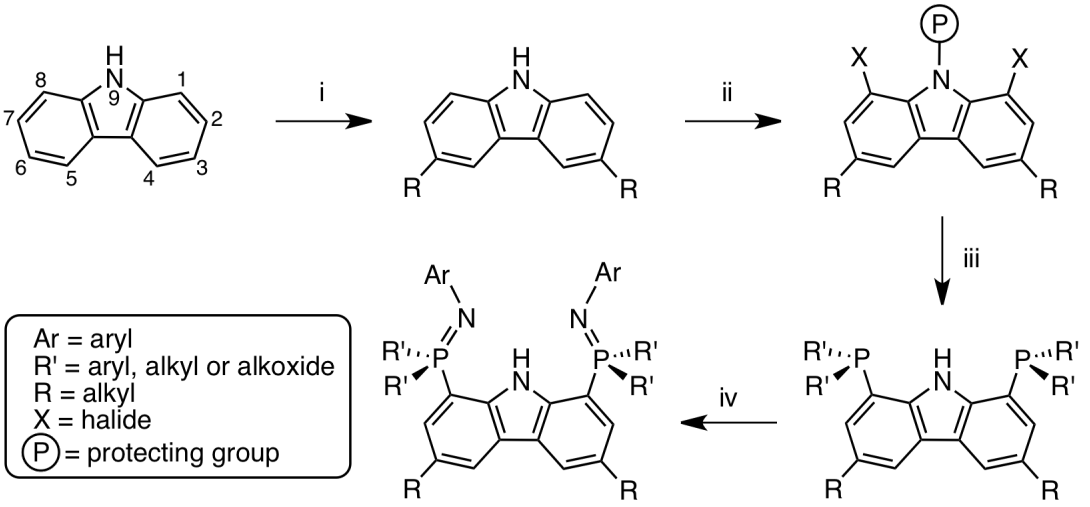

Scheme 2.3 General synthetic approach for preparing the bis(phosphinimine)carbazole ligand

2.4.2 Precursors Known From the Literature

As the synthetic feedstock for preparing the bis(phosphinimine)carbazole ligand, carbazole was selected as it is a commercially available and inexpensive reagent.

Carbazole (Cz) exhibits a regioselective preference for electrophilic substitution at the 3 and 6 sites of the aromatic ring system rather than the desired 1 and 8 positions. Consequently, functionalization of the carbazole ring system at the 3 and 6 sites was required prior to installation of phosphine moieties at the 1 and 8 locations. Furthermore, substitution at the 3 and 6 positions provides a convenient means for controlling both the ligand solubility and the electronic and steric properties of the aromatic ring system.

There are various methods available in the literature for functionalization of carbazole at the 3 and 6 positions. For example, *tert*-butyl groups can be installed at these sites via Friedel-Crafts alkylation.[136,137] Alternatively, derivatization with phenyl rings can be accomplished by (i) iodination of carbazole at the 3 and 6 sites followed by (ii) a Suzuki coupling reaction with $PhB(OH)_2$.[138] In this thesis, a carbazole ring system derivatized with methyl groups at the 3 and 6 sites has been pursued and can be synthesized by a variety of methods (Scheme 2.4). For example, two equivalents of commercially available 2-bromo-4-methylaniline can be coupled using a Pd/In catalytic system to generate 2,2′-diamino-5,5′-dimethylbiphenyl.[139] A subsequent ring closing reaction of 2,2′-diamino-5,5′-dimethylbiphenyl in dilute sulfuric acid liberates 3,6-dimethylcarbazole (Route A, Scheme 2.4[140] Alternatively, di-*p*-tolylamine can be subjected to either photolysis or pyrolysis reactions to give 3,6-dimethylcarbazole (Route B, Scheme 2.4).[141] Both of the above-mentioned methods are unattractive due to the high cost of the required reagents; the first route requires an expensive palladium catalyst in order to prepare 2,2′-diamino-5,5′-dimethylbiphenyl, while the second strategy requires the expensive precursor di-*p*-tolylamine making it unsuitable for scale-up. As mentioned previously, carbazole is an inexpensive starting material and as such it is attractive to use

as a chemical feedstock. Accordingly, 3,6-dimethylcarbazole can be prepared from carbazole in two synthetic steps. First, carbazole can be brominated at the 3 and 6 positions using NBS to afford 3,6-dibromocarbazole.[142] The second step involves installation of a trimethylsilyl *N*-protecting group, lithium halogen exchange using 4.1 equivalents of *tert*-butyllithium, subsequent reaction with iodomethane and finally, acidic workup to remove the protecting group (Route C, Scheme 2.4).[143]

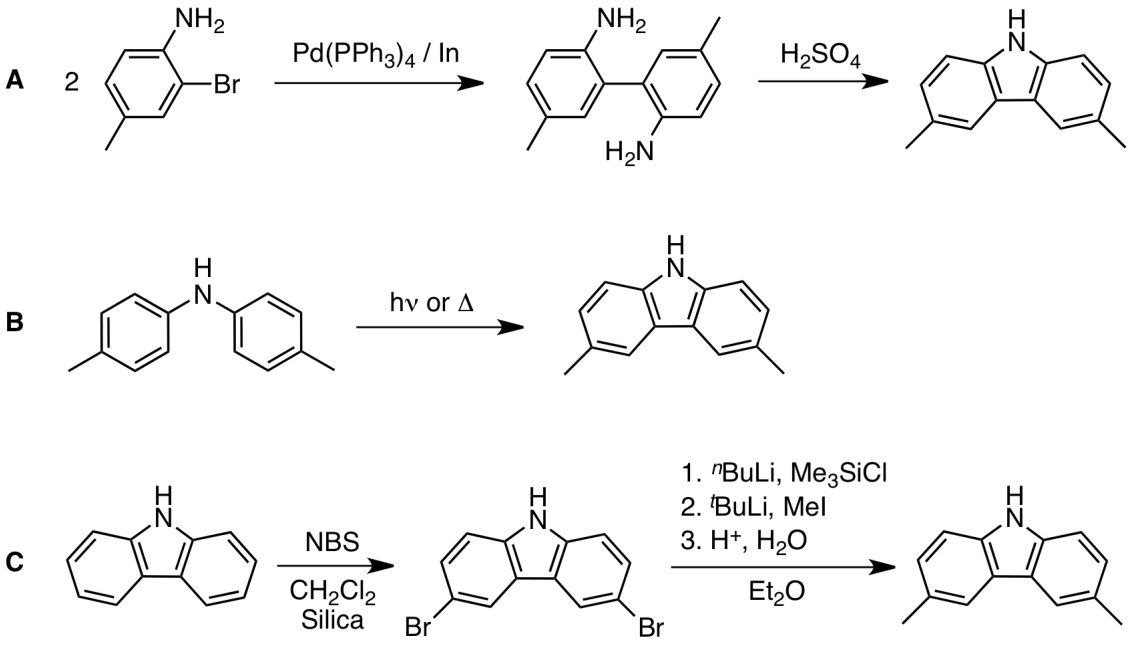

Scheme 2.4 Synthetic routes to 3,6-dimethylcarbazole

From 3,6-dimethylcarbazole, the strategy utilized to install phosphines at the 1 and 8 positions of the aromatic backbone requires initial bromination of carbazole at the 1 and 8 positions, followed by *N*-protection with a suitable protecting group. Phosphine moieties can then be installed by a lithium halogen exchange reaction using *tert*-butyllithium followed by reaction with two equivalents of a chlorophosphine. The requisite precursor 1,8-dibromo-3,6-dimethylcarbazole is a known molecule and can be readily synthesized by brominating 3,6-dimethylcarbazole with two equivalents of NBS

(Scheme 2.5).[143] The following section describes *N*-protection of 1,8-dibromo-3,6-dimethylcarbazole and subsequent installation of phosphine moieties.

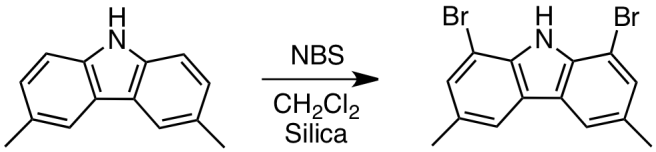

Scheme 2.5 Synthesis of 1,8-dibromo-3,6-dimethylcarbazole

2.4.3 Evaluation of *N*-Protecting Groups

Prior to installation of phosphine subunits onto the carbazole backbone, a suitable *N*-protecting group was required. Initially, the use of a trimethylsilyl group was explored for this purpose. Accordingly, 1,8-dibromo-3,6-dimethylcarbazole was reacted with one equivalent of *n*-butyllithium followed by trimethylsilyl chloride to afford 1,8-dibromo-3,6-dimethyl-9*N*-trimethylsilylcarbazole *in situ*. Subsequently, a lithium halogen exchange reaction was performed by addition of *tert*-butyllithium and the lithiated species was then quenched with an excess of chlorodiphenylphosphine. Following workup, it was quickly discovered that the isolated product was not the expected 1,8-bis(diphenylphosphino)-3,6-dimethylcarbazole, but rather, the compound 1,8,9*N*-tris(diphenylphosphino)-3,6-dimethylcarbazole **1** had been prepared (Scheme 2.6).

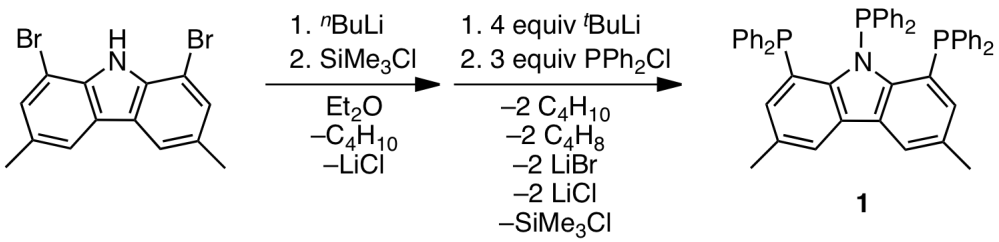

Scheme 2.6 Synthesis of 1,8,9*N*-tris(diphenylphosphino)-3,6-dimethylcarbazole **1**

Upon re-evaluation of the reaction conditions, the resultant formation of **1** was not entirely surprising. For example, in the preparation of dichalcogenoimidodiphosphinates ($(E{=}PR_2)_2NH$, E = O, S, Se), the method of choice involves the reaction of a chlorophosphine (PR_2Cl, R = Ph, ^{i}Pr) with hexamethyldisilazane to afford a $(PR_2)_2NH$ product, which is then oxidized to the corresponding dichalcogenoimidodiphosphinate.[144] As such, the reaction of a chlorophosphine (PR_2Cl) with an $R'_2N–SiR''_3$, bond is quite facile and proceeds with the formation of an $R'_2N–PR_2$ product and corresponding loss of chlorosilane $ClSiR''_3$.

Despite the unexpected formation of **1**, it could be readily prepared in high yield and purity. Its $^{31}P\{^{1}H\}$ NMR spectrum (chloroform-*d*) exhibited a triplet at δ 53.3 (1P, J_{PP} = 69.5 Hz) and a doublet at δ −17.2 (2P, J_{PP} = 69.5 Hz) indicating coupling between the 1,8-Cz phosphines and the *N*-bound phosphine. The ^{1}H and $^{13}C\{^{1}H\}$ NMR spectra corroborated the expected structure of **1** and suggested C_{2v} symmetry in solution.

Single crystals of **1** were obtained from a concentrated toluene solution at −35 °C and the solid-state structure was determined by X-ray crystallography. The compound crystallized in the orthorhombic space group $Pna2_1$ (#33) with one molecule of toluene in the asymmetric unit. The molecular structure is depicted in Figure 2.2 as a thermal ellipsoid plot and selected metrical parameters are listed in Table 2.1.

The C–P bond lengths in **1** are unexceptional (average C–P = 1.836 Å, range = 1.818(2) – 1.846(3) Å). The N–P bond distance of 1.742(2) Å also falls within the normal range. In the compound, P1 lies within the plane defined by the carbazole backbone; however, P2 lies below the same plane by 0.918 Å and P3 lies above by 0.611 Å. This

twisting of the diphenylphosphino moieties in and out of the carbazole plane is likely due to steric crowding.

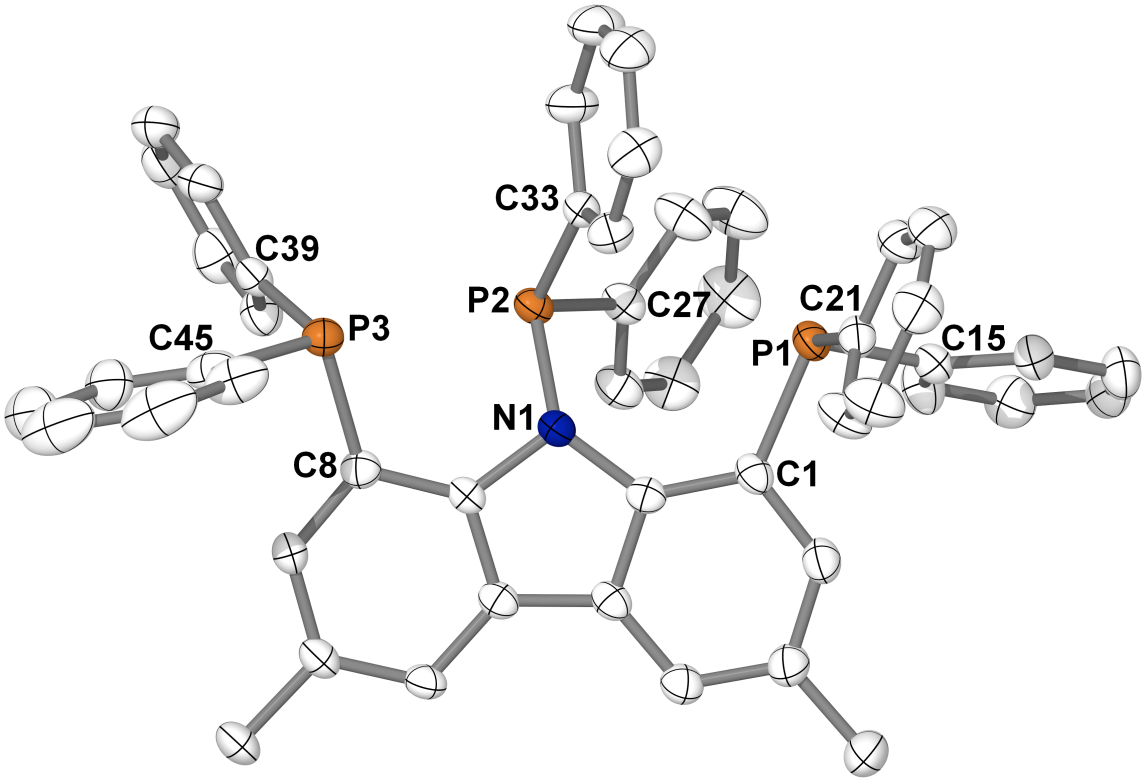

Figure 2.2 Thermal ellipsoid plot (50% probability) of **1**. Hydrogen atoms and toluene solvent molecule are omitted for clarity.

Table 2.1 Selected bond distances /Å and angles /° for **1**

P1–C1	1.845(2)	P1–C21	1.842(2)
P1–C15	1.836(2)	N1–P2	1.742(2)
P2–C33	1.818(2)	P2–C27	1.831(2)
P3–C8	1.844(2)	P3–C39	1.829(3)
P3–C45	1.846(3)	P1···P2	3.673(1)
P3···P2	3.111(1)		
C15–P1–C21	102.7(1)	C21–P1–C1	102.1(1)
C15–P1–C1	99.0(1)	C27–P2–N1	103.7(1)
C33–P2–N1	105.9(1)	C27–P2–C33	106.8(1)
C39–P3–C45	101.2(1)	C45–P3–C8	100.7(1)
C39–P3–C8	105.3(1)		

Gratifyingly, compound **1** can be reacted with $[Et_3NH]I$ in methylene chloride to cleave the P–N bond and liberate the desired compound 1,8-bis(diphenylphosphino)-3,6-dimethylcarbazole (**2**), iododiphenylphosphine and triethylamine (Scheme 2.7).

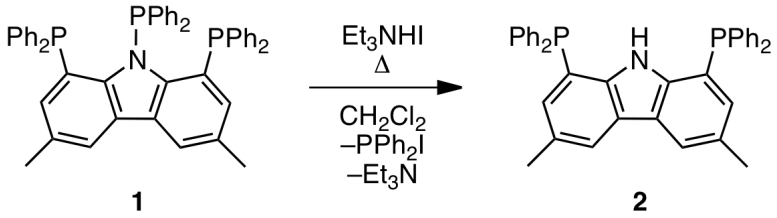

1 **2**

Scheme 2.7 Conversion of **1** to diphosphine **2**

While the compound 1,8-bis(diphenylphosphino)-3,6-dimethylcarbazole can be readily prepared from **1**, its purification was not trivial. Removal of the iododiphenylphosphine byproduct proved difficult and samples of **2** consistently retained ~5-10% iododiphenylphosphine (as indicated by ^{31}P NMR spectroscopy). As such, an alternative approach to the synthesis of **2** was explored.

Since the use of a trimethylsilyl *N*-protecting group led to cleavage of the N–Si bond, different *N*-protecting groups for use with 1,8-dibromo-3,6-dimethylcarbazole were investigated. The use of CO_2 as a protecting group has precedent in lithiation reactions involving carbazole.[136,145] By this approach, the carbazole NH is deprotonated with butyllithium and subsequently reacted with CO_2 to generate a carbamic acid anion. Unfortunately, this method was met with little success, and a *tert*-butoxycarbonyl *N*-protecting group was pursued instead.

Installation of a BOC protecting group onto 1,8-dibromo-3,6-dimethylcarbazole was achieved by reaction with di-*tert*-butyl dicarbonate (*t*-BOC_2O) in the presence of

catalytic 4-dimethylaminopyridine. This reaction proceeded cleanly to afford the *N*-protected compound 1,8-dibromo-3,6-dimethyl-9-BOC-carbazole, **3**. A subsequent lithium halogen exchange reaction of **3** with *tert*-butyllithium, followed by reaction with chlorodiphenylphosphine generated the corresponding BOC protected diphosphine **4** in 96.0% yield. Removal of the protecting group was efficiently achieved under thermal conditions (160 °C for 4.5 h) liberating deprotected compound **2**. The approach described above allowed for the preparation of **2** in high yield and purity as an off-white microcrystalline powder (Scheme 2.8).

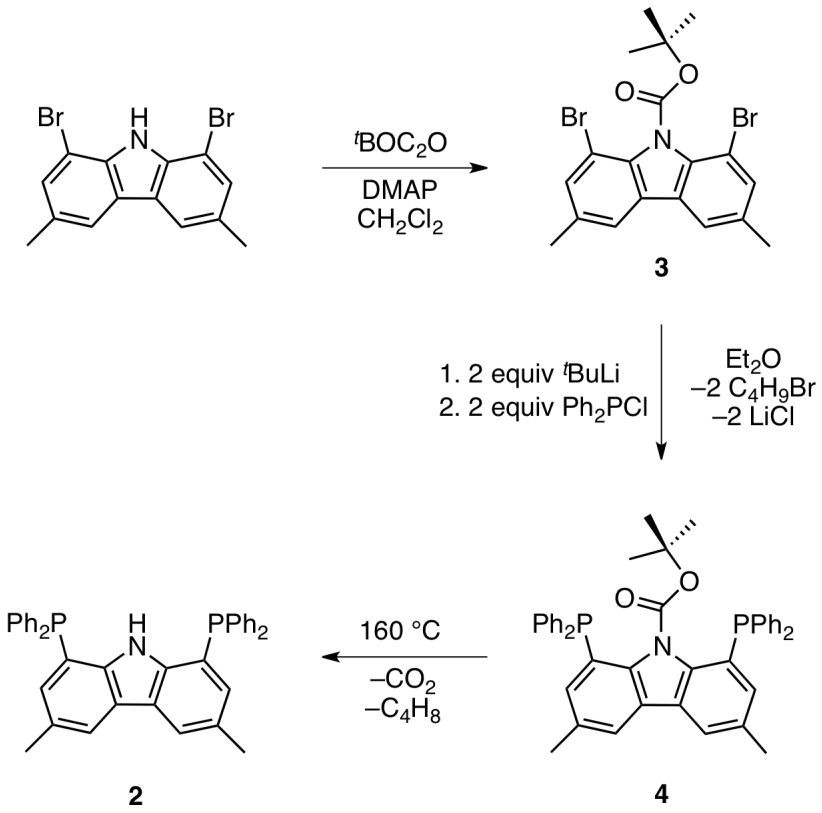

Scheme 2.8 Alternative method for synthesis of diphosphine **2**

2.4.4 Staudinger Reaction

The final step of the ligand synthesis involves reaction of diphosphine **2** with an appropriate aryl azide under standard Staudinger conditions to generate the phosphinimine functionality. To this end, reaction of **2** with two equivalents of mesityl azide at ambient temperature afforded the proteo ligand ($H\mathbf{L}_{\mathbf{A}}^{\mathbf{Mes}}$, **5**) in high yield with concomitant loss of N_2 (Scheme 2.9). The compound exhibited a single resonance in its $^{31}P\{^1H\}$ NMR spectrum at δ −6.5 (benzene-d_6) and its ^1H and $^{13}C\{^1H\}$ NMR spectra suggested C_{2v} symmetry in solution. The proton NMR spectrum (benzene-d_6) had a broad NH peak at δ 12.18, an expectedly complicated aromatic region and three methyl resonances at δ 2.26, 2.22 and 1.95 corresponding to the *p*-mesityl, 3,6-carbazole and *o*-mesityl methyl signals, respectively. The high frequency of the NH resonance signifies that the group is likely involved in a hydrogen bonding interaction.

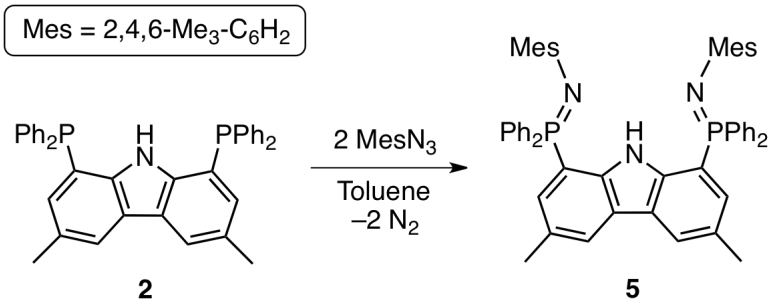

Scheme 2.9 Synthesis of mesityl substituted bis(phosphinimine) ligand **5**

Single crystals of **5** suitable for an X-ray diffraction experiment were grown from a concentrated toluene solution at −35 ºC. The ligand crystallized in the space group $P\bar{1}$ with two crystallographically independent molecules in the asymmetric unit; both structures are depicted in Figure 2.3 as thermal ellipsoid plots.

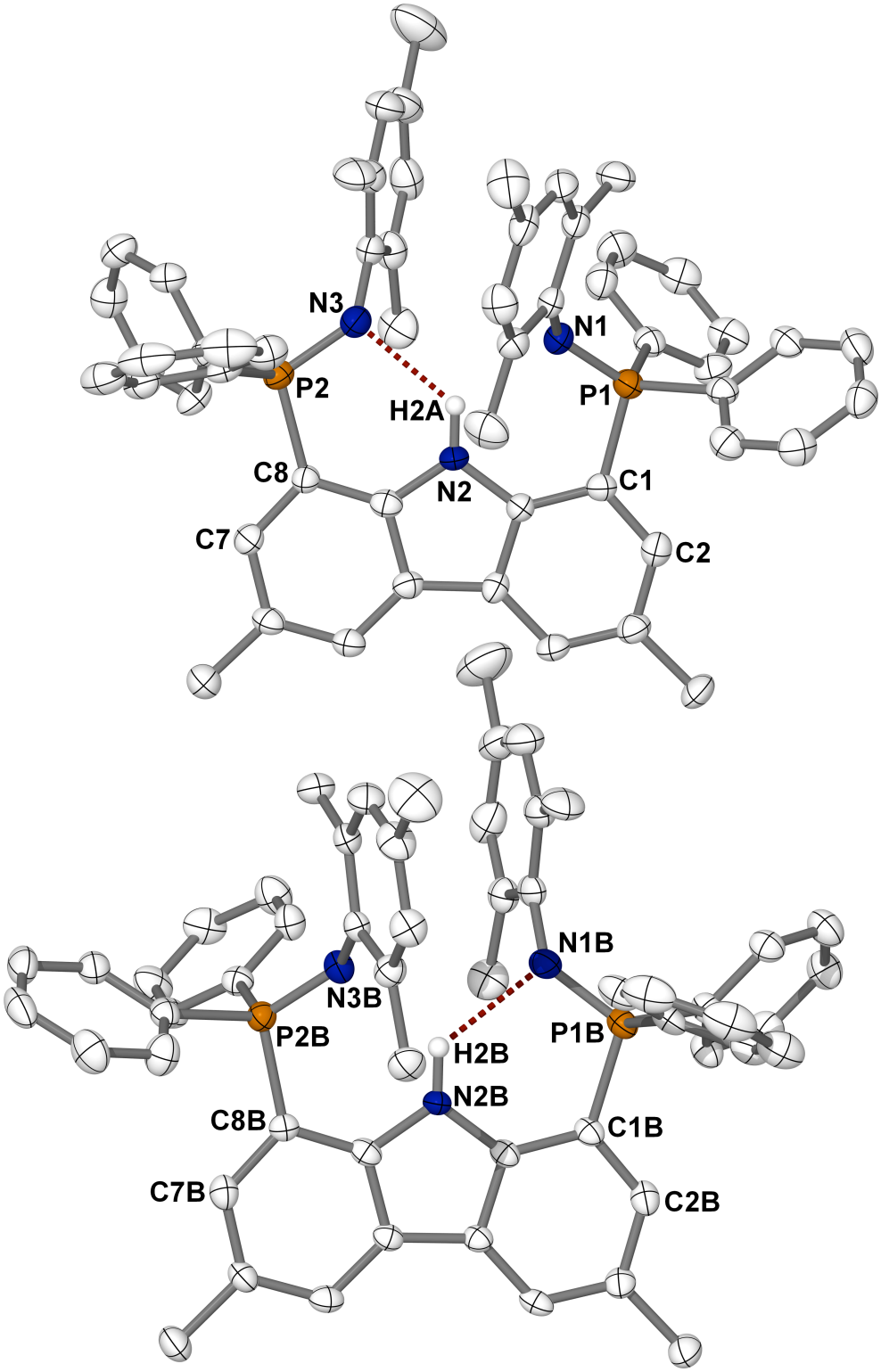

Figure 2.3 Thermal ellipsoid plots (50% probability) depicting two crystallographically independent molecules of HL_A^{Mes} (**5**). Hydrogen atoms (except H2A and H2B) and toluene solvent molecules are omitted for clarity.

The solid-state structure of **5** corroborated the expected composition of the ligand, as previously determined from multinuclear NMR spectroscopy. In each independent molecular unit of the structure, one phosphinimine nitrogen donor interacts with the carbazole N–H through a hydrogen bond (d(N2···N3) = 2.805(4) Å, d(N2B···N1B) = 2.835(4) Å). The phosphinimine arms are rotated periplanar to the aromatic carbazole backbone with N1–P1–C1–C2 and N3–P2–C8–C9 torsion angles of −154.4(3)° and −173.4(3)° in one molecule, and 153.2(3)° and 165.5(3)° in the other. A survey of selected metrical parameters from both independent molecules of **5** (Table 2.2) indicated a high degree of agreement between the two structures.

Table 2.2 Selected bond distances /Å, angles /° and torsion angles /° for the crystallographically independent molecules of compound **5**

P1–N1	1.549(3)	P1B–N1B	1.551(3)
P2–N3	1.560(3)	P2B–N3B	1.551(3)
N2···N3	2.805(4)	N2B···N1B	2.835(4)
N1–P1–C1	111.7(2)	N1B–P1B–C1B	110.3(2)
N3–P2–C8	110.1(2)	N3B–P2B–C8B	112.5(2)
N1–P1–C1–C2	−154.4(3)	N1B–P1B–C1B–C2B	165.5(3)
N3–P2–C8–C7	−173.4(3)	N3B–P2B–C8B–C7B	153.2(3)

2.5 Protonolysis Reactivity

In an effort to access an organolanthanide complex of the bis(phosphinimine) ligand via alkane elimination, proteo ligand **5** was reacted with one equivalent of the trialkyl lanthanide precursor $Y(CH_2SiMe_3)_3(THF)_2$ at ambient temperature. When the reaction was followed *in situ* by NMR spectroscopy in benzene-d_6 solution, the initial

formation of a product was evident after 1 h. At this point, the $^{31}P\{^{1}H\}$ NMR spectrum revealed the formation of a doublet at δ 24.1 ($^{2}J_{PY}$ = 6.2 Hz) and unreacted proteo ligand at δ −6.5 with relative integrations of 20:80. Continued reaction at ambient temperature over the course of 24 h resulted in complete conversion to product. The doublet at δ 24.1 was indicative of the formation of a new yttrium complex, especially with apparent coupling between ^{89}Y (100% abundant, I = ½) and the phosphorus nuclei of the ancillary ligand.

Analysis of the product by ^{1}H and $^{13}C\{^{1}H\}$ NMR spectroscopy revealed that the expected dialkyl yttrium complex had not been isolated, but rather, a doubly cyclometalated product. The complex consisted of the ligand bound to the yttrium centre in a κ^5 mode through its three nitrogen atoms and two *ortho*-metalated *P*-phenyl rings. A lack of symmetry in the ^{1}H and $^{13}C\{^{1}H\}$ NMR spectra of the product was apparent and signals in the aromatic regions corresponded to inequivalent *P*-phenyl rings. A particularly diagnostic signal in the $^{13}C\{^{1}H\}$ NMR spectrum was the metalated carbon attached directly to yttrium. This *ipso* carbon was highly deshielded and resonated far downfield as a doublet of doublets at δ 198.1 (dd, $^{1}J_{CY}$ = 42.5 Hz, $^{2}J_{CP}$ = 38.8 Hz). It was also found that the ^{1}H and $^{13}C\{^{1}H\}$ NMR spectra of the product were consistent with a complex where the mesityl rings were locked in position and incapable of free rotation on the NMR experiment time scale at ambient temperature. This was likely due to extreme steric crowding in the complex.

It is presumed that formation of the observed yttrium complex occurred as outlined in Scheme 2.10. First, reaction of **5** with $Y(CH_2SiMe_3)_3(THF)_2$ liberated the dialkyl yttrium complex **6** as a highly reactive species with loss of one equivalent of

tetramethylsilane. Subsequently, **6** rapidly reacted by intramolecular cyclometalative alkane elimination to afford doubly cyclometalated product **7**.

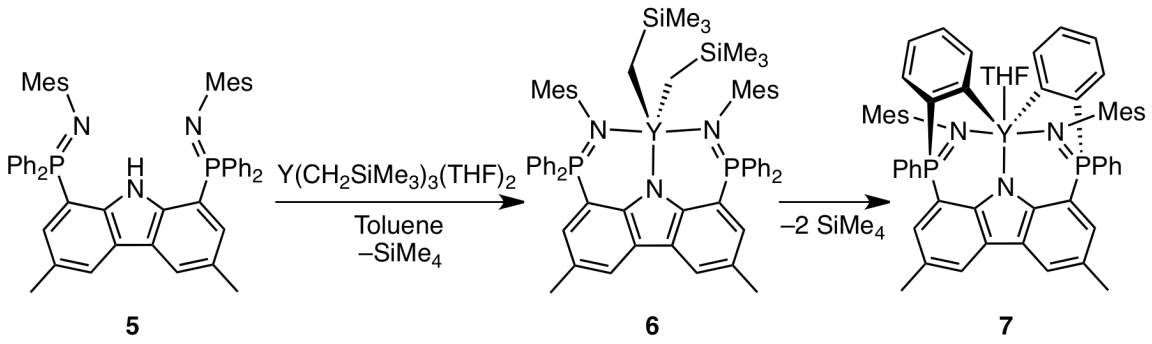

Scheme 2.10 Protonolysis reactivity of HL_A^{Mes} (**5**) and double *ortho*-metalation

Complex **7** can be obtained as a pure microcrystalline solid in reasonable yield (69.4%) after recrystallization. Unfortunately, single crystals suitable for an X-ray diffraction experiment could not be obtained despite repeated attempts. Consequently, the solid-state structure of **7** was not determined.

In light of the fact that the dialkyl yttrium complex of L_A^{Mes} was thermally unstable and only spectroscopic data could be obtained for its decomposition product, the alkane elimination reactivity of **5** with rare earth trialkyl reagents was not investigated any further. Accordingly, the synthesis of more thermally robust rare earth species was of interest, including their structural characterization, in order to be able to assess the coordination ability and other properties of the ligand. To this end, alternate rare earth complexation strategies such as salt metathesis were pursued.

2.6 Salt Metathesis Reactivity

2.6.1 Ligand Lithiation

Reaction of **5** with *n*-butyllithium was facile and resulted in quantitative conversion to the lithiated derivative **8**, ($\mathbf{L_A^{Mes}}$-κ^3*N*)Li, with loss of butane (Scheme 2.11). Compound **8** exhibited a $^{31}P\{^1H\}$ NMR resonance at δ 11.0 (benzene-d_6), which was downfield from that observed for the proteo ligand. In general, the chemical shift of the $^{31}P\{^1H\}$ phosphinimine resonance was found to be highly sensitive to the coordination environment of the ligand with a downfield shift being indicative of strong σ-donation from the phosphinimine functionalities. Like the proteo derivative, the ^1H and $^{13}C\{^1H\}$ NMR spectra of **8** were suggestive of C_{2v} symmetry in solution.

X-ray quality single crystals of **8** were readily obtained from a concentrated toluene solution at −35 °C and its molecular structure was determined. Compound **8** crystallized in the space group $P\bar{1}$ with one disordered molecule of toluene in the asymmetric unit. The solid-state structure of **8** is depicted in Figure 2.4 as a thermal ellipsoid plot and selected metrical parameters are listed in Table 2.3.

The geometry of the ligand in **8** promotes tridentate coordination of the lithium cation through the three nitrogen atoms. Notably, the ligand has sufficient steric bulk to saturate the coordination sphere of the cation; as such, lithio derivative **8** is both monomeric and solvent-free. In the solid state, the complex exhibits N–Li contacts that are relatively similar (N1–Li1 = 2.008(5) Å, N3–Li1 = 2.011(5) Å, N2–Li1 = 1.945(5) Å) and short P–N bonds (P1–N1 = 1.585(2) Å, P2–N3 = 1.570(2) Å). The short P–N bonds are consistent with double bond character. In the ligand, there is rotation of the pincer

phosphinimine arms out of the plane defined by the carbazole backbone (N1–P1–C1–C2 and N3–P2–C8–C7 torsion angles of 134.6(2)° and −129.4(3)°, respectively). As a result of this twisting, the lithium cation sits below the plane of the aromatic backbone by 0.771 Å. An interesting feature in the solid-state structure of **8** is a π-stacking interaction between the mesityl aromatic rings. Both mesityl rings exhibit a close to parallel alignment and have a centroid–centroid distance of 4.156 Å.

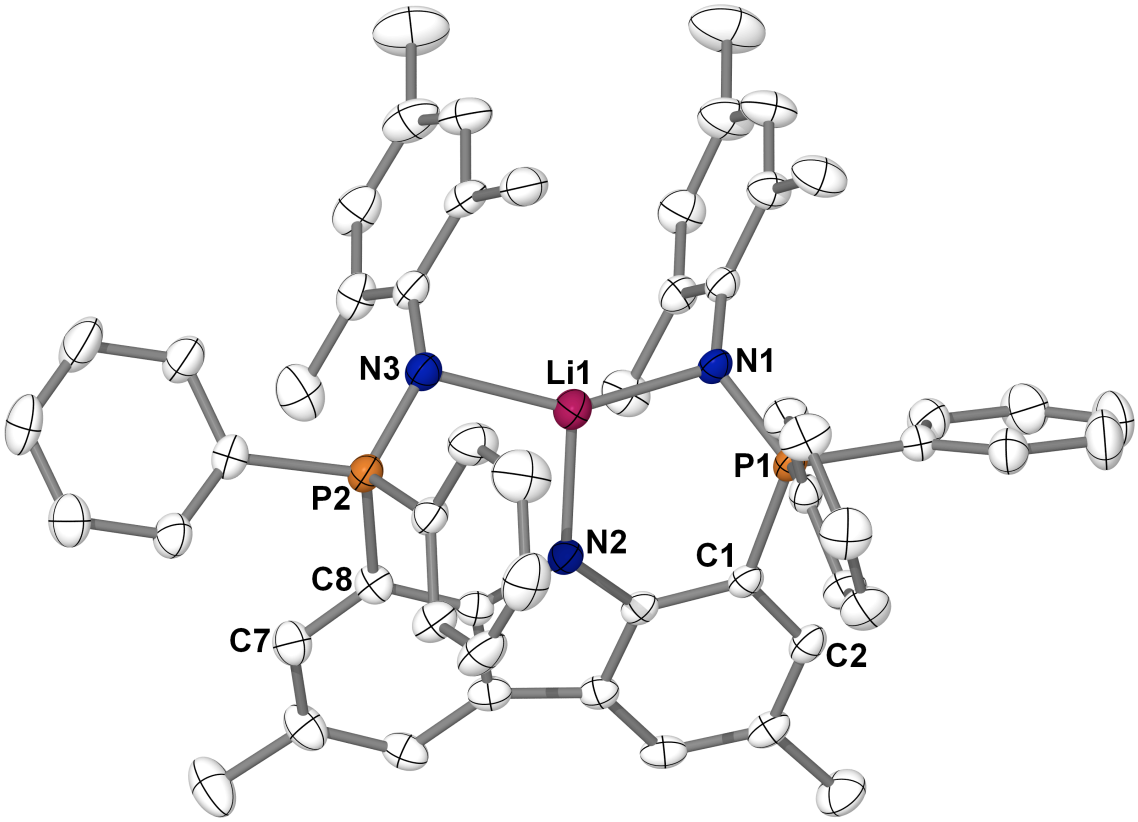

Figure 2.4 Thermal ellipsoid plot (50% probability) of ($\mathbf{L_A^{Mes}}$-κ^3*N*)Li (**8**). Hydrogen atoms and toluene solvent molecule are omitted for clarity.

Table 2.3 Selected bond distances /Å, angles /° and torsion angles /° for compounds **8**, **9** and **10**

	8	**9**	**10**
P1–N1	1.585(2)	1.619(4)	1.608(2)
P2–N3	1.570(2)	1.619(4)	1.615(2)
N1–M[a]	2.008(5)	2.221(3)	2.356(2)
N3–M[a]	2.011(5)	2.188(4)	2.317(2)
N2–M[a]	1.945(5)	2.200(4)	2.358(2)
Cl1–M[a]	—	2.392(1)	2.532(1)
Cl2–M[a]	—	2.434(1)	2.570(1)
P1–N1–M[a]	108.6(2)	121.0(2)	121.8(1)
P2–N3–M[a]	107.7(2)	126.1(2)	126.3(1)
N2–M–N1[a]	104.1(2)	85.3(1)	82.41(7)
N2–M–N3[a]	103.6(2)	84.5(1)	81.92(8)
N1–M–Cl2[a]	—	88.7(1)	90.06(6)
N3–M–Cl2[a]	—	92.9(1)	95.93(6)
N2–M–Cl1[a]	—	96.9(1)	96.82(5)
Cl2–M–Cl1[a]	—	98.44(5)	99.82(3)
N1–M–Cl1[a]	—	111.3(1)	113.38(5)
Cl1–M–N3[a]	—	101.1(1)	100.52(6)
N1–P1–C1–C2	134.6(2)	−139.1(4)	−137.6(2)
N3–P2–C8–C7	−129.4(3)	170.0(3)	168.0(2)

Note: [a]M corresponds to the atom Li1 for compound **8**, Sc1 for compound **9** and Y1 for compound **10**.

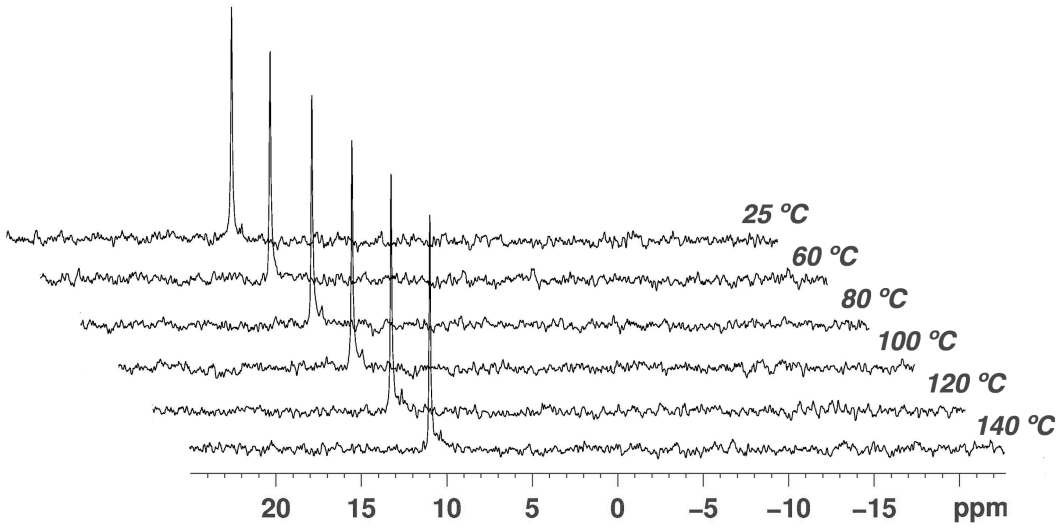

Figure 2.5 Stacked plot depicting $^{31}P\{^{1}H\}$ NMR spectra of **8** in benzene-d_6 following thermal treatment

Lithio ligand **8** was found to be highly thermally robust. A solution of **8** in benzene-d_6 could be heated to 140 °C in a J-Young NMR tube with absolutely no sign of ligand decomposition or conversion to proteo ligand (Figure 2.5). The thermal stability of **8** was a desirable feature because salt metathesis reactions of bulky ligands with rare earth metal halides can sometimes require forcing thermal conditions.[78,79]

2.6.1 Rare Earth Complexation by Salt Metathesis

Lithio ligand **8** can be readily complexed with rare earth metal chlorides via salt metathesis to afford the corresponding dichloride complexes (Scheme 2.11). For example, reaction of **8** with the THF adducts of scandium or yttrium trichloride ($ScCl_3(THF)_3$ or $YCl_3(THF)_{3.5}$) in toluene solution at 50 °C afforded the corresponding base-free group 3 dichloride complexes ($\mathbf{L}_{\mathbf{A}}^{\mathbf{Mes}}$-$\kappa^3$*N*)$LnCl_2$ (Ln = Sc, **9**; Y, **10**). The NMR spectral properties of **9** and **10** were quite similar, with the exception of ^{89}Y coupling observed in **10**. Complex **9** exhibited a single resonance in its $^{31}P\{^1H\}$ NMR spectrum at δ 26.4 while **10** gave rise to a doublet at δ 25.2 ($^2J_{PY}$ = 2.3 Hz).

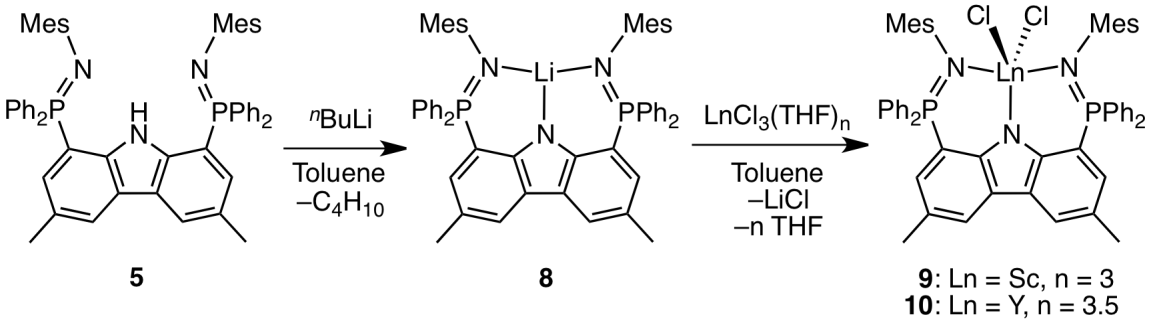

Scheme 2.11 Ligand coordination via salt metathesis

Recrystallization of complexes **9** and **10** from concentrated toluene solutions at −35 °C generated yellow crystals suitable for X-ray diffraction. Both complexes were isostructural and crystallized in the rhombohedral space group $R\bar{3}$ (#148). A representative structure of **10** is depicted in Figure 2.6 as a thermal ellipsoid plot. The similar geometries of **9** and **10** are reflected in the highly comparable metrical parameters of each complex (Table 2.3).

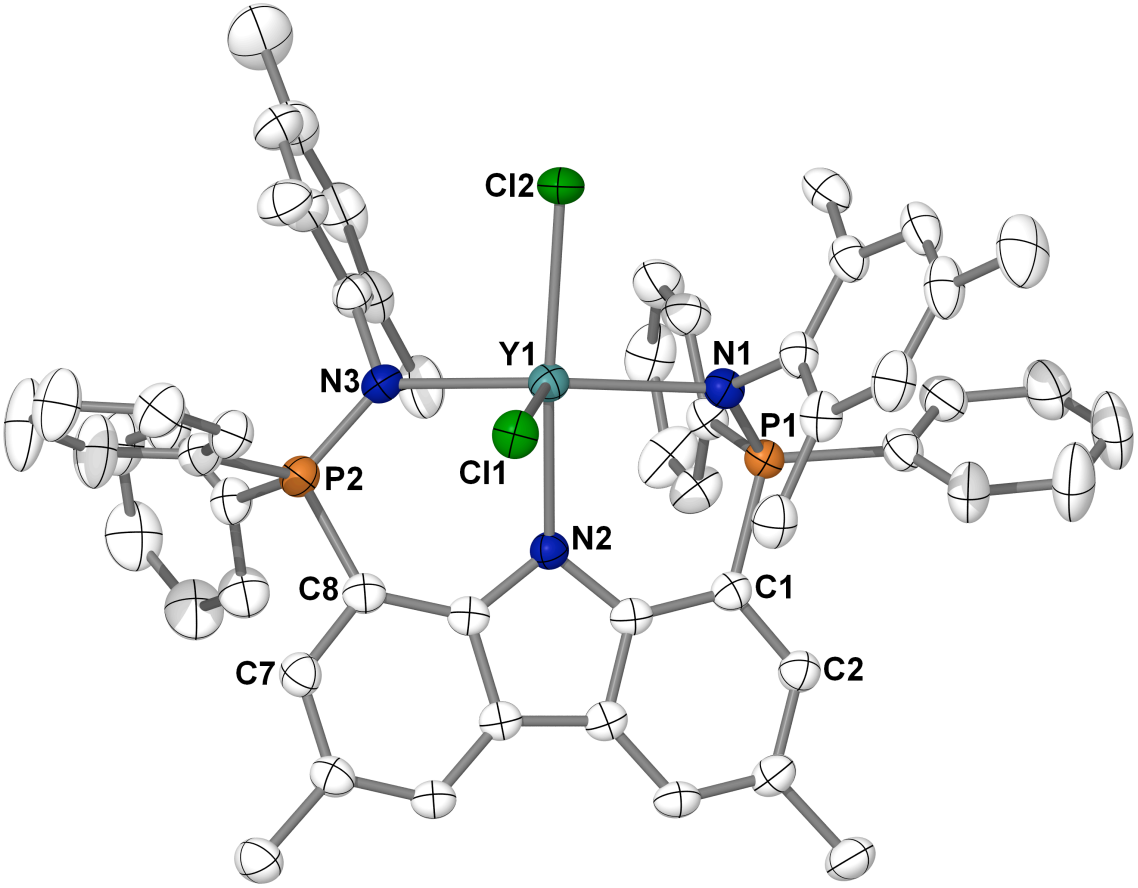

Figure 2.6 Thermal ellipsoid plot (50% probability) of **10** ($\mathbf{L_A^{Mes}}$-κ^3*N*)YCl_2 with hydrogen atoms and solvent molecules of crystallization omitted for clarity. The solid-state structure of (L_A^{Mes}-κ^3*N*)$ScCl_2$ (**9**) is isostructural to that of **10**.

In the solid state, complexes **9** and **10** are monomeric and adopt a distorted square pyramidal geometry at the metal centre defined by coordination of two chloride ligands

and the κ^3 bound pincer ligand. The nitrogen atoms of the ancillary ligand (N1, N2 and N3) and one chloride (Cl2) make up the base of the pyramid while Cl1 occupies the apical site. The bond angles around the base of the pyramid are close to 90° (N2–Sc1–N1 = 85.3(1)°, N2–Sc1–N3 = 84.5(1)°, N1–Sc1–Cl2 = 88.7(1)°, N3–Sc1–Cl2 = 92.9(1)°, **9**; N2–Y1–N1 = 82.41(7)°, N2–Y1–N3 = 81.92(8)°, N1–Y1–Cl2 = 90.06(6)°, N3–Y1–Cl2 = 95.93(6)°, **10**), and the apical atom (Cl1) is positioned relatively perpendicular to this base (average perpendicular angle = 101.9°, **9**; 102.6°, **10**). As expected, the Y–Cl bond lengths (2.532(1) Å and 2.570(1) Å) are slightly longer than the Sc–Cl distances (2.392(1) Å and 2.434(1) Å) due to the larger radius of yttrium.

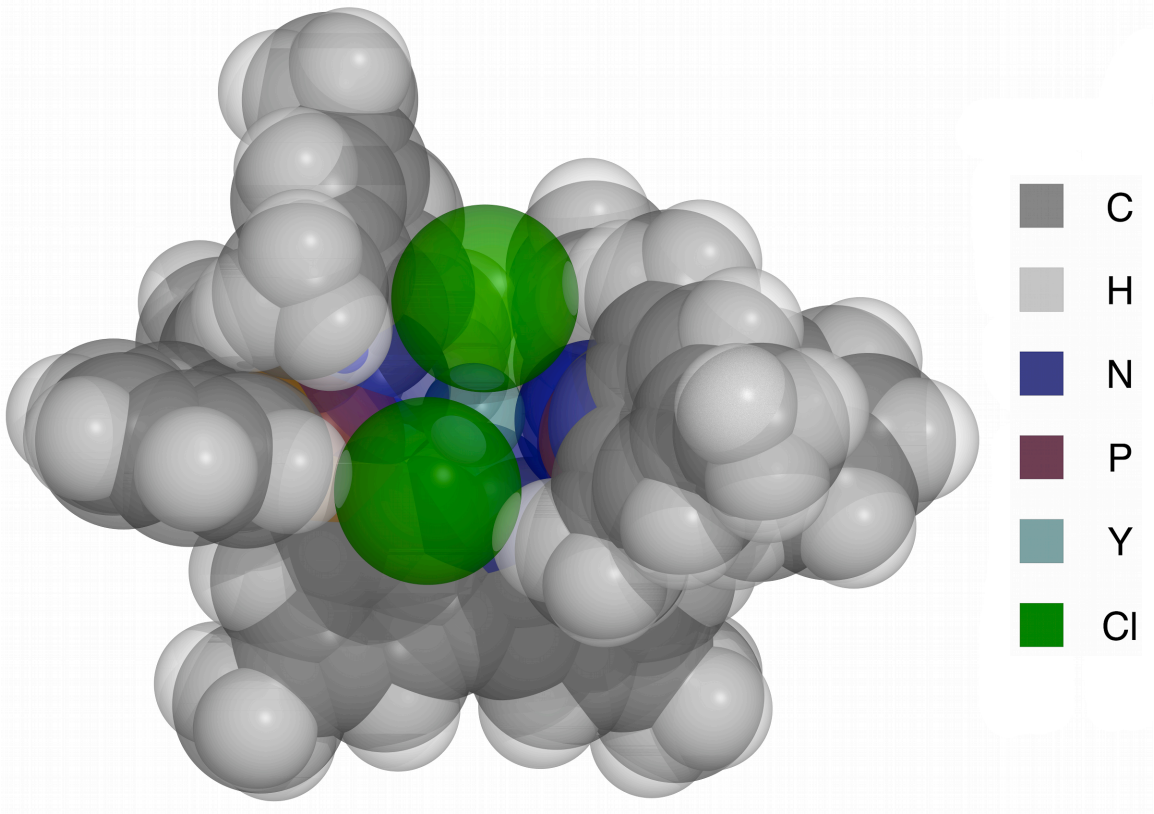

Figure 2.7 Space-filling diagram of **10** ($\mathbf{L}_{\mathbf{A}}^{\mathbf{Mes}}$-$\kappa^3$*N*)$YCl_2$ with atoms drawn at their respective van der Waals radii.

The ancillary ligand appears to provide significant steric shielding of the metal centre. A space-filling diagram of **10** is depicted in Figure 2.7 to illustrate this feature. In the diagram, the metal is largely obscured by the chloride ligands; however, the coordination of nitrogen donor atoms to the metal is quite evident. The combination of phenyl and mesityl aryl rings on the ancillary ligand provides a sterically crowded coordination pocket for the metal, and essentially sandwiches the chloride ligands in place. Evidently, the steric bulk of this ligand leaves little space at the metal centre for any ligands larger than chlorides. In light of this, it was suspected that the instability of the fleeting dialkyl complex ($\mathbf{L}_{\mathbf{A}}^{\mathbf{Mes}}$-$\kappa^3$*N*)Y($CH_2SiMe_3$)$_2$ **6** (which contained two bulky –CH_2SiMe_3 ligands in the metal coordination pocket), and its resultant cyclometalative C–H bond activation chemistry, was likely a result of high steric pressure imparted by the ancillary ligand.[24]

2.7 Conclusions

In this chapter, the design and synthesis of a novel mesityl-substituted bis(phosphinimine)carbazole pincer ligand (H$\mathbf{L}_{\mathbf{A}}^{\mathbf{Mes}}$, **5**) was described and its ability to coordinate rare earth metals was demonstrated. It was found that the presence of bulky mesityl rings on the ligand imparted a sterically demanding coordination pocket for rare earth metals and as such, ligand coordination via alkane elimination proved to be slow. Furthermore, the high degree of steric pressure inflicted by the ligand caused a dialkyl yttrium complex to be highly susceptible to a cyclometalative C–H bond activation process resulting in a doubly *ortho*-metalated derivative. Ligand **5** proved to be suitable

for salt metathesis reactivity; the deprotonated derivative reacted readily with the THF adducts of rare earth trichlorides to afford dichloride complexes of the ligand in high yield. The developed complexes acted as useful models to study the reactivity patterns of the ancillary ligand and its ability to support rare earth metal complexes.

Chapter 3

Steric Influences: Modulation of *N*-Aryl Rings

3.1 Overview

The bis(phosphinimine)carbazole ligand ($\mathbf{L_A^{Mes}}$) described in Chapter 2 exhibited good chelating properties and afforded highly stable and monomeric rare earth dichloride complexes. However, the incorporation of bulky mesityl rings at the *N*-aryl position of the scaffold caused a high degree of steric crowding at the ligand coordination pocket. This was particularly evident in dialkyl rare earth complexes of $\mathbf{L_A^{Mes}}$, whereby severe steric crowding at the metal centre was speculated to influence cyclometalative complex decomposition. Specifically, the *P*-phenyl rings of the phosphinimine functionality underwent cyclometalation reactions with loss of alkane. As a consequence, the isolation of well-defined dialkyl rare earth complexes of $\mathbf{L_A^{Mes}}$ was not possible.

In an attempt to mitigate the metalative decomposition problem, a variety of bis(phosphinimine)carbazole ligands with reduced steric bulk at the *N*-aryl ring were

devised. It was speculated that incorporation of less bulky *N*-aryl groups would reduce the steric crowding at the coordination pocket of the ligand and hopefully yield rare earth dialkyl complexes with enhanced stability.

3.2 Tuning Steric Bulk

Three novel derivatives of the bis(phosphinimine)carbazole ligand were prepared whereby the mesityl group at the *N*-aryl site of the scaffold was replaced with phenyl (Ph), *para*-isopropylphenyl (Pipp) and pyrimidine (Pym) rings. Following the protocol utilized in the synthesis of $H\mathbf{L}_{\mathbf{A}}^{\mathbf{Mes}}$ (**5**), the compound 1,8-bis(diphenylphosphino)-3,6-dimethylcarbazole **2** was reacted with an appropriate aryl azide to generate the desired phosphinimine functionality in high yield. Utilization of phenyl azide, *para*-isopropylphenyl azide and 2-azidopyrimidine[§] in this reaction afforded a family of proteo ligands $H\mathbf{L}_{\mathbf{A}}^{\mathbf{Ph}}$ (**11**), $H\mathbf{L}_{\mathbf{A}}^{\mathbf{Pipp}}$ (**12**) and $H\mathbf{L}_{\mathbf{A}}^{\mathbf{Pym}}$ (**13**), respectively, with varied steric and electronic properties.

The proteo ligands **11**, **12** and **13** are C_{2v} symmetric on the NMR time scale. Each ligand exhibits a sharp singlet (δ 6.2, **11**; δ 5.5, **12**; δ 18.5, **13**) in its $^{31}P\{^{1}H\}$ NMR spectrum (benzene-d_6). The proton NMR spectrum of **11** (chloroform-*d*) has a single methyl resonance at δ 2.44, a broad NH peak at δ 11.8 and an expectedly complicated aromatic region consisting of resonances corresponding to carbazole, *N*-phenyl and

[§] In solution, 2-azidopyrimidine is susceptible to valance tautomerism and exists in equilibrium with its tetrazole form (tetrazolo[1,5-a]pyrimidine). The equilibrium is influenced by choice of solvent and temperature but lies strongly to the tetrazole side. As a result, the Staudinger reaction of **2** with 2-azidopyrimidine is significantly slower than the analogous reaction with phenyl azide or *para*-isopropylphenyl azide.

P-phenyl protons. Similarly, the ^{1}H NMR spectrum of **12** (chloroform-*d*) contains a singlet at δ 2.45 corresponding to the symmetric methyl groups of the carbazole backbone and a broad NH peak at δ 11.7. The ^{1}H NMR spectrum of **12** also features isopropyl resonances at δ 2.74 (sp, C*H*) and δ 1.17 (d, CH_3) in addition to a well-defined AB spin pattern (δ 6.74, d; δ 6.64, d) corresponding to protons on the *N*-aryl rings. Finally, the ^{1}H NMR spectrum of **13** (benzene-d_6) exhibits similar spectral features to that of proteo ligands **11** and **12**, *i.e.* a single carbazole methyl resonance at δ 2.16, a broad NH peak at δ 12.2 and the expected aromatic signals. In particular, the pyrimidine rings on **13** give rise to a triplet at δ 5.97 and a doublet at δ 8.02 corresponding to the *para* and *meta* protons, respectively.

In addition to characterization of **11**, **12** and **13** by multinuclear NMR spectroscopy, the proteo ligands were also characterized by single-crystal X-ray diffraction. Single crystals of **11** · C_6H_6 suitable for an X-ray diffraction study were readily obtained from a benzene solution layered with pentane at ambient temperature. The molecular structure of **11** is illustrated in Figure 3.1 as a thermal ellipsoid plot and selected metrical parameters are listed in Table 3.1. In the solid state, N1 lies approximately periplanar to the carbazole backbone (N1–P1–C1–C12 torsion angle of −11.1(4)°). However, N3 lies significantly out of this plane with an N3–P2–C8–C9 torsion angle of 68.4(4)°. The rotation of the P2–N3 arm out of the plane of the carbazole backbone is likely due to steric interactions between the two *N*-phenyl groups on the phosphinimine moiety. The periplanar orientation of N1 to the carbazole backbone in the solid state is likely due to the hydrogen bonding interaction that exists between it and

H2A. The distance between the donor and acceptor nitrogen atoms in the N2–H2A···N1 interaction in **11** is 2.789(5) Å.

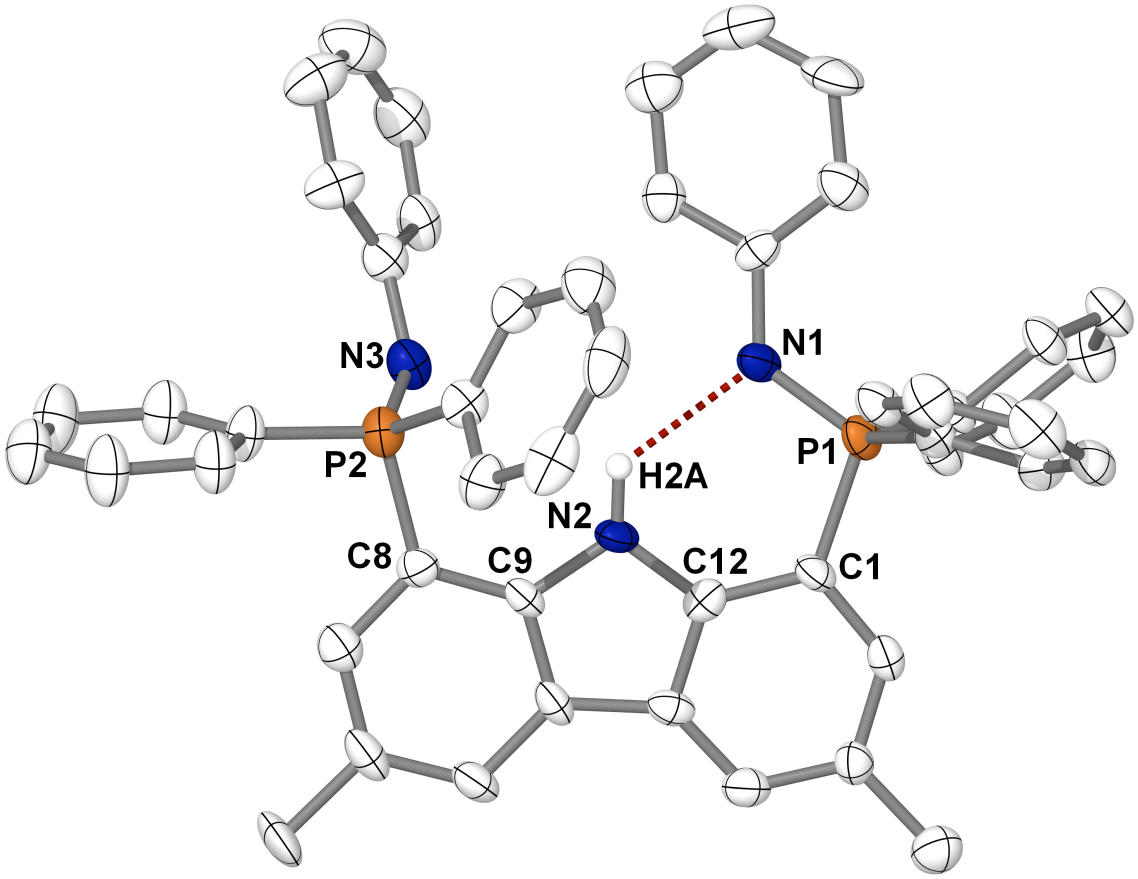

Figure 3.1 Thermal ellipsoid plot (50% probability) of HL_A^{Ph} (**11**) with hydrogen atoms (except H2A) and benzene molecule of crystallization omitted for clarity.

Similar to **11**, single crystals of **12** · 2 C_6H_6 were obtained from a concentrated benzene solution layered with pentane. The molecular structure of **12**, as determined from an X-ray diffraction experiment, is depicted in Figure 3.2 and selected metrical parameters are listed in Table 3.1. Analogous to that described for **11**, ligand **12** has one nitrogen donor (N1) lying periplanar to the carbazole backbone and one (N3) out of the plane. The N1–P1–C1–C12 and N3–P2–C8–C9 torsion angles of 7.8(2)° and −70.7(2)°, respectively, correspond well with that observed for **11**. In comparison to that of **11**, the

N3 group in **12** is rotated about 2° further out of plane from the aromatic backbone, while the N1 group is approximately 2° closer to the plane of the carbazole backbone. This small, but statistically relevant difference may be attributed to the presence of the isopropyl groups in the *para* positions of the *N*-aryl rings of **12**, which create slightly greater steric repulsion between the *N*-aryl rings. It is notable that only minor differences in the geometry of **11** and **12** are observed, a fact which correlates well with the identical reaction rates of ligand metalation observed for complexes **14** and **15** (*vide infra*).

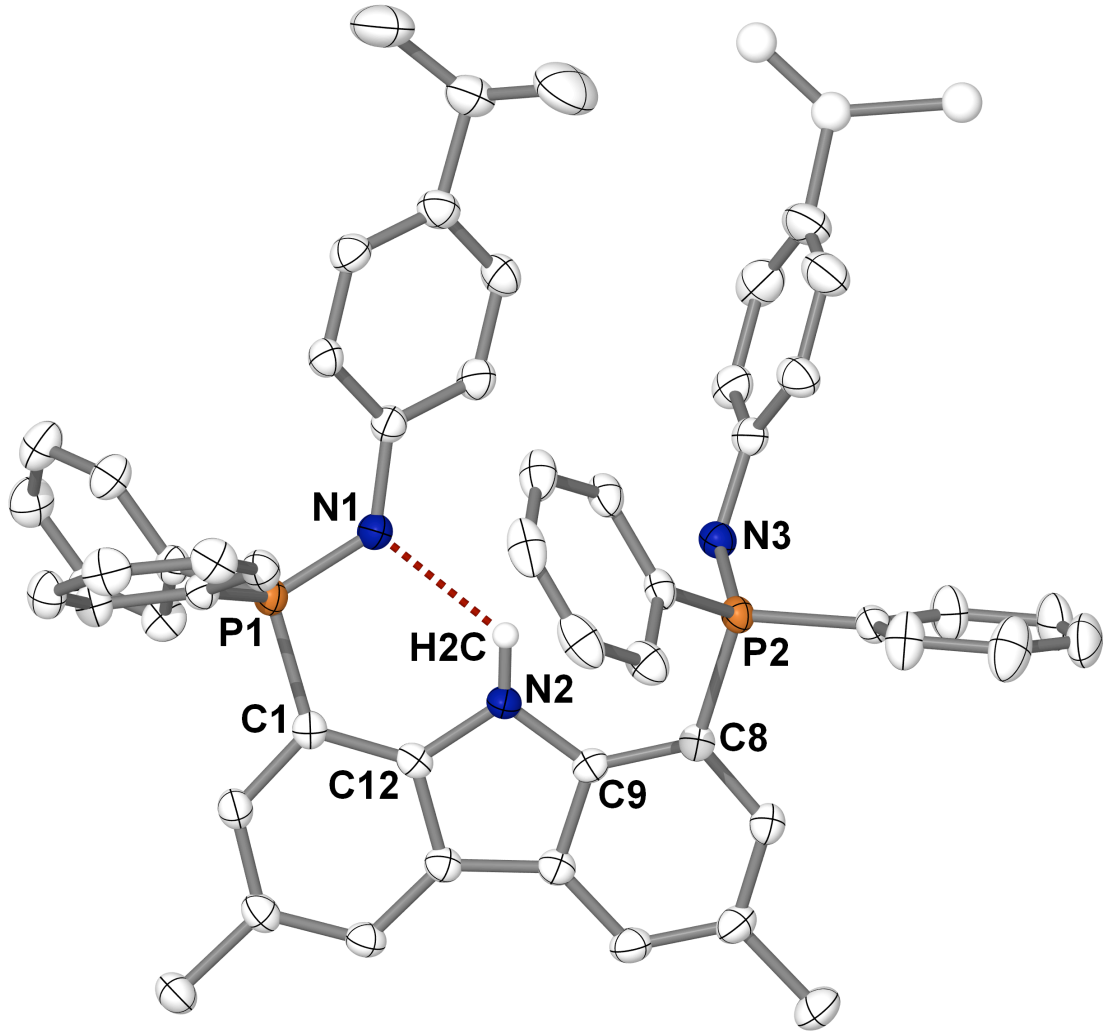

Figure 3.2 Thermal ellipsoid plot (50% probability) of HL_A^{Pipp} (**12**) with hydrogen atoms (except H2C) and two benzene molecules omitted for clarity. Positionally disordered atoms are depicted as spheres of arbitrary radius.

Proteo ligand HL_A^{Pym} (**13**) crystallized from a concentrated chloroform-*d* solution in the space group $P2_1/c$ with two solvent molecules. The molecular structure is depicted in Figure 3.3 as a thermal ellipsoid plot and selected metrical parameters are listed in Table 3.1. In a manner similar to **11** and **12**, one phosphinimine donor (N1) participates in a hydrogen bond interaction with the carbazole N–H (d(N···N) = 2.838(5) Å; however, it lies out of the dimethylcarbazole backbone plane (N1–P1–C1–C12 torsion angle of 33.6(4)°). The other phosphinimine group (P2–N3) is rotated significantly away from the carbazole N–H (N3–P2–C8–C9 torsion angle of 159.1(3)°). The phosphinimine double bond lengths in **13** (1.597(3) Å and 1.592(3) Å) are slightly elongated compared to the corresponding distances in **11** and **12**, which range from 1.570(4) Å to 1.581(4) Å.

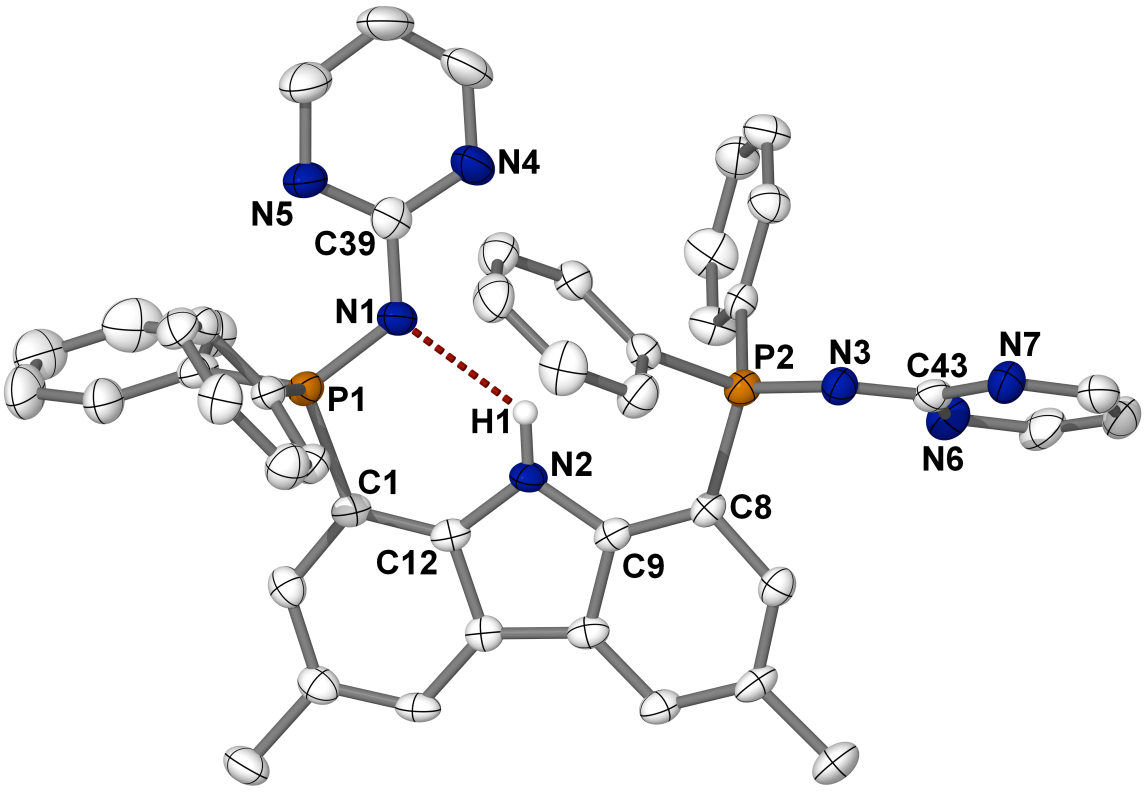

Figure 3.3 Thermal ellipsoid plot (50% probability) of HL_A^{Pym} (**13**) with hydrogen atoms (except H1) and two chloroform-*d* solvent molecules omitted for clarity.

Table 3.1 Selected bond distances /Å, angles /° and torsion angles /° for compounds **11**, **12** and **13**

	11	**12**	**13**
P1–N1	1.581(4)	1.574(2)	1.597(3)
P2–N3	1.570(4)	1.575(2)	1.592(3)
N2–H···N1	2.790(5)	2.742(3)	2.838(5)
N1–P1–C1	107.2(2)	105.3(1)	103.4(2)
N3–P2–C8	106.0(2)	106.8(1)	114.7(2)
N1–P1–C1–C12	−11.1(4)	7.8(2)	33.6(4)
N3–P2–C8–C9	68.4(4)	−70.7(2)	159.1(3)

3.3 Protonolysis Reactivity

In order to assess the ability of ligands **11**, **12** and **13** to support well-defined organolanthanide complexes, the corresponding lutetium dialkyl derivatives were prepared. Proteo ligands **11**, **12** and **13** reacted readily with $Lu(CH_2SiMe_3)_3(THF)_2$ to give the respective lutetium dialkyl compounds via alkane elimination. When these reactions were followed *in situ* on an NMR tube scale in benzene-d_6, they proceeded rapidly with formation of the desired metal dialkyl complexes, one equivalent of $SiMe_4$ and two equivalents of liberated THF. Interestingly, the Ph and Pipp ligands gave rise to lutetium complexes ($(\mathbf{L}_{\mathbf{A}}^{\mathbf{Ph}}\text{-}\kappa^3N)Lu(CH_2SiMe_3)_2$, **14**; $(\mathbf{L}_{\mathbf{A}}^{\mathbf{Pipp}}\text{-}\kappa^3N)Lu(CH_2SiMe_3)_2$, **15**) with significantly different properties from that of the Pym ligand ($(\mathbf{L}_{\mathbf{A}}^{\mathbf{Pym}}\text{-}\kappa^5N)Lu(CH_2SiMe_3)_2$, **16**). As such, the properties and reactivity of **14** and **15** are discussed separately from that for **16**.

3.4 Dialkyl Lutetium Complexes of $\mathbf{L}_{\mathbf{A}}^{\mathbf{Ph}}$ and $\mathbf{L}_{\mathbf{A}}^{\mathbf{Pipp}}$

The lutetium dialkyl complexes of the Ph and Pipp ligands (**14** and **15**) were both found to be highly thermally sensitive compounds with the ligand coordinated to the metal in a κ^3 manner through its three nitrogen atoms (Scheme 3.1). Due to the thermal sensitivity of dialkyl species **14** and **15**, neither complex could be isolated as a pure solid. All attempts to do so resulted in samples contaminated with the thermodynamic decomposition products (*vide infra*). However, both complexes were quantitatively generated *in situ* at low temperature and used in this form to further investigate reactivity. Complexes **14** and **15** were fully characterized by multinuclear NMR spectroscopy at low temperature (−2 °C and −24 °C, respectively) with no sign of decomposition over the course of the experiments.

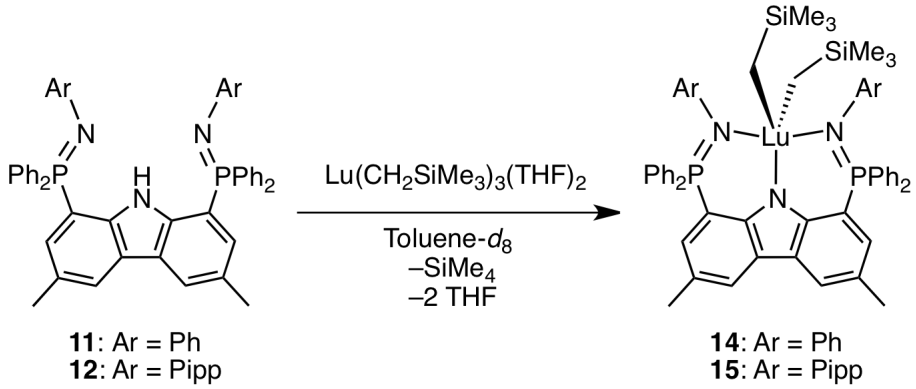

Scheme 3.1 Synthesis of dialkyl lutetium complexes **14** and **15**

The ^{1}H NMR spectra of **14** and **15** in toluene-d_8 exhibit diagnostic methyl and methylene resonances upfield of 0 ppm for the protons of the trimethylsilylmethyl groups (**14**, 271.3K: δ −0.06 (CH_3), −0.79 (CH_2); **15**, 249.1K: δ −0.01 (CH_3), −0.72 (CH_2)). Upon cooling solutions of **14** or **15** below −60 °C the two trimethylsilylmethyl moieties become inequivalent with splitting of the methylene resonances indicating a reduction in

molecular symmetry from C_{2v} to C_s. In the $^{31}P\{^1H\}$ NMR spectra (toluene-d_8), a significant downfield shift of the phosphinimine resonance is observed upon complexation with lutetium (**14**, 271.3 K: δ 29.6; **15**, 249.1 K: δ 29.4). As the phosphinimine functionality is highly sensitive to its coordination environment, the large downfield shift is indicative of complexation with the electropositive lutetium centre. In addition, the sharp single resonances in the $^{31}P\{^1H\}$ NMR spectra corroborate that the ancillary is bound to lutetium in a symmetric κ^3 coordination mode. Although two equivalents of THF were present in the *in situ*-generated reaction mixture, it was found that the dialkyl lutetium complexes were 5-coordinate with no THF donors bound to the metal. Specifically, toluene-d_8 solutions of the dialkyl complexes at temperatures between 249.1 K and 295.7 K exhibited resonances in the ^1H and $^{13}C\{^1H\}$ NMR spectra consistent with free THF. This comparison is outlined in Table 3.2 for ^1H NMR signals observed in the spectra of the reaction mixture containing dialkyl **14** and THF. There is a high degree of correlation across the temperature range between the THF signals observed in the reaction mixture with those measured for a free THF standard in toluene-d_8. These values can be compared to significantly different chemical shifts that occur when a THF molecule is coordinated to a rare earth metal, for example, as in the complex $Lu(CH_2SiMe_3)_3(THF)_2$.

Table 3.2 Residual THF ^1H NMR resonances at various temperatures (toluene-d_8)

T /K	**14**	Free THF	$Lu(CH_2SiMe_3)_3(THF)_2$
249.1	3.54, 1.35	3.54, 1.39	3.90, 1.25
271.3	3.54, 1.38	3.55, 1.42	3.93, 1.32
295.7	3.54, 1.37	3.54, 1.43	3.97, 1.38

3.4.1 Ligand Cyclometalation

At temperatures above 0 °C, toluene solutions of **14** and **15** rapidly undergo two sequential intramolecular metalative alkane eliminations whereby both alkyl groups are liberated as RH through a σ-bond metathesis pathway with the *ortho* C–H bonds of the adjacent *P*-phenyl rings. Upon monitoring the decomposition by ^{1}H and ^{31}P{^{1}H} NMR spectroscopy, the formation of an asymmetric intermediate with C_1 symmetry was observed (Scheme 3.2). This transient species, assigned as a monometalated complex (**17** and **18**), then undergoes a second intramolecular σ-bond metathesis process with a phenyl ring from the other phosphinimine phosphorus (*vide infra*), releasing a second equivalent of tetramethylsilane. The final C_2 symmetric products **19** and **20** are the result of a double *ortho*-metalation process. These κ^5-bound lutetium diaryl species consist of two 6-membered metallacycles complete with bridging phenyl rings, and are similar to the cyclometalated yttrium complex, **7**, described in Chapter 2.

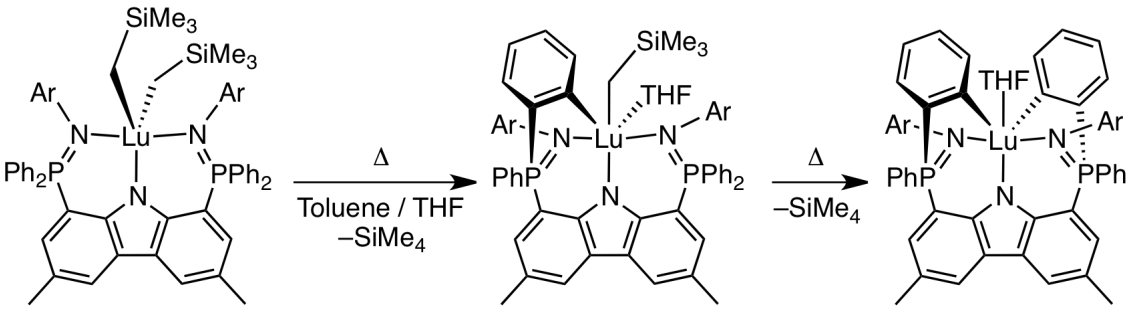

14: Ar = Ph
15: Ar = Pipp

17: Ar = Ph
18: Ar = Pipp

19: Ar = Ph
20: Ar = Pipp

Scheme 3.2 Sequential intramolecular metalative alkane elimination reaction

The lower symmetry in the final thermodynamic products, **19** and **20**, compared to the initial dialkyl complexes (**14** and **15**), was difficult to ascertain through ^{1}H NMR spectroscopy due to overlapping signals in the aromatic region of the spectrum. However,

$^{13}C\{^{1}H\}$ NMR spectroscopy proved to be diagnostic in this regard. The metalated *ipso* carbon attached directly to lutetium is highly deshielded and resonates far downfield as a doublet of doublets at δ 204.6 (dd, $^{2}J_{PC}$ = 41.2 Hz, $^{4}J_{PC}$ = 1.1 Hz, **19**) and δ 204.7 ($^{2}J_{PC}$ = 40.9 Hz, $^{4}J_{PC}$ = 1.2 Hz, **20**). Such values correspond well with the shifts reported for other neutral lutetium aryl species such as $LuPh_3(THF)_2$ (δ 198.7, benzene-d_6),[146] Lu(*p*-tol)$_3$(THF)$_2$ (δ 195.2, benzene-d_6),[146] Lu(C_6H_4-*p*-Et)$_3$(THF)$_2$ (δ 194.2, benzene-d_6),[146] (Cp*)$_2$LuPh (δ 198.5, cyclohexane-d_{12})[88] and Lu(*o*-$C_6H_4CH_2NMe_2)_3$ (δ 196.7, benzene-d_6).[147]

3.4.2 Kinetic Analysis of Ligand Metalation

The decomposition from derivative **14** to **17** was quantitatively monitored by $^{31}P\{^{1}H\}$ NMR spectroscopy and revealed to be first order in the dialkyl species. The reaction progress at 293.5 K (from t = 1760 s to t = 15500 s) is depicted in Figure 3.4 as a stacked plot of $^{31}P\{^{1}H\}$ NMR spectra. As can be seen from the plot, the decreasing concentration of **14** (δ 29.4) is accompanied by the growth of two broad peaks resonating at δ 27.5 and δ 22.7 for asymmetric intermediate **17**. Within 4 h at this temperature complex **17** gradually converts exclusively to thermodynamic product **19** (δ 25.6).

The reaction was followed over a broad range of temperatures (282.4 K to 326.9 K; Figure 3.5), with observed $t_{1/2}$ values ranging from 5690 s to 44.7 s (Table 3.3). Construction of an Eyring plot (Figure 3.6) allowed for extraction of the activation parameters, $\Delta H^{\ddagger}$ = 80.5 ± 1.4 kJ·mol^{-1} and $\Delta S^{\ddagger}$ = −34.5 ± 4.7 J·K^{-1}·mol^{-1}, for the cyclometalation process from **14** to **17**. These values correspond to that expected for a

highly ordered four-centred transition state[34,146] and agree well with others reported for intramolecular σ-bond metathesis reactions.[79,80,148]

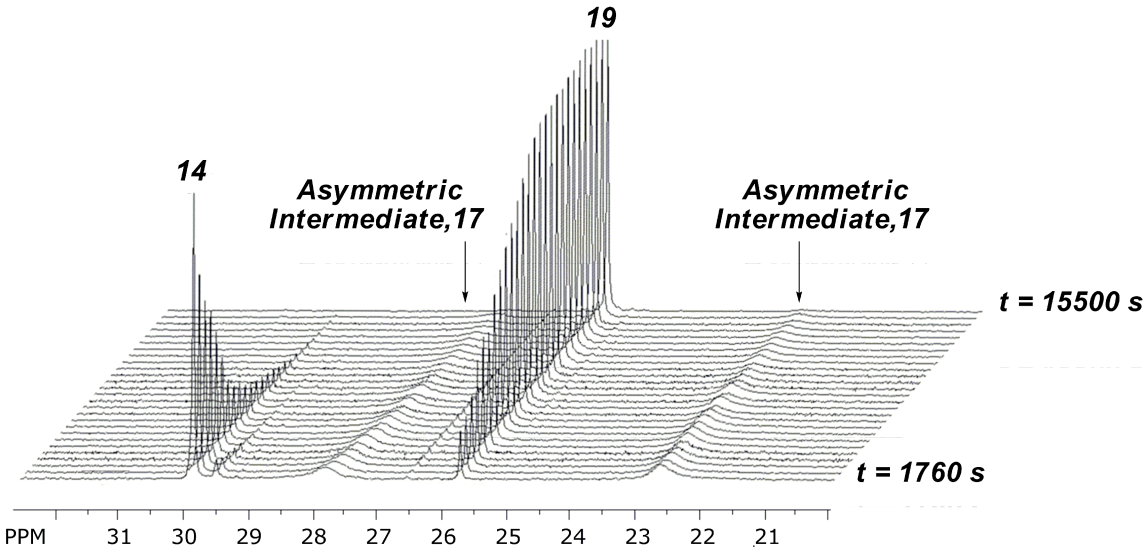

Figure 3.4 Stacked plot of $^{31}P\{^{1}H\}$ NMR spectra (toluene-d_8) depicting the decomposition of **14** to **19** (via intermediate **17**) at 293.5 K from t = 1760 s to t = 15500 s.

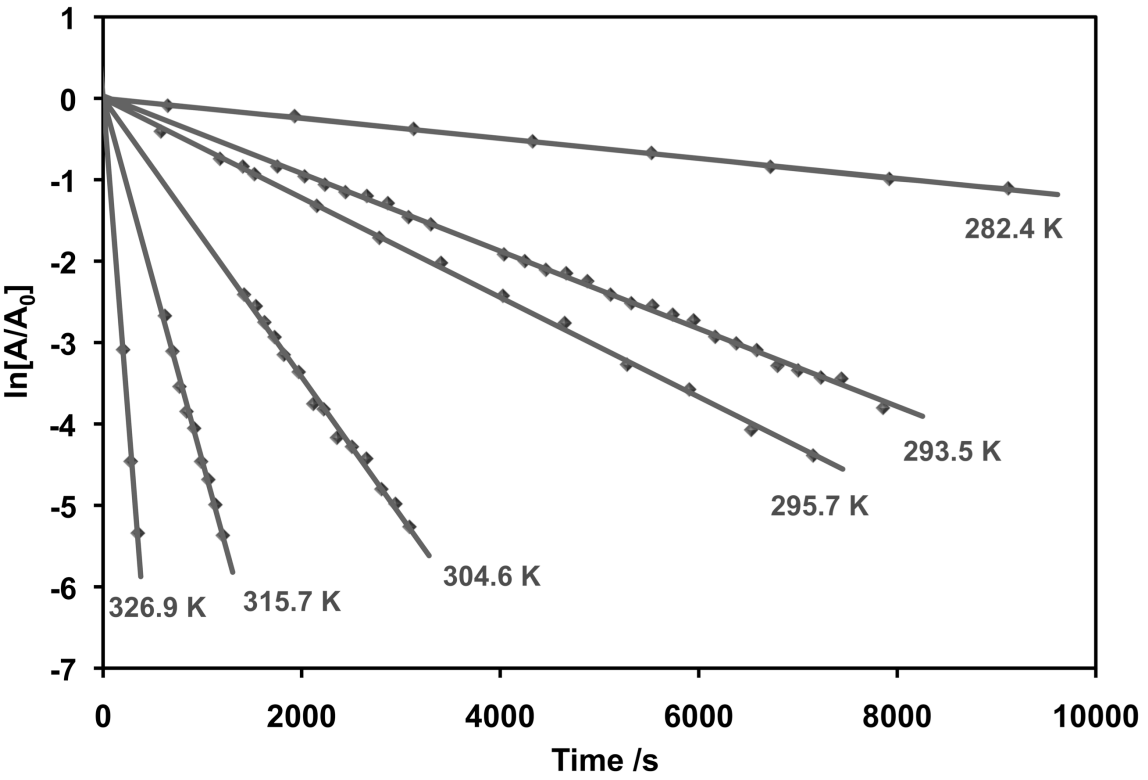

Figure 3.5 First order plots of the cyclometalation of **14** at various temperatures.

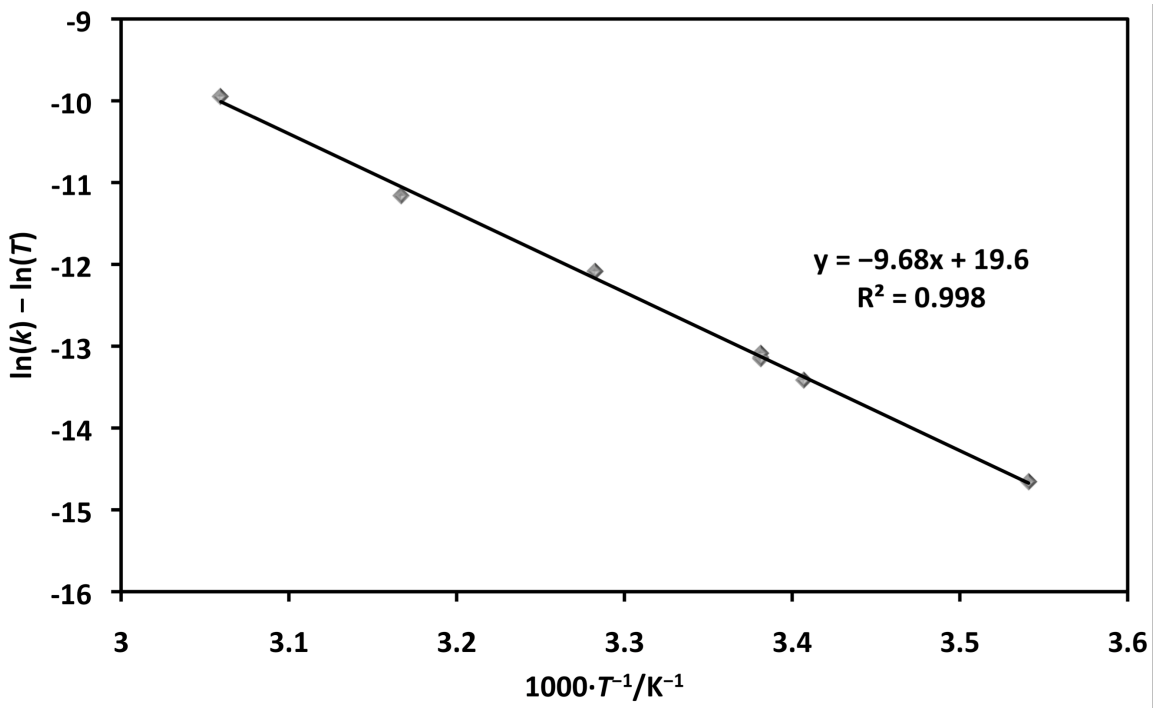

Figure 3.6 Eyring plot for the cyclometalation of **14**

Kinetic data for the conversion of **17** to **19** was not ascertained due to problems in accurately determining the concentration of **17** over the course of decomposition. Such difficulty stemmed from the broad peaks for **17** in the $^{31}P\{^{1}H\}$ NMR spectra which could not be reproducibly integrated due to the low signal-to-noise ratio. In addition, certain temperature ranges gave rise to an overlap of resonances for **17** and **19**. As such, the sum of the concentration of **17** and **19** could be readily determined at those temperatures; however, it was not always possible to establish the concentration of each individual species without introducing significant error.

At 295.7 K, metalation of **14** proceeded at a rate of 5.89×10^{-4} s^{-1}, while that for **15** was found to be 5.98×10^{-4} s^{-1} (Table 3.3). The high degree of correlation between these two rates suggests that the presence of the isopropyl groups in the *para* positions of the *N*-aryl rings of **15** does not significantly alter reactivity. This result was anticipated as

the incorporation of isopropyl groups on **15** was intended solely for the purposes of (a) increasing solubility; (b) increasing crystallinity; and (c) providing more diagnostic ^{1}H NMR resonances for the *N*-aryl ring, compared to that available for complex **14**. Furthermore, the solid-state structures of proteo ligands, **11** and **12**, which were used to prepare **14** and **15**, were essentially isostructural (*vide supra*).

Table 3.3 Observed rate constants for the intramolecular metalation of compounds **14** and **15** to **17** and **18** at temperatures ranging from 282.4 to 326.9 K

Compound	T /K	k_{obs} /s^{-1}	$t_{1/2}$ /s
14	282.4	1.22×10^{-4}	5690
14	293.5	4.37×10^{-4}	1590
14	295.7	5.89×10^{-4}	1180
14	304.6	1.71×10^{-3}	405
14	315.7	4.46×10^{-3}	155
14	326.9	1.55×10^{-2}	44.7
15	295.7	5.98×10^{-4}	1160

3.4.3 Solid State Characterization of Ligand Metalation

In order to unambiguously establish that the C–H bond activation of the ancillary ligand occurred through the *ortho* carbon of the phenyl rings on phosphorus, single-crystal X-ray diffraction studies were performed. Crystals of **18** were serendipitously obtained from an *in situ*-generated solution of **15** in a 4:1 mixture of toluene and THF at −35 °C over the course of one week. As **15** slowly decomposed at this temperature, intermediate **18** selectively crystallized out of solution. Under these dynamic and highly variable conditions the crystallinity of **18** was of low quality, and repeated attempts to grow higher quality crystals of this unstable intermediate were unsuccessful. Despite the

challenges encountered with crystal quality, a reliable set of low intensity single-crystal data was obtained for complex **18**. Such data was sufficient for unambiguously establishing the connectivity of the structure; however, no meaningful comments on the metrical parameters can be made at this time.

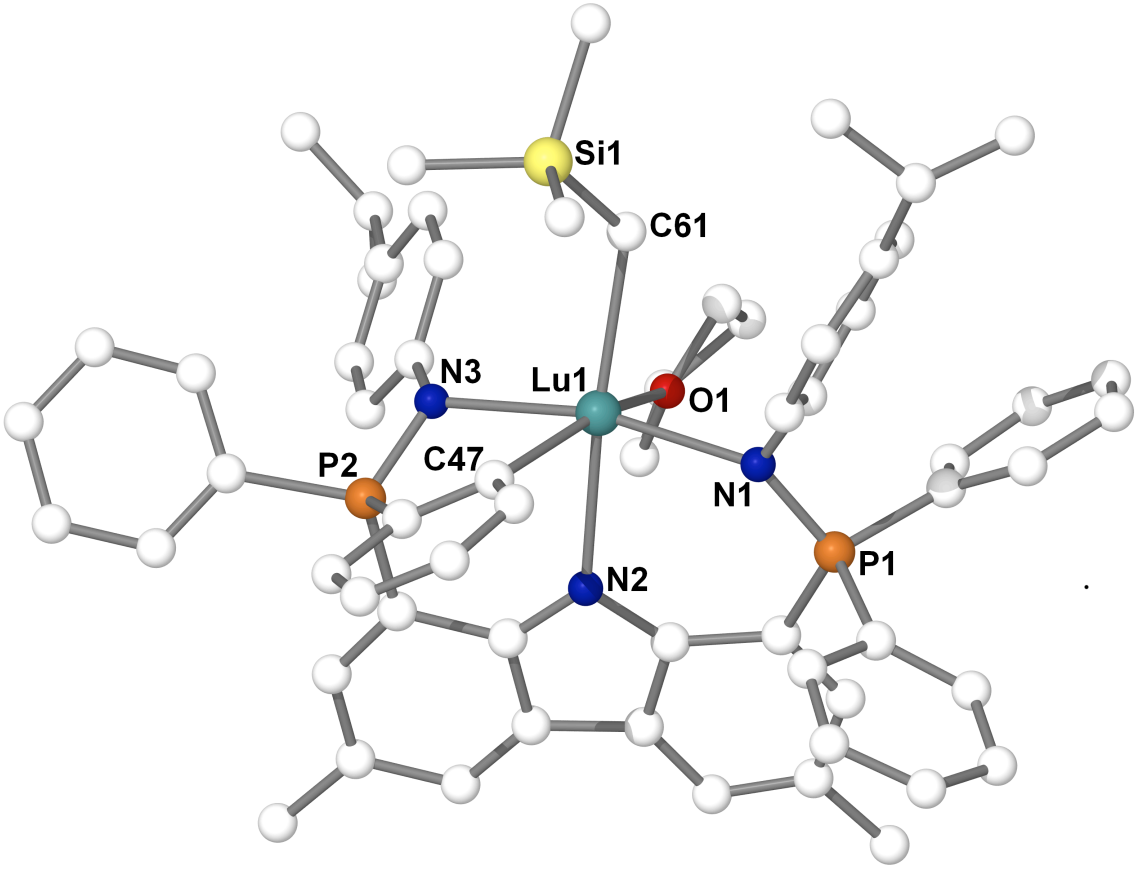

Figure 3.7 Molecular structure of ($\mathbf{L}_{\mathbf{A}}^{\mathbf{Pipp}}$-$\kappa^3$*N*,$\kappa$*C*$^{P\text{-Ph}}$)Lu($CH_2SiMe_3$)(THF) (**18**) with hydrogen atoms omitted for clarity.

The molecular structure of **18** is depicted in Figure 3.7. The solid-state structure confirms that the ligand is bound to lutetium in a κ^4 fashion, through three nitrogen atoms, as well as via an *ortho* carbon of one *P*-phenyl ring. One trimethylsilylmethyl group remains attached to lutetium as well as one THF donor, giving rise to a structure with distorted octahedral geometry. This structural information corroborates the

postulated intermediate in the conversion of dialkyl complex **15** to diaryl species **20** (Scheme 3.2). Due to the very small (< 10 mg) crop of crystals obtained from the crystallization of **18**, insufficient material was available for further characterization.

In contrast to the unstable nature of **18**, diaryl lutetium **20** can easily be prepared on a multigram scale. Reaction of **12** with $Lu(CH_2SiMe_3)_3(THF)_2$ in benzene for 18 h at ambient temperature generated **20** which was isolated as a pure yellow crystalline solid. Recrystallization from a benzene solution layered with pentane at ambient temperature afforded large needles of **20** that were suitable for X-ray diffraction. It was found that complex **20** crystallized with two independent molecules in the asymmetric unit, in addition to one pentane and three benzene solvent molecules. These independent structures, **20** and **20′**, are enantiomers of one another, and are depicted as thermal ellipsoid plots in Figure 3.8.

At *ca.* 1.61 Å, complexes **20** and **20′** exhibit P–N bonds that are elongated relative to that of the free ligand (average P–N = 1.575 Å). Such lengthening is indicative of strong donation from the phosphinimine functionality to the metal centre; however, such a distance is still consistent with a formal phosphorus-nitrogen double bond.[83] The Lu–C_{aryl} contacts in **20** and **20′** range from 2.425(8) Å in **20′** to 2.472(8) Å in **20**. These values fall within the normal range for neutral Lu–C_{aryl} bonds.[81,82,147,149-154] Complexes **20** and **20′** both exhibit distorted octahedral geometry at the lutetium centre, with the ancillary ligand occupying five of the six coordination sites. The sixth site composing the octahedron is defined by a THF donor. No attempt has yet been made to remove or exchange the coordinated Lewis base.

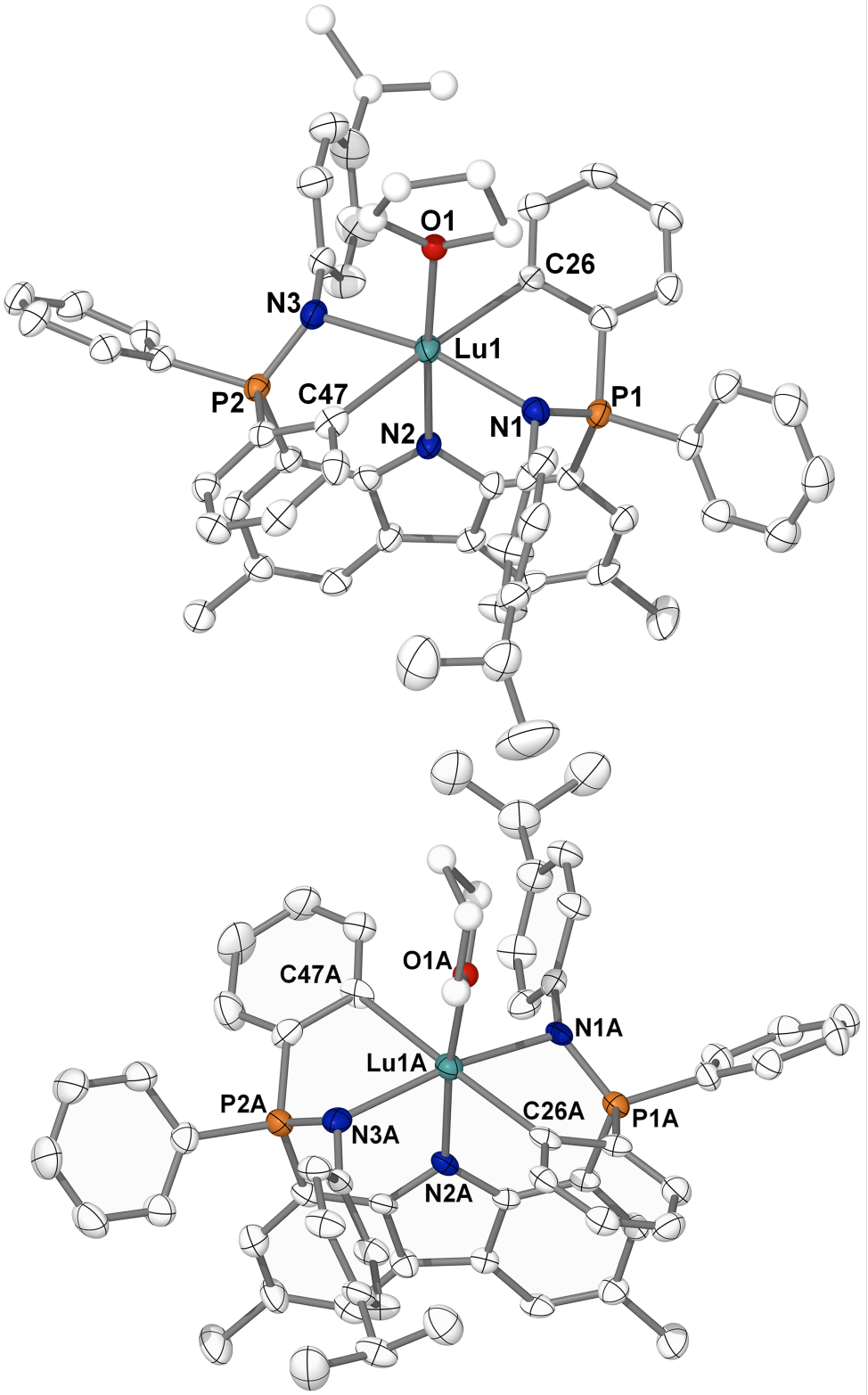

Figure 3.8 Thermal ellipsoid plot (50% probability) depicting two crystallographically independent molecules of ($\mathbf{L}_{\mathbf{A}}^{\mathbf{Pipp}}$-$\kappa^3N,\kappa^2C^{P\text{-Ph}}$)Lu(THF) (**20** and **20′**) with hydrogen atoms omitted for clarity. Positionally disordered atoms are depicted as spheres of arbitrary radius.

Table 3.4 Selected bond distances /Å and angles /° for **20** and **20′**

	20	**20′**
Lu1–N1	2.294(6)	2.290(6)
Lu1–N3	2.286(6)	2.298(6)
Lu1–N2	2.343(6)	2.348(6)
Lu1–C26	2.472(8)	2.450(8)
Lu1–C47	2.431(8)	2.425(8)
Lu1–O1	2.303(14)	2.341(14)
P1–N1	1.620(6)	1.606(6)
P2–N3	1.606(7)	1.611(6)
N1–Lu1–N3	166.3(2)	167.3(2)
C26–Lu1–C47	176.4(3)	178.1(2)
N2–Lu1–O1	174.6(4)	173.9(5)

3.5 Dialkyl Lutetium Complex of $\mathbf{L}_{\mathbf{A}}^{\mathbf{Pym}}$

In contrast to ligands $\mathbf{L}_{\mathbf{A}}^{\mathbf{Ph}}$ and $\mathbf{L}_{\mathbf{A}}^{\mathbf{Pipp}}$, the pyrimidine-substituted ligand $\mathbf{L}_{\mathbf{A}}^{\mathbf{Pym}}$ presents a chelation environment whereby a nitrogen atom from each pyrimidine ring can coordinate to the metal centre, in addition to the two phosphinimine donors and carbazole nitrogen. As such, the alkane elimination reaction of $Lu(CH_2SiMe_3)_3(THF)_2$ with $H\mathbf{L}_{\mathbf{A}}^{\mathbf{Pym}}$ resulted in a dialkyl lutetium complex ($\mathbf{L}_{\mathbf{A}}^{\mathbf{Pym}}$-$\kappa^5$*N*)$Lu(CH_2SiMe_3)_2$ (**16**) whereby the ligand was bound κ^5 through five nitrogen atoms (Scheme 3.3). In complex **16**, the presence of two extra nitrogen donors provided enhanced electron donation to the metal centre, and as a result, enhanced thermal stability. Compared to dialkyl species **14** and **15**, which exhibited half lives on the order of only 20 min at ambient temperature (*vide supra*), complex **16** can be left in solution (benzene-d_6 / THF) at ambient temperature for over 5 h with only minimal signs of decomposition. Eventually, **16** does decompose to a

single new product (*vide infra*); this decomposition is rapidly accelerated by increased temperature. Unfortunately, attempts to isolate **16** as a pure solid were unsuccessful and always resulted in mixtures of **16** and its decomposition product. However, **16** can be quantitatively generated *in situ* at low temperature and used in this form to further investigate reactivity.

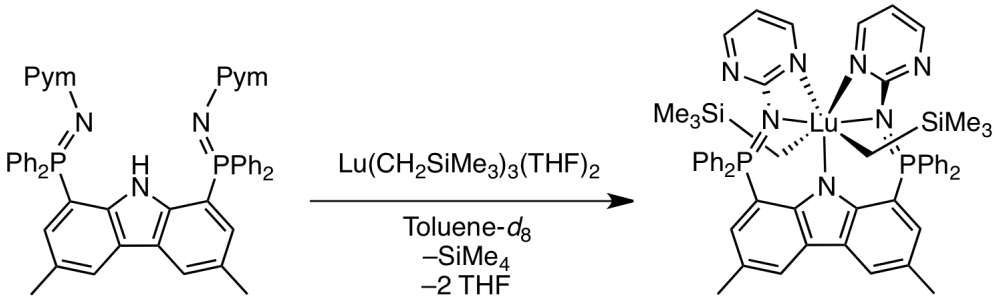

13 **16**

Scheme 3.3 Synthesis of κ^5 dialkyl lutetium complex **16**

In the $^{31}P\{^1H\}$ NMR spectrum (toluene-d_8, 263.2 K), a downfield shift of the phosphinimine resonance was observed for ($\mathbf{L}_{\mathbf{A}}^{\mathbf{Pym}}$-$\kappa^5$*N*)Lu($CH_2SiMe_3$)$_2$ (**16**) at δ 27.2. The ^1H NMR spectrum revealed the corresponding methylene (δ −1.22) and trimethylsilyl signals (δ −0.33) as sharp singlets, integrating to 4 and 18 protons, respectively. In the aromatic region of the spectrum, three separate signals corresponding to pyrimidine protons were observed at δ 8.28 (br m, 2H), 7.74 (m, 2H) and 6.08 (dd, 2H). From this, it was concluded that a nitrogen atom on both pyrimidine rings was coordinated to the lutetium centre, thus giving a metal complex where the ancillary ligand was coordinated in a κ^5*N* mode.

3.5.1 Pyrimidine Ligand Reactivity

Interestingly, **16** is not susceptible to an intramolecular metalative alkane elimination decomposition pathway as was the case for dialkyl complexes **14** and **15**. Rather, **16** undergoes an unusual double 1,5-alkyl shift, whereby the alkyl groups on the metal migrate to the 4 position of both pyrimidine rings, *para* to the nitrogen atom coordinated to lutetium. A consequence of the double alkyl migration reaction is dearomatization of the pyrimidine rings and formation of a negative charge on the coordinated pyrimidine nitrogen atoms. The product of this sigmatropic shift is an asymmetric bimetallic complex $[(\mathbf{L}_{\mathbf{A}}^{\mathbf{Pym*}}\text{-}\kappa^5\textit{N})\text{Lu}]_2(\text{THF})$, **21**, whereby the ligand is κ^5-coordinated to lutetium through five nitrogen atoms (three anionic nitrogen atoms and two neutral phosphinimine donors).

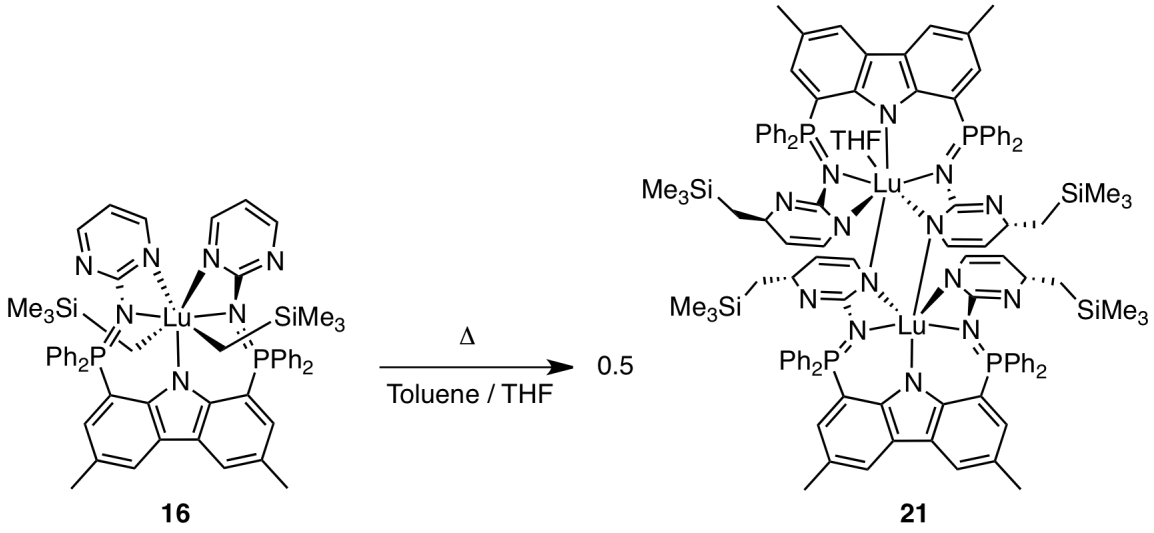

Scheme 3.4 Double [1,5]-CH_2SiMe_3 sigmatropic shift

Due to the complexity of the reaction product, the structure was ascertained through a single-crystal X-ray diffraction experiment. The solid-state structure is depicted in Figure 3.9 as a thermal ellipsoid plot and selected metrical parameters are listed in

Table 3.5. For clarity, the two subunits of the bimetallic complex are also depicted as independent species in Figure 3.10.

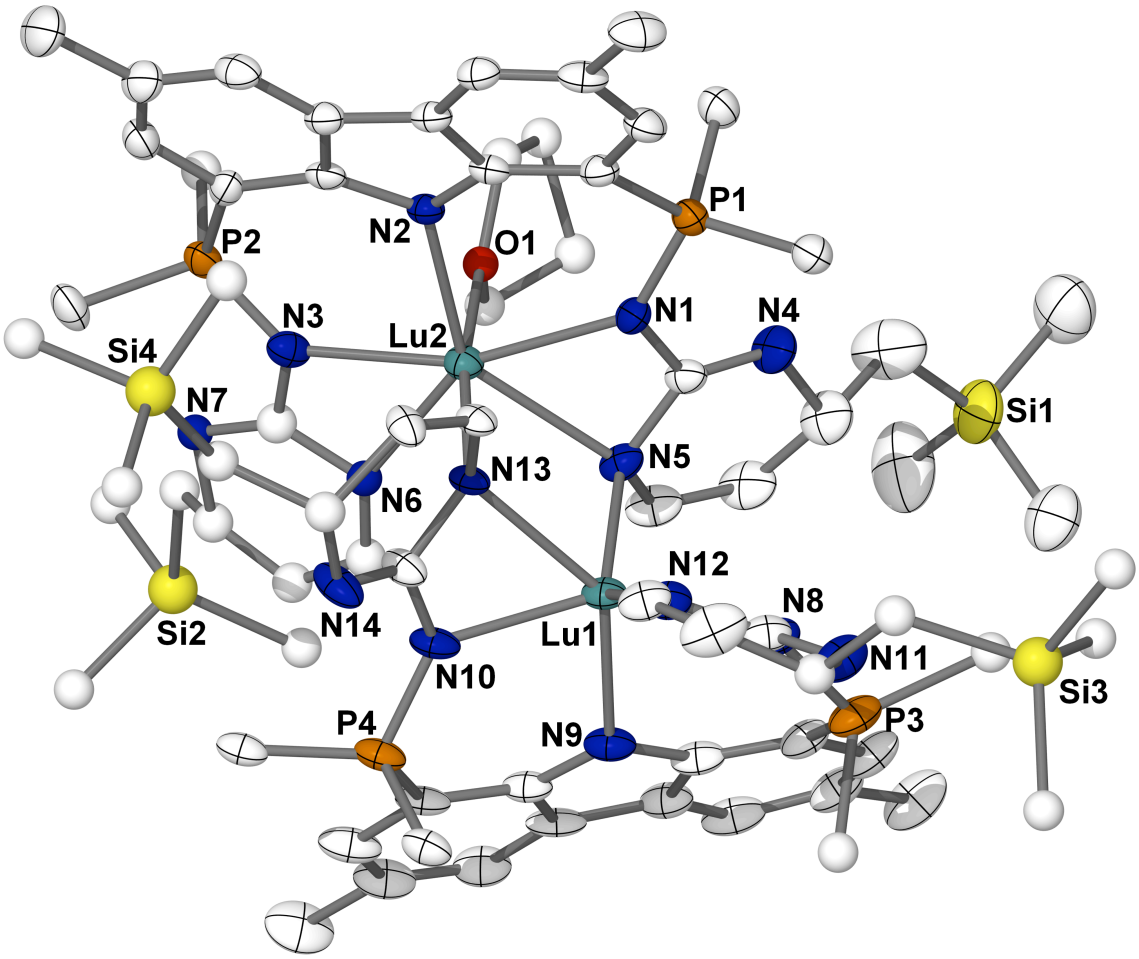

Figure 3.9 Thermal ellipsoid plot (30% probability) of [($\mathbf{L}^{\mathbf{Pym*}}_{\mathbf{A}}$-κ^5*N*)Lu]$_2$(THF), **21** with hydrogen atoms and *P*-phenyl rings (except for *ipso* carbons) omitted for clarity. Positionally disordered atoms are depicted as spheres of arbitrary radius.

In the solid state, the complex was found to dimerize via bridging nitrogen atoms (N5 and N13) of the dearomatized pyrimidine rings. As each bridging pyrimidine nitrogen atom has a negative charge, it bonds to one lutetium centre as an anionic ligand, and the other metal centre as a Lewis acid-base adduct. Interestingly, N5 exhibits short

(2.315(6) Å) and long (2.493(6) Å) bonds to Lu1 and Lu2, respectively. Likewise, N13 is bonded to Lu1 and Lu2 by long and short interactions (2.436(5) Å and (2.354(5) Å), respectively). These bond distances suggest that the bimetallic complex is held together not by Lewis acid-base interactions, but rather by the anionic ligand-to-metal bonds.

In the complex, one lutetium centre (Lu2) is 7-coordinate and the other metal centre (Lu1) is 6-coordinate. The geometry at Lu2 is best described as pentagonal bipyramidal with five nitrogen atoms from one ligand subunit (N1, N2, N3, N5 and N6) occupying the equatorial plane (average N–Lu–N angle = 72.0°). The apical sites of the pentagonal bipyramid are defined by coordination of one THF ligand (O1) and a bridging pyrimidine nitrogen atom (N13). The N13–Lu2–O1 angle of the apical atoms was found to be relatively linear at 170.2(4)°. In contrast to Lu2, the molecular geometry at Lu1 is not easily defined. Upon initial inspection, a distorted trigonal prismatic geometry was considered with the trigonal faces defined by N9, N8 and N5; and N10, N12 and N13. The N–N–N bond angles measured on the N9, N8, N5 trigonal face range from 50.0(2)° to 65.6(2)° and are in relatively good agreement with the expected value of 60°. However, the N–N–N bond angles measured on the N10, N12, N13 trigonal face are largely distorted (ranging from 38.4(2)° to 80.2(2)°); the result of this being a trigonal prismatic geometry with significant twist. Perhaps a better description of the geometry at Lu1 is as a bicapped tetrahedron,[155] whereby the tetrahedron is defined by N5, N9, N10 and N12 while N8 and N13 are the capping atoms. The average tetrahedral angle at Lu1 was calculated at 107.8° which is slightly less than the ideal value of 109.5°. A large angle of 138.6(2)° was measured between the capping atoms of the tetrahedron (N8–Lu1–N13), suggesting distortion in the geometry.

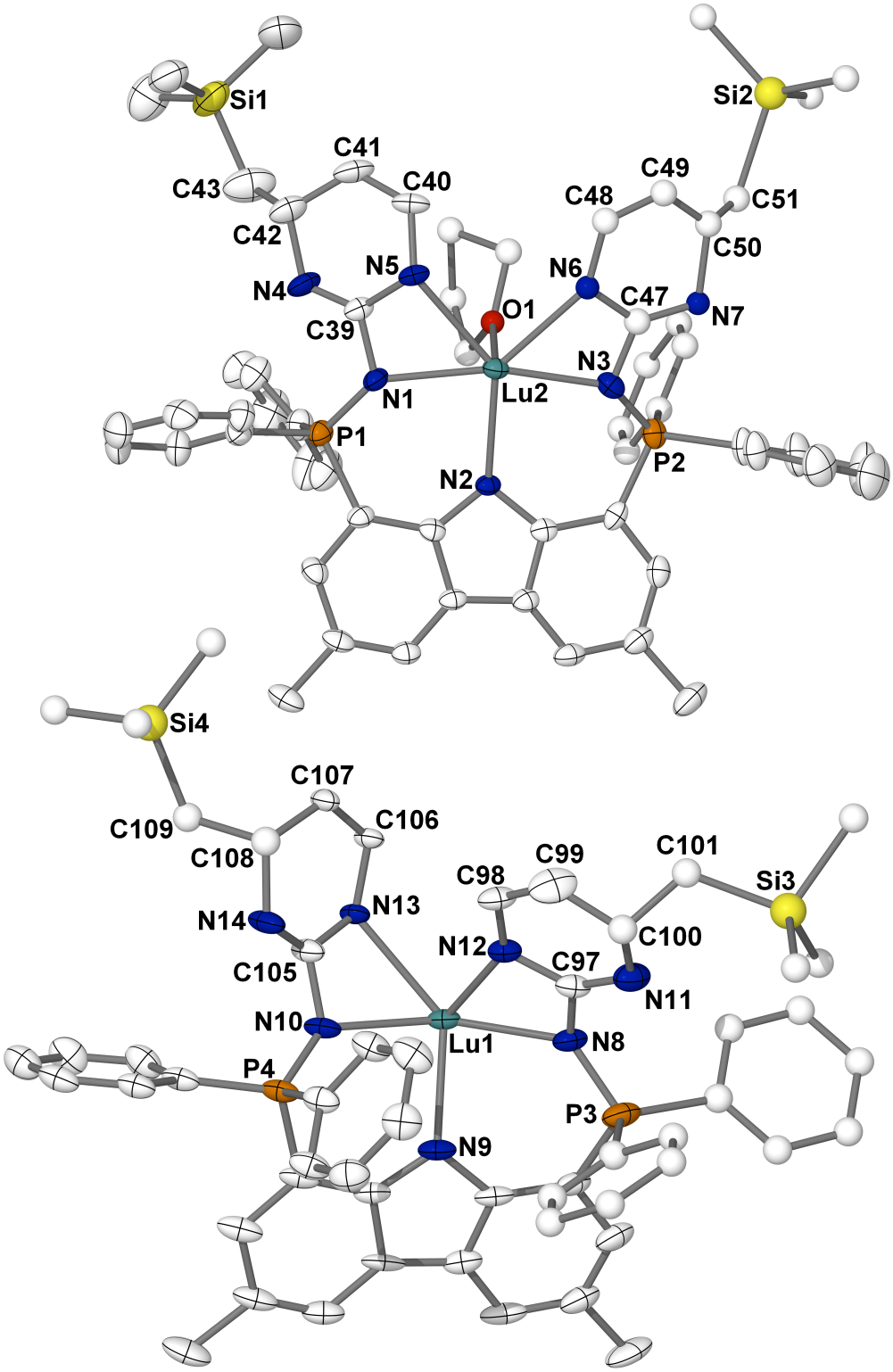

Figure 3.10 Thermal ellipsoid plots (30% probability) depicting the two subunits of [($\mathbf{L}_{\mathbf{A}}^{\mathbf{Pym*}}$-$\kappa^5$*N*)Lu]$_2$(THF), **21** with hydrogen atoms omitted for clarity. Positionally disordered atoms are depicted as spheres of arbitrary radius.

Table 3.5 Selected bond distances /Å and angles /° for **21**

Lu2–N2	2.412(5)	N13–Lu2–O1	170.2(4)
Lu2–N3	2.297(6)	N3–Lu2–N2	81.4(2)
Lu2–N1	2.321(5)	N2–Lu2–N1	81.0(2)
Lu2–N5	2.493(6)	N1–Lu2–N5	56.4(2)
Lu2–N13	2.354(5)	N5–Lu2–N6	87.2(5)
Lu2–N6	2.389(16)	N6–Lu2–N3	53.8(5)
Lu1–N13	2.436(5)	N12–Lu1–N5	129.0(2)
Lu1–N10	2.264(6)	N12–Lu1–N10	105.1(2)
Lu1–N5	2.315(6)	N12–Lu1–N9	118.1(2)
Lu1–N9	2.327(5)	N9–Lu1–N10	81.1(2)
Lu1–N8	2.305(6)	N10–Lu1–N5	110.7(2)
Lu1–N12	2.240(6)	N9–Lu1–N5	102.6(2)
O1–Lu2	2.341(11)	N8–Lu1–N13	138.6(2)

The unusual reactivity observed in the dialkyl lutetium complex of $\mathbf{L}_{\mathbf{A}}^{\mathbf{Pym}}$ is not completely unprecedented. In 2006, Kiplinger *et al*. reported a 1,3-alkyl migration that occurred in lutetium alkyl complexes supported by 2,2′:6′,2″-terpyridine (terpy) and 4,4′,4″-tri-*tert*-butyl-2,2′:6′,2″-terpyridine ligands (Scheme 3.5).[156]

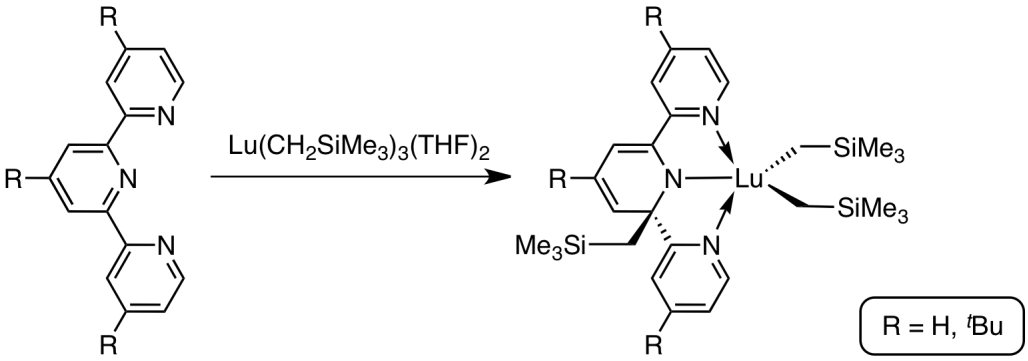

Scheme 3.5 Example of a 1,3-alkyl migration in a lutetium terpy complex

With the terpy-based scaffold, migration of only one alkyl group occurred, converting the neutral terpy ligand into a monoanionic ligand. Despite the dearomatization and functionalization of the terpy ligand, a stable dialkyl lutetium

complex was obtained as the final product. As such, two valences were still retained at the lutetium centre for further derivatization of the metal and reactivity studies.[157]

In terms of the reactivity involving the bis(phosphinimine)carbazole ligand, the double 1,5-alkyl migration converted the monoanionic ligand $\mathbf{L}_{\mathbf{A}}^{\mathbf{Pym}}$ into a trianionic and functionalized derivative $\mathbf{L}_{\mathbf{A}}^{\mathbf{Pym*}}$. In the corresponding lutetium complex [($\mathbf{L}_{\mathbf{A}}^{\mathbf{Pym*}}$-$\kappa^5$*N*)Lu]$_2$(THF), **21**, the trianionic ligand used all of the metal valences, leaving none for further reactivity. Unfortunately, due to the irreversible nature of this form of ligand functionalization, no further reactivity was investigated with complex **21**.

3.6 Conclusions

In summary, the synthesis and characterization of a versatile family of pincer ligands, which represent a new platform for preparing low coordinate organometallic species, has been described. These carbazole-based ligands have been utilized to prepare base-free dialkyl lutetium complexes. All dialkyl lutetium complexes were thermally sensitive and found to be highly susceptible to intramolecular reactivity involving the ancillary ligand. Interestingly, the observed reactivity varied depending on the nature of the *N*-aryl substituent.

The ligands $\mathbf{L}_{\mathbf{A}}^{\mathbf{Ph}}$ and $\mathbf{L}_{\mathbf{A}}^{\mathbf{Pipp}}$ afforded highly electrophilic lutetium dialkyl complexes that were susceptible to a rare double cyclometalative reaction involving the *ortho* C–H bonds of the *P*-phenyl rings. This unique reactivity led to complexes whereby the ancillary ligand was bound to the metal via three nitrogen atoms and two *ortho*-metalated *P*-phenyl rings.

The pyrimidine-substituted ligand $\mathbf{L}_{\mathbf{A}}^{\mathbf{Pym}}$ was utilized to prepare a lutetium dialkyl complex that was resistant to *ortho* cyclometalative decomposition. However, this species was prone to a double 1,5-alkyl sigmatropic shift that resulted in functionalization and dearomatization of the ligand pyrimidine rings.

Despite the unexpected nature of the reactivity in the developed compounds, a variety of well-defined lutetium complexes have been prepared. These complexes serve as useful models to study the reactivity patterns of the bis(phosphinimine)carbazole ligand and its ability to support highly reactive organolanthanide complexes.

Chapter 4

Metallacycle Ring Opening Reactivity

4.1 Overview

From a synthetic perspective, a ligand cyclometalation process can have diverse consequences. For example, in the context of an olefin polymerization catalyst, the cyclometalative C–H bond activation often results in catalyst deactivation and deprivation of any living polymerization processes.[158,159] Furthermore, ligand metalation may occur through numerous competing intramolecular C–H bond activation pathways and at different sites. If multiple products are generated, it often proves difficult to separate or characterize the mixture.

While frequently unfavourable, ligand metalation processes can sometimes be exploited to achieve desired reactivity; notable examples involving lanthanide complexes are outlined in Chapter 1. In early transition metal chemistry, a recent example reported by Waterman *et al*. involved a cyclometalated zirconium trisamidoamine species that

exhibited catalytic reactivity for the selective dehydrocoupling of phosphines and arsines (Scheme 4.1),[160,161] in addition to catalytic hydrophosphination of terminal alkynes.[162]

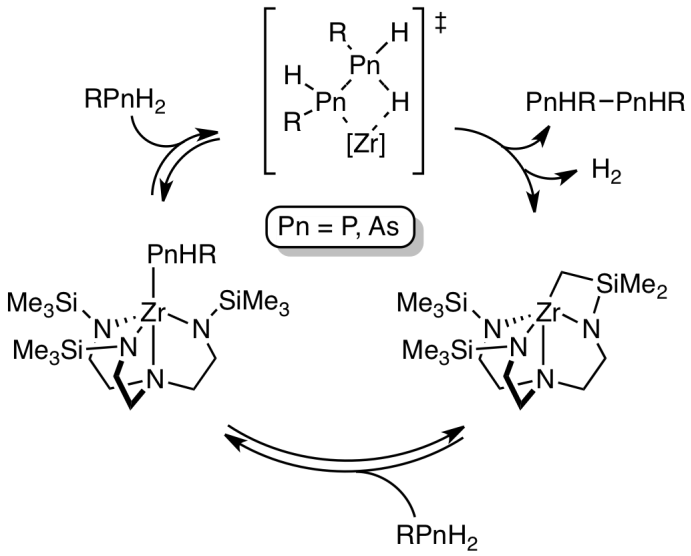

Scheme 4.1 Mechanism of pnictogen dehydrocoupling

Another prominent example reported by Tilley *et al*. utilized a doubly metalated tungsten tuck-in complex to access a tungsten silylene product (Scheme 4.2).[163,164] In this reaction, it can be speculated that the tungsten tuck-in complex acts as a synthon for the 14-electron coordinatively unsaturated cation $[Cp^*(dmpe)W]^+$, whereby the hydride ligands have reversibly migrated back to the Cp* ring. A range of silanes react with the synthon to give the corresponding tungsten silylene dihydride cation $[Cp^*(dmpe)H_2W{=}SiR_2]^+$. Notably, deuterium labeling experiments (*e.g.* reaction of the synthon with diphenylsilane-d_2) yielded $Cp^*(dmpe)D_2W{=}SiR_2]^+$ with >90% deuterium incorporation at the tungsten hydride positions.[106]

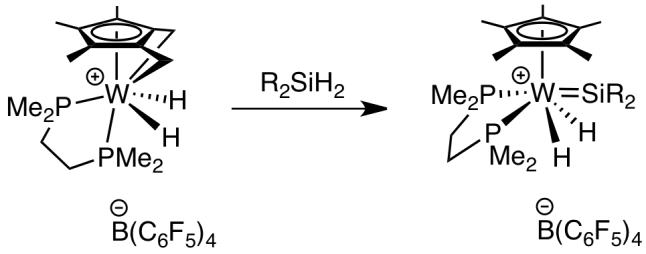

Scheme 4.2 Access to a tungsten silylene via a doubly metalated species

In Chapter 3, the synthesis of bis(phosphinimine)carbazolide pincer ligands $\mathbf{L}_{\mathbf{A}}^{\mathbf{Ph}}$ and $\mathbf{L}_{\mathbf{A}}^{\mathbf{Pipp}}$ and their use in the preparation of well-defined organolutetium complexes was described. It was found that dialkyl lutetium complexes of $\mathbf{L}_{\mathbf{A}}^{\mathbf{Ph}}$ and $\mathbf{L}_{\mathbf{A}}^{\mathbf{Pipp}}$ were thermally unstable and rapidly underwent two sequential intramolecular metalative alkane elimination processes. The final product of this transformation contained the ligand bound in a κ^5 manner through the three nitrogen atoms of the ligand framework and two *ortho*-metalated *P*-phenyl rings ($\mathbf{L}_{\mathbf{A}}^{\mathbf{Ar}}$-$\kappa^3$*N*,$\kappa^2$*C*$^{P\text{-Ph}}$)Lu(THF) (Ar = Ph, **19**; *para*-isopropylphenyl, **20**).

This chapter reports an investigation into the reactivity patterns of the *ortho*-metalated organolutetium complexes through the process of metallacycle ring opening. In particular, diiodide and bis(anilide) lutetium complexes supported by $\mathbf{L}_{\mathbf{A}}^{\mathbf{Ph}}$ and $\mathbf{L}_{\mathbf{A}}^{\mathbf{Pipp}}$, as well as a mixed aryl/anilide lutetium complex were prepared by means of metallacycle ring opening. The viability of the latter was assessed for its potential to liberate a lutetium imido complex ($\mathbf{L}_{\mathbf{A}}^{\mathbf{Ar}}$Lu=NR) by thermolysis. As a result of this study, novel reactivity patterns were uncovered in conjunction with the clean formation of complexes that exhibit unique bonding modes and structures.

4.2 Metallacycle Ring Opening Reactivity

4.2.1 Synthesis of a Lutetium Diiodide Complex

In the context of exploring the potentially reactive Lu–C bonds in **19** and **20**, it was expected that these species would serve as useful precursors for further derivatization at the metal centre. Specifically, it was anticipated that access to a lutetium iodide derivative could be achieved through the acid-base reaction of the doubly *ortho*-metalated complex with the "iodide delivery reagent" $[Et_3NH]I$. As expected, treatment of **20** with two equivalents of $[Et_3NH]I$ cleanly afforded the diiodide complex, ($\mathbf{L}_{\mathbf{A}}^{\mathbf{Pipp}}$-$\kappa^3$*N*)$LuI_2(THF)$ (**22**), with simultaneous production of triethylamine (Scheme 4.3).

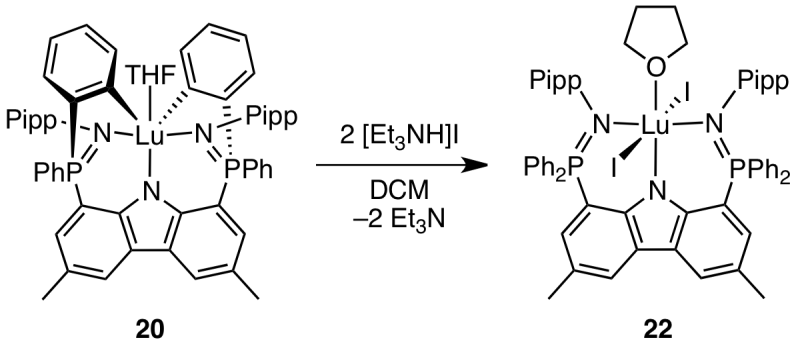

20 **22**

Scheme 4.3 Synthesis of a lutetium diiodide complex

Recrystallization of complex **22** from a toluene/THF solution at −35 °C generated yellow crystalline blocks suitable for an X-ray diffraction experiment. Under these conditions, complex **22** crystallized in triclinic space with one molecule of benzene and is depicted in Figure 4.1 as a thermal ellipsoid plot. In the solid state, **22** is defined by coordination of two iodide ligands, one THF donor and the bis(phosphinimine)carbazole ligand bound κ^3 through three nitrogen atoms. The lutetium centre exhibits octahedral

geometry with the iodide ligands *trans* to one another, and meridional coordination by the ancillary ligand. Complex **22** exhibits relatively long Lu–I contacts of 2.9989(3) Å and 2.9626(3) Å, which are slightly longer than values previously reported for other structurally characterized neutral lutetium iodide compounds (2.896(1) Å – 2.914(2) Å).[165,166]

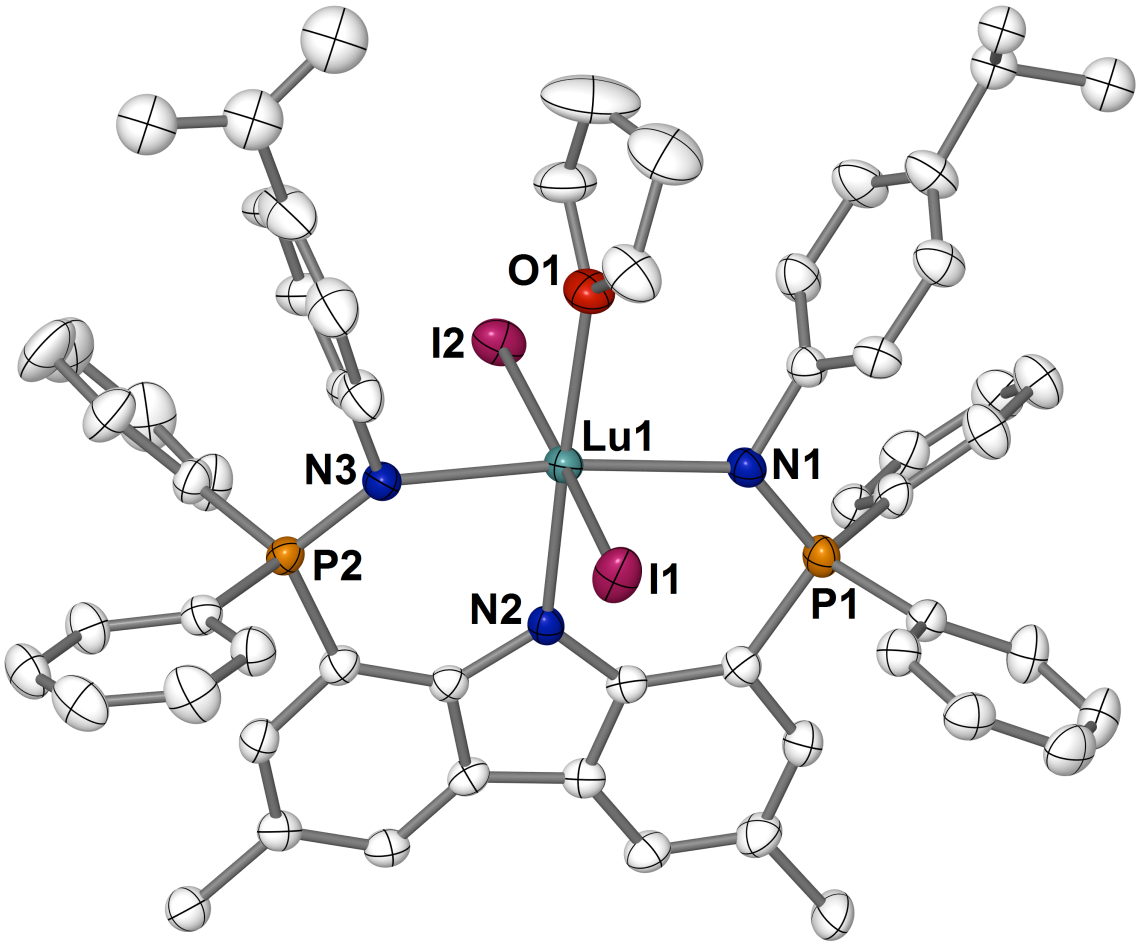

Figure 4.1 Thermal ellipsoid plot (50% probability) of **22** with hydrogen atoms and benzene molecule of crystallization omitted for clarity. Positionally disordered atoms are depicted as spheres of arbitrary radius.

Table 4.1 Selected bond distances /Å and angles /º for compound **22**

Lu1–I1	2.9989(3)	N3–Lu1–N2	88.0(1)
Lu1–I2	2.9626(3)	N2–Lu1–N1	87.5(1)
Lu1–N1	2.297(3)	N1–Lu1–O1	89.6(1)
Lu1–N2	2.284(3)	O1–Lu1–N3	95.2(1)
Lu1–N3	2.302(3)	I2–Lu1–N3	90.15(8)
Lu1–O1	2.369(3)	N3–Lu1–I1	86.75(8)
P1–N1	1.606(3)	I1–Lu1–N1	89.56(7)
P2–N3	1.605(3)	N1–Lu1–I2	93.86(7)
I1–Lu1–O1	89.29(7)	I2–Lu1–N2	89.48(7)
O1–Lu1–I2	87.16(7)	N2–Lu1–I1	94.25(7)

The method described above for the preparation of diiodide complex **22** is a slight variation of a procedure previously developed for the synthesis of erbium diiodide complexes.[78] The synthesis of lanthanide iodide complexes is of interest due to their unique properties; the Ln–I bond is typically more labile than other Ln–X bonds (X = Cl, Br), and often results in different reactivity patterns.[166] This is likely due to the fact that iodide ligands are relatively soft and can be displaced from lanthanide centres under milder conditions than the corresponding lanthanide chlorides. Despite this fact, complexes of lanthanide iodides are studied to a far lesser extent than their chloride analogues; this is possibly because lanthanide iodide precursors (*i.e.* LnI_3) are less available and more expensive than lanthanide chloride reagents.[167] In account of this, a variety of methods do exist in the literature for the preparation of lanthanide iodide complexes.[168] For example, the salt metathesis reaction of anionic ligands with LnI_3 reagents;[128,129,165,169,170] halide exchange reactions of lanthanide chlorides with NaI[166] or trimethylsilyliodide;[78] oxidation of divalent lanthanide complexes or Ln(0) reagents with iodine or alkyl iodides;[171-173] or the reaction of lanthanide hydride or alkyl complexes with various iodo reagents.[171,172] Unfortunately, the above-mentioned methods are limited

in that they require the use of a stable lanthanide chloride, hydride, alkyl or low-valent precursor. As such, the procedure described herein involving $[Et_3NH]I$ provides a general route for the preparation of lanthanide iodides in high yield from cyclometalated lanthanide complexes. As a mild synthetic method, it is anticipated that this route should be relevant to a diverse array of cyclometalated lanthanide complexes and thus, of high applicability. It is also expected that convenient access to lanthanide iodide complexes will serve as a platform for the development of new forms of reactivity and bonding through subsequent derivatization. For example, this may be achieved by salt metathesis substitution reactions with an assortment of potassium reagents.

4.2.2 Lutetium Anilide Complexes

In an effort to further explore the metallacycle ring opening reactivity of complexes **19** and **20**, an investigation was made into their reactivity with other protic reagents. To this end, the *ortho*-metalated lutetium aryl complexes **19** and **20** can be reacted with various anilines in toluene solution at ambient temperature to give the corresponding anilide product. For example, treatment of **19** with two equivalents of 2,4,6-trimethylaniline ($MesNH_2$) resulted in immediate reaction whereby ring opening of the metalated *P*-phenyl rings liberated the bis(anilide) complex **23**, $(\mathbf{L}_{\mathbf{A}}^{\mathbf{Ph}}\text{-}\kappa^3 N)Lu(NHMes)_2$ (Scheme 4.4). Similar reactivity has been previously documented in rare earth complexes supported by an anilido-phosphinimine ligand.[81,82]

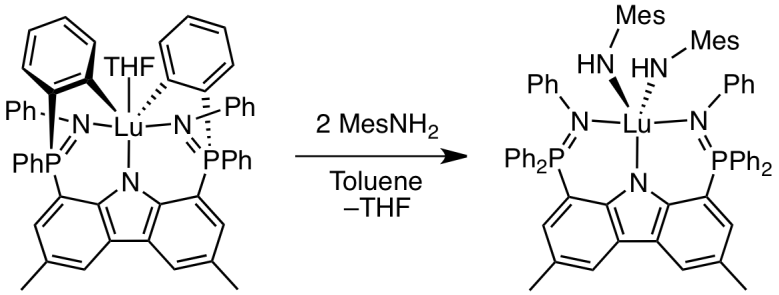

19 **23**

Scheme 4.4 Metallacycle ring opening reaction of complex **19** with $MesNH_2$

The bis(anilide) lutetium complex **23** is C_{2v} symmetric in the solution state, as depicted by a sharp singlet (δ 30.6) in its $^{31}P\{^{1}H\}$ NMR spectrum (benzene-d_6). The ^{1}H NMR spectrum for complex **23** exhibits the expected signals for the ancillary ligand, in addition to a set of resonances corresponding to two mesityl anilide ligands. In particular, the NH anilide protons of complex **23** give rise to a singlet at δ 3.97 with an integration of 2H (benzene-d_6).

Single crystals of complex **23** · C_6H_6 suitable for an X-ray diffraction study were readily obtained from a benzene solution layered with pentane at ambient temperature. The molecular structure of **23** is illustrated in Figure 4.2 as a thermal ellipsoid plot. In the solid state, complex **23** is defined by coordination of two 2,4,6-trimethylanilide ligands and the ancillary pincer ligand bound in a κ^3 fashion through its three nitrogen atoms. The five-coordinate lutetium centre exhibits distorted trigonal bipyramidal geometry with the anilide ligands (N1 and N2) and N4 of the ancillary in the equatorial positions. The phosphinimine nitrogen donors of the pincer ligand (N3 and N5) occupy the apical sites. The metal centre sits above the plane of the dimethylcarbazole backbone by 0.770 Å. At 2.178(2) Å (Lu1–N1) and 2.175(2) Å (Lu1–N2), the lutetium anilide bond lengths agree well with values previously reported for neutral lutetium anilides.[157,174-177] Similarly, the

ancillary ligand coordinates to lutetium with bond lengths of 2.348(2) Å (Lu1–N3), 2.360(2) Å (Lu1–N4) and 2.359(2) Å (Lu1–N5), which correspond well with structural parameters discussed in Chapters 2 and 3.

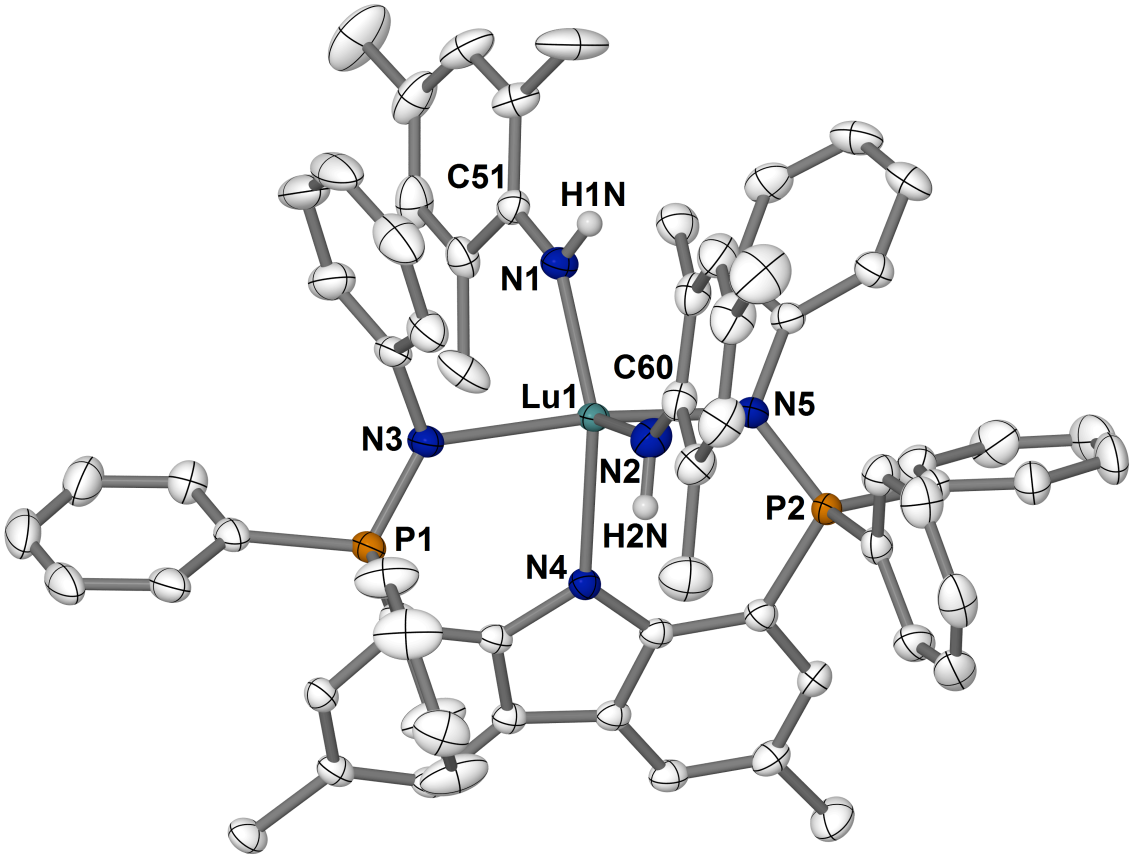

Figure 4.2 Thermal ellipsoid plot (50% probability) of **23** with hydrogen atoms (except H1N and H2N) and benzene molecule of crystallization omitted for clarity.

Of particular interest was the installation of only one anilide group on lutetium so as to afford a mixed aryl/anilide species. The impetus behind this goal stemmed from the idea that thermolysis of a mixed aryl/anilide complex may promote intramolecular metallacycle ring opening to yield an unprecedented terminal lutetium imido complex.[91,178] Accordingly, the reaction of complex **19** with only one equivalent of $MesNH_2$ was explored in the prospect of generating the mono(anilide) congener of **23**.

Unfortunately, repeated attempts resulted in reaction mixtures whereby only the bis(anilide) complex, **23**, could be isolated. It is possible that this reaction was hampered by a Schlenk-type ligand redistribution process that involved formation of the bis(anilide) complex, **23**, alongside additional unknown byproducts. Similar reactivity has previously been documented in the preparation of other rare earth mono(anilide) complexes.[179]

Table 4.2 Selected bond distances /Å and angles /º for compounds **23** and **24**

	23	**24**
Lu1–N1	2.178(2)	2.203(7)
Lu1–N2	2.175(2)	2.170(8)
Lu1–N3	2.348(2)	2.331(8)
Lu1–N4	2.360(2)	2.323(7)
Lu1–N5	2.359(2)	2.339(7)
P1–N3	1.594(2)	1.576(8)
P2–N5	1.610(2)	1.600(7)
N3–Lu1–N5	168.76(6)	170.8(3)
N3–Lu1–N4	86.38(6)	84.9(3)
N4–Lu1–N5	84.44(6)	86.4(3)
N1–Lu1–N2	118.11(7)	110.1(3)
Lu1–N1–C51[a]	144.0(2)	—
Lu1–N2–C60[a]	151.3(2)	—
Lu1–N1–C57[b]	—	146.5(7)
Lu1–N2–C72[b]	—	143.8(7)

Notes: [a]The listed angle pertains only to complex **23**; [b]The listed angle pertains only to complex **24**.

In a further effort to prepare a mono(anilide) lutetium complex, the premise of metallacycle ring opening using anilines of steric bulk even greater than that of $MesNH_2$ was pursued. The concept behind this approach was to install a sufficiently bulky anilide ligand to inhibit further intermolecular metallacycle ring opening. Thus, reaction of complex **20** with various anilines of gradually increasing steric bulk was investigated. For

this purpose, the reagents 2,4,6-triisopropylaniline ($TripNH_2$) and 2,4,6-tri-*tert*-butylaniline (Mes^*NH_2) were utilized.

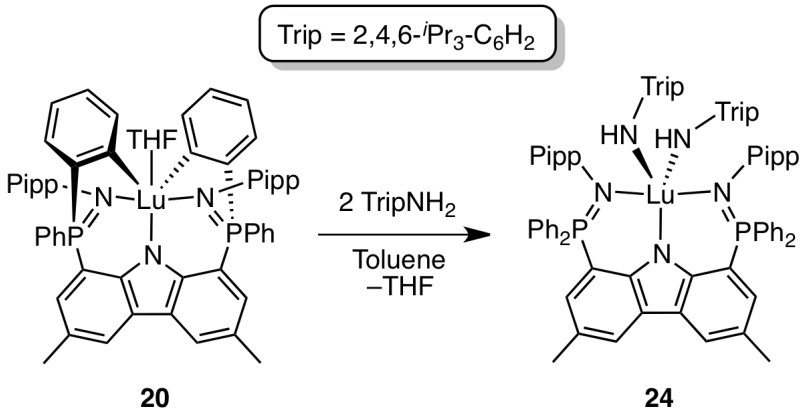

20 **24**

Scheme 4.5 Metallacycle ring opening reaction of complex **24** with $TripNH_2$

Reaction of complex **20** with two equivalents of $TripNH_2$ afforded the double metallacycle ring opening product ($\mathbf{L}_{\mathbf{A}}^{\mathbf{Pipp}}$-$\kappa^3$*N*)Lu(NHTrip)$_2$, **24**, analogous to bis(anilide) **23** (Scheme 4.5). Similar to **23**, complex **24** exhibits C_{2v} symmetry in solution on the NMR time scale. In the $^{31}P\{^1H\}$ NMR spectrum of **24**, a sharp singlet resonating at δ 30.6 (benzene-d_6) can be observed; this shift is coincidental to the $^{31}P\{^1H\}$ NMR signal for complex **23**. The ^1H NMR spectrum consists of the expected resonances for the ancillary ligand as well as signals corresponding to two Trip anilide groups. Similar to the $^{31}P\{^1H\}$ chemical shift, the two NH protons for complex **24** resonate with the same frequency as complex **23** (δ 3.97, benzene-d_6).

Single crystals of complex **24** · C_5H_{12} were obtained by recrystallization from a concentrated pentane solution at ambient temperature. The solid-state structure of **24**, as determined from an X-ray diffraction experiment, is depicted in Figure 4.3. Similar to that observed in **23**, the lutetium centre in complex **24** adopts a trigonal bipyramidal geometry with two Trip anilide ligands and the ancillary pincer bound in a κ^3 fashion

through its three nitrogen atoms. Likewise, the anilide ligands (N1 and N2) and N4 of the ancillary occupy the equatorial positions, while N3 and N5 define the apical sites. The lutetium anilide bond lengths in complex **24** are comparable to that of **23** with distances of 2.203(7) Å and 2.169(8) Å for Lu1–N1 and Lu1–N2, respectively (Table 4.2). In addition, the Lu–N–C anilide bond angles in both complexes **23** and **24** are similar with values ranging from 143.8(7)° to 151.3(2)°.

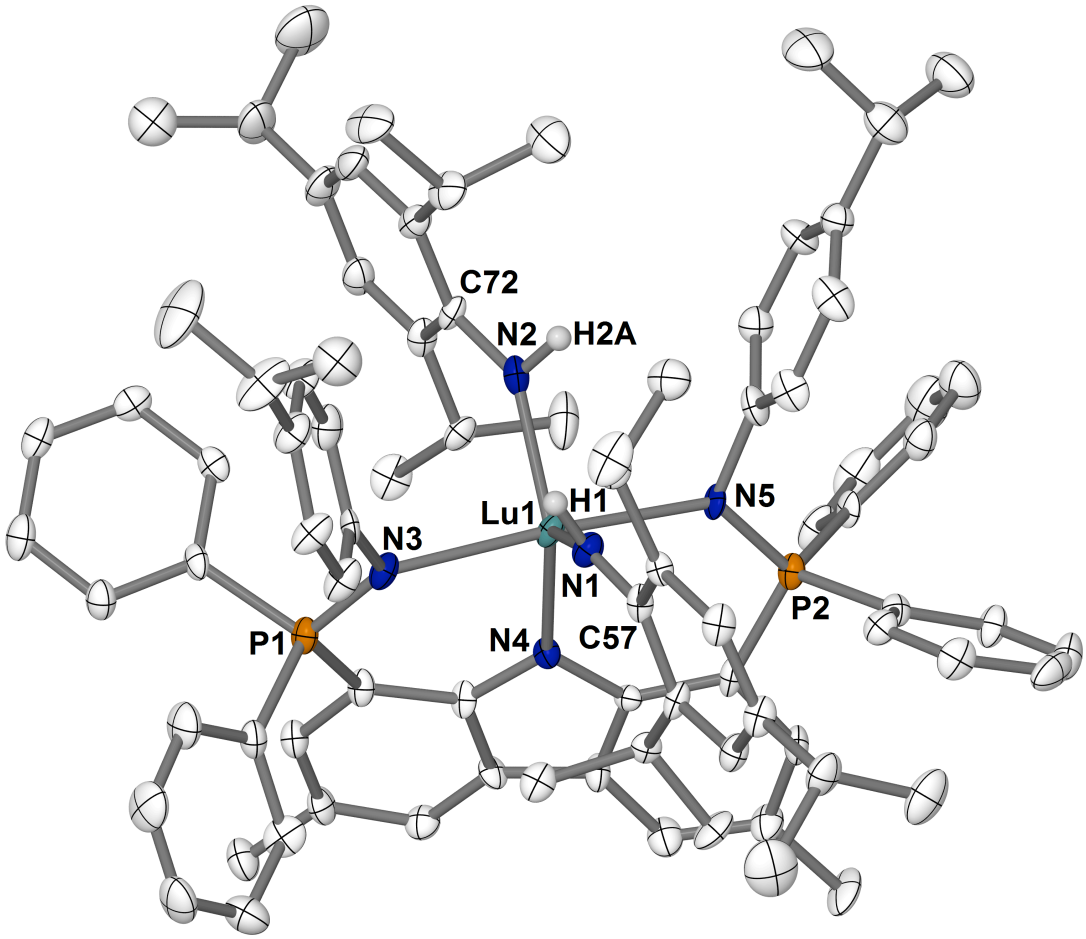

Figure 4.3 Thermal ellipsoid plot (30% probability) of **24** with hydrogen atoms (except H1 and H2A) and pentane molecule of crystallization omitted for clarity. Positionally disordered atoms are depicted as spheres of arbitrary radius.

In contrast to the reactivity observed upon reaction of **19** and **20** with $MesNH_2$ and $TripNH_2$, addition of one equivalent of 2,4,6-tri-*tert*-butylaniline (Mes^*NH_2) to **20**

only promoted metallacycle ring opening of a single *ortho*-metalated *P*-phenyl group generating the desired mono(anilide) complex ($\mathbf{L}_{\mathbf{A}}^{\mathbf{Pipp}}$-$\kappa^3N,\kappa C^{P\text{-Ph}}$)Lu(NHMes*), **25** (Scheme 4.6). Even under forcing conditions (100 °C for 24 h) with two equivalents of Mes*NH_2, it was found that double substitution of **20** (to make ($\mathbf{L}_{\mathbf{A}}^{\mathbf{Pipp}}$- κ^3N)Lu(NHMes*)$_2$) was not possible.

Interestingly, complex **25** was highly unstable toward a thermally induced intramolecular rearrangement to the structural isomer ($\mathbf{L}_{\mathbf{A}}^{\mathbf{Pipp}}$-$\kappa^3N,\kappa C^{N\text{-Pipp}}$)Lu(NHMes*) **26** (Scheme 4.6). Unfortunately, the high thermal instability of **25** precluded its isolation as a solid. Complex **25** could, however, be readily observed *in situ* by $^{31}P\{^1H\}$ NMR spectroscopy throughout the transformation from **20** to **26**. The $^{31}P\{^1H\}$ NMR spectrum of **25** revealed a marked difference from that observed for **23** and **24**. In the solution state, complex **25** exhibits low symmetry (C_1) as demonstrated by two singlets of equal intensity in the $^{31}P\{^1H\}$ NMR spectrum at δ 31.8 and δ 22.6 (benzene-d_6), corresponding to the chemically inequivalent phosphinimine groups. Attempts to fully characterize **25** *in situ* by other NMR nuclei (^1H or $^{13}C\{^1H\}$) were unsuccessful due to the severity of overlapping signals corresponding to complexes **20**, **25** and **26**.

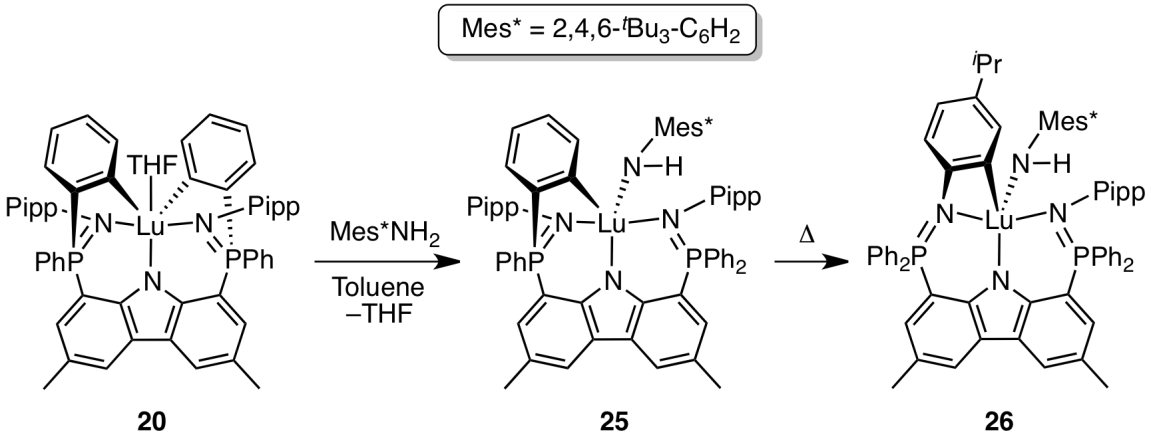

20 **25** **26**

Scheme 4.6 Metallacycle ring opening reaction of **20** with one equivalent of Mes*NH_2

The thermal transformation of **25** to **26** liberated a structural isomer whereby the ancillary ligand is *ortho*-metalated via an *N*-aryl ring in **26**, as compared to a *P*-phenyl ring in **25**. The $^{31}P\{^{1}H\}$ NMR spectrum of complex **26** contains two resonances (δ 29.96 and δ 11.83 (benzene-d_6)) slightly upfield of those observed for **25**. The ^{1}H and $^{13}C\{^{1}H\}$ NMR spectra of **26** were found to be extremely complicated, especially in the aromatic regions, due to the low symmetry (C_1) of the complex; however, the expected resonances for the ancillary ligand and one 2,4,6-tri-*tert*-butylanilide moiety were observed. In particular, the NH anilide proton of complex **26** gives rise to a singlet in the ^{1}H NMR spectrum at δ 4.88 with an integration of 1H (benzene-d_6).

In order to unambiguously establish the connectivity of **26**, a single-crystal X-ray diffraction study was performed. Complex **26** was found to be highly crystalline and single crystals were readily obtained from a concentrated toluene solution layered with pentane at −35 °C. As depicted in the molecular structure of **26** (Figure 4.4), the low symmetry of the complex in the solid state (C_1) matched that observed in solution. The complex adopts a five-coordinate geometry with one site occupied by a 2,4,6-tri-*tert*-butylanilide ligand. The remaining four coordination sites are defined by the ancillary ligand bound in a κ^4 fashion through the three nitrogen atoms and the *ortho* carbon of one Pipp group. At 1.554 Å, the lutetium centre sits substantially out of the plane of the dimethylcarbazole ligand backbone, presumably due to the extremely sterically demanding nature of the ligands coordinated to it. Of particular interest in complex **26** is the unusual four-membered metallacycle constituted by Lu1, N2, C39 and C40. In the solid state the metallacycle takes on a kite-shaped geometry defined by two long bonds (Lu1–N2, 2.307(3) Å; Lu–C40, 2.337(4) Å) and two short bonds (C39–N2, 1.444(5) Å;

C39–C40, 1.408(5) Å). The sum of the angles within the metallacycle is 359.0°, indicating a nearly planar conformation. The Lu–N1–C57 anilide bond angle in **26** (164.2(3)°) is substantially more linear than that observed in complexes **23** and **24** (which range from 143.8(7)° to 151.3(2)°). This difference is likely due to the increased steric bulk of the 2,4,6-tri-*tert*-butylanilide ligand. Selected bond distances and angles for complex **26** are listed in Table 4.3.

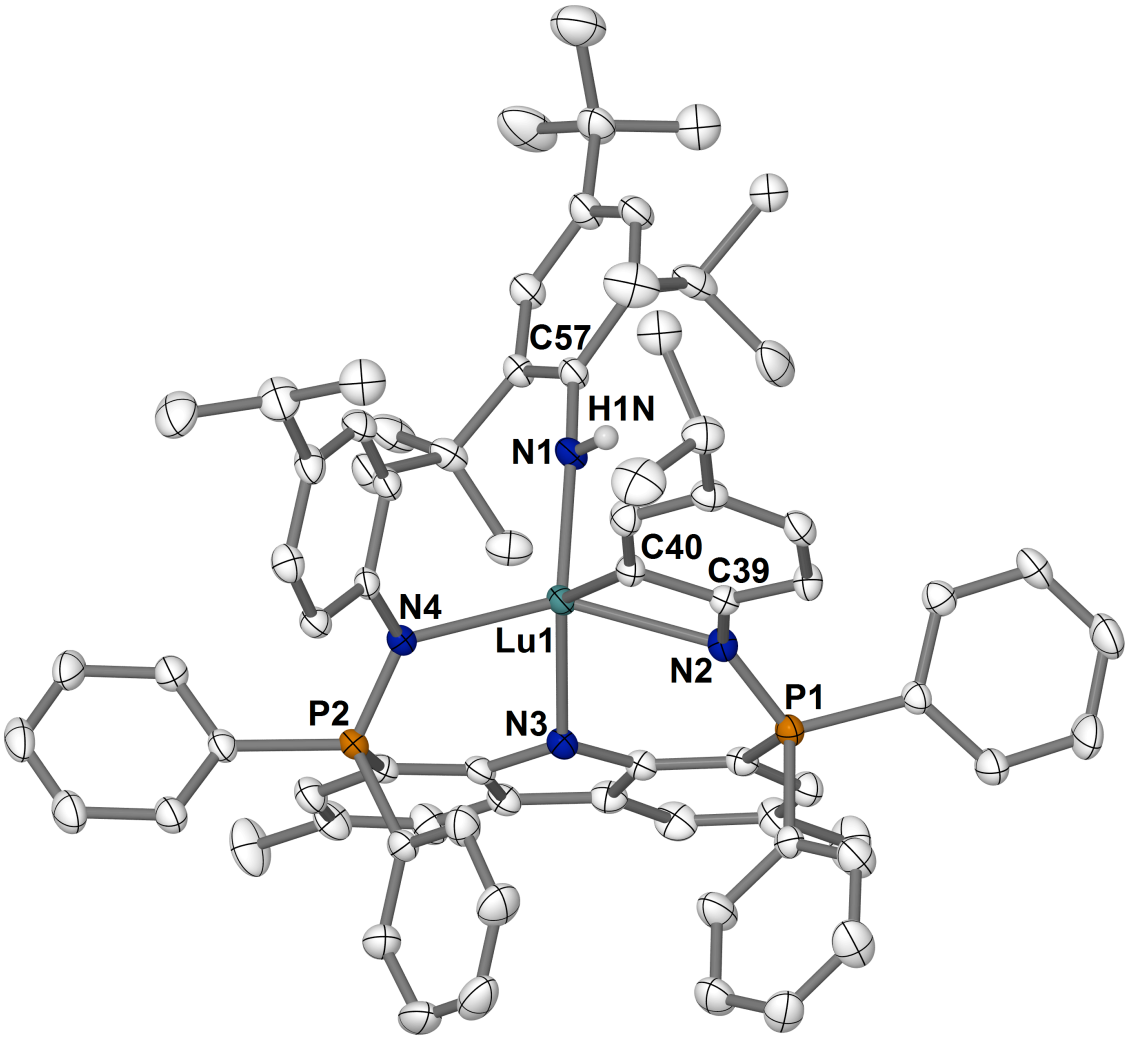

Figure 4.4 Thermal ellipsoid plot (50% probability) of **26** with hydrogen atoms (except H1N) and pentane molecules of crystallization omitted for clarity. Positionally disordered atoms are depicted as spheres of arbitrary radius.

Table 4.3 Selected bond distances /Å and angles /º for compound **26**

Lu1–N1	2.163(3)	N2–Lu1–N4	142.5(1)
Lu1–N2	2.307(3)	N2–Lu1–N3	81.8(1)
Lu1–N3	2.312(3)	N3–Lu1–N4	86.5(1)
Lu1–N4	2.312(3)	N1–Lu1–N3	125.2(1)
Lu1–C40	2.337(4)	Lu1–N1–C57	164.2(3)
C39–C40	1.408(5)	Lu1–N2–C39	92.9(2)
C39–N2	1.444(5)	N2–Lu1–C40	61.3(1)
P1–N2	1.584(3)	Lu1–C40–C39	92.6(3)
P2–N4	1.614(3)	N2–C39–C40	112.3(3)

4.3 Kinetic Analysis of Metallacycle Ring Opening

Due to its rapid rate of decomposition, complex **25** could neither be isolated nor fully characterized by ^{1}H or $^{13}C\{^{1}H\}$ NMR spectroscopy. However, the formation of **25** from **20**, followed by its decomposition to complex **26** (Equation 4.1), was quantitatively monitored by $^{31}P\{^{1}H\}$ NMR spectroscopy. The progress of reaction at 296.9 K (from t = 185 s to t = 157000 s) is portrayed in Figure 4.5 as a stacked plot of $^{31}P\{^{1}H\}$ NMR spectra (toluene-d_8) recorded at predefined time intervals. Over the course of the reaction, the decreasing concentration of **20** (δ 29.7) is accompanied by the formation of asymmetric intermediate **25**, depicted by two resonances at δ 31.7 and 22.4. Within two days at this temperature, complex **25** gradually undergoes an intramolecular metalation exchange to exclusively afford product **26** (δ 29.7 and 11.4).

$$\mathbf{20} + \mathrm{Mes{*}NH_2} \xrightarrow{k_1} \mathbf{25} \xrightarrow{k_2} \mathbf{26} \qquad \text{Equation 4.1}$$

The observed rate constant ($k_{1(obs)}$) for the formation of complex **25** was obtained from a second order plot of the reaction of **20** with Mes*NH_2. The reaction was monitored over a broad range of temperatures (296.9 to 349.1K), with observed $t_{1/2}$ values spanning from 18500 to 198 s for the first half-life of the reaction (Table 4.4). An Eyring plot was constructed that allowed for extraction of the activation parameters $\Delta H^{\ddagger} = 73.5 \pm 1.4$ kJ·mol^{-1} and $\Delta S^{\ddagger} = -50.3 \pm 4.5$ J·K^{-1}·mol^{-1} for this transformation (Figure 4.6a). The large negative entropy of activation suggests a highly ordered transition state, consistent with the expected mechanism for this reaction.

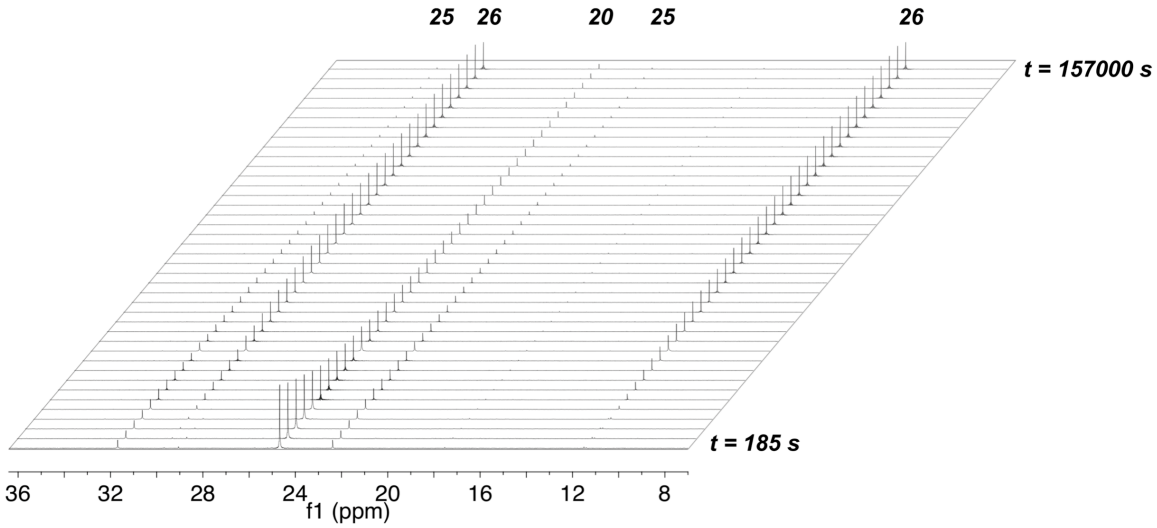

Figure 4.5 Stacked $^{31}P\{^{1}H\}$ NMR spectra depicting the metallacycle ring opening reaction of complex **20** to **25** followed by transformation to complex **26**.

In contrast to the second order reaction that converted complex **20** to **25**, the transformation from **25** to **26** involved significantly more complicated kinetic behaviour. No simple mathematical rate law could be derived for the expression of k_2 due to the complexity of the consecutive reactions. Thus, no values for $k_{2(obs)}$ could be determined from the experimental data. However, using the kinetic simulation software COPASI,[180] the two-step process from **20** to **26** was modeled. As such, the modeled data-set allowed

for calculation of the simulated rate constants, $k_{1(calc)}$ and $k_{2(calc)}$, for the consecutive reactions; these values are listed in Table 4.4 and Table 4.5, respectively. The $k_{1(calc)}$ values agree fairly well with the $k_{1(obs)}$ values; however, it should be noted that the calculated rate constants were consistently slightly slower (by 5 to 14%) than the observed rate constants. Due to this observation, it is reasonable to assume that the calculated rate constants for k_2 (Table 4.5) may also be slow by a similar margin of error. However, a visual inspection of the simulated reaction progress over time indicated good agreement with the experimental reaction plots.

Table 4.4 Observed and calculated rate constants for the metallacycle ring opening reaction of complex **20** with Mes*NH_2 at temperatures ranging from 296.9 to 349.1 K

T/K	$k_{1(obs)}$/$M^{-1}\cdot s^{-1}$	$t_{1/2(obs)}$/s	$k_{1(calc)}$/$M^{-1}\cdot s^{-1}$	$t_{1/2(calc)}$/s
296.9	1.81×10^{-3}	18500	1.69×10^{-3}	19900
304.6	3.43×10^{-3}	9660	3.22×10^{-3}	10300
315.7	9.96×10^{-3}	3330	9.44×10^{-3}	3510
326.8	3.07×10^{-2}	1070	2.68×10^{-2}	1230
338.0	7.44×10^{-2}	445	6.42×10^{-2}	517
349.1	1.66×10^{-1}	198	1.49×10^{-1}	222

Note: $t_{1/2}$ values are reported for the first half-life only.

Table 4.5 Calculated rate constants for the intramolecular rearrangement of complex **25** to complex **26** at temperatures ranging from 296.9 to 349.1 K

T/K	$k_{2(calc)}$/s^{-1}	$t_{1/2(calc)}$/s
296.9	3.17×10^{-5}	21900
304.6	8.46×10^{-5}	8200
315.7	2.54×10^{-4}	2730
326.8	6.84×10^{-4}	1010
338.0	2.02×10^{-3}	342
349.1	5.14×10^{-3}	135

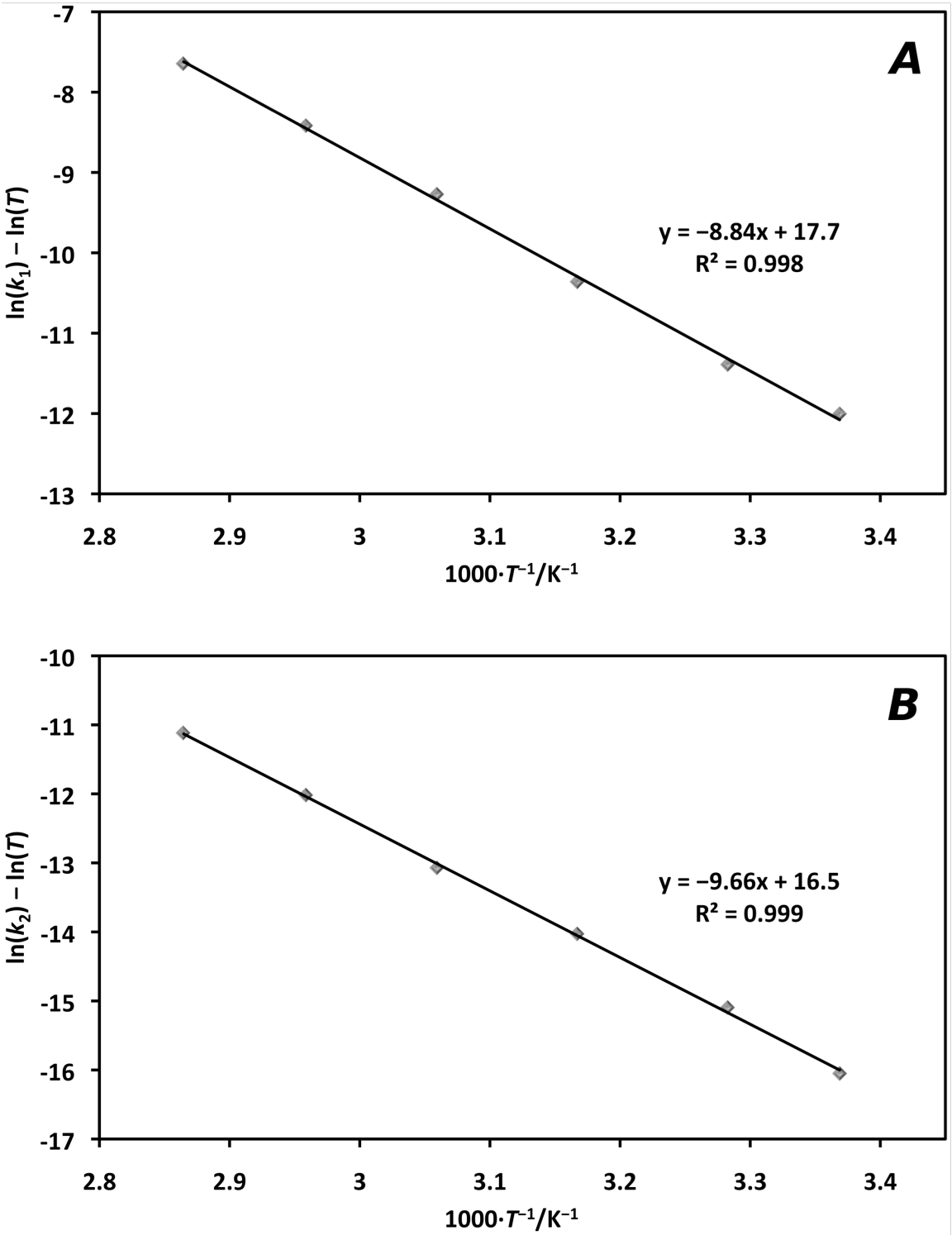

Figure 4.6 (a) Eyring plot for the metallacycle ring opening reaction of **20** to **25** (derived from $k_{1(obs)}$). (b) Eyring plot for the intramolecular rearrangement of **25** to **26** (derived from $k_{2(calc)}$).

As with the observed rate constant $k_{1(obs)}$, Eyring plots were constructed to express the temperature dependence of the simulated rate constants $k_{1(calc)}$ and $k_{2(calc)}$. From these plots, the activation parameters of $\Delta H^{\ddagger} = 72.3 \pm 1.0$ kJ·mol^{-1} and $\Delta S^{\ddagger} = -55.0 \pm 3.2$ J·K^{-1}·mol^{-1}; and $\Delta H^{\ddagger} = 80.3 \pm 1.1$ kJ·mol^{-1} and $\Delta S^{\ddagger} = -60.0 \pm 3.4$ J·K^{-1}·mol^{-1} were extracted for $k_{1(calc)}$ and $k_{2(calc)}$, respectively (Table 4.6). The parameters obtained for $k_{1(calc)}$ agree very well with those obtained from $k_{1(obs)}$. For the activation parameters obtained from the $k_{2(calc)}$ rate constants, the enthalpic barrier and entropy of activation both remained similar to that observed for k_1.

Table 4.6 Transition state activation parameters for the transformation of complex **20** to **26**

Rate Constant	$\Delta H^{\ddagger}$/kJ·mol^{-1}	$\Delta S^{\ddagger}$/J·K^{-1}·mol^{-1}
$k_{1(obs)}$	73.5 ± 1.4	−50.3 ± 4.5
$k_{1(calc)}$	72.3 ± 1.0	−55.0 ± 3.2
$k_{2(calc)}$	80.3 ± 1.1	−60.0 ± 3.4

4.4 Deuterium Labeling and Mechanism

The structure of complex **26**, confirmed by solution multinuclear NMR spectroscopy and solid-state X-ray diffraction analysis, suggests that an unusual reaction mechanism is operative in its formation from starting material **20**. It is evident that the mechanism for the generation of **26** from **20** requires multiple steps, due to the intermediacy of **25**. Several pathways for this transformation can be envisioned, the two most plausible of which will be described in depth. The first mechanism (Pathway 1) involves the metallacycle ring opening reaction of complex **20** with Mes*NH_2 to give mono(anilide) **25**, followed by direct metalation exchange of the aryl rings between *P*-Ph

and *N*-Pipp groups of the ancillary ligand to afford complex **26** as the final product. An alternate mechanism (Pathway 2) could involve the formation of **25** as in Pathway 1. Following this, intramolecular metallacycle ring opening of complex **25** could give rise to a transient lutetium imido complex, whereby C–H addition across the Lu=N bond by an *N*-Pipp group would afford the final product **26**. Although there have been no terminal, unconstrained lutetium imides reported to date,[181,182] there are several examples of rare earth metal complexes that are formed via a transient terminal imido intermediate.[47,91,178,183] More recently, the isolation of a terminal scandium imide has been realized,[92] thus suggesting that the paucity of such species in the literature is not due to thermodynamic limitations. In order to establish which mechanism is operative in the formation of **26** from **20**, two independent deuterium labeling experiments were performed (Scheme 4.7 and Scheme 4.8).

The first deuterium labeling experiment involved the reaction of complex **20** with Mes*ND_2. As outlined in Scheme 4.7, if Pathway 1 was operative, the labeled anilide formed upon initial reaction (**25**-*N*-d_1-*ring*-d_1) would retain a deuterium atom on the anilide nitrogen throughout the transformation to give the final product **26**-*N*-d_1-*ring*-d_1, with a deuterium-labeled anilide nitrogen. Conversely, if Pathway 2 was operative, the deuterium on the anilide nitrogen of **25**-*N*-d_1-*ring*-d_1 would become scrambled into the *P*-phenyl rings upon imido formation. This would be followed by re-metalation of an *N*-Pipp group, thus installing a proton onto the anilide nitrogen atom of the final putative product, **26**-*ring*-d_2. Upon following this reaction on an NMR tube scale by ^{1}H NMR spectroscopy, it was unambiguously determined that the final product of the transformation contained a deuterium atom on the anilide nitrogen, thus suggesting that

Pathway 1, rather than Pathway 2, was operative. This conclusion was supported by the lack of a resonance at δ 4.88 in the ^{1}H NMR spectrum of **26**-*N*-d_1-*ring*-d_1. The aromatic region in the ^{1}H NMR spectrum of **26**-*N*-d_1-*ring*-d_1 would also be expected to integrate as one less proton than **26**; however, this small difference in integration could not be accurately determined. Other than these details, the ^{1}H NMR spectrum of **26**-*N*-d_1-*ring*-d_1 was identical to that of the proteo control, **26**, where the NH signal can be clearly observed at δ 4.88 (Figure 4.7).

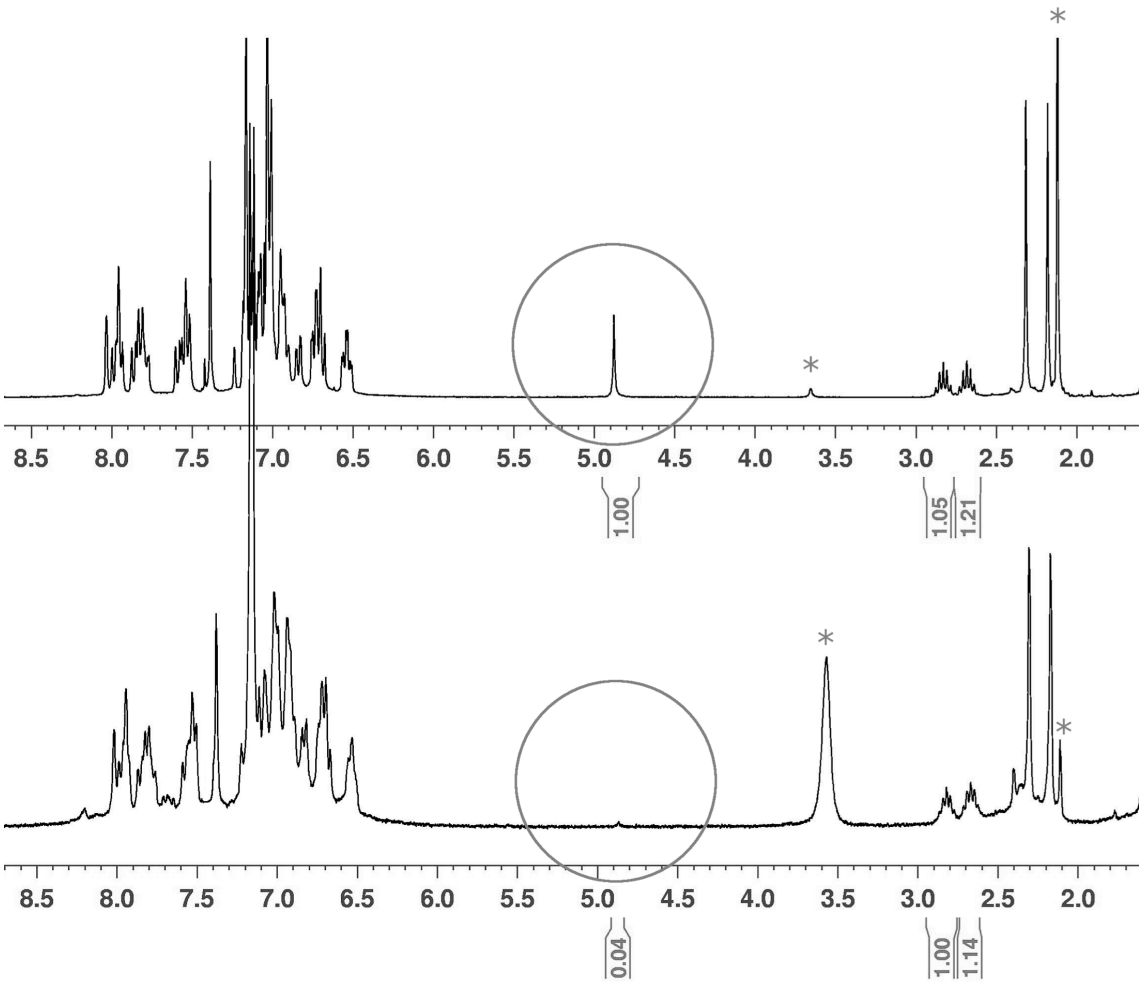

Figure 4.7 ^{1}H NMR spectra for deuterium labeling experiment 1. Top: Reaction of **20** with Mes*NH_2 (protonated control). Bottom: Reaction of **20** with Mes*ND_2 (labeling experiment). Solvent signals (THF and toluene) are denoted by an asterisk. Mes*ND_2 with >95% deuterium incorporation at nitrogen was used in this experiment.

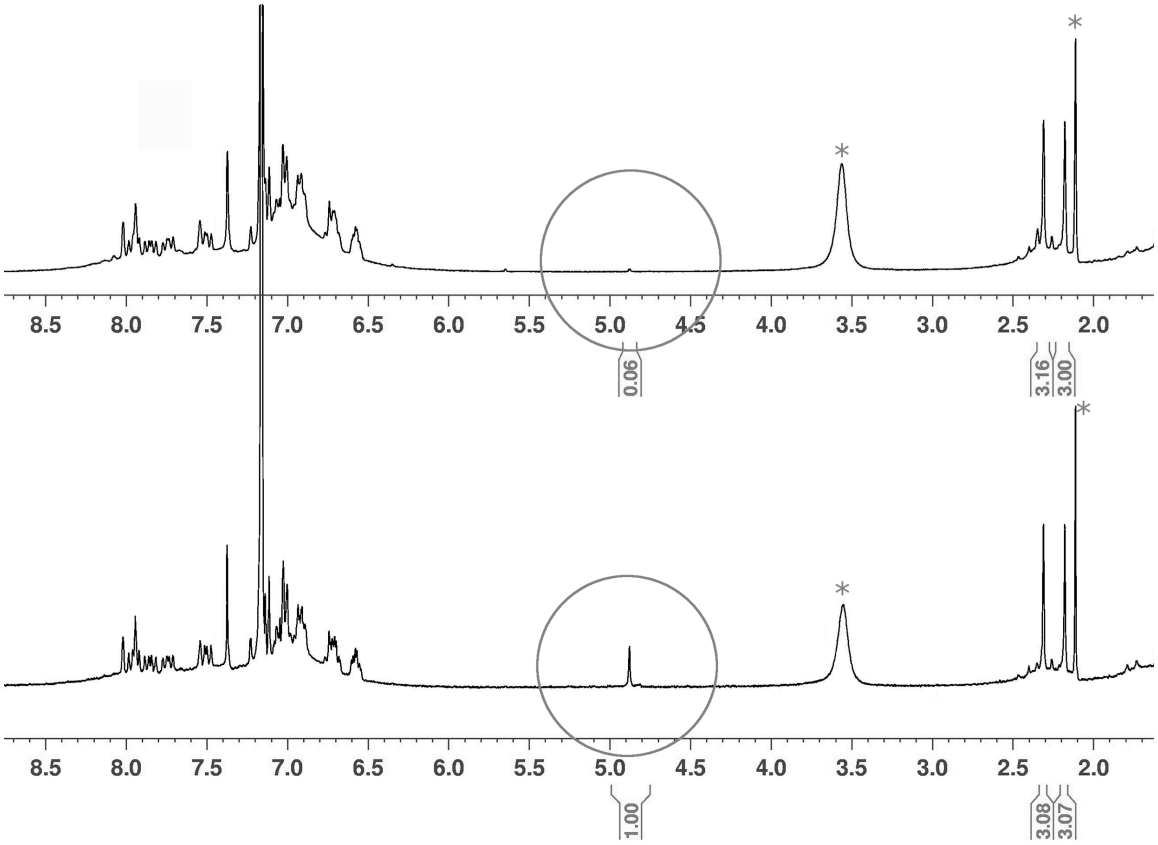

Figure 4.8 ^{1}H NMR spectra for deuterium labeling experiment 2. Top: Reaction of **19**-*ring*-d_{10} with Mes*ND_2 (deuterated control). Bottom: Reaction of **19**-*ring*-d_{10} with Mes*NH_2 (labeling experiment). Solvent signals (THF and toluene) are denoted by an asterisk. **19**-*ring*-d_{10} with >98% deuterium incorporation in the phenyl rings was used in this experiment.

The second deuterium labeling experiment involved the reaction of fully protonated Mes*NH_2 with a deuterium labeled lutetium analogue of **20**, **19**-*ring*-d_{10}, (Scheme 4.8). The starting material **19**-*ring*-d_{10} contained fully deuterated *N*-phenyl groups as opposed to the proton-containing 4-isopropylphenyl groups in **20**. Despite the lack of an isopropyl group in the *para* position of the *N*-aryl ring, it could be assumed with confidence that **19**-*ring*-d_{10} would react in an identical manner to that of **20**, excluding any kinetic isotope effects. The identical reactivity patterns and kinetic behaviour of **19** (the protonated version of **19**-*ring*-d_{10}) and **20** was previously

documented in Chapter 3. As depicted in Scheme 4.8, Pathway 1 dictates that reaction of **19**-*ring*-d_{10} with Mes*NH_2 would result in the products **25′**-*ring*-d_{10} and **26′**-*ring*-d_{10}, whereby a proton is retained on the anilide nitrogen throughout the entire process. Conversely, Pathway 2 would result in loss of the anilide proton upon imido formation, followed by re-metalation of a deuterium-labeled *N*-aryl ring, thus installing a deuterium atom on the anilide nitrogen. Upon following the transformation by ^{1}H NMR spectroscopy, the final product of the reaction of **19**-*ring*-d_{10} with Mes*NH_2 was clearly observed to be **26′**-*ring*-d_{10} with a proton bound to the anilide nitrogen (Figure 4.8). Thus, deuterium labeling experiment 2 corroborated the results from experiment 1, in that Pathway 1, rather than 2, appears to be operative.

Two additional mechanisms (Pathways 3 and 4) have also been considered, but quickly disproven. Pathway 3 involves the reaction of complex **25** with a second equivalent of Mes*NH_2 to give the bis(anilide) complex analogous to **23** and **24**. From such a species, loss of 2,4,6-tri-*tert*-butylaniline with concomitant metalation of an *N*-Pipp group would result in **26**. Pathway 3 is not considered to be a probable mechanism on grounds of steric hindrance. It does not appear to be possible to fit two 2,4,6-tri-*tert*-butylanilide groups into the coordination pocket defined by the ancillary ligand because of too much steric crowding. Furthermore, Pathway 3 was nullified through the above-mentioned deuterium labeling studies. For example, in deuterium labeling experiment 1, the reaction of **20** with two equivalents of Mes*ND_2 would result in the intermediate ($\mathbf{L}_{\mathbf{A}}^{\mathbf{Pipp}}$-$\kappa^3$*N*-*ring*-$d_2$)Lu(NDMes*)$_2$ if Pathway 3 were operative. This species would then undergo loss of Mes*NHD to give the final product **26**-*N*-d_1-*ring*-d_2. It can be expected then, that in subsequent reactions, competition between **20** reacting with Mes*ND_2 or

Mes*NHD would occur. As a result, deuterium incorporation on the anilide nitrogen of complex **26** would not be either 100% or 0% (as for Pathways 1 and 2, respectively), but rather, a statistical mixture. In Pathway 4, the anilide ligand in complex **25** could serve to shuttle an H atom from the *N*-aryl group to the metalated *P*-phenyl moiety via intermediate (**L**-$\kappa^3 N$,$\kappa C^{P\text{-Ph}}$,$\kappa C^{N\text{-Ar}}$)Lu(NH_2Mes*). This mechanism was disproven by both deuterium labeling experiments because Mes*NHD, which would afford a statistical mixture of D and H incorporation on the anilide nitrogen of complex **26**, would be produced in both cases.

The mechanistic work presented herein suggests that the formation of complex **26** occurs via two sequential metallacycle ring opening reactions. The first ring opening is induced by the reaction of **20** with Mes*NH_2 to give complex **25**, which possesses a metalated *P*-phenyl ring. Complex **25** then undergoes a thermal rearrangement via a rare direct metalation exchange between an *N*-aryl ring and the metalated *P*-phenyl ring to yield structural isomer **26**. The results from deuterium labeling experiments argue against the possibility of a transient lutetium imido species being formed as an intermediate in this transformation.

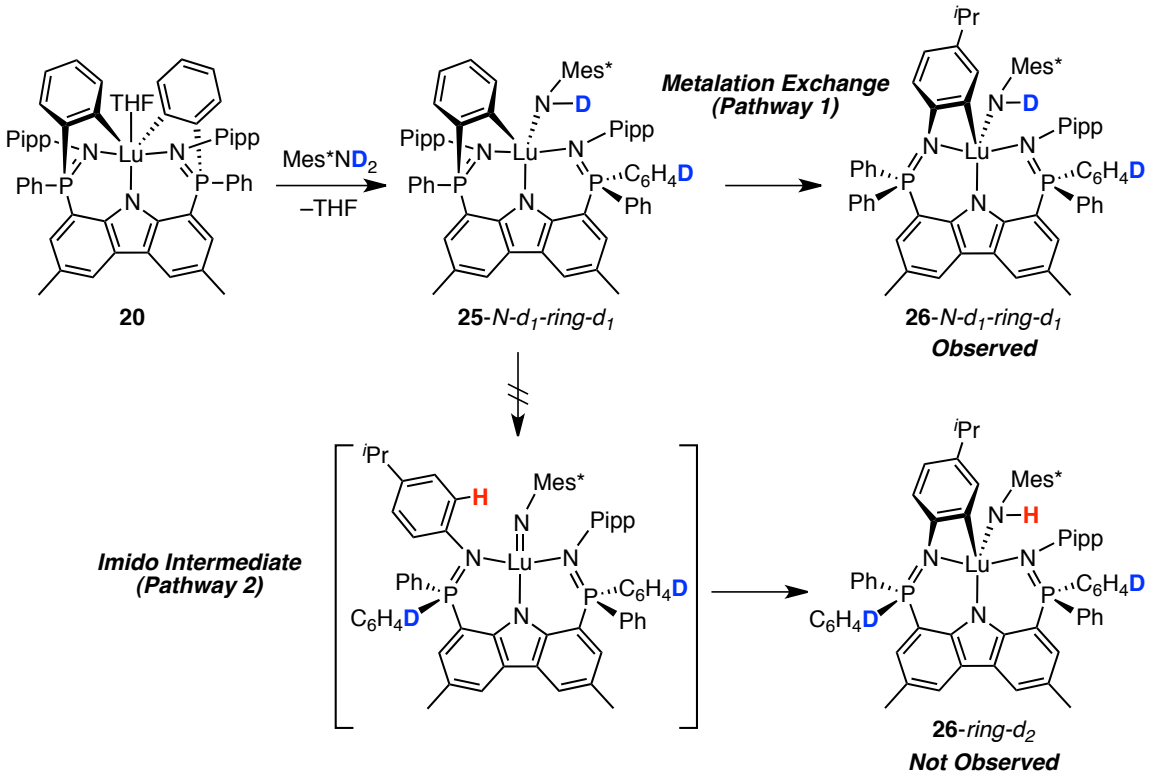

Scheme 4.7 Deuterium labeling experiment 1: reaction of complex **20** with Mes*ND_2

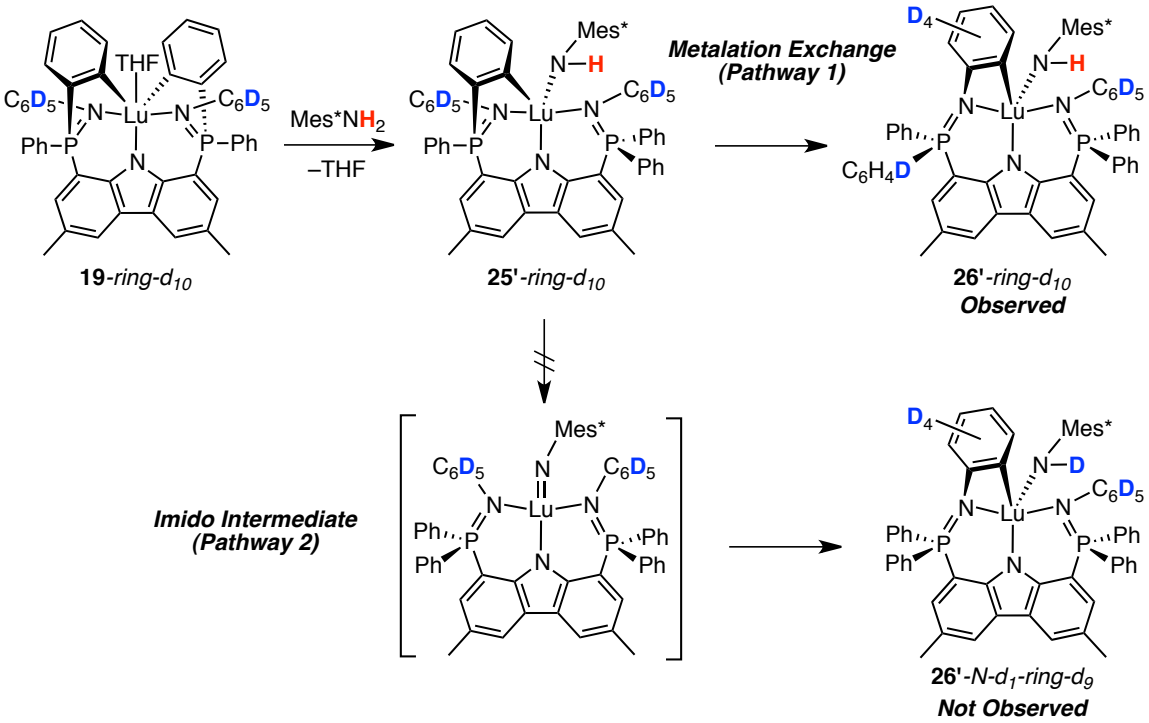

Scheme 4.8 Deuterium labeling experiment 2: reaction of complex **19**-*ring-*d_{10} with Mes*NH_2

4.5 Access to a Lutetium Mixed Alkyl/Anilide Complex

Although the formation of complex **26** did not proceed via a transient lutetium imido intermediate, the prospect of accessing such an elusive target was sufficiently enticing to warrant further study into the matter. A strategy commonly encountered in the preparation of imido complexes of the early d-block metals is the thermolysis of a mixed alkyl/anilide precursor to give the M=NR functionality with loss of alkane.[184,185] For this reason, the viability of this route with respect to 4f metals was investigated.[181]

In Chapter 3 it was demonstrated that the alkane elimination reaction of $Lu(CH_2SiMe_3)_3(THF)_2$ with $H\mathbf{L}^{\mathbf{Pipp}}_{\mathbf{A}}$ results in formation of the dialkyl complex ($\mathbf{L}^{\mathbf{Pipp}}_{\mathbf{A}}$-$\kappa^3$*N*)$Lu(CH_2SiMe_3)_2$, **15**, with loss of one equivalent of $SiMe_4$. Therefore, it was reasoned that an analogous alkane elimination protocol whereby reaction of $H\mathbf{L}^{\mathbf{Pipp}}_{\mathbf{A}}$ with a reagent of form $Lu(CH_2SiMe_3)_2(NHMes^*)(THF)_2$, **27**, might give rise to the mixed alkyl/anilide species ($\mathbf{L}^{\mathbf{Pipp}}_{\mathbf{A}}$-$\kappa^3$*N*)$Ln(CH_2SiMe_3)NHMes^*$, **28**, with loss of $SiMe_4$.

The lutetium reagent **27** was synthesized through the protonolysis reaction of $Lu(CH_2SiMe_3)_3(THF)_2$ with one equivalent of 2,4,6-tri-*tert*-butylaniline. This facile reaction proceeded in toluene solution at ambient temperature to give $Lu(CH_2SiMe_3)_2(NHMes^*)(THF)_2$ as the sole product with loss of one equivalent of $SiMe_4$. Complex **27** was alternatively prepared in high yield (84.0%) via the one-pot salt metathesis reaction of anhydrous $LuCl_3$ with two equivalents of $LiCH_2SiMe_3$ and one equivalent of KNHMes* in a toluene/THF solution (Scheme 4.9).

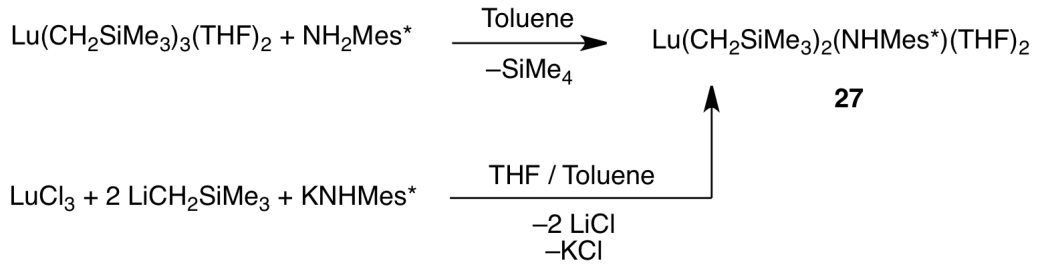

Scheme 4.9 Synthesis of $Lu(CH_2SiMe_3)_2(NHMes^*)(THF)_2$, **27**

The ^1H NMR spectrum of complex **27** exhibits the expected resonances corresponding to one 2,4,6-tri-*tert*-butylanilide moiety, two trimethylsilylmethyl ligands and two THF donors. In particular, the NH signal was found to resonate at δ 3.85 (benzene-d_6) with an integration of 1H. The methyl and methylene resonances for the alkyl groups were observed as singlets at δ 0.36 and −0.75 (benzene-d_6), with integrations of 18H and 4H, respectively. Complex **27** is related to other examples of dialkyl lutetium complexes containing a 2,4,6-tri-*tert*-butylanilide ligand such as the 4,4′-di-*tert*-butyl-2,2′-bipyridyl stabilized complex, $Lu(CH_2SiMe_3)_2NHMes^*(^tBu_2bpy)$, and the triphenylphosphine oxide analogue, $Lu(CH_2SiMe_3)_2NHMes^*(OPPh_3)_2$.[177]

Single crystals of **27** suitable for X-ray diffraction were readily obtained from a concentrated pentane solution at −35 °C. The molecular structure of **27** is depicted in Figure 4.9 as a thermal ellipsoid plot and selected metrical parameters are listed in Table 4.7. In the solid state, **27** is defined by coordination of two trimethylsilylmethyl groups, one 2,4,6-tri-*tert*-butylanilide ligand and two THF donors. The five-coordinate lutetium centre exhibits distorted trigonal bipyramidal geometry with the anilide and two alkyl ligands in the equatorial positions. The apical sites of the complex are occupied by coordination of two THF ligands. The equatorial ligands lie essentially in the same plane,

with a sum of angles about the metal equal to 359.9°. The apical THF ligands coordinate to lutetium with a close to linear O1–Lu1–O2 bond angle of 175.56(7)°.

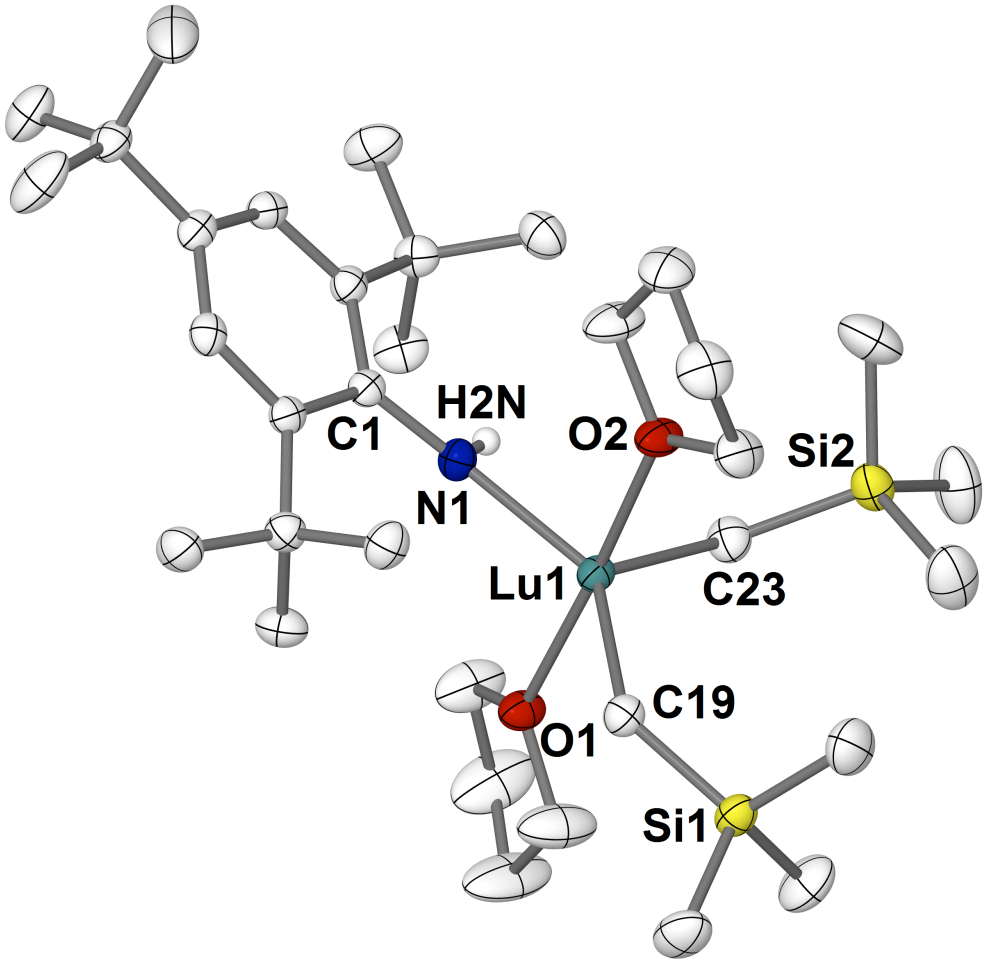

Figure 4.9 Thermal ellipsoid plot (50% probability) of $Lu(CH_2SiMe_3)_2(NHMes^*)(THF)_2$ **27** with hydrogen atoms (except H2N) omitted for clarity.

Table 4.7 Selected bond distances /Å and angles /º for compound **27**

Lu1–N1	2.192(3)	Lu1–N1–C1	155.3(2)
Lu1–C19	2.393(3)	C19–Lu1–N1	134.7(1)
Lu1–C23	2.353(3)	C23–Lu1–N1	103.1(1)
Lu1–O1	2.313(2)	C19–Lu1–C23	122.0(1)
Lu1–O2	2.337(2)	O1–Lu1–O2	175.56(7)

Complex **27** is structurally similar to the previously reported triphenylphosphine oxide analogue, $Lu(CH_2SiMe_3)_2NHMes^*(OPPh_3)_2$.[177] Of note, the Lu1–N1 bond length of **27** at 2.192(3) Å is slightly shorter than the corresponding bond in $Lu(CH_2SiMe_3)_2NHMes^*(OPPh_3)_2$ at 2.224(7) Å. The elongation of this bond in $Lu(CH_2SiMe_3)_2NHMes^*(OPPh_3)_2$ is likely due to the increased steric demand of the triphenylphosphine oxide ligands compared to the THF ligands in **27**.

The protonolysis reactivity of **27** with $H\mathbf{L}_{\mathbf{A}}^{\mathbf{Pipp}}$ (**12**) was monitored on NMR tube scale in benzene-d_6 solution. The reaction was found to proceed rapidly at ambient temperature; however, it was not selective for alkane elimination. Rather, two competing reactions transpired, whereby both amine and alkane elimination occurred. As a result of this, the complexes **15** and **28** both formed with loss of Mes^*NH_2 and $SiMe_4$, respectively. To further complicate matters, complex **15** is quite thermally sensitive (as discussed in Chapter 3) and rapidly decomposes to afford the doubly *ortho*-metalated product **20**. Due to the multiple products generated by this protonolysis reaction, it was evident that the isolation and full characterization of the desired mixed alkyl/anilide complex (**28**) would be extremely challenging and was not pursued. It was discovered, however, that if the reaction mixture (containing **20**, **28**, Mes^*NH_2 and $SiMe_4$) was heated to 100 ºC, then complex **26** could be obtained as the single thermodynamic product. During this reaction, **20** reacts with Mes^*NH_2 via metallacycle ring opening to give **26** as previously discussed (Scheme 4.6). Complex **28** reacts by losing one equivalent of $SiMe_4$ with concomitant *ortho*-metalation of either a *P*-Ph or *N*-aryl ring to give **25** or **26**, respectively. If **25** formed then it would react as previously outlined via

metalation exchange to give **26** as the final thermodynamic product (Scheme 4.10). In all cases, complex **26** was formed as the sole reaction product and could be cleanly isolated.

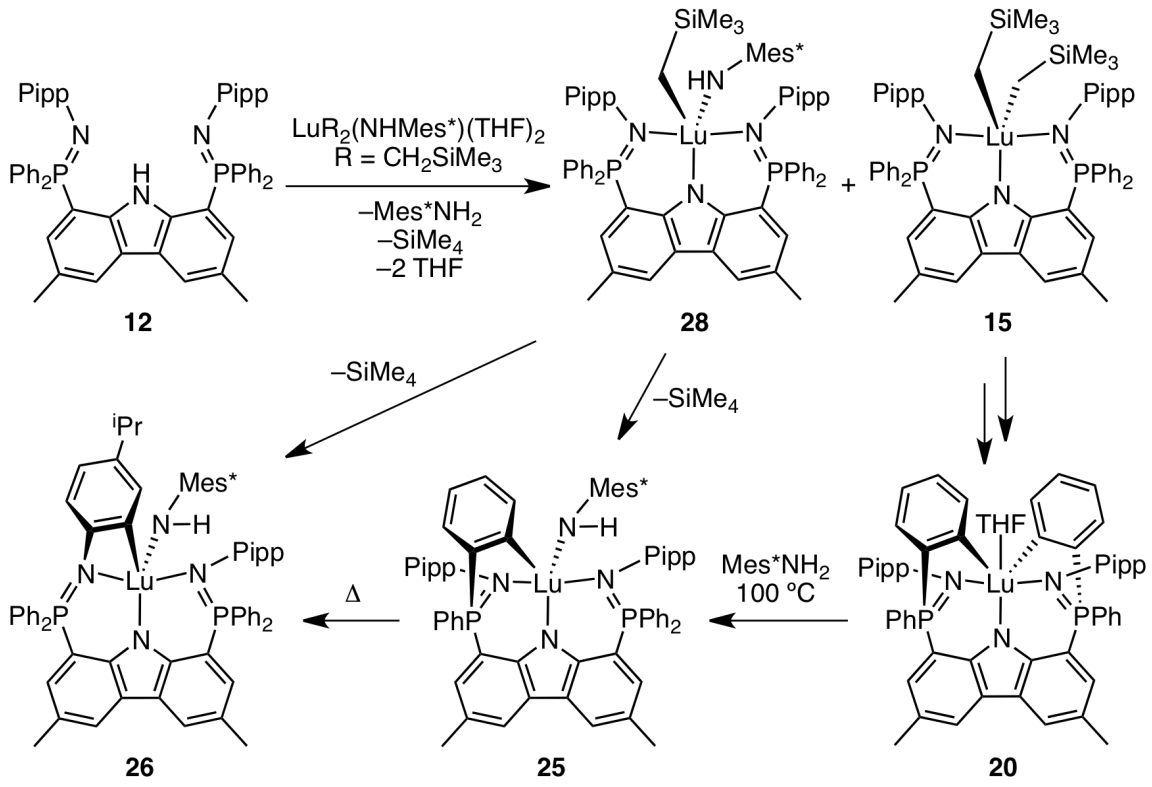

Scheme 4.10 Reactivity of **12** with $Lu(CH_2SiMe_3)(NHMes^*)(THF)_2$

In the thermolysis of **28**, it can be speculated that perhaps instead of proceeding as described above, the complex may rather lose one equivalent of $SiMe_4$, with the formation of a transient lutetium imido intermediate, that then undergoes *N*-aryl metalation to give **26**. This possibility was disproven through a deuterium labeling study, whereby deuterated proteo ligand (**11**-ring-d_{10}) was reacted with **27** (Scheme 4.11).

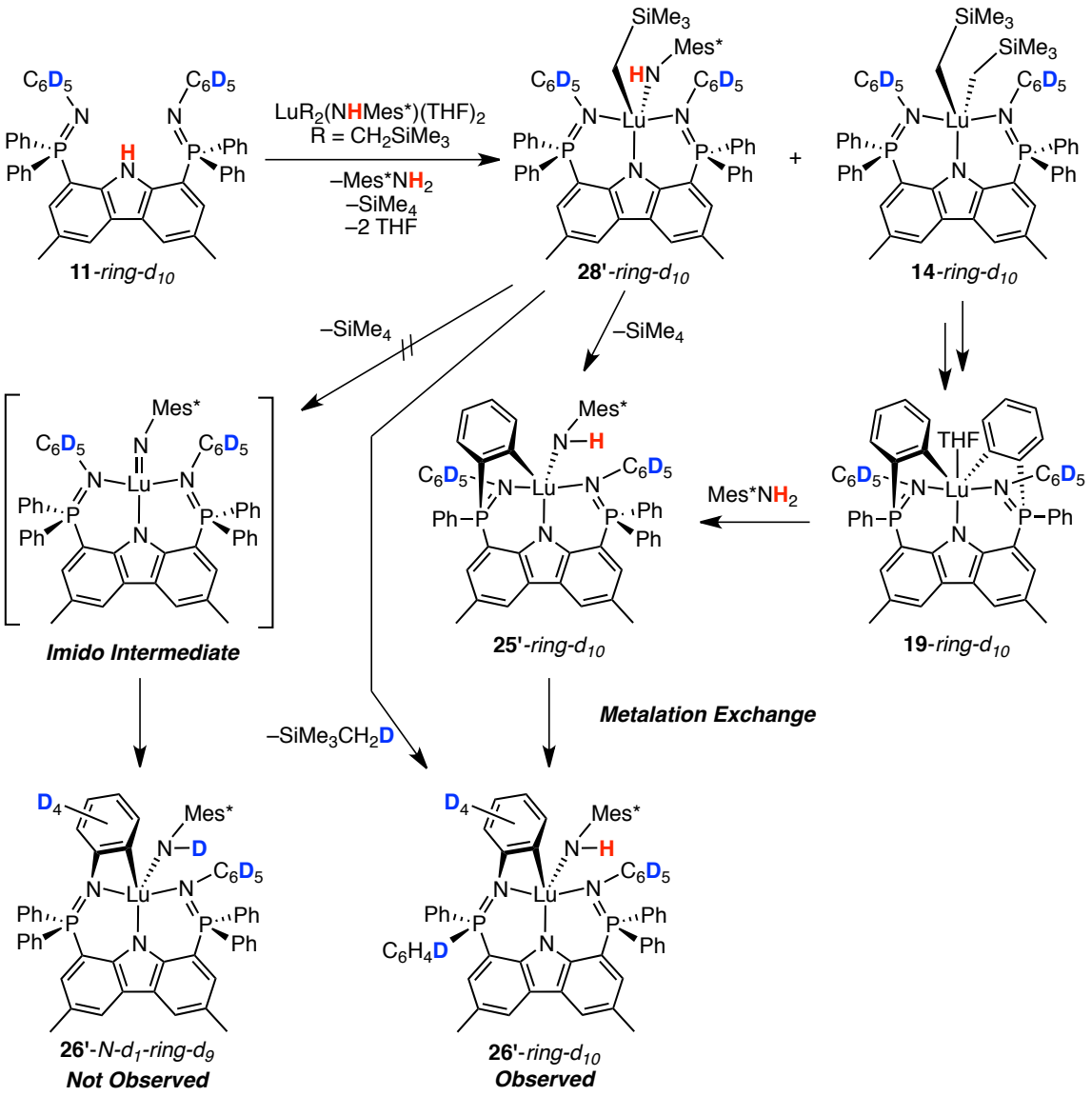

Scheme 4.11 Deuterium labeling experiment 3: reaction of complex **11**-*ring*-d_{10} with $Lu(CH_2SiMe_3)_2(NHMes^*)(THF)_2$, **27**

The starting material **11**-ring-d_{10} contained fully deuterated *N*-phenyl groups as opposed to the proton-containing 4-isopropylphenyl groups in **12**. Much to the same extent as in deuterium labeling experiment 2 (*vide supra*), the lack of an isopropyl group in the *para* position of the *N*-aryl ring, was not expected to cause any variation in the reactivity of **11**-ring-d_{10} compared to **12** (excluding any kinetic isotope effects). As depicted in Scheme 4.11, reaction of **11**-ring-d_{10} with $Lu(CH_2SiMe_3)(NHMes^*)(THF)_2$

would result in the mixture of products **28′**-*ring*-d_{10} and **14**-*ring*-d_{10}, whereby a proton is retained on the anilide nitrogen of **28′**-*ring*-d_{10}. Loss of tetramethylsilane with concomitant *ortho*-metalation would result in final product **26′**-*ring*-d_{10} with a proton retained on the anilide nitrogen. Conversely, in the scenario of a transient lutetium imido intermediate, the anilide proton would be lost upon imido formation, followed by re-metalation of a deuterium-labeled *N*-aryl ring, thus installing a deuterium atom on the anilide nitrogen. Upon following the transformation by ^{1}H NMR spectroscopy, the final product of the reaction of **11**-ring-d_{10} with Lu(CH_2SiMe_3)(NHMes*)$(THF)_2$ was observed to be **26′**-*ring*-d_{10} with a proton bound to the anilide nitrogen. Therefore, deuterium labeling experiment 3 suggests that the thermolysis of **28** does not proceed through a transient lutetium imido intermediate.

4.6 Conclusions

The process of metallacycle ring opening has been probed in detail using a doubly *ortho*-metalated lutetium aryl complex. This acid-base reaction was initially probed using the reagent [Et_3NH]I to promote double metallacycle ring opening of ($\mathbf{L}_{\mathbf{A}}^{\mathbf{Pipp}}$-$\kappa^3N,\kappa^2C^{P\text{-Ph}}$)Lu(THF) to afford the diiodide complex ($\mathbf{L}_{\mathbf{A}}^{\mathbf{Pipp}}$-$\kappa^3N$)$LuI_2$(THF). Similarly, reaction of ($\mathbf{L}_{\mathbf{A}}^{\mathbf{Ar}}$-$\kappa^3N,\kappa^2C^{P\text{-Ph}}$)Lu(THF) with bulky anilines ($MesNH_2$, $TripNH_2$) resulted in double metallacycle ring opening to generate the corresponding bis(anilide) lutetium complexes. Utilization of the extremely sterically demanding Mes*NH_2 promoted single metallacycle ring opening to afford the mono(anilide) complex, ($\mathbf{L}_{\mathbf{A}}^{\mathbf{Pipp}}$-$\kappa^3N,\kappa C^{P\text{-Ph}}$)Lu(NHMes*), **25**, exclusively. The latter product was found to be highly

thermally reactive and rapidly underwent an unusual metalation exchange process to yield ($\mathbf{L}_{\mathbf{A}}^{\mathbf{Pipp}}$-$\kappa^3$*N*,$\kappa$*C*$^{N\text{-Pipp}}$)Lu(NHMes*), **26** in high yield. Through various deuterium labeling and kinetic studies it was determined that complex **26** forms through direct metalation exchange with no evidence of a transient imido intermediate.

Synthesis of the mixed alkyl/anilide complex ($\mathbf{L}_{\mathbf{A}}^{\mathbf{Pipp}}$-$\kappa^3$*N*)Ln($CH_2SiMe_3$)NHMes*, **28**, via the reagent Lu(CH_2SiMe_3)$_2$(NHMes*)(THF)$_2$, **27**, failed to proceed cleanly and resulted in the generation of **15** (and subsequently **20**) as byproducts. The thermolysis reactivity of **28**, generated *in situ* as a mixture, could be followed by deuterium labeling and interestingly, it was found to decompose via *ortho*-metalation to afford **26** as the final thermodynamic product with no evidence of proceeding through a transient imido intermediate.

In an effort to access elusive Lu=E functionalities, future work will explore the reactions of complexes **19** and **20** with the heavier group 15 analogues of Mes*NH_2. These larger congeners may exhibit significantly different reactivity patterns whereby a complex possessing a terminal lutetium-main-group multiple bond may be realized through a metallacycle ring opening pathway.

Chapter 5

Ligand Modulation at Phosphorus

5.1 Overview

A fine balance is required when tuning the steric properties of an ancillary ligand for use in rare earth metal chemistry. Sufficiently bulky groups must be retained on the ligand for the purpose of sterically shielding the metal centre; however, too much bulk can result in extreme steric crowding and dynamic ligand behaviour such as cyclometalation. Chapter 3 outlined structural modifications to the ligand *N*-aryl groups; however, the developed dialkyl lutetium complexes were thermally sensitive and susceptible to intramolecular reactivity by either *ortho*-metalation ($\mathbf{L}_{\mathbf{A}}^{\mathbf{Pipp}}$ and $\mathbf{L}_{\mathbf{A}}^{\mathbf{Ph}}$) or 1,5-alkyl migration ($\mathbf{L}_{\mathbf{A}}^{\mathbf{Pym}}$). The latter problem can be circumvented by avoiding pyrimidine rings in the ligand scaffold. The cyclometalation issue surrounding $\mathbf{L}_{\mathbf{A}}^{\mathbf{Pipp}}$ and $\mathbf{L}_{\mathbf{A}}^{\mathbf{Ph}}$ is more complex due to the fact that these scaffolds are capable of *ortho*-metalation through both the *N*-aryl and *P*-phenyl rings. To address the phosphinimine metalation issue, this

chapter investigates the effect of replacing phenyl rings at phosphorus with less bulky and geometrically constrained moieties.

5.2 Approach to Ligand Modulation at Phosphorus

It was expected that a reduction of steric bulk around the exterior edge of the ligand would dampen undesired cyclometalation pathways. For this purpose, a variety of alternatives to the diphenylphosphine subunit (i, Chart 5.1) have been considered. For example, incorporation of dimethylphosphine groups (ii, Chart 5.1) into the ligand would result in a framework with significantly reduced peripheral steric properties. This structural change would also consequently integrate other beneficial qualities into the ligand framework, such as improved ligand solubility in aliphatic solvents and diagnostic $^2J_{HP}$ NMR coupling.

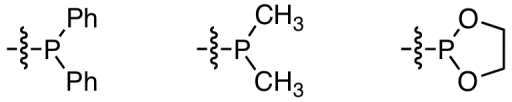

i **ii** **iii**

Chart 5.1 Various $-PR_2$ moieties

In addition to a reduction in steric bulk, it was expected that linking the R groups on phosphorus together could also reduce the propensity for cyclometalation reactions of the phosphinimine functionality. The intention of this approach was to generate a cyclic phosphorus-containing ring with a constrained geometry so that metalative C–H bond activation would be restricted by raising the energy barrier for a highly ordered σ-bond metathesis transition state. Accordingly, the inexpensive and commercially available

dioxaphospholane ring was considered for this purpose (iii, Chart 5.1). Notably, the dioxaphospholane ring possesses both a constrained geometry and oxygen atoms in the α-position to phosphorus, thus eliminating potential for C–H bond activation to occur at those sites. Furthermore, the oxygen atoms were considered to be potential Lewis basic donors, should the ring be able to pivot to within close proximity of the metal centre. To this end, an investigation regarding the effect of dioxaphospholane incorporation into the bis(phosphinimine)carbazole ligand framework and the potential of this geometrically constrained ligand to support highly reactive rare earth dialkyl species was undertaken.

5.3 Synthesis of a Dioxaphospholane Ligand Derivative

Due to the fact that this chapter focuses on modulation of the ligand at the PR_2 sites rather than the *N*-aryl position, *para*-isopropylphenyl rings were selected as the only *N*-aryl group to be used in all ligand derivatives discussed. Compared to other *N*-aryl rings outlined in previous chapters (mesityl, phenyl and pyrimidine) the incorporation of *para*-isopropylphenyl groups has tended to provide a ligand scaffold with the best balance of desirable features. For example, complexes of $\mathbf{L}_{\mathbf{A}}^{\mathbf{Pipp}}$ exhibited reduced steric crowding at the metal coordination pocket compared to the mesityl-substituted ligand $\mathbf{L}_{\mathbf{A}}^{\mathbf{Mes}}$. In terms of reactivity, $\mathbf{L}_{\mathbf{A}}^{\mathbf{Pipp}}$ paralleled that of $\mathbf{L}_{\mathbf{A}}^{\mathbf{Ph}}$ quite closely; however, $\mathbf{L}_{\mathbf{A}}^{\mathbf{Pipp}}$ exhibited superior ^{1}H NMR spectral properties and afforded complexes with enhanced crystallinity. Finally, *para*-isopropylphenyl rings do not have a propensity to undergo 1,5-alkyl shift reactions analogous to that observed with the pyrimidine rings in $\mathbf{L}_{\mathbf{A}}^{\mathbf{Pym}}$.

Using a similar synthetic protocol to that previously reported, the targeted bis(phosphinimine)carbazole ligand containing dioxaphospholane moieties was readily synthesized over three steps from 1,8-dibromo-3,6-dimethyl-9-BOC-carbazole, **2**, as outlined in Scheme 5.1. Dioxaphospholane rings were first installed onto the carbazole framework by lithiation of **2** with four equivalents of *t*-BuLi in diethyl ether followed by addition of 2.2 equivalents of 2-chloro-1,3,2-dioxaphospholane to generate the BOC-protected derivative, **29**. Thermal deprotection of **29** at 160 ºC liberated the desired bis(dioxaphospholane), **30**. Finally, the phosphinimine functionality was installed onto the ligand via a Staudinger reaction of **30** with *para*-isopropylphenyl azide with concomitant loss of N_2 to afford $H\mathbf{L}_{\mathbf{B}}^{\mathbf{Pipp}}$, **31**, in 45.2% overall yield.

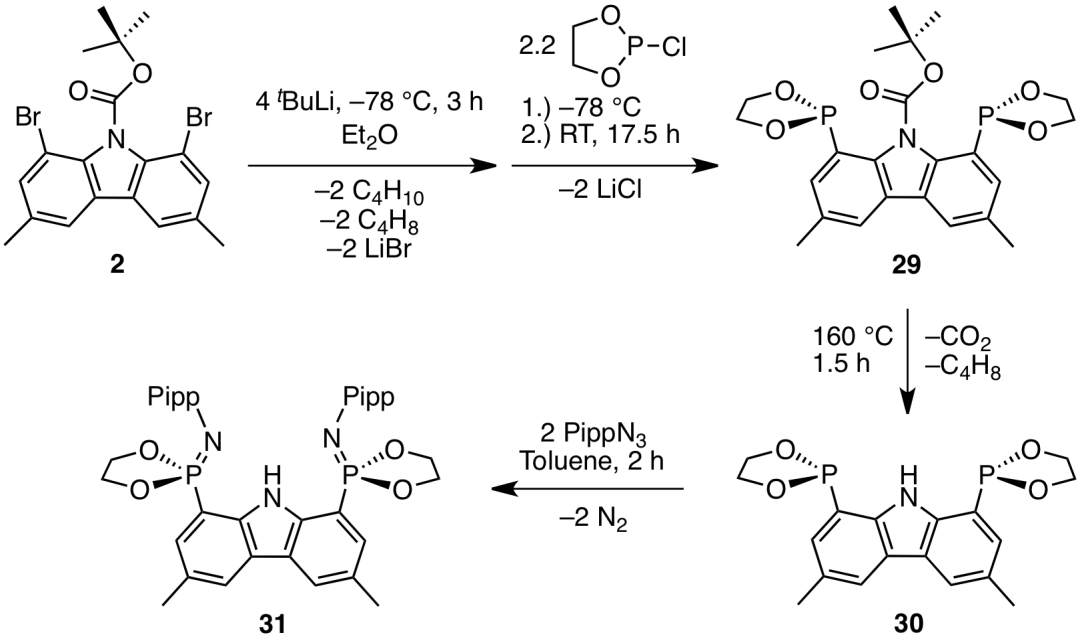

Scheme 5.1 Ligand synthesis incorporating dioxaphospholane rings

The $^{31}P\{^{1}H\}$ NMR resonances (benzene-d_6) of **29** and **30** at δ 148.7 and 167.9, respectively, were observed relatively far downfield, similar to that of the starting

material 2-chloro-1,3,2-dioxaphospholane. However, upon oxidation of the dioxaphospholane centre via the Staudinger reaction, an upfield shift in the $^{31}P\{^{1}H\}$ NMR resonance of **31** was observed (δ 24.2, benzene-d_6).

In order to gain insight into the geometrically constrained nature of the dioxaphospholane ring when attached to the dimethylcarbazole backbone, single-crystal X-ray diffraction experiments were performed on compounds **30** and **31**. Of particular relevance was an investigation into the extent to which the dioxaphospholane ring could pivot about the C–P bond; this information would allow for a qualitative assessment of its conformational influence on the structure of the ancillary ligand.

Recrystallization of **30** from a concentrated pentane solution at ambient temperature afforded single crystals that were suitable for a diffraction experiment. The bis(dioxaphospholane) compound crystallized in the space group $P\bar{1}$ and the molecular structure is depicted in Figure 5.1 as a thermal ellipsoid plot.

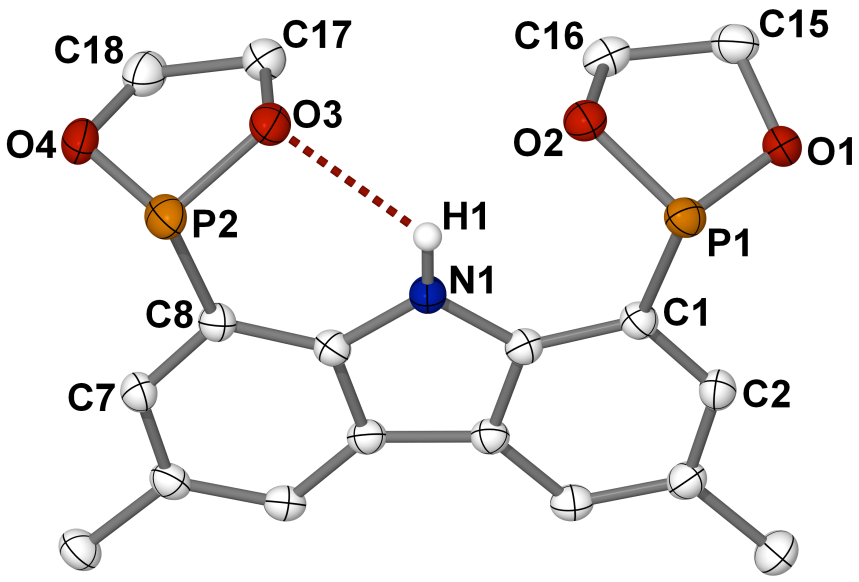

Figure 5.1 Thermal ellipsoid plot (50% probability) of **30** with hydrogen atoms (except H1) omitted for clarity.

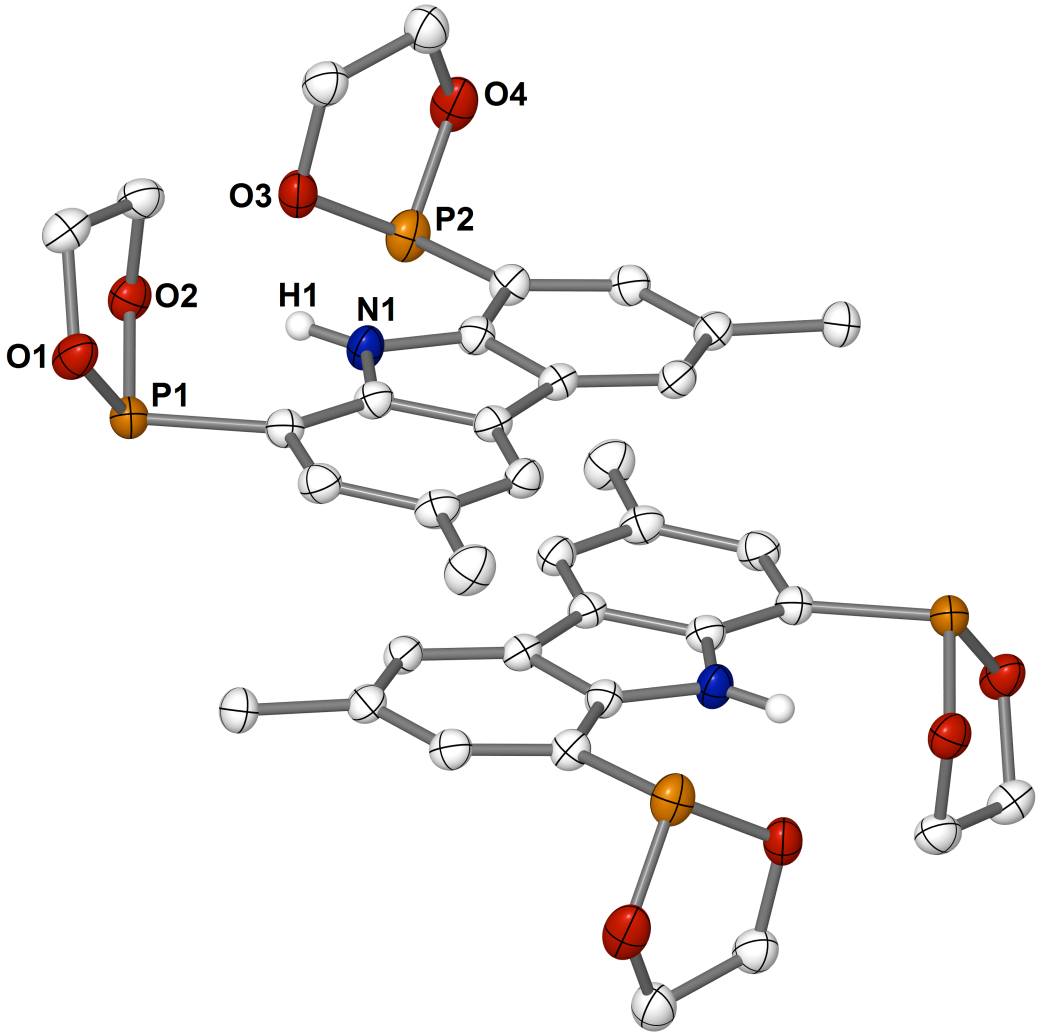

Figure 5.2 Packing diagram of **30** with hydrogen atoms (except H1) omitted for clarity.

In the solid-state structure, both dioxaphospholane rings are positioned so that they are orientated toward the same face of the planar dimethylcarbazole backbone (O2–P1–C1–C2 torsion angle of 152.0(2)° and O3–P2–C8–C7 torsion angle of −155.2(2)°). This particular conformation of the two dioxaphospholane moieties can be attributed to two factors: (i) A hydrogen bonding interaction can occur between an oxygen atom of the dioxaphospholane ring and the carbazole proton. The distance between the donor and acceptor atoms in the N1–H1···O3 interaction in **30** is 2.857(2) Å. A similar contact can

also occur via O2, whereby the donor-acceptor distance for the N1–H1···O2 interaction has been calculated to be 2.877(2) Å. These distances are comparable to the (d(N···N) lengths measured for the N–H···N hydrogen bond in proteo ligands $H\mathbf{L}_{\mathbf{A}}^{\mathbf{Mes}}$, $H\mathbf{L}_{\mathbf{A}}^{\mathbf{Ph}}$, $H\mathbf{L}_{\mathbf{A}}^{\mathbf{Pipp}}$ and $H\mathbf{L}_{\mathbf{A}}^{\mathbf{Pym}}$ in Chapters 2 and 3. (ii) The orientation also allows for energetically favourable aromatic π-π stacking interactions between the carbazole ring systems of two adjacent molecules of **30** in the solid state (average centroid-centroid distance = 3.930 Å). This packing arrangement is depicted in Figure 5.2.

A comparison of the metrical parameters of each dioxaphospholane ring in the molecule revealed slight variations in the P–O bond distances. In one ring, the P1–O2 distance is slightly longer at 1.643(1) Å, compared to the P1–O1 distance of 1.635(1) Å. It is the same case in the other ring, whereby the P2–O3 distance is slightly longer at 1.640(1) Å, compared to the P2–O4 distance of 1.628(2) Å. This elongation in bond lengths for P1–O2 and P2–O3 may be a result of the fact that O2 and O3 are capable of interacting in a hydrogen bond with H1.

Recrystallization of proteo ligand **31** from a concentrated benzene solution layered with pentane at ambient temperature afforded colourless prisms that were suitable for X-ray diffraction. The ancillary ligand crystallized in the orthorhombic space group *Pbca* (#61) and the molecular structure is depicted in Figure 5.3 as a thermal displacement plot. The solid-state structure of **31** adopts a conformation whereby one phosphinimine arm (N1–P1) is held periplanar to the dimethylcarbazole backbone (N1–P1–C1–C2 torsion angle of −165.1(1)°) and the other arm (N3–P2) is rotated further out of the aromatic plane (N3–P2–C8–C7 torsion angle of −140.7(1)°). The alignment of the N1–P1 phosphinimine group is influenced by a hydrogen bond contact between N1 of the

phosphinimine and the carbazole N–H (d(N···N) = 2.817(2) Å). In **31**, the N–P bond distance of the phosphinimine functionalities was measured to be 1.535(1) Å for N1–P1 and 1.534(1) Å for N3–P2. This phosphinimine distance is consistent with the expected double bond character.

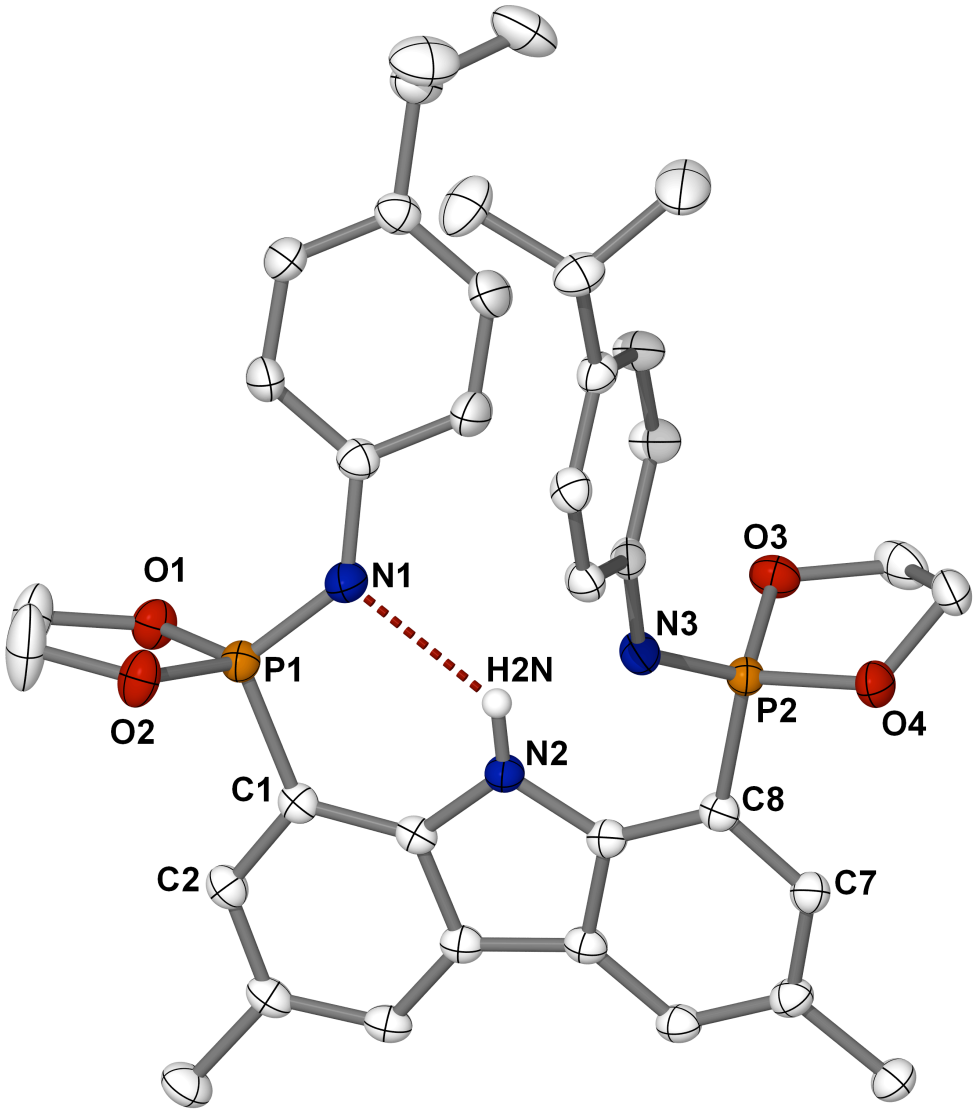

Figure 5.3 Thermal ellipsoid plot (50% probability) of **31** with hydrogen atoms (except H2N) omitted for clarity.

Table 5.1 Selected bond distances /Å, angles /º and torsion angles /º for compounds **30** and **31**

	30	**31**
P1–O1	1.635(1)	1.601(1)
P1–O2	1.643(1)	1.606(1)
P2–O3	1.640(1)	1.610(1)
P2–O4	1.628(2)	1.600(1)
C1–P1	1.839(2)	1.777(2)
C8–P2	1.829(2)	1.777(2)
N1–P1[b]	—	1.535(1)
N3–P2[b]	—	1.534(1)
N2···N1[b]	—	2.817(2)
N2···N3[b]	—	3.048(2)
N1···O2[a]	2.877(2)	—
N1···O3[a]	2.857(2)	—
O1–P1–O2	95.47(7)	96.37(6)
O3–P2–O4	94.56(7)	96.66(6)
C1–P1–O2	100.66(8)	107.76(7)
C1–P1–O1	101.35(8)	107.46(7)
C8–P2–O3	100.56(8)	108.32(7)
C8–P2–O4	101.84(8)	106.99(7)
C1–P1–N1[b]	—	106.82(7)
C8–P2–N3[b]	—	108.14(7)
C2–C1–P1–O2	152.0(2)	66.4(1)
C2–C1–P1–O1	54.2(2)	−36.5(1)
C7–C8–P2–O3	−155.2(2)	91.7(1)
C7–C8–P2–O4	−58.2(2)	−11.6(2)
C2–C1–P1–N1[b]	—	−165.2(1)
C7–C8–P2–N3[b]	—	−140.7(1)

Note: [a]The listed parameter pertains only to complex **30**. [b]The listed parameter pertains only to complex **31**.

Each phosphorus atom in the proteo ligand exhibits roughly tetrahedral geometry. Of particular interest are the O–P–O bond angles of 96.37(6)° and 96.66(6)° for O1–P1–O2, and O3–P2–O4, respectively. Both of these angles are significantly smaller than the average tetrahedral angle at phosphorus (avg = 109.32° for P1 and P2), and from this it can be inferred that the nature of the dioxaphospholane rings indeed constrain the oxygen

atoms to the peripheral edge of the ligand. As such, the solid-state geometry of **31** suggests that when the ligand is coordinated in a tridentate mode to a metal via N1, N2, and N3, the tetrahedral bond angles at phosphorus would persist and the dioxaphospholane moiety would be held away from the metal. This described geometry is ideal for the purpose of designing a ligand that is resistant to cyclometalation of the PR_2 groups.

5.4 Ring Opening Insertion Reactivity

The proteo ligand was readily complexed with lutetium via the alkane elimination reation of **31** with $Lu(CH_2SiMe_3)_3(THF)_2$ (Scheme 5.2). *In situ* observation of the reaction in benzene-d_6 solution revealed the rapid formation of dialkyl complex **32** at ambient temperature with concurrent loss of one equivalent of $SiMe_4$ and two equivalents of THF. Unfortunately, **32** was found to be quite thermally reactive and rapidly decomposed to a new product; consequently, the dialkyl lutetium complex could not be isolated as a solid.

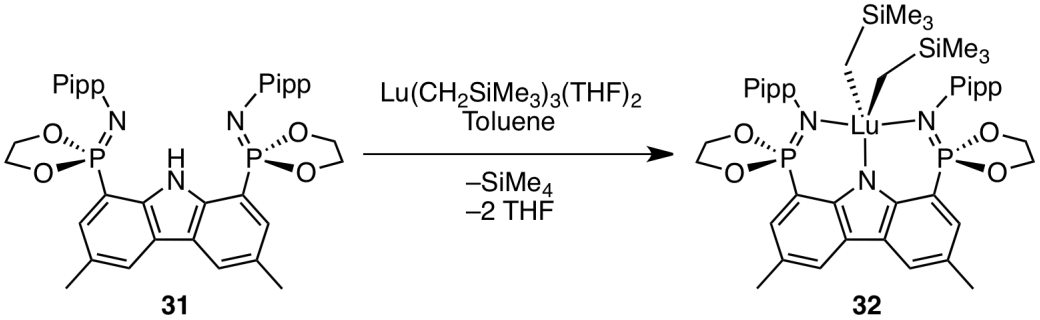

Scheme 5.2 Metal complexation of HL_B^{Pipp}

Full NMR characterization of **32** at low temperature (−10 ºC) in toluene-d_8 was attempted; however, even at reduced temperature, the spectra were found to be consistently contaminated with signals arising from reaction intermediates and the final decomposition product, resulting in ambiguous peak assignments. To a large degree, the NMR signals corresponding to the final decomposition product (*vide infra*) could be subtracted from the spectra of **32**, allowing for fair confidence in ^{1}H and ^{31}P{^{1}H} NMR assignments. Unfortunately, this process was not suitable for assigning ^{13}C{^{1}H} NMR signals for **32**, due to the complexity of the spectrum. In the ^{31}P{^{1}H} NMR spectrum (benzene-d_6) of **32**, a downfield shift was observed from that of free proteo ligand to 56.2 ppm. The expected methylene and $SiMe_3$ signals were observed in the ^{1}H NMR spectrum (benzene-d_6) at δ −0.28 and 0.24, respectively.

When the thermal decomposition of **32** was followed *in situ* at ambient temperature in benzene-d_6 solution, the ^{31}P{^{1}H} NMR spectrum revealed the initial formation of four new signals with equal integrations and a decrease in the dialkyl resonance. Likewise, the ^{1}H NMR spectrum (benzene-d_6) also displayed four sets of new signals with equal integrations growing in place of those for **32**. Particularly evident in the ^{1}H NMR spectrum was the presence of four new $SiMe_3$ signals at δ −0.167, −0.212, −0.400, and −0.562 and four carbazole methyl signals at δ 2.60, 2.51, 2.47 and 2.42 (Figure 5.4). If left overnight at ambient temperature, full conversion of **32** to a new product **33** occurred. Alternatively, heating a solution of **32** to 100 ºC for 80 min allowed for rapid synthesis of the decomposition product **33**.

While it was evident from the NMR spectra that **33** was an asymmetric bimetallic complex, its identity could not initially be assigned with confidence. The presence of four

$SiMe_3$ signals in the ^1H NMR spectrum and zero formation of tetramethylsilane as a decomposition byproduct suggested that the thermal reactivity of **32** did not involve a cyclometalative alkane elimination mechanism (as previously observed wtih **14** and **15**). Particularly perplexing, however, was the fact that while four $SiMe_3$ signals were observed slightly upfield of 0 ppm in the ^1H NMR spectrum, there was no sign of any methylene signals in that region of the spectrum, as would be expected for a complex containing $Lu–CH_2SiMe_3$ groups. Rather, various methylene signals were observed further downfield in the spectrum as series of overlapping multiplets between 4.7–3.2 ppm and 2.0–1.4 ppm (Figure 5.4).

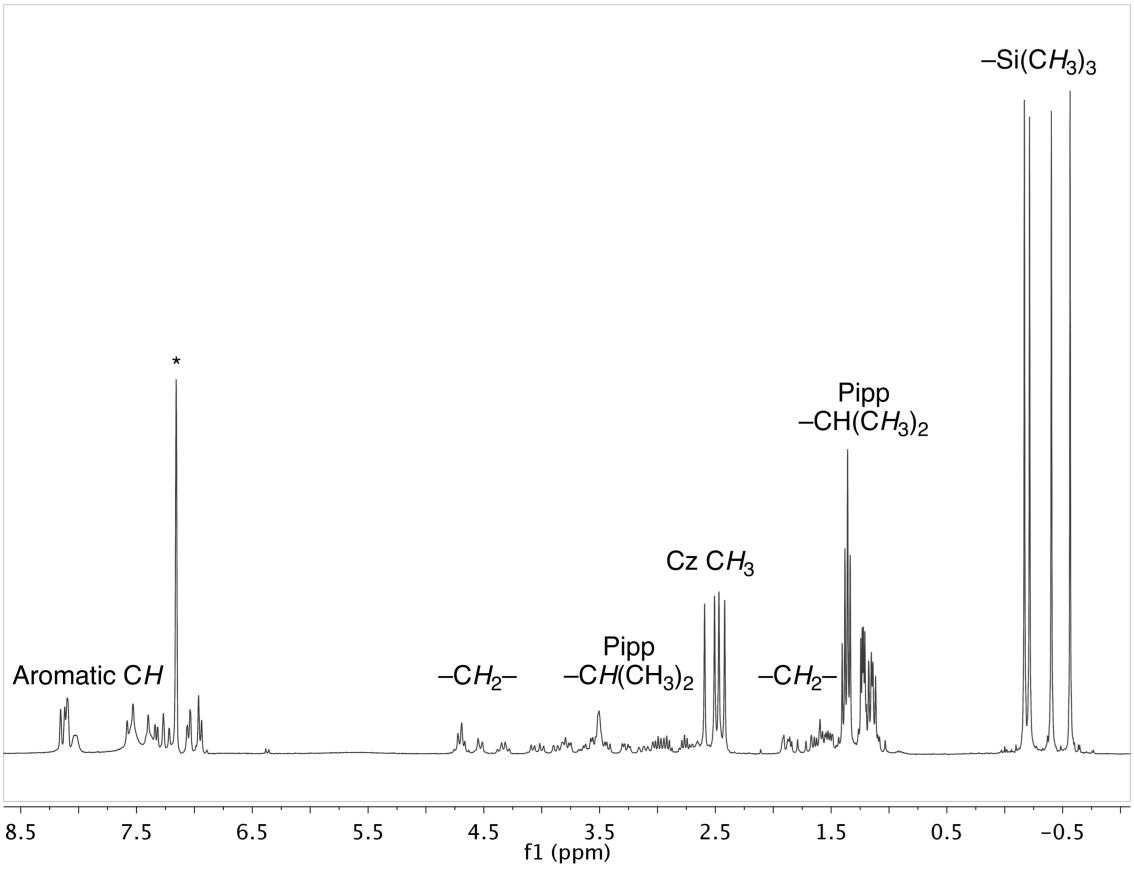

Figure 5.4 ^1H NMR spectrum (benzene-d_6) of **33**. Solvent signal is denoted by an asterisk

Analysis of the complex by a DEPT-135 NMR experiment revealed twelve different methylene signals, eight of which could be catagorized as –O*C*H_2– moieties, and four as –*C*H_2SiMe_3 groups (Figure 5.5). Of the eight –O*C*H_2– methylene signals, five were split into doublets by J_{CP} spin-spin coupling of varying degrees. Four of the five exhibited coupling constants between 7 and 11 Hz, suggesting 2-bond coupling between carbon and phosphorus; while the fifth displayed a smaller coupling constant of 5 Hz, indicative of longer range (3-bond) coupling. All four signals corresponding to the –*C*H_2SiMe_3 methylene carbon atoms were split into doublets by J_{CP} coupling. Interestingly, the –*C*H_2SiMe_3 methylene doublets exhibited very large J values between 84 and 93 Hz, which was suggestive of 1-bond coupling between carbon and phosphorus. On these grounds, the methylene signals in the spectrum were consistent with a compound that contained four inequivalent PCH_2SiMe_3 moieties and four $POCH_2CH_2O$– chains.

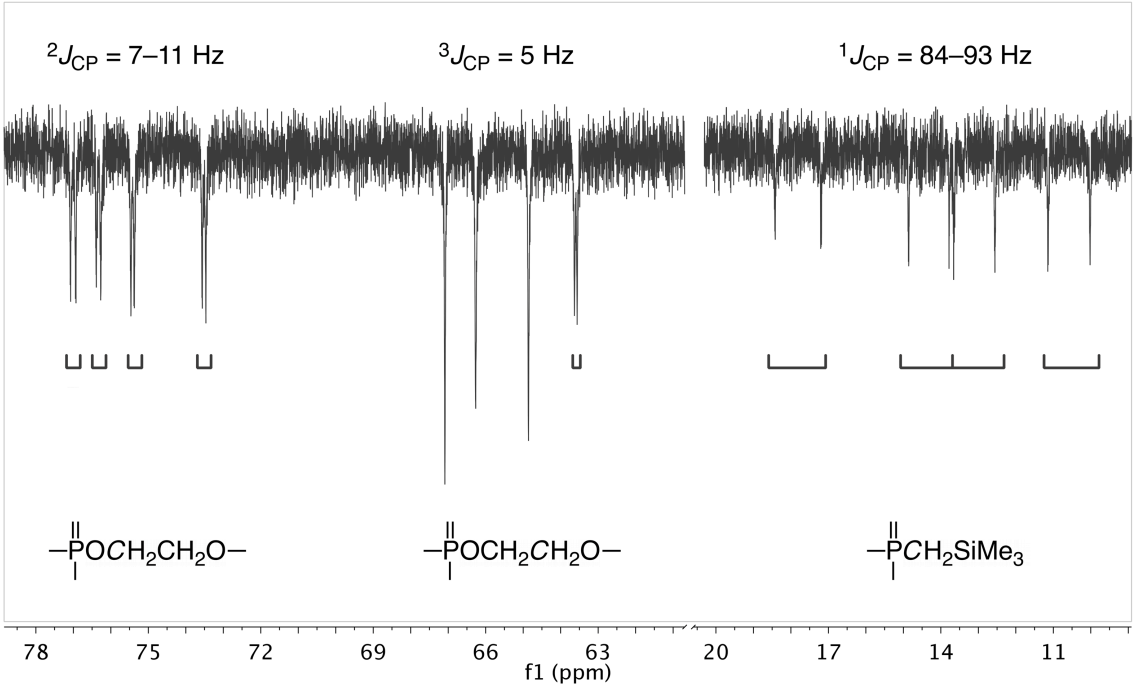

Figure 5.5 Methylene regions in the DEPT-135 NMR spectrum of **33**

From the described NMR data, it was premised that the structure of **33** was likely the product of a ring opening insertion reaction of the ligand dioxaphospholane rings into the lutetium alkyl bonds of **32**. Accordingly, the expected structure would contain trimethylsilylmethyl groups bound to phosphorus and ethylene glycoxide moieties connecting lutetium to a phosphorus atom of the ligand. The product of this reaction is depicted in Scheme 5.3 as an asymmetric bimetallic complex.

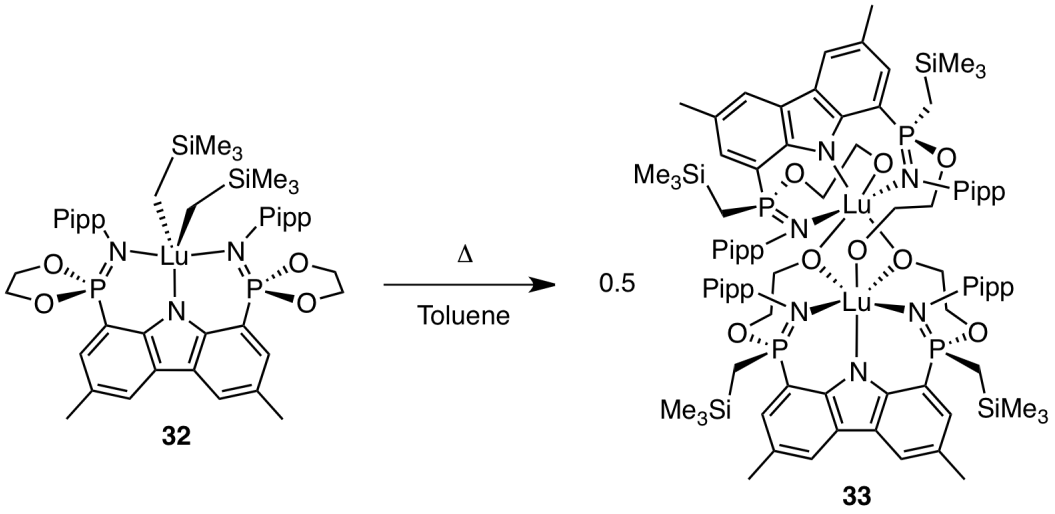

Scheme 5.3 Dioxaphospholane ring opening insertion

In order to unambigously determine the structure of **33**, a single-crystal X-ray diffraction experiment was performed. Single crystals suitable for diffraction analysis were obtained from a concentrated benzene solution layered with pentane; the molecular structure is depicted in Figure 5.6 as a thermal displacement plot. As suggested by the NMR spectroscopic data, the solid-state structure of **33** was found to be an asymmetric bimetallic complex with one trimethylsilylmethyl group bound to each phosphorus atom, in addition to ethylene glycoxide moieties linking each phosphorus atom to a lutetium metal centre.

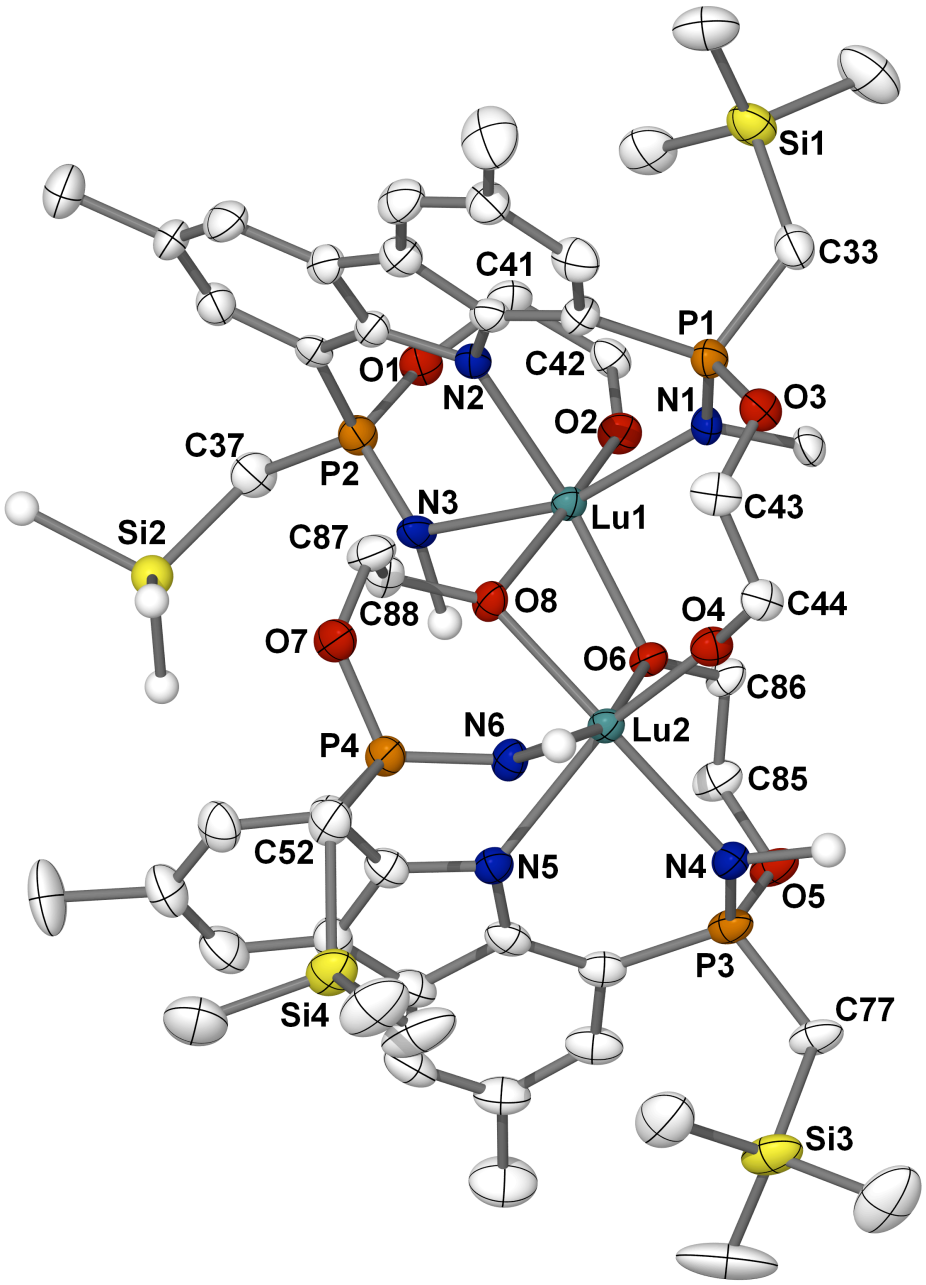

Figure 5.6 Thermal ellipsoid plot (50% probability) of **33** with hydrogen atoms and *para*-isopropylphenyl rings (except for *ipso* carbons) omitted for clarity. Positionally disordered atoms are depicted as spheres of arbitrary radius.

A unique structural feature of this bimetallic complex is that the two subunits are held together through Lewis acid-base interactions via the bridging alkoxy groups (O6 and O8), as well as by an anionic ligand-to-metal bonding interaction whereby the

ethylene glycoxide moiety from one subunit is tethered to the other subunit through the O4–Lu2 bond. As expected, the bridging lutetium alkoxide bonds are longer (2.228(4) Å, 2.245(4) Å, 2.285(4) Å, and 2.207(4) Å for Lu1–O6, Lu2–O6, Lu1–O8, and Lu2–O8, respectively) than the terminal lutetium alkoxide distances (2.058(4) Å and 2.028(4) Å for Lu1–O2 and Lu2–O4, respectively). The complex exhibits typical bond angles of 104.3(2)° and 103.7(1)° for the bridging Lu1–O6–Lu2 and Lu1–O8–Lu2 interactions, respectively).

Table 5.2 Selected bond distances /Å and angles /º for compound **33**

Lu1–N1	2.337(5)	Lu2–N4	2.379(5)
Lu1–N2	2.358(5)	Lu2–N5	2.359(5)
Lu1–N3	2.385(5)	Lu2–N6	2.423(4)
Lu1–O2	2.058(4)	Lu2–O4	2.028(4)
Lu1–O6	2.228(4)	Lu2–O6	2.245(4)
Lu1–O8	2.285(4)	Lu2–O8	2.207(4)
P1–N1	1.585(5)	P3–N4	1.591(5)
P2–N3	1.581(5)	P4–N6	1.581(5)
Lu1–O6–Lu2	104.3(2)	Lu1–O8–Lu2	103.7(1)
O6–Lu1–N2	155.3(1)	N4–Lu2–O8	157.8(2)
N3–Lu1–N1	163.6(2)	N5–Lu2–O4	156.7(2)
O2–Lu1–O8	168.0(2)	N6–Lu2–O6	160.8(1)

In **33**, each lutetium centre exhibits distorted octahedral geometry with three sites occupied by alkoxide ligands and the remaining coordination sites defined by the ancillary ligand. Interestingly, the pincer ligand chelated to Lu1 adopts a meridional geometry around the metal via N1, N2 and N3, while a facial geometry is enforced at Lu2 as a result of the unique coordination mode of N4, N5 and N6 to the metal. The facial coordination mode of the ligand at Lu2 is somewhat surprising considering that the pincer design of the ancillary ligand was intended to enforce solely a meridional geometry. At the same time, the ligand was also designed to support highly reactive

organolanthanide complexes rather than react with them so it can be surmised that this particular ligand scaffold possesses the ability to deviate from its intended reaction behaviour.

5.5 Mechanistic Considerations

The ring opening insertion reactivity that led to the formation of **33** is the first example of a lanthanide alkyl cleaving a phosphonimidate ester P–O bond. Comparable reactivity has previously been documented in early transition metal chemistry. For example, a titanium benzyne species cleaved a P–O bond of trimethylphosphite to afford a titanium aryl/alkoxide product.[186] Likewise, the reaction of trialkylphosphites with group 1 and group 2 organometallic reagents is an analogous transformation. In the generation of **33**, the mechanism presumably proceeds by coordination of an oxygen atom of the dioxaphospholane ring to lutetium, followed by ring opening insertion via a four-centred transition state. This process is repeated a total of four times, either in parallel or sequentially, to afford product **33** (Scheme 5.4).

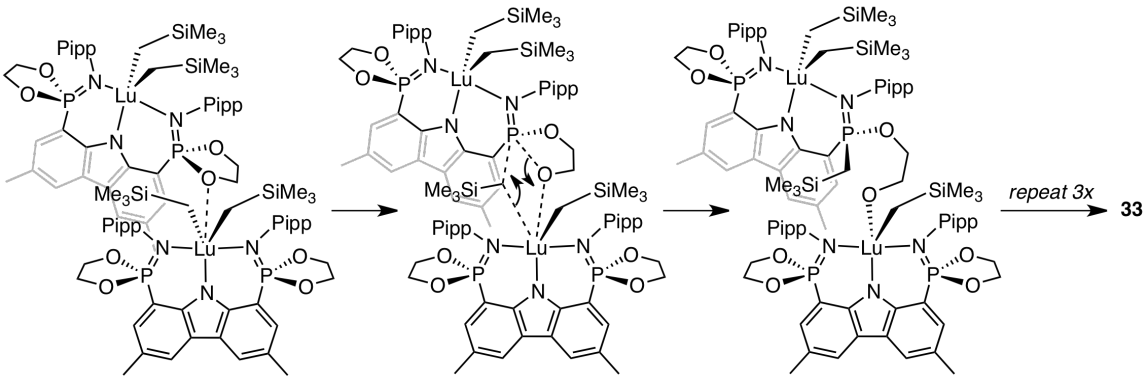

Scheme 5.4 Proposed mechanism for dioxaphospholane ring opening insertion

While the cyclic, constrained geometry of the dioxaphospholane rings on the pincer ligand seemed well suited towards the restriction of cyclometalation reactions at the PR_2 sites, the presence of phosphonimidate ester P–O bonds caused detrimental effects. Due to the high reactivity of lanthanide alkyl bonds with the phosphonimidate ester functionality of the dioxaphospholane rings, $\mathbf{L_B^{Pipp}}$ was found to be unsuitable for further use as a ligand in rare earth organometallic chemistry. Research into the oxygen-free phospholane analogue to $\mathbf{L_B^{Pipp}}$ as a "cyclometalation resistant" pincer ligand is currently underway in the Hayes research group (Chart 5.2).[187] In the absence of reactive phosphonimidate ester P–O bonds, it is expected that the constrained geometry of a five-membered phospholane ring in the bis(phosphinimine)carbazole pincer framework should afford a ligand that is capable of supporting highly reactive organolanthanide complexes.

dioxaphospholane ***phospholane***

Chart 5.2 Dioxaphospholane and phospholane rings

5.6 Synthesis of a Dimethylphosphino Ligand Derivative

Due to the propensity for the dioxaphospholane moieties in $\mathbf{L_B^{Pipp}}$ to react via ring opening insertion with lanthanide alkyls, a different R group at phosphorus was required. To this end, the phosphonite ester P–O bond reactivity of the dioxaphospholane rings on the ligand was exploited in order to derivatize phosphorus with methyl groups. Reaction

of **30** with five equivalents of methyllithium in a toluene/THF mixture at 100 ºC, followed by aqueous workup resulted in the clean formation of 1,8-bis(dimethylphosphino)-3,6-dimethylcarbazole, **34**, in high yield (81.4%). Subsequent reaction of **34** with *para*-isopropylphenyl azide liberated ligand $H\mathbf{L}_{\mathbf{C}}^{\mathbf{Pipp}}$, **35**, with loss of dinitrogen.

While compound **30** proved to be a useful reagent for preparing **34**, it was found that the BOC-protected derivative **29** was not suitable for use in an analogous reaction with methyllithium. It was observed that methyllithium does not react with the phosphonite ester P–O bonds at ambient temperature and must be heated to 100 ºC in order to promote substitution. However, the BOC-protecting group is thermally reactive (hence why a thermal deprotection strategy is used in this thesis), and heating complex **29** results in loss of the BOC group as CO_2 and isobutene. For this reason, it was more efficient to utilize the deprotected compound **30** in the reaction rather than BOC-protected **29**.

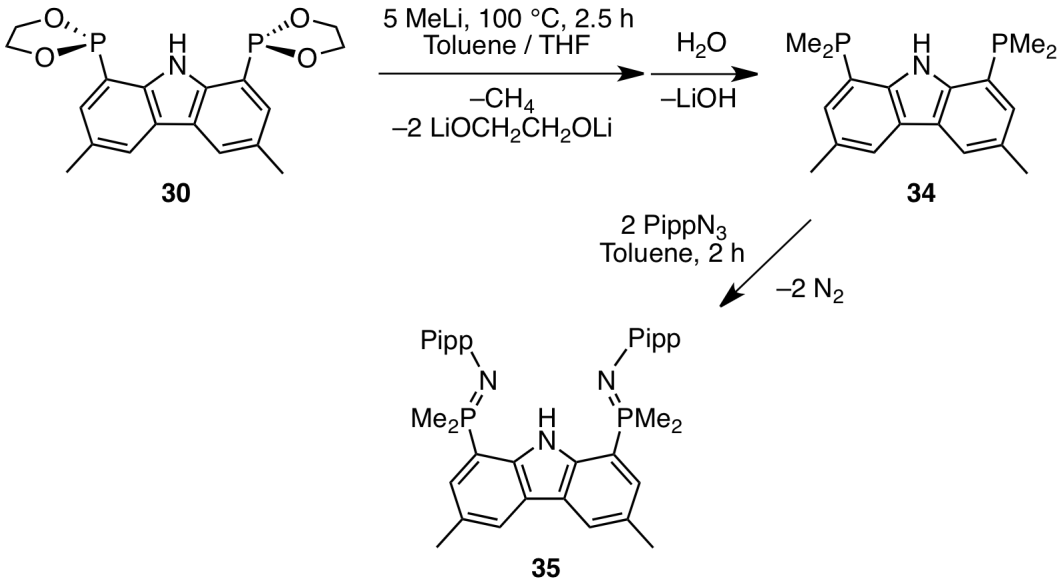

Scheme 5.5 Synthesis of dimethylphosphine-substituted ligand $\mathbf{HL}_{\mathbf{C}}^{\mathbf{Pipp}}$ (**35**)

The $^{31}P\{^{1}H\}$ NMR spectrum (benzene-d_6) of proteo ligand **35** gives rise to a single resonance at δ 5.4 and the ^{1}H NMR spectrum (chloroform-*d*) supports the expected structure (Figure 5.7). In particular, a doublet at δ 1.82 corresponding to the *P*-methyl groups ($^{2}J_{HP}$ = 12.7 Hz, 12H) is evident in the spectrum. The methyl groups on carbazole give rise to a singlet at δ 2.55 (6H) and the NH proton resonates as a broad singlet at δ 11.18 (1H). In the aromatic region, the expected *para*-isopropylphenyl (δ 6.87, d; δ 6.78, d) and carbazole CH protons (δ 7.99; δ 7.37, d) can be easily identified.

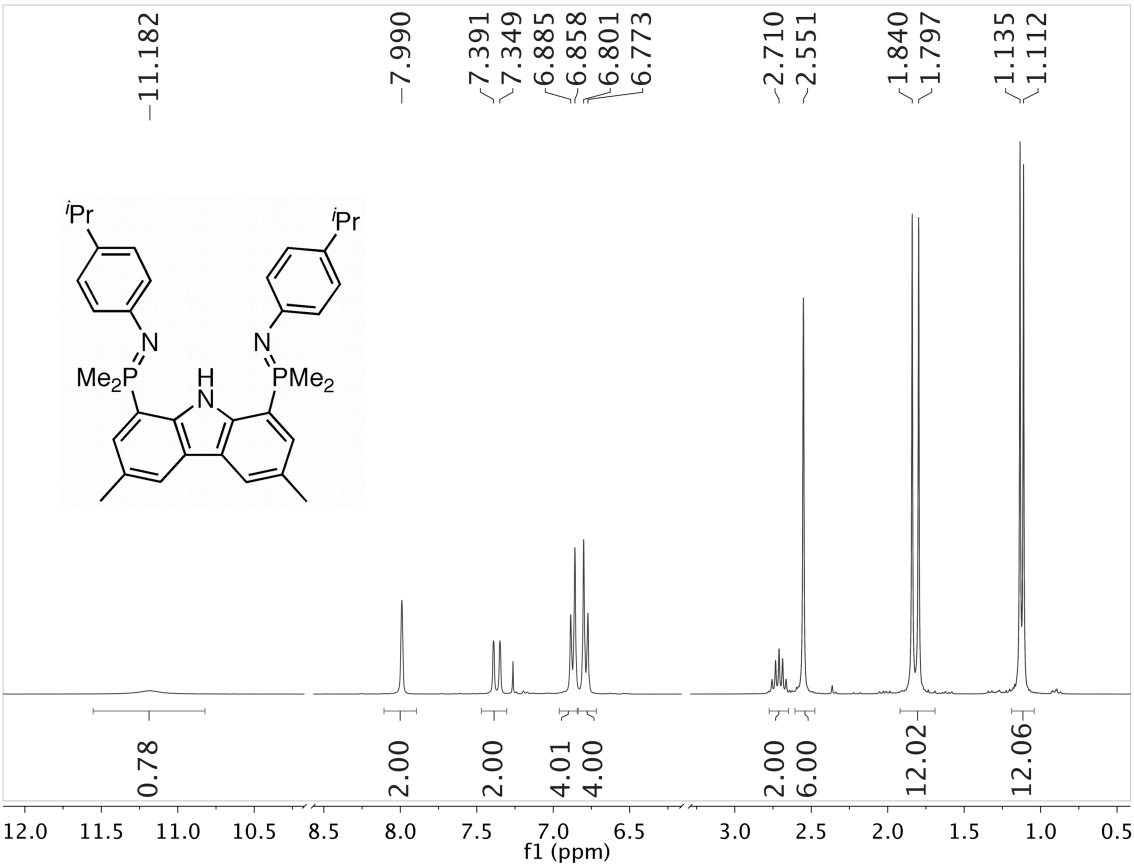

Figure 5.7 ^{1}H NMR spectrum (chloroform-*d*) of $\mathbf{HL}_{\mathbf{C}}^{\mathbf{Pipp}}$ (**35**)

In addition to full characterization of **35** by multinuclear NMR spectroscopy, its solid-state structure was also determined by single-crystal X-ray diffraction. The

molecular structure is depicted in Figure 5.8 as a thermal ellipsoid plot and selected metrical parameters are listed in Table 5.3.

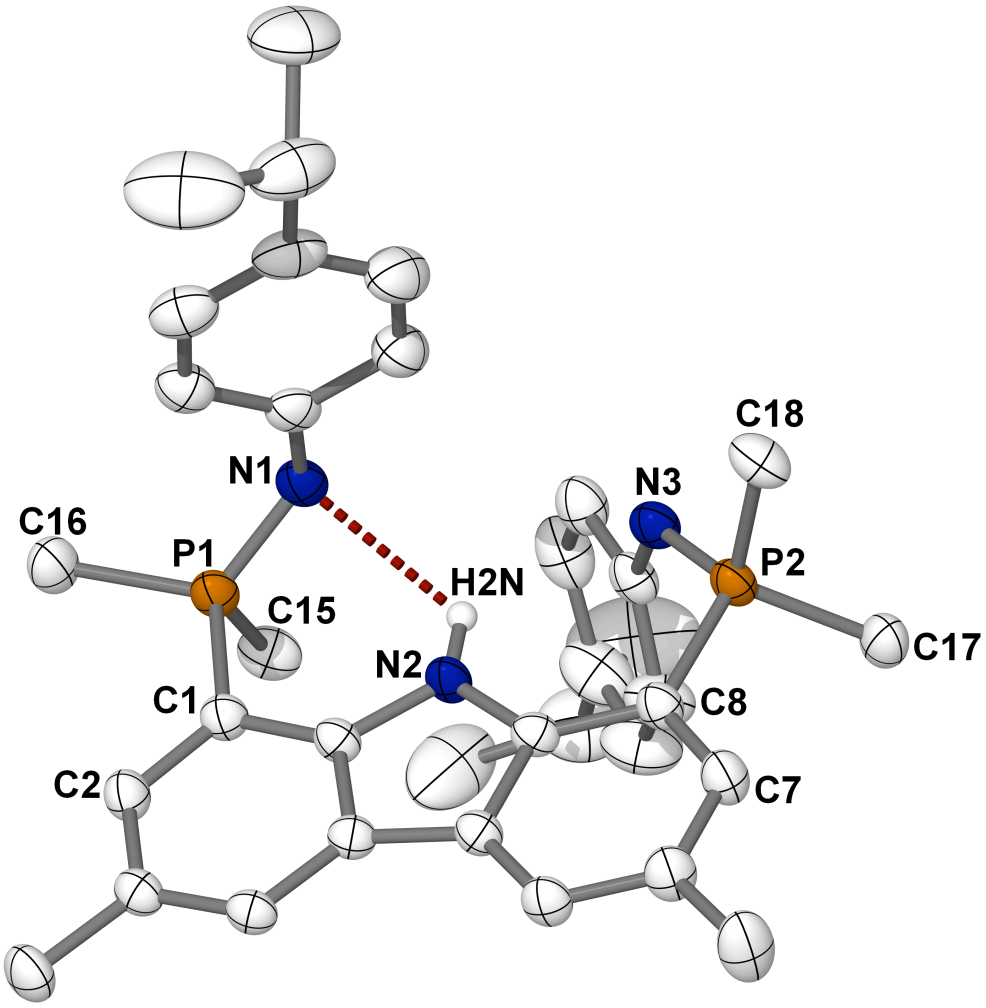

Figure 5.8 Thermal ellipsoid plot (50% probability) of **35** with hydrogen atoms (except H2N), omitted for clarity.

Ligand **35** adopts a comparable solid-state structure to the other structurally characterized proteo ligands described previously. Accordingly, one phosphinimine group (N3–P2) is held periplanar to the dimethylcarbazole backbone (N3–P2–C8–C7 torsion angle of 170.8(2)°) and the other arm (N1–P1) is rotated away from the aromatic plane (N1–P1–C1–C2 torsion angle of 147.9(2)°). Relatively long hydrogen bond

contacts can exist between the carbazole N–H and the nitrogen atoms of both phosphinimine subunits (d(N2···N1) = 2.972(2) Å and d(N2···N3) = 3.010(2) Å). Despite being rotated further away from the aromatic plane, N1 exhibits a shorter distance to N2 compared to the N2···N3 bond length. This discrepancy can be attributed to the more acute N1–P1–C1 bond angle of 111.83(8)º, compared to the N3–P2–C8 angle of 115.36(7)º. The phosphinimine double bond lengths in **35** are similar to each other with distances of 1.580(1) Å and 1.579(1) Å for N1–P1 and N3–P2, respectively.

Compared to the dioxaphospholane proteo ligand **31**, the bond angles measured at each phosphorus atom in **35** exhibit marked differences. Specifically, the bond angles of 105.1(1)° and 105.8(1)° for C15–P1–C16 and C17–P2–C18, respectively, were substantially larger than the corresponding O–P–O bond angles in **31** (96.37(6)° and 96.66(6)°). This difference can be explained by the fact that the geometry at phosphorus in **35** is not constrained into a five-membered ring, as is the case in compound **31**.

Table 5.3 Selected bond distances /Å, angles /º and torsion angles /º for compound **35**

P1–C15	1.788(2)	P1–C16	1.806(2)
P2–C17	1.805(2)	P2–C18	1.793(2)
C1–P1	1.808(2)	C8–P2	1.809(2)
N1–P1	1.580(1)	N3–P2	1.579(1)
N2···N1	2.972(2)	N2···N3	3.010(2)
C15–P1–C16	105.1(1)	C17–P2–C18	105.8(1)
C1–P1–C15	107.0(1)	C1–P1–C16	106.3(1)
C8–P2–C17	105.1(1)	C8–P2–C18	106.4(1)
C1–P1–N1	111.83(8)	C8–P2–N3	115.36(7)
C2–C1–P1–C15	−95.6(2)	C7–C8–P2–C18	−71.4(2)
C2–C1–P1–C16	16.2(2)	C2–C1–P1–N1	147.9(2)
C7–C8–P2–C17	40.5(2)	C7–C8–P2–N3	170.8(2)

5.7 Reactivity of Ligand H$\mathbf{L}_{\mathbf{C}}^{\mathbf{Pipp}}$

In order to probe the ability of H$\mathbf{L}_{\mathbf{C}}^{\mathbf{Pipp}}$, **35**, to support dialkyl lutetium complexes, the ligand was reacted with $Lu(CH_2SiMe_3)_3(THF)_2$ in benzene-d_6 at ambient temperature and the reaction was monitored by ^1H and $^{31}P\{^1H\}$ NMR spectroscopy. Unfortunately, the result of this experiment was a mixture of ill-defined products. It is probable that the alkane elimination reaction initially proceeded as expected to afford ($\mathbf{L}_{\mathbf{C}}^{\mathbf{Pipp}}$-$\kappa^3$*N*)$Lu(CH_2SiMe_3)_2$; however, this product was likely extremely thermally unstable and rapidly decomposed via unknown routes. It is possible that the complex decomposed by a combination of intra- and inter-molecular ligand cyclometalation of *N*-aryl rings and/or *P*-methyl groups, but this has not been established due to the complexity of the resultant mixture of products.

It was reasoned that incorporation of additional σ-donor ligands into the complex would assist in stabilizing an organometallic complex of $\mathbf{L}_{\mathbf{C}}^{\mathbf{Pipp}}$. Two equivalents of THF were already known to be present in the reaction mixture as byproducts of the alkane elimination reaction of proteo ligand with the reagent $Lu(CH_2SiMe_3)_3(THF)_2$. As a donor ligand, THF can impart significant stability to a metal complex by providing electron density and occupying a coordination site. It was expected however, that replacement of THF with a stronger σ-donor ligand would afford a more thermally robust product.

The lutetium alkyl reagent, $Lu(CH_2SiMe_3)_3(THF)_2$, can be used to illustrate this point. With the coordination of two THF donors, $Lu(CH_2SiMe_3)_3(THF)_2$ is thermally sensitive and will decompose at a moderate rate at ambient temperature. However, replacement of the THF ligands with strongly electron donating groups has yielded

complexes with improved thermal sensitivity, such as (^{t}Bu$_2$bpy)Lu(CH_2SiMe_3)$_3$,[177] (^{i}Pr-trisox)Lu(CH_2SiMe_3)$_3$,[188] and (12-crown-4)Lu(CH_2SiMe_3)$_3$,[189] where ^{t}Bu$_2$bpy = 4,4″-di-*tert*-butyl-2,2″-bipyridyl, ^{i}Pr-trisox = 1,1,1-tris[(*S*)-4-isopropyloxazolinyl]ethane and 12-crown-4 = 1,4,7,10-tetraoxacyclododecane. In this work, replacement of the THF moieties with 4-dimethylaminopyridine (DMAP) ligands as strong σ-donors has been pursued. DMAP has proved to be an effective σ-donor ligand in rare earth metal chemistry and was in fact recently celebrated for its role as a Lewis base in stabilizing the first unambiguous example of a terminal scandium imido complex (Scheme 5.6).[92]

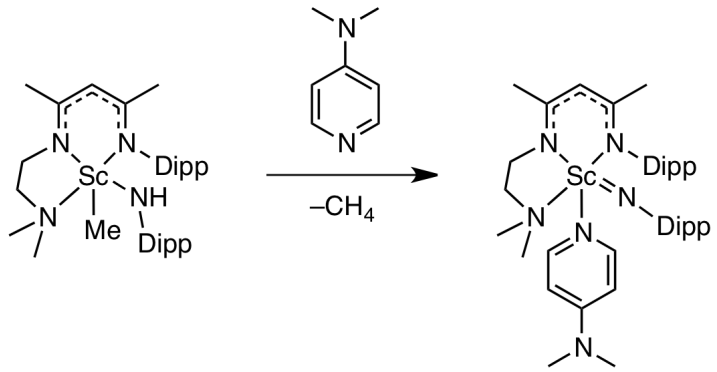

Scheme 5.6 Synthesis of a terminal scandium imido complex

The novel complex Lu(CH_2SiMe_3)$_3$(DMAP)$_2$, **36**, was readily synthesized by reaction of Lu(CH_2SiMe_3)$_3$(THF)$_2$ with two equivalents of DMAP in toluene solution and the THF byproduct was easily removed under vacuum (Scheme 5.7). In benzene-d_6, the ^{1}H NMR spectrum of **36** exhibits methylene and methyl signals at δ −0.24 and δ 0.42, integrating to 6 and 27 protons, respectively. The spectrum also contains a singlet at δ 2.05 corresponding to the dimethylamino group of DMAP and two doublets at δ 6.00 and δ 8.74, each integrating to 4H, corresponding to the DMAP aromatic protons.

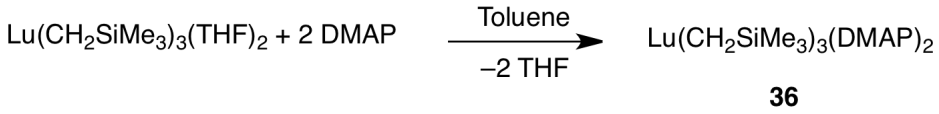

Scheme 5.7 Synthesis of $Lu(CH_2SiMe_3)_3(DMAP)_2$, **36**

The solid-state structure of **36** was obtained by single-crystal X-ray diffraction and is depicted in Figure 5.9 as a thermal ellipsoid plot. Selected metrical parameters are listed in Table 5.4. Complex **36** adopts a monomeric, five coordinate geometry at the lutetium centre. The geometry can be described as distorted trigonal bipyramidal with three alkyl groups in the equatorial plane (C26–Lu1–C22 = 114.6(1)º, C22–Lu1–C18 = 133.7(1)º, C18–Lu1–C26 = 111.7(1)º) and two DMAP ligands in the apical positions (N1–Lu1–N3 = 177.3(1)º). The Lu–C bond lengths (2.373(3) Å, 2.384(3) Å, 2.354(3) Å) and Lu–C–Si bond angles (126.5(2)º, 123.0(2)º, 129.8(2)º) are comparable to other lutetium complexes containing three trimethylsilylmethyl ligands.[177,188,189]

Table 5.4 Selected bond distances /Å and angles /º for compound **36**

C18–Lu1	2.373(3)	N1–Lu1	2.408(3)
C22–Lu1	2.384(3)	N3–Lu1	2.414(3)
C26–Lu1	2.354(3)		
C26–Lu1–C22	114.6(1)	Si1–C22–Lu1	126.5(2)
C22–Lu1–C18	133.7(1)	Si3–C26–Lu1	123.0(2)
C18–Lu1–C26	111.7(1)	Si2–C18–Lu1	129.8(2)
N1–Lu1–N3	177.3(1)		

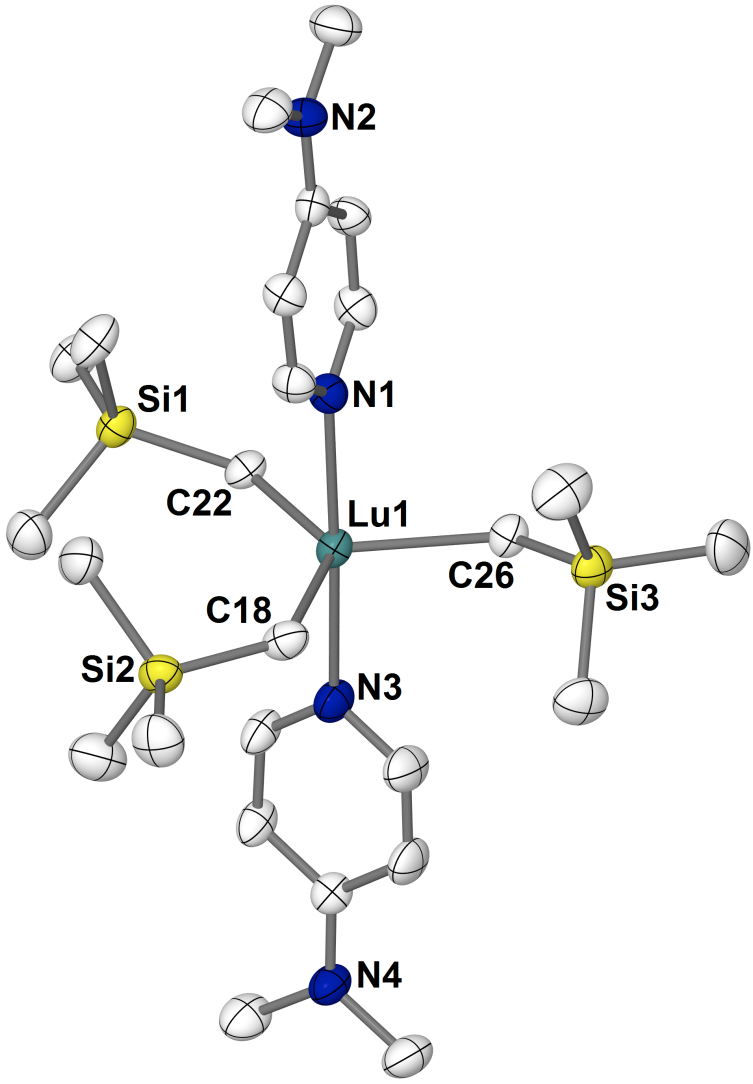

Figure 5.9 Thermal ellipsoid plot (50% probability) of $Lu(CH_2SiMe_3)_3(DMAP)_2$, **36**, with hydrogen atoms omitted for clarity.

Reaction of complex **36** with HL_C^{Pipp}, **35**, proceeded cleanly at ambient temperature to afford a single product **37**. From the ^1H NMR spectrum of **37**, it was evident that the product was a doubly cyclometalated complex, $(L_C^{Pipp}\text{-}\kappa^3N,\kappa^2C)Lu(DMAP)_2$, whereby the ligand was coordinated via three nitrogen atoms and two metalated *P*-methyl groups. Particularly diagnostic features in the ^1H NMR spectrum (benzene-d_6) of **37** include the *P*-methyl signal, which appears as a

doublet at δ 1.99 ($^2J_{HP}$ = 12.4 Hz) and integrates to 6H; and the cyclometalated P–CH_2 moieties, which resonate as a multiplet at δ 0.58 with an integration of 4H.

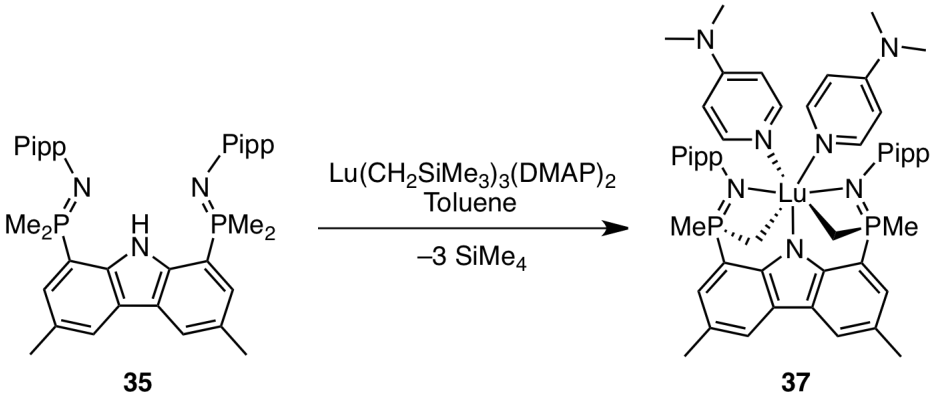

Scheme 5.8 Synthesis of doubly cyclometalated complex $\mathbf{L}_{\mathbf{C}}^{\mathbf{Pipp}}$-κ^3*N*,κ^2*C*)Lu(DMAP)$_2$, **37**

It is probable that the reaction of **36** with H$\mathbf{L}_{\mathbf{C}}^{\mathbf{Pipp}}$ proceeded with initial loss of one equivalent of tetramethylsilane to form a putative dialkyl complex of the ligand, ($\mathbf{L}_{\mathbf{C}}^{\mathbf{Pipp}}$-κ^3*N*)Lu($CH_2SiMe$)$_2$(DMAP)$_n$, (n = 0, 1 or 2). While it is likely that this dialkyl complex can be observed *in situ* by NMR spectroscopy at low temperature, no attempt to do so has been made at this time. Subsequent formation of product **37** then arose via a mechanism similar to the sequential *ortho*-metalation reactivity described in Chapter 3, whereby cyclometalation of two *P*-methyl groups and loss of two further equivalents of tetramethylsilane liberated the final doubly cyclometalated complex. Similar reactivity was previously documented in a scandium dimethyl complex of an anilido phosphinimine ligand, whereby cyclometalation of a dimethylphosphine group occurred with loss of one equivalent of methane.[83]

In order to unambiguously confirm the structure of **37**, an X-ray diffraction experiment was performed. Single crystals of the compound were obtained by slow diffusion of pentane into a benzene solution and it was found to crystallize in the

monoclinic space group $P2_1/c$. The molecular structure of **37** is depicted in Figure 5.10 and selected metrical parameters are listed in Table 5.5.

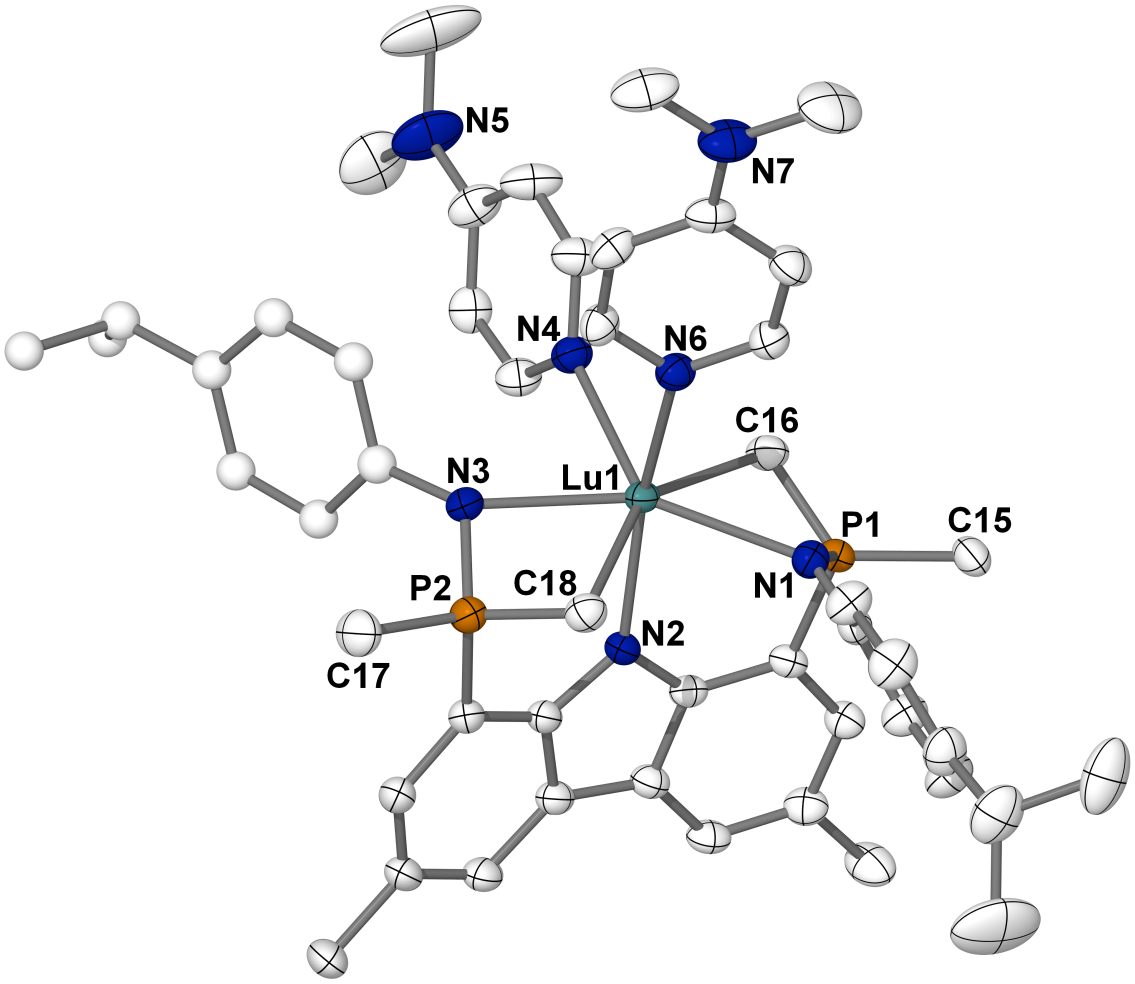

Figure 5.10 Thermal ellipsoid plot (50% probability) of ($\mathbf{L}_{\mathbf{C}}^{\mathbf{Pipp}}$-$\kappa^3N,\kappa^2C$)Lu(DMAP)$_2$, **37**, with hydrogen atoms and two benzene molecules of crystallization omitted for clarity. Positionally disordered atoms are depicted as spheres of arbitrary radius.

The metal centre in **37** is seven-coordinate and adopts a distorted pentagonal bipyramidal geometry with the equatorial plane defined by N1, C16, N4, N3 and C18 (N1–Lu1–C16 = 62.70(6)º, C16–Lu1–N4 = 72.92(7)º, N4–Lu1–N3 = 75.29(6)º, N3–

Lu1–C18 = 63.58(7)º, C18–Lu1–N1 = 89.53(7)º) and the apical positions occupied by N2 and N6 (N2–Lu1–N6 = 163.42(6)º).

Table 5.5 Selected bond distances /Å and angles /º for compound **37**

Lu1–C16	2.548(2)	P1–N1	1.633(2)
Lu1–C18	2.529(2)	P2–N3	1.626(2)
Lu1–N1	2.393(2)	P1–C15	1.810(2)
Lu1–N2	2.325(2)	P1–C16	1.715(2)
Lu1–N3	2.391(2)	P2–C17	1.814(2)
Lu1–N4	2.445(2)	P2–C18	1.724(2)
Lu1–N6	2.413(2)		
N2–Lu1–N6	163.42(6)	C15–P1–C16	119.6(1)
N1–Lu1–C16	62.70(6)	C17–P2–C18	118.1(1)
C16–Lu1–N4	72.92(7)	N1–P1–C15	111.2(1)
N4–Lu1–N3	75.29(6)	N1–P1–C16	100.5(1)
N3–Lu1–C18	63.58(7)	N3–P2–C17	110.5(1)
C18–Lu1–N1	89.53(7)	N3–P2–C18	101.5(1)

The Lu–C bond lengths in **37** are quite long at 2.548(2) Å and 2.529(2) Å and are comparable to the Lu–C bond distances in a phosphonium bis(ylide) complex, $Cp^*Lu((CH_2)_2PPh_2)_2$ (2.493(2) Å, 2.526(2) Å, 2.465(2) Å and 2.480(2) Å).[190] Interestingly, the bonding mode of the N–P–C moieties in **37** has some resemblance to that of a phosphonium ylide ligand. Particularly evident are the short P1–C16 and P2–C18 bond lengths of 1.715(2) Å and 1.724(2) Å, respectively. These can be compared to the longer P1–C15 and P2–C17 bond distances (1.810(2) Å and 1.814(2) Å, respectively) as well as the P–Me bonds in **35** (1.788(2) Å, 1.806(2) Å, 1.805(2) Å, 1.793(2) Å). For this reason, it could be speculated that there is some electron delocalization within the N–P–C moieties of **37** (Scheme 5.9). Unfortunately, limited data exists to support this notion beyond the metrical parameters obtained from the solid-state structure of **37**. Evidence

that argues against this conjecture includes the NMR chemical shifts for the metalated CH_2 subunits. For example, in the ^1H NMR spectrum of **37**, the CH_2 moiety gives rise to a multiplet with a chemical shift of δ 0.58. Accordingly, this chemical shift is far more representative of an alkyl-type $–CH_2^–$ ligand bonded to lutetium rather than an olefinic $=CH_2$ group.

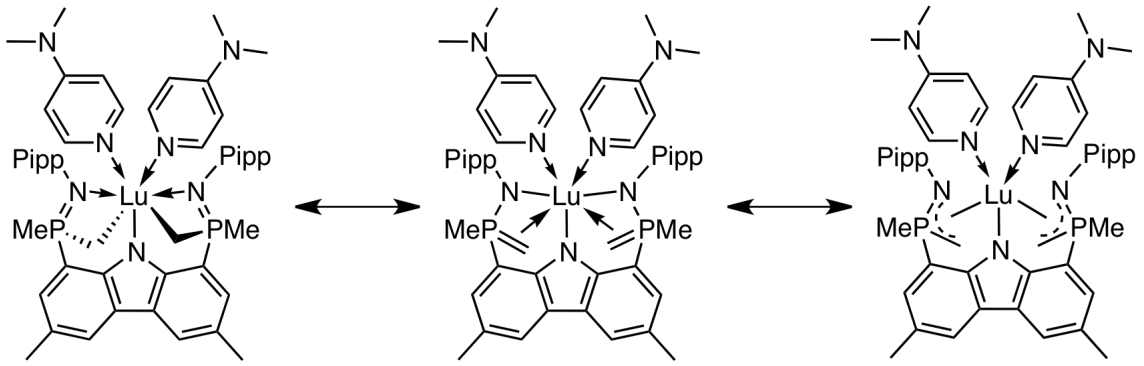

Scheme 5.9 Possible electron delocalization in **37**

Much to the same degree as the experiments in Chapter 4, the metallacycle ring opening reactivity of **37** with a variety of anilines was tested; unfortunately, the complex showed no signs of reactivity towards these substrates, even at elevated temperatures (100 ºC, 48 h). It can be surmised that the two DMAP ligands coordinated to the metal centre in **37** stabilize the complex to a degree where it appears to be inert towards this form of reactivity. On these grounds, $\mathbf{L}_{\mathbf{C}}^{\mathbf{Pipp}}$ and its lutetium complex were not considered to be particularly useful for the objective of exploring novel forms of reactivity and unique bonding modes, and consequently were not pursued any further.

5.8 Conclusions

In an effort to modify the bis(phosphinimine)carbazole ligand so as to make it resistant to cyclometalation decomposition pathways, the steric bulk around the peripheral edge of the ligand was reduced by adjusting the R groups at phosphorus. Installation of geometrically constrained and cyclic dioxaphospholane rings at the PR_2 site afforded a novel ligand $H\mathbf{L}_{\mathbf{B}}^{\mathbf{Pipp}}$, **31**, with unique geometry. A dialkyl lutetium complex of **31** was prepared; however, it was susceptible to degradation via an unusual ring opening insertion reaction. This decomposition route appears to have proceeded by an intra- and inter-molecular cascade involving the insertion reaction of four dioxaphospholane rings into four Lu-alkyl bonds to give a final "ring opened" lutetium alkoxide bimetallic complex **33**. Notably, this was the first example of a lanthanide alkyl cleaving a phosphonimidate ester bond in this manner.

Replacement of the dioxaphospholane rings with dimethylphosphine moieties afforded ancillary ligand $H\mathbf{L}_{\mathbf{C}}^{\mathbf{Pipp}}$, **35**. The alkane elimination reaction of **35** with the novel organolutetium reagent $Lu(CH_2SiMe_3)_3(DMAP)_2$, resulted in the isolation of lutetium complex, **37**, with cyclometalated *P*-methyl groups. In account of this, it was evident that even with reduction of steric bulk around the peripheral edge of the bis(phosphinimine)carbazole pincer ligand, dialkyl rare earth complexes are still highly susceptible to cyclometalative decomposition. Sufficient evidence is now available to conclude that the inherent nature of the bis(phosphinimine)carbazole geometry lends itself to promote metalative decomposition routes with reactive metal centres.

Chapter 6

Pyrrole Framework

6.1 Overview

To mitigate the cyclometalation problem encountered using the bis(phosphinimine)carbazole ligand, considerations have been taken to modify the geometry of the pincer framework. The original bis(phosphinimine)carbazole scaffold forms two six-membered chelate rings with a metal upon tridentate coordination (for example, as in complex **8**). It was envisioned that the bite of the ligand could be enlarged if upon tridentate coordination to a metal, two five-membered chelate rings were formed instead.[143] To this end, this chapter investigates the incorporation of pyrrole into the ligand framework in place of carbazole.

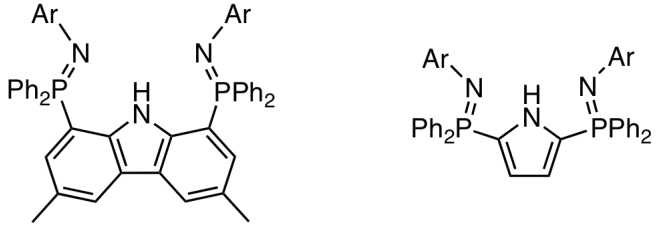

Chart 6.1 Bis(phosphinimine)carbazole and bis(phosphinimine)pyrrole ligands

6.2 Pyrrole-Based Ligands in the Literature

Over the past decade, a variety of pincer ligand designs have been reported that involve a pyrrole backbone. Selected examples include bis(imino)pyrrole (i),[191,192] bis((dialkylamino)methyl)pyrrole (ii),[193-196] and bis(oxazoline)pyrrole (iii)[197,198] ligands (Chart 6.2).

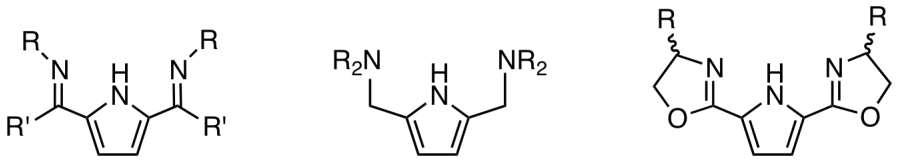

i ii iii

Chart 6.2 Selected pyrrole-based pincer ligands

Of these frameworks, the bis(imino)pyrrole (i) and bis((dialkylamino)methyl)pyrrole (ii) ligands have previously been utilized to prepare stable rare earth metal complexes.[191,194] Limited investigations regarding the bis(oxazoline)pyrrole (iii) ligand have been reported; however, late transition metal complexes of iii have been prepared and demonstrated to be active cross coupling catalysts.[139]

With regard to the bis(imino)pyrrole ligand, some tribulations have been previously encountered. For example, the ancillary framework is susceptible to nucleophilic attack at the imine carbon atom, which can lead to undesired ligand functionalization.[133] Additionally, in metal complexes of the bis(imino)pyrrole ligand, variable coordination modes have been described. As depicted in Chart 6.3, the ligand can bind a metal in either a κ^3 or κ^2 mode.[191] Factors such as metal ion size and the steric bulk of R groups attached to the imine nitrogen have been implicated to influence the

coordination mode of the ligand. Similar chelation properties have also been described in complexes involving the bis(dialkylamino)methylpyrrole ligand[195,199,200] and bis(oxazoline)pyrrole[139] frameworks. As a detrimental consequence of the κ^2-coordination mode in these frameworks, metal complexes have been found to dimerize or oligomerize through the uncoordinated donor group.[139] Furthermore, it can be expected that rare earth complexes of a bidentate ligand would be (i) inherently less stable than those supported by a tridentate chelate because of less electron donation, and (ii) more prone to retain Lewis basic solvents due to a sterically unsaturated coordination sphere.

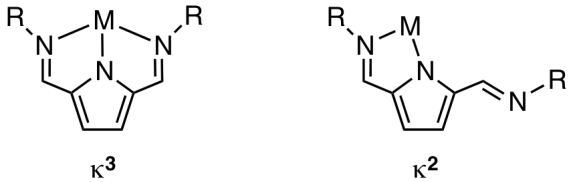

Chart 6.3 Coordination modes of a bis(imino)pyrrolyl ligand

Accordingly, the design and synthesis of a bis(phosphinimine)pyrrole ancillary was expected to afford a ligand framework with notable differences from i, ii and iii in terms of steric and electronic properties. In comparison to the bis(phosphinimine)carbazole ligand design, a bis(phosphinimine)pyrrole pincer would also exhibit a larger coordination pocket. These properties made it an ideal target to pursue as a ligand for stabilizing highly reactive rare earth metals.

6.3 Synthesis of a Bis(phosphinimine)pyrrole Ligand

Synthesis of the target bis(phosphinimine)pyrrole ligand was achieved in high yield over three steps from the *N*-BOC protected derivative of 2,5-dibromopyrrole,[201] as

outlined in Scheme 6.1. Lithium-halogen exchange of 2,5-bis(diphenylphosphino)-*N*-(*tert*-butoxycarbonyl)pyrrole with *n*-BuLi in THF,[202] followed by reaction with chlorodiphenylphosphine, afforded the BOC-protected diphosphine, **38**. Thermal removal of the BOC group was performed at 155 °C to liberate 2,5-bis(diphenylphosphino)-1H-pyrrole, **39**. Finally, the phosphinimine functionality was installed onto the ligand via a Staudinger reaction of **39** with *para*-isopropylphenyl azide, with concomitant loss of N_2 to afford **40** in 60% overall yield.

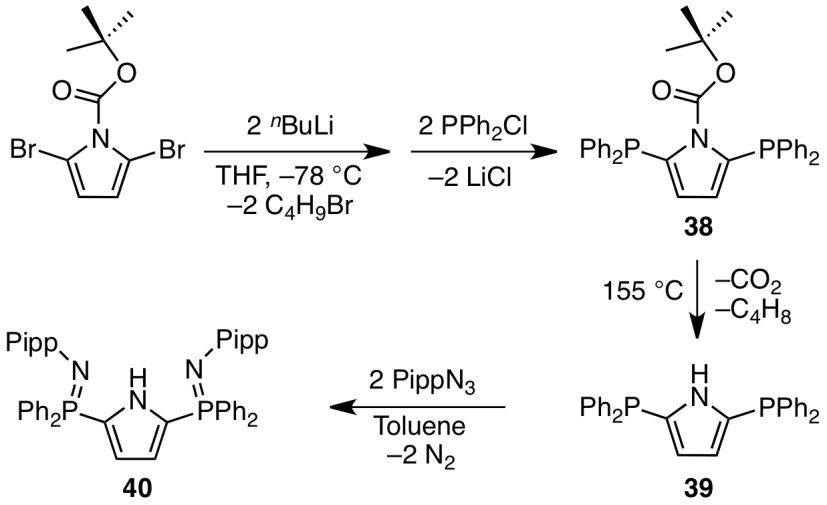

Scheme 6.1 Synthesis of bis(phosphinimine)pyrrole ligand **40**

Proteo ligand **40** contains chemically equivalent phosphorus nuclei in solution and exhibits a single resonance in its $^{31}P\{^{1}H\}$ NMR spectrum at δ −8.1 (benzene-d_6). The ^{1}H and $^{13}C\{^{1}H\}$ NMR spectra corroborate the expected structure of the ligand. Single crystals of **40** suitable for an X-ray diffraction experiment were obtained from a concentrated toluene solution at ambient temperature. The molecular structure of **40** is depicted in Figure 6.1 as a thermal ellipsoid plot and selected metrical parameters are listed in Table 6.1.

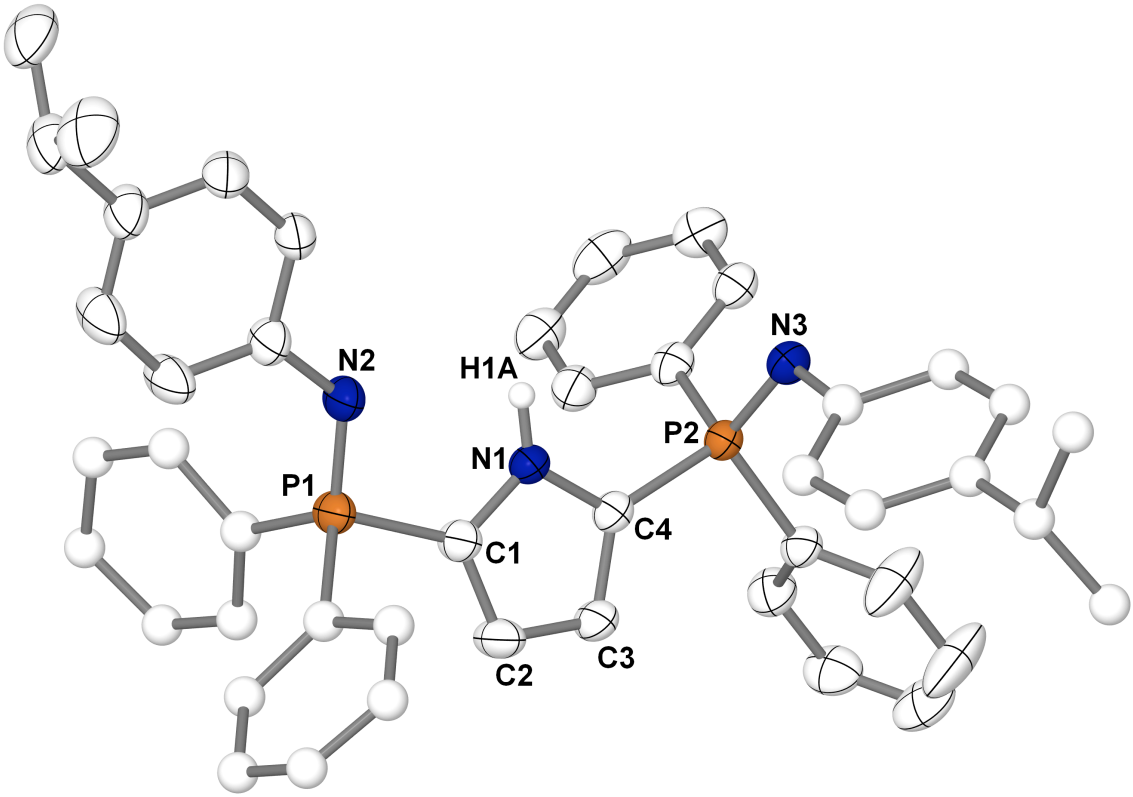

Figure 6.1 Thermal ellipsoid plot (50% probability) of **40** with hydrogen atoms (except H1A) omitted for clarity. Positionally disordered atoms are depicted as spheres of arbitrary radius.

In the same sense as the bis(phosphinimine)carbazole ligand design, tridentate pincer ligand **40** is intended to chelate metals in a meridional fashion via N1, N2, and N3. Accordingly, when coordinated to a metal, it would be expected that the pincer arms (N2 and N3) would occupy a common plane with the pyrrole backbone. In the solid state, N2 is close to the plane of the pyrrole backbone (N2–P1–C1–N1 torsion angle of 23.3(3)°). Conversely, N3 lies significantly further out of this plane with an N3–P2–C4–N1 torsion angle of 54.6(3)°. This rotation is influenced by intermolecular hydrogen bonds in the crystal structure (*vide infra*). Other metrical parameters of interest include the phosphinimine P–N bond lengths of 1.562(2) Å (P1–N2) and 1.572(2) Å (P2–N3). These

values correlate well with other examples in the literature whereby the phosphinimine functionality exhibits significant P=N double bond character.[83,203]

Table 6.1 Selected bond distances /Å, angles /º and torsion angles /º for compound **40**

P1–N2	1.562(2)	N2–P1–C1–N1	23.3(3)
P2–N3	1.572(2)	N3–P2–C4–N1	54.6(3)
N1–H1A···N3[a]	2.851(3)		
C1–P1–N2	106.3(1)	C4–P2–N3	119.4(1)
N2–P1–C5A	118.0(2)	C4–P2–C23	101.8(1)
C5A–P1–C11A	104.9(3)	C4–P2–C17	106.5(1)
C11A–P1–C1	104.9(2)	N3–P2–C17	108.0(1)
N2–P1–C11A	115.0(2)	N3–P2–C23	114.7(1)
C5A–P1–C1	106.7(2)	C23–P2–C17	105.5(1)

[a] This bond length represents the intermolecular H-bond between two molecules of **40** in the unit cell

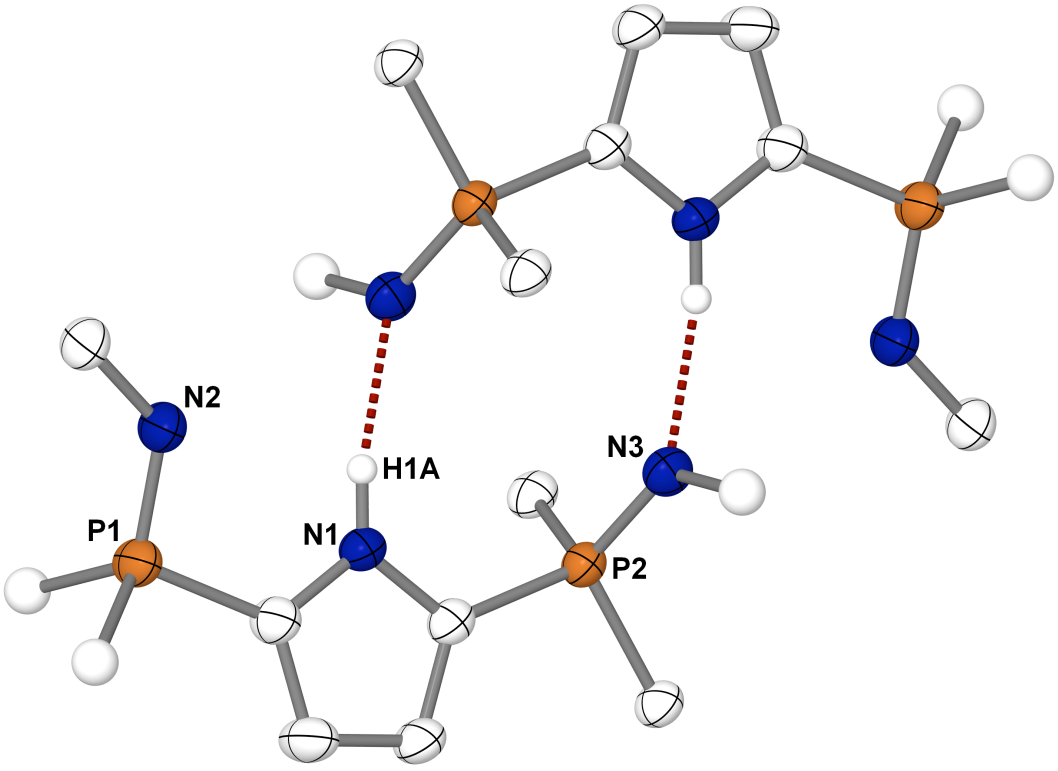

Figure 6.2 Packing diagram of **40** with hydrogen atoms (except H1A), phenyl and *para*-isopropylphenyl rings (except for *ipso* carbons) omitted for clarity.

Interestingly, the compound crystallized in the triclinic space group $P\bar{1}$ as centrosymmetric hydrogen-bonded pairs, with the pyrrole N–H group on each molecule associating with an imine nitrogen (N3) on the other (d(N···N) = 2.851(3) Å). A packing diagram depicting this assembly of the centrosymmetric pairs in the solid state is illustrated in Figure 6.2.

Proteo ligand **40** ($H\mathbf{L}_{\mathbf{D}}^{\mathbf{Pipp}}$) can readily be complexed with a variety of metal precursors at ambient temperature. For example, dialkyl lanthanide complexes of the ligand were readily prepared via an alkane elimination reaction of **40** with $Ln(CH_2SiMe_3)_3(THF)_2$, Ln = Er, Lu, Sc (Scheme 6.2). When these reactions were followed *in situ* by NMR spectroscopy in benzene-d_6, they proceeded rapidly at ambient temperature with the formation of the corresponding metal dialkyl complexes, one equivalent of $SiMe_4$ and two equivalents of uncoordinated THF. Upon scale-up of the reactions in toluene solution, the dialkyl products, ($\mathbf{L}_{\mathbf{D}}^{\mathbf{Pipp}}$-$\kappa^3$*N*)$Ln(CH_2SiMe_3)_2$, (Ln = Er, **41**; Lu, **42**; Sc, **43**), were obtained in high yield (81%, 82% and 81%, respectively) after recrystallization.

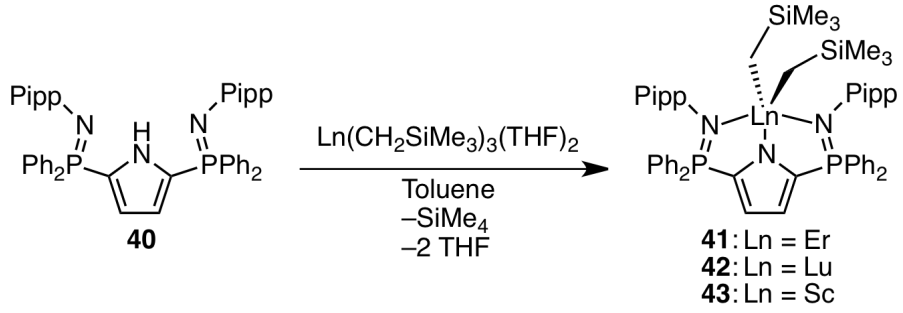

Scheme 6.2 Lanthanide complexation through alkane elimination

In the $^{31}P\{^1H\}$ NMR spectra (benzene-d_6), a significant downfield shift of the phosphinimine resonance was observed upon complexation of **40** with diamagnetic rare

earth metals (**42** δ 25.0; **43**, δ 23.8). Despite the paramagnetic nature of erbium, the broad $^{31}P\{^{1}H\}$ NMR resonance of **41** (δ −0.29, benzene-d_6) also proved to be a diagnostic indicator of ligand coordination. The ^{1}H NMR spectra of diamagnetic **42** and **43** revealed the corresponding $–CH_2SiMe_3$ methylene (δ −0.20, **42**; 0.55, **43**) and methyl signals (δ 0.18, **42**; 0.11, **43**) as sharp singlets, each integrating to 4 and 18 protons, respectively.

Notably, the dialkyl rare earth complexes were all base-free and the lutetium and scandium derivatives exhibited high thermal stability in both the solid and solution states. For example, complexes **42** and **43** can be left in benzene-d_6 solution at ambient temperature for at least one week with no apparent decomposition (as evidenced by multinuclear NMR spectroscopy). This is a dramatic improvement in thermal stability compared to the analogous carbazole-based dialkyl lutetium complex **15** that exhibited a half-life at ambient temperature (295.7 K) of only 1160 s. Perhaps even more significant is the fact that preliminary experiments indicate that **42** is stable in solution at 60 °C with no sign of decomposition over 4.5 hours.

In order to unambiguously establish the connectivity of the rare earth dialkyl complexes, X-ray diffraction analyses were performed. Single crystals of **41** and **42** were obtained from concentrated toluene/THF mixtures and their molecular structures were determined. Complexes **41** and **42** were found to be isostructural and a representative thermal displacement plot of **42** is depicted in Figure 6.3. While a solid-state structure of **43** was not obtained, it is reasonable to assume that it would possess an isostructural geometry to that of the lutetium and erbium derivatives.

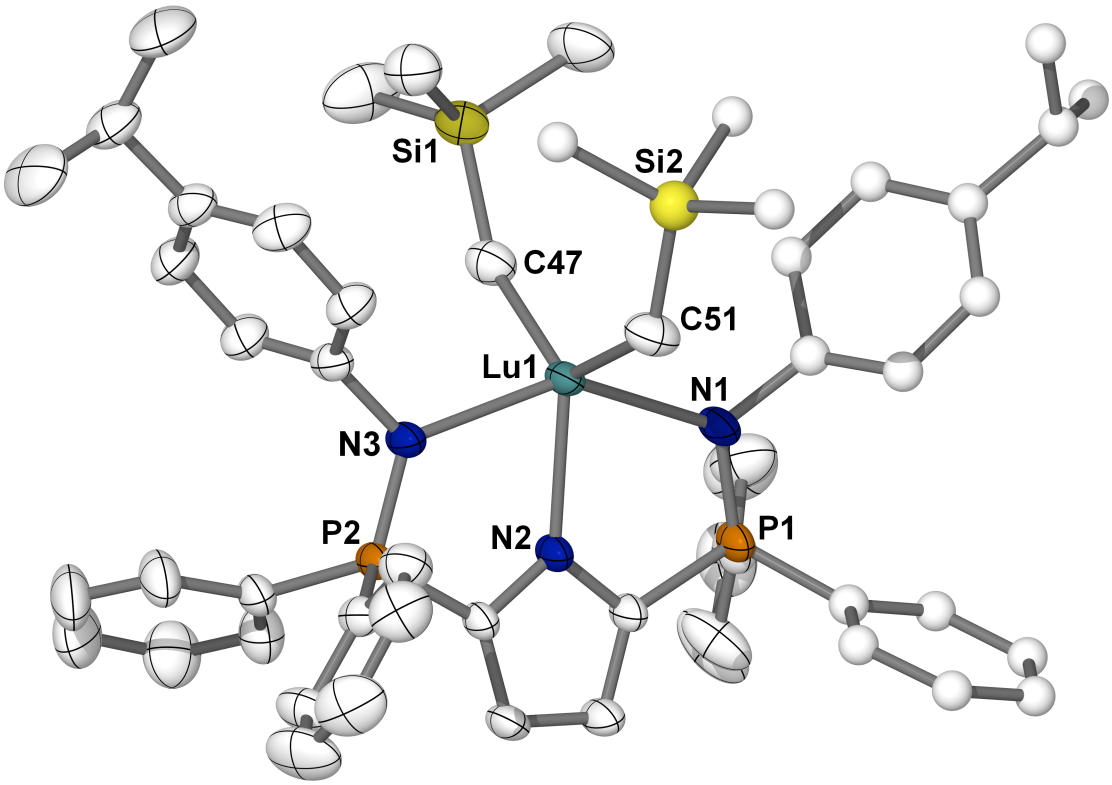

Figure 6.3 Thermal ellipsoid plot (50% probability) of ($\mathbf{L}_{\mathbf{D}}^{\mathbf{Pipp}}$-$\kappa^3$*N*)Lu($CH_2SiMe_3$)$_2$ (**42**) with hydrogen atoms omitted for clarity. The solid-state structure of ($\mathbf{L}_{\mathbf{D}}^{\mathbf{Pipp}}$-$\kappa^3$*N*)Er($CH_2SiMe_3$)$_2$ (**41**) is isostructural to that of **42**. Positionally disordered atoms are depicted as spheres of arbitrary radius.

The lanthanide complexes **41** and **42** are monomeric with five-coordinate metal centres that are bound to the pincer ligand in a κ^3 fashion through the three nitrogen atoms. The geometry is best described as distorted trigonal bipyramidal with the equatorial plane defined by N2 and the alkyl groups (C47 and C51). The phosphinimine donors (N1 and N3) occupy the apical sites. The bond angles about the equatorial plane in each complex are close to the ideal value of 120° (N2–Er1–C47 = 115.7(1)°, N2–Er1–C51 = 117.0(1)°, C47–Er1–C51 = 127.3(2)°, **41**; N2–Lu1–C47 = 117.2(1)°, N2–Lu1–C51 = 116.0(1)°, C47–Lu1–C51 = 126.8(1)°, **42**); however, the apical bond angle (N1–Ln–N3) deviates significantly from 180° (142.4(1)°, **41**; 144.3(1)°, **42**). The Ln–C–Si

bond angles fall within the normal range for rare earth trimethylsilylmethyl complexes (129.4(2)°, 136.6(2)°, **41**; 130.7(2)°, 136.9(2)°, **42**). The Er–C bond lengths in **41** (2.375(4) Å and 2.398(5) Å) agree well with other recent structurally characterized organoerbium complexes such as (nacnac)Er(CH_2SiMe_3)$_2$ (2.342(3) Å and 2.380(2) Å)[78] and (Czx)Er(CH_2SiMe_3)$_2$ (2.398(3) Å and 2.404(3) Å),[204] where nacnac = 2,6-^{i}Pr-C_6H_3 substituted β-diketiminate and Czx = carbazole-bis(oxazoline). Complex **42** exhibits slightly shorter Lu–C bond lengths (2.347(4) Å and 2.355(4) Å) than the corresponding contacts in the erbium congener, but the distances fall within the range expected for typical Lu–CH_2SiMe_3 bonds.[**]

Table 6.2 Selected bond distances /Å, angles /º and torsion angles /º for **41** and **42**

	41	**42**
Ln–C47	2.398(5)	2.347(4)
Ln–C51	2.375(4)	2.355(4)
Ln–N2	2.338(3)	2.297(2)
Ln–N1	2.361(3)	2.364(3)
Ln–N3	2.396(3)	2.332(2)
P1–N1	1.606(3)	1.608(3)
P2–N3	1.610(3)	1.608(2)
N2–Ln–C47	115.7(1)	117.2(1)
N2–Ln–C51	117.0(1)	116.0(1)
C47–Ln–C51	127.3(2)	126.8(1)
N1–Ln–N3	142.4(1)	144.3(1)
Ln–C47–Si1	129.4(2)	136.9(2)
Ln–C51–Si2	136.6(2)	130.7(2)
C1–P1–N1–Ln	−5.0(2)	−8.4(2)
C4–P2–N3–Ln	−8.4(3)	−4.6(2)

[**] An analysis of 47 entries in the Cambridge Structural Database (CSD version 5.32, updated Aug. 2011) for neutral bis(trimethylsilylmethyl) lutetium complexes of the generic form (L)$_n$Lu(CH_2SiMe_3)$_2$ suggested an average Lu–CH_2SiMe_3 bond length of 2.35 Å (range = 2.293–2.406 Å).

In **41** and **42**, the metal sits in the centre of the ancillary ligand binding pocket. Both of the complexes exhibit Ln–pyrrole bond distances that are significantly shorter than the Ln–phosphinimine lengths (Er1–N2 = 2.338(3) Å *c.f.* Er1–N1 = 2.361(3) Å and Er1–N3 = 2.396(3) Å, **41**; Lu1–N2 = 2.297(2) Å *c.f.* Lu1–N3 = 2.332(2) Å and Lu1–N1 = 2.364(3) Å, **42**). The P–N bonds in the dialkyl complexes (ranging from 1.606(3) Å to 1.610(3) Å) are elongated by *ca*. 3% compared to those in the free proteo ligand, suggesting strong donation from the phosphinimine functionality to the rare earth metal.

6.4 Reactivity Studies

Preliminary reactivity studies of **42** (on NMR tube-scale, benzene-d_6) have revealed rich reaction chemistry. For instance, reaction of **42** with one equivalent of the oxonium acid, $[H(OEt_2)_2]^+[B(C_6F_5)_4]^-$,[205] proceeds at ambient temperature over 4.5 h to liberate the expected cationic species as a diethyl ether adduct, $(\mathbf{L}_{\mathbf{D}}^{\mathbf{Pipp}}\text{-}\kappa^3N)Lu(CH_2SiMe_3)(OEt_2)_2]^+[B(C_6F_5)_4]^-$, **44** (Scheme 6.3). Alternatively, reaction of **42** with one equivalent of Mes*NH_2 in the presence of DMAP at 100 °C (over 1.5 h) resulted in the clean formation of the mixed alkyl/anilide complex, $(\mathbf{L}_{\mathbf{D}}^{\mathbf{Pipp}}\text{-}\kappa^3N)Lu(CH_2SiMe_3)$(NHMes*)(DMAP), **45**, with loss of one equivalent of $SiMe_4$ (Scheme 6.3). The neutral (**41**, **42** and **43**) and cationic (**44**) complexes are of interest as catalysts for various applications (*e.g.* lactone and olefin polymerization) and their efficacy for mediating such processes is currently under evaluation. As an analogue to the elusive mixed alkyl/anilide complex encountered in chapter 4, it is expected that complex **45** may provide fundamental insight into the structure and reactivity of lanthanide

alkyl/anilide complexes. Alternatively, **45** might act as a useful model towards the development of a hydroamination catalyst.

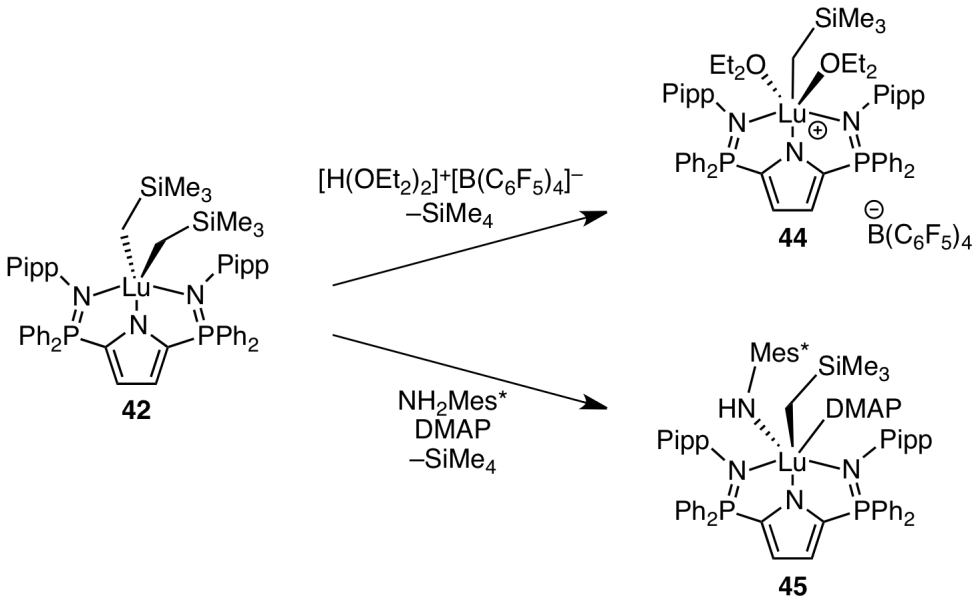

Scheme 6.3 Reaction chemistry of $(\mathbf{L}_{\mathbf{D}}^{\mathbf{Pipp}}\text{-}\kappa^3\textit{N})\text{Lu}(\text{CH}_2\text{SiMe}_3)_2$, **42**

6.5 Conclusions

In summary, a new ancillary ligand comprised of a modular bis(phosphinimine)pyrrole framework (**40**) has been prepared. The versatility of this ligand was demonstrated in that it can readily be complexed to lanthanide metals via an alkane elimination protocol to generate thermally robust rare earth dialkyl species. Current efforts are underway to investigate the small molecule reactivity of complexes **41**–**45** in order to exploit the full range of their utility for various applications.

Chapter 7

Future Work and Conclusions

7.1 Future Reactivity Studies of Existing Frameworks

7.1.1 Pyrrole Ligand Organometallic Chemistry

The bis(phosphinimine)pyrrole ligand framework discussed in Chapter 6 exhibits agreeable steric and electronic properties that has allowed for the preparation and isolation of thermally stable rare earth dialkyl complexes. Preliminary work has already demonstrated that the lutetium dialkyl complex, ($\mathbf{L}_{\mathbf{D}}^{\mathbf{Pipp}}$-$\kappa^3$*N*)Lu($CH_2SiMe_3$)$_2$, **42**, can be readily derivatized to afford a cationic species, ($\mathbf{L}_{\mathbf{D}}^{\mathbf{Pipp}}$-$\kappa^3$*N*)Lu($CH_2SiMe_3$)($OEt_2$)$_2$]$^+$ [B(C_6F_5)$_4$]$^-$, **44**, and the mixed alkyl/anilide compound, ($\mathbf{L}_{\mathbf{D}}^{\mathbf{Pipp}}$-$\kappa^3$*N*)Lu($CH_2SiMe_3$)-(NHMes*)(DMAP), **45**.

A plethora of organometallic chemistry can likely be harvested from the developed dialkyl complexes and their derivatives. For example, the cationic lutetium compound **44** is expected to be a useful catalyst for industrially relevant processes such

as olefin or lactone polymerization. It would also be useful to compare the catalytic activity of **44** to that of the corresponding neutral dialkyl complex. While only the lutetium cation has been prepared to date, it is highly probable that the corresponding erbium and scandium analogues can be prepared from **41** and **43**, respectively via a similar means to that established in Chapter 6. It should be noted that reactivity variability based on metal ion size is a well-established concept in lanthanide chemistry,[1,8,206] and different chemistry may be witnessed upon modulation of the metal ion. In the case of developing a polymerization catalyst, this can be beneficial in terms of tuning the catalyst for optimal activity. This concept was recently outlined in a study comparing the ethylene polymerization ability of aminopyridinate-stabilized organolanthanide cations of Sc, Lu, Er and Y. These four rare earth complexes were isostructural, however, it was found that the erbium congener exhibited the highest catalytic activity by a substantial margin.[207]

Beyond polymerization chemistry, the organometallic complexes developed in Chapter 6 may prove to be useful in facilitating other important chemical transformations. In particular, the activation and functionalization of small molecules such as carbon dioxide or methane is of interest. Global levels of these greenhouse gases have dramatically increased in recent years and a viable solution to reduce their atmospheric levels is yet to be realized. Accordingly, the development of chemical methods to activate and then subsequently transform these gases into useful molecules or fuels, such as methanol, is an intriguing topic to pursue.[208-210] While this is clearly a significantly challenging objective, it has high potential to yield rewarding results. Initial forays into this direction might begin by studying the insertion reactivity of CO_2 into the

lanthanide alkyl bonds of complexes **41**–**43** to give the corresponding carboxylate complexes.

7.1.2 Scandium Organometallic Chemistry

Preliminary investigations involving scandium complexes of the *N*-phenyl substituted ligand ($\mathbf{L}_{\mathbf{A}}^{\mathbf{Ph}}$) have revealed rich reaction behaviour. For example, the scandium dialkyl complex ($\mathbf{L}_{\mathbf{A}}^{\mathbf{Ph}}$-$\kappa^3$*N*)Sc($CH_2SiMe_3$)$_2$, which can be prepared by the alkane elimination reaction of H$\mathbf{L}_{\mathbf{A}}^{\mathbf{Ph}}$ with Sc(CH_2SiMe_3)$_3$(THF)$_2$, appears to exhibit significantly different reaction behaviour from that observed with the lutetium analogue ($\mathbf{L}_{\mathbf{A}}^{\mathbf{Ph}}$-$\kappa^3$*N*)Lu($CH_2SiMe_3$)$_2$, **14**. Initial studies suggest that the scandium dialkyl is thermally susceptible to an intramolecular metalative alkane elimination reaction; however, it is believed that this process proceeds by γ-cyclometalation of a –CH_2SiMe_3 group with loss of one equivalent of tetramethylsilane to form ($\mathbf{L}_{\mathbf{A}}^{\mathbf{Ph}}$-$\kappa^3$*N*)Sc($CH_2$)$_2$SiMe$_2$. Notably, the γ-cyclometalated derivative can be prepared independently by reaction of the dichloride complex ($\mathbf{L}_{\mathbf{A}}^{\mathbf{Ph}}$-$\kappa^3$*N*)$ScCl_2$ with the dilithium reagent [THF(LiCH$_2$)$_2$SiMe$_2$]$_6$ (Scheme 7.1)[211]

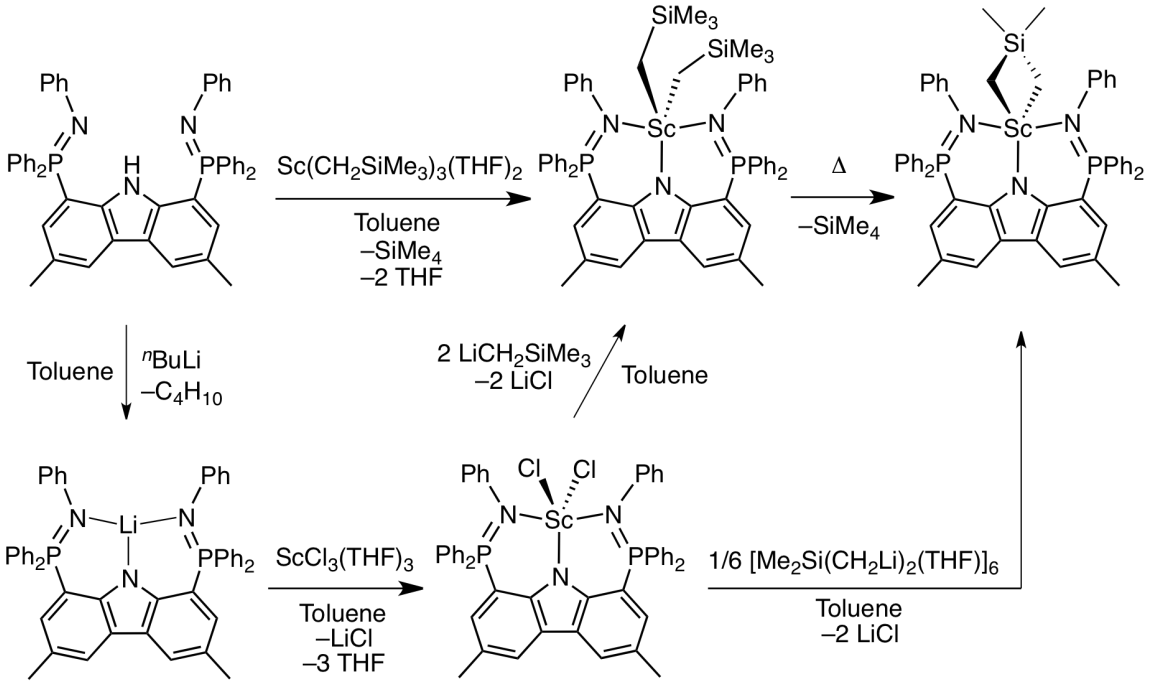

Scheme 7.1 γ-Cyclometalation in a scandium complex of $\mathbf{L}_{\mathbf{A}}^{\mathbf{Ph}}$

Other related γ-cyclometalated complexes, such as $Cp^*_2Th(CH_2)_2SiMe_2$ and $Cp^*_2Th(CH_2)_2CMe_2$, have been shown to exhibit remarkable organometallic chemistry. For example, the thoracyclobutane compound $Cp^*_2Th(CH_2)_2CMe_2$ is capable of activating methane at the relatively mild temperature of 60 ºC (Scheme 7.2).[212,213] It can be speculated that the γ-cyclometalated scandium complex ($\mathbf{L}_{\mathbf{A}}^{\mathbf{Ph}}$-κ^3*N*)$Sc(CH_2)_2SiMe_2$ might be capable of similar hydrocarbon activation chemistry. In account of this, a detailed investigation into the structure and reactivity of organoscandium complexes supported by $\mathbf{L}_{\mathbf{A}}^{\mathbf{Ph}}$ should be pursued.

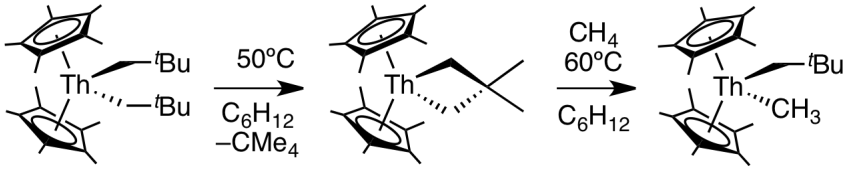

Scheme 7.2 Formation of a thoracyclobutane complex via γ-metalation and its subsequent application in methane activation

7.2 Phosphinimine Ligand Modifications

Through the installation of pyrimidine rings into the phosphinimine functionality, a pentadentate *NNNNN* ligand was obtained ($H\mathbf{L}_{\mathbf{A}}^{\mathbf{Pym}}$). Enhanced thermal stability of dialkyl lutetium complexes of this ligand was observed compared to analogous complexes of the tridentate ligand derivatives ($H\mathbf{L}_{\mathbf{A}}^{\mathbf{Mes}}$, $H\mathbf{L}_{\mathbf{A}}^{\mathbf{Ph}}$, $H\mathbf{L}_{\mathbf{A}}^{\mathbf{Pipp}}$). Unfortunately, the pyrimidine rings were susceptible to subsequent dearomatization and functionalization through an alkyl migration reaction; for this reason the retention of pyrimidine rings in the ligand scaffold was undesirable.

From these observations, the synthesis of a pentadentate ligand without pyrimidine rings would be expected to afford rare earth complexes with heightened stability over tridentate analogues. To this end, a rational ligand modification involving the attachment of pendant *N,N*-dimethylethylamino groups onto the nitrogen atom of the phosphinimine functionality would result in a ligand with the potential to coordinate a metal in a pentadentate mode through five nitrogen atoms. This ligand derivative could be readily synthesized by the Staudinger reaction of the diphosphine **2** with two equivalents of 2-azido-*N,N*-dimethylethylamine[214,215] (Scheme 7.3).

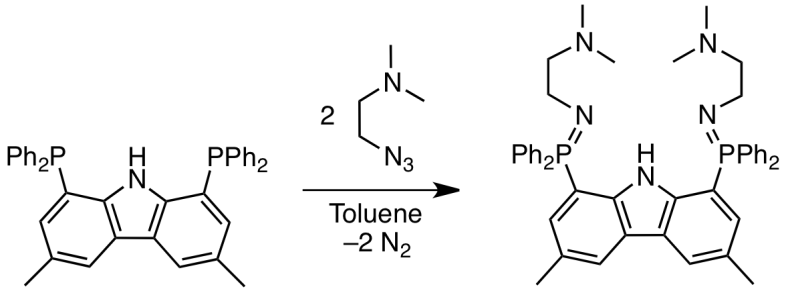

Scheme 7.3 Installation of *N,N*-dimethylethylamino moieties

A similar approach involves installation of aryl rings that contain a pendant donor group in the *ortho* position. For example, 1-azido-2-dimethylaminbenzene[216] or 1-azido-2-methoxybenzene[217] could be applied in the Staudinger reaction to access ligands of an *NNNNN* or *NNNOO* type, respectively (Chart 7.1).

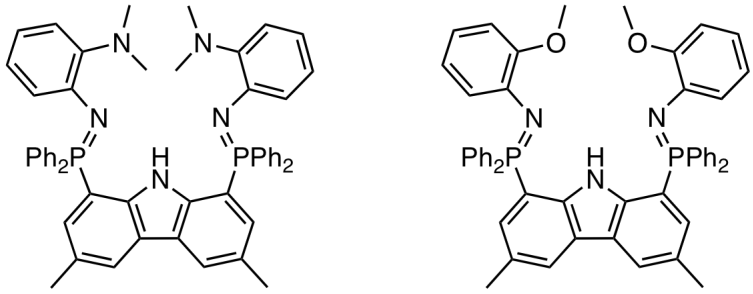

Chart 7.1 Aryl rings with pendant dimethylamine and methoxy groups

7.3 Alternative Ligand Frameworks

As described in Chapters 2 through 5, the ligand geometry based on a bis(phosphinimine)carbazole framework presents a sterically crowded environment for supporting rare earth alkyl complexes. Consequently, intramolecular metalative alkane elimination reactions were found to be quite prevalent in complexes encompassing this framework. While attempts to pursue other highly reactive functionalities at the metal centre were precluded by the ligand metalation problem, the results encountered along the way have provided insight into which ligand features are important for stabilizing highly reactive rare earth complexes.

Investigations are already underway into the development of ligands that contain potentially "metalation resistant" phosphinimine functionalities. These ligands include geometrically constrained phospholane rings as analogues to the dioxaphospholane

derivatives presented in Chapter 5. The incorporation of phospholane rings into the ligand framework is expected to give a structure with a similar constrained geometry to the dioxaphospholane analogue, but without the drawback of being susceptible to intra- and inter-molecular ring opening insertion of the dioxaphospholane into metal alkyl bonds. It should be pointed out, however, that while the phospholane geometry is constrained and will likely lead to a ligand that is resistant to *intra*-molecular C–H bond activation of the PR_2 group, the phospholane ring may still be susceptible to the analogous *inter*-molecular reaction. Such a notion is not completely unprecedented in this family of ligands; inter-molecular bond activation reactions were in fact observed at the PR_2 site of the ligand in complex **33**. Furthermore, it is evident from results observed in Chapter 4, that the phosphinimine functionality is prone to metalation via not only the PR_2 moiety, but alternatively via the *N*-aryl ring (*i.e.*, complex **26**).

The propensity for the phosphinimine functionality to participate in metalative alkane elimination reactions in rare earth complexes stems in part from the geometry that the donor phosphinimine arms impose at the metal centre. In the case of the bis(phosphinimine)carbazole ligands, a tight coordination pocket is enforced by the ligand geometry, and as a result, the phosphinimine R groups become situated in close proximity to the metal. This leads to high steric crowding at the metal centre and promotes metalative alkane elimination reactivity as a faucet to minimize the steric pressure.

Conversely, the bis(phosphinimine)pyrrole ligand tends to chelate metal ions with a larger coordination pocket and as a consequence of this, the phosphinimine R groups become situated further from the metal. In the case of rare earth alkyl complexes of the

bis(phosphinimine)pyrrole framework, the ligand was found to impose minimal steric crowding at the metal centre. This allowed for the isolation of quite thermally robust rare earth alkyl complexes that were not prone to ligand metalation via the phosphinimine moieties.

While the phosphinimine functionality seems to be well-suited in terms of sterics and geometry for the bis(phosphinimine)pyrrole ligand, it is believed that it is far too sterically crowding for use in the analogous carbazole ligand. As such, it is suggested that the multitude of metalation issues arising in the bis(phosphinimine)carbazole ligand be mitigated by removal of the phosphinimine functionality and replacement with alternative donor moieties. For example, previously reported carbazole frameworks with imino[143] or pyridyl[137] donors may prove suitable for use as supporting ligands in rare earth chemistry. Alternatively, a particularly attractive and novel substitute to the phosphinimine functionality is incorporation of pyrazolyl donor groups onto a carbazole ligand framework.

7.3.1 A Bis(pyrazolyl)carbazole Ligand

The tris(pyrazolyl)borate (Tp) ligand is an anionic tridentate ancillary with three pyrazolyl rings bound to a borate anion.[218,219] The Tp ligand family is considered to be among the most versatile ligands in inorganic chemistry and has garnered increased use in rare earth chemistry in recent years.[220-224] This is in part due to the scorpionate geometry of the ligand, but also due to its strong donor properties. On each pyrazolyl ring of the ligand, the nitrogen atom not bound to boron is Lewis basic and can act as an

electron donor to a metal ion. Due to the ability of pyrazolyl rings to act as suitable donors to rare earth metals, it is expected that a fusion of the donor properties of the Tp ligand with the backbone framework of a carbazole pincer ligand would afford a novel hybrid ancillary with remarkable properties.

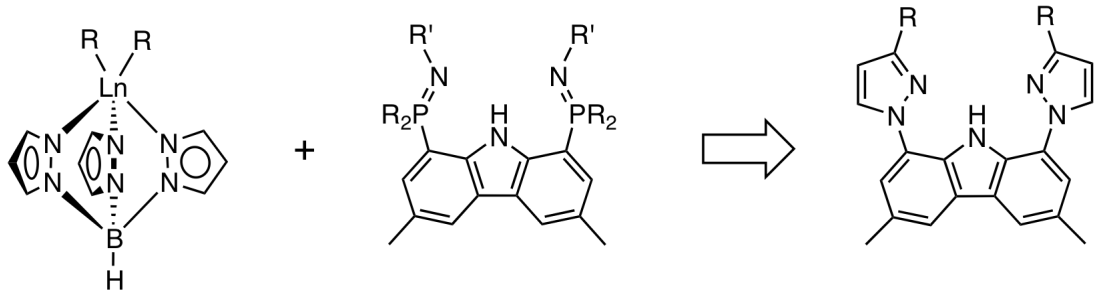

Scheme 7.4 A novel hybrid ancillary ligand with pyrazolyl donors

Synthesis of the novel ligand 3,6-dimethyl-1,8-bis(pyrazolyl)carbazole (CzPz) should be possible via the straight-forward Ullmann coupling reaction of 1,8-dibromo-3,6-dimethylcarbazole with substituted pyrazoles (R = H, Me, ^{i}Pr) in the presence of copper(I) oxide as a catalyst (Scheme 7.5).[225] Once prepared, rare earth metal complexes of the CzPz ligand should be easily accessible via standard synthetic methods such as alkane elimination or salt metathesis.

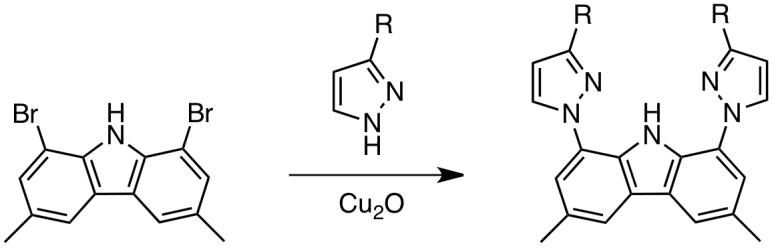

Scheme 7.5 Synthesis of a bis(pyrazolyl)carbazole pincer ligand

A variant to the CzPz ligand involves the incorporation of 1,2,3-triazole rings onto a carbazole backbone at the 1 and 8 positions. It is expected that such a ligand could readily be synthesized via a click chemistry approach.[226] For example, starting from

commercially available 1,8-diaminocarbazole, formation of the diazonium salt followed by reaction with sodium azide would result in 1,8-diazidocarbazole. Subsequent treatment with an appropriate alkyne in the presence of a copper(I) catalyst would generate two 1,2,3-triazole rings by means of an azide alkyne Huisgen cycloaddition reaction[227] (Scheme 7.6). It is likely that the carbazole ligand with 1,2,3-triazole rings (CzTz) would act as a complementary analogue to the CzPz scaffold.

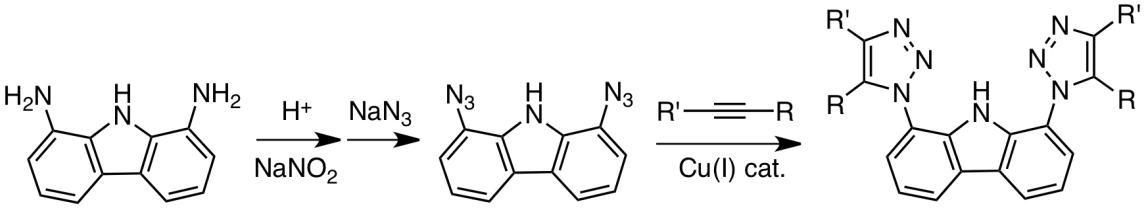

Scheme 7.6 Synthesis of 1,2,3-triazole ligand by click chemistry

7.4 Summary and Conclusions

This thesis presented the development of novel bis(phosphinimine) pincer ligands and their application in the preparation of well-defined rare earth organometallic complexes. Two ligand classes based on bis(phosphinimine)carbazole and bis(phosphinimine)pyrrole frameworks were synthesized, and the effect of steric and electronic modulation of the *N*-aryl and PR_2 sites was explored. Accordingly, through the systematic development of the ancillary ligand frameworks, rare earth metal species with unique structure and reactivity were encountered.

Several of the developed ligand derivatives of the bis(phosphinimine)carbazole framework were prone to cyclometalative C–H bond activation reactivity with rare earth alkyl complexes. The cyclometalation process was monitored by spectroscopy and

kinetic parameters related to the transformation were obtained. Protonolysis reactivity of cyclometalated lutetium complexes was also examined through the process of metallacycle ring opening. Mechanistic and kinetic insights into these transformations were obtained through an array of deuterium labeling and kinetic experiments. Other forms of reactivity that were encountered over the course of this work include the dearomatization and functionalization of ligand pyrimidine rings by a 1,5-alkyl migration, and ring opening insertion of dioxaphospholane rings.

Rare earth complexes of the bis(phosphinimine)pyrrole ligand were found to be quite thermally stable. Accordingly, this well-designed ancillary ligand has been shown to stabilize the coordination environment of rare earth metals so as to be able to control their reactivity. This class of compound presents itself as a promising platform for future study of organolanthanide reactivity and chemical transformations.

Chapter 8

Experimental

8.1 General Procedures

8.1.1 Laboratory Equipment and Apparatus

All reactions were carried out under an argon atmosphere with the rigorous exclusion of oxygen and water using standard glovebox (MBraun) or high vacuum techniques, unless specified otherwise. All thermally unstable compounds were stored in a −35 °C freezer within a glovebox. Specialty glassware included thick walled (5 mm) glass reaction vessels equipped with Kontes Teflon stopcocks (referred to herein as 'bombs') and swivel frit assemblies. All glassware was either heated at 115 °C in an oven for a minimum of 2 hours or flame-dried with a Bunsen burner immediately before use.

8.1.2 Solvents

The solvents THF, diethyl ether, methylene chloride, pentane, benzene and toluene were dried and purified using a solvent purification system (MBraun) and stored in evacuated 500 mL bombs over sodium benzophenone ketyl (THF and diethyl ether), CaH_2 (methylene chloride) or "titanocene" (pentane, benzene and toluene). Deuterated solvents were dried over sodium benzophenone ketyl (benzene-d_6 and toluene-d_8) or CaH_2 (chloroform-*d* and dichloromethane-d_2), degassed via three freeze–pump–thaw cycles, distilled under vacuum and stored in glass bombs under argon. Unless otherwise specified, all solvents required for air-sensitive reactions were introduced directly into reaction flasks by vacuum transfer with condensation at −78 °C. For manipulations involving air-stable molecules, the solvents THF, diethyl ether, methylene chloride and *n*-hexane were purchased from EMD Chemicals and used without further purification.

Liquid nitrogen (−196 °C), liquid nitrogen/acetone (−94 °C) dry ice/acetone (−78 °C) and water/ice (0 °C) baths were used for cooling receiving flasks and to maintain low temperature conditions of reactions performed on a vacuum line or in a fume hood. For synthetic protocols performed within a glovebox, sealed reaction flasks were placed in a −35 °C freezer to cool synthetic mixtures and maintain low temperature conditions.

8.1.3 NMR Spectroscopy

Samples for NMR spectroscopy were recorded on a 300 MHz Bruker Avance II ultrashield spectrometer (^{1}H 300.13 MHz, ^{13}C{^{1}H} 75.47 MHz, ^{31}P{^{1}H} 121.49 MHz, ^{19}F

282.42 MHz and ^{11}B 96.29 MHz) and referenced relative to either $SiMe_4$ (0 ppm) through the residual solvent resonance(s) for ^{1}H and $^{13}C\{^{1}H\}$; or an external standard (85% H_3PO_4 (0 ppm) for $^{31}P\{^{1}H\}$, boron trifluoride diethyl etherate (0 ppm) for ^{11}B, or α,α,α-trifluorotoluene (−63.7 ppm) for ^{19}F NMR). All NMR spectra were recorded at ambient temperature (295 K) unless otherwise specified.

8.1.4 Other Instrumentation and Analysis

FT-IR spectra were recorded on a Bruker ALPHA FT infrared spectrometer with ATR sampling. Elemental analyses were performed using an Elementar Americas Vario MicroCube instrument.

8.1.5 Materials

The reagents di-*tert*-butyl dicarbonate, dimethylaminopyridine, sodium azide, urea, 2,4,6-trimethylaniline and 4-isopropylaniline (Alfa Aesar); chlorodiphenylphosphine, anhydrous lutetium(III) chloride and anhydrous erbium(III) chloride (Strem Chemicals); sodium nitrite (J. T. Baker); 2,4,6-tri-*tert*-butylaniline (Frinton Laboratories); and 2-chloro-1,3,2-dioxaphospholane (TCI America) were used as received. Solutions of *t*-BuLi (1.7 M in pentane), *n*-BuLi (1.6 M in hexane), $LiCH_2SiMe_3$ (1.0 M in pentane) and MeLi (1.6 M in Et_2O) were obtained from Sigma-Aldrich. The solvent was removed from the $LiCH_2SiMe_3$ and MeLi solutions under vacuum to yield the reagents as a white amorphous powder, which were then stored as

solids in a glovebox freezer at −35 °C. All deuterated solvents and reagents were purchased from Cambridge Isotope Laboratories.

Mes*ND_2 was prepared via the exchange reaction of Mes*NH_2 with D_2O under the presence of a catalytic amount of anhydrous HCl in diethyl ether. This resulted in >95% deuterium incorporation at the N atom of Mes*ND_2. The precursor *N*-(*tert*-butoxycarbonyl)-2,5-dibromopyrrole was prepared by a slightly modified literature procedure: all synthetic conditions were maintained as previously reported,[201] with the exception that chloroform was used to extract the product in place of carbon tetrachloride. A comparable product yield was obtained following recrystallization from anhydrous ethanol at −35 °C. The reagent $[Et_3NH]I$ was synthesized as previously described,[228] and subsequently purified by recrystallization from an acetone-methanol mixture (1:1) at −35 °C and dried thoroughly under vacuum. Mesityl azide,[229] phenyl azide,[230] tosyl azide,[231] 2-iodopyrimidine,[232] 1,8-dibromo-3,6-dimethylcarbazole,[143] $ScCl_3(THF)_3$,[233] $YCl_3(THF)_{3.5}$,[234] $Y(CH_2SiMe_3)_3(THF)_2$,[235] $TripNH_2$,[236] Mes*NHK,[237] and $[H(OEt_2)_2]^+[B(C_6F_5)_4]^-$,[205] were prepared according to literature procedures.

8.1.6 Preparation of Reagents by Modified Procedures

Synthesis of $Lu(CH_2SiMe_3)_3(THF)_2$

In a glovebox, $LuCl_3$ (2.10 g, 7.45 mmol) was slurried with THF (7 mL) in a 25 mL Erlenmeyer flask (caution: exothermic). After 2 minutes, pentane (3 mL) was added to the suspension and the mixture was then stirred for 20 minutes. The suspension was cooled to −35 °C and a solution of $LiCH_2SiMe_3$ (2.07 g, 22.0 mmol, 2.95 equiv) in

pentane (10 mL) was added dropwise at this temperature. The reaction mixture was allowed to warm to ambient temperature and was stirred for 1 h resulting in a colourless solution and an oily precipitate. All volatile components were removed from the flask under vacuum to give an oily white residue. The product was extracted into toluene and then filtered through a fine porosity frit. The solvent was removed from the clear and colourless filtrate under reduced pressure to give an oily residue. Upon standing at −35 °C, the residue crystallized into a solid mass. The product was dried thoroughly under reduced pressure to remove any traces of solvent, leaving a white crystalline solid. Yield: 4.024 g (94.6%). ^{1}H NMR (benzene-d_6): δ 3.96 (m, 8H, OCH_2CH$_2$), 1.29 (m, 8H, OCH$_2$CH_2), 0.30 (s, 27H, Si(CH_3)$_3$), −0.88 (s, 6H, CH_2). The spectroscopic analysis of this compound agrees with previously published data for the fully characterized product.[238]

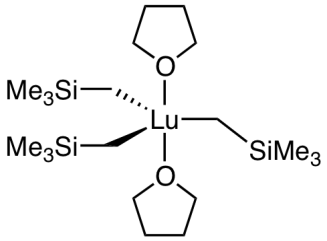

Synthesis of Sc(CH$_2$SiMe$_3$)$_3$(THF)$_2$

In a glovebox, ScCl$_3$(THF)$_3$ (0.860 g, 2.34 mmol, 1 equiv) was suspended in a mixture of pentane (3 mL) and THF (1 mL) in a 25 mL Erlenmeyer flask at −35 °C. A solution of LiCH$_2$SiMe$_3$ (0.649 g, 6.89 mmol, 2.95 equiv) in a mixture of pentane (10 mL) and THF (1 mL) was added slowly in portions over 30 min while keeping the solution cold with agitation. The cloudy white reaction mixture was allowed to warm to ambient temperature and was stirred for exactly 20 minutes. At this point, the solution began to take on a pale pink hue suggesting initial stages of thermal

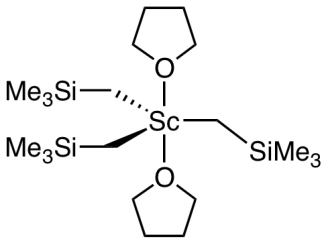

decomposition. Reaction completion was evidenced by the consumption of all sparingly soluble $ScCl_3(THF)_3$ in the flask and formation of a milky white oily layer at the bottom of the flask amongst the slightly cloudy and colourless solution. All volatile components were removed from the flask under vacuum to give a white solid residue. The product was extracted into toluene (5 × 1 mL) followed by pentane (3 × 1 mL). All extracts were combined and then filtered through a fine porosity frit. The solvent was removed from the clear and colourless filtrate under reduced pressure to give an off-white solid. (Note: if no solid is obtained, but rather an oily residue, then standing the oil at −35 °C for 30 min will induce crystallization. The crystalline mass can then be dried thoroughly under vacuum.) Yield: 0.909 g (86.3%). ^{1}H NMR (benzene-d_6): δ 4.04 (m, 8H, OCH_2CH$_2$), 1.34 (m, 8H, OCH$_2$CH_2), 0.277 (s, 27H, Si(CH_3)$_3$), −0.223 (s, 6H, CH$_2$). The spectroscopic analysis of this compound agrees with previously published data for the fully characterized product.[13]

Synthesis of Er(CH$_2$SiMe$_3$)$_3$(THF)$_2$

In a glovebox, $ErCl_3$ (1.91 g, 6.98 mmol) was slurried with THF (4 mL) in a 25 mL Erlenmeyer flask (caution: exothermic). After 2 minutes, pentane (4 mL) was added to the suspension and the mixture was then stirred for 20 minutes. The suspension was cooled to −35 °C and a solution of $LiCH_2SiMe_3$ (1.94 g, 20.6 mmol, 2.95 equiv) in pentane (12 mL) was added dropwise at this temperature. The reaction mixture was allowed to warm to ambient temperature and was stirred for 1 h resulting in a cloudy pink solution. All volatile components were removed from the flask

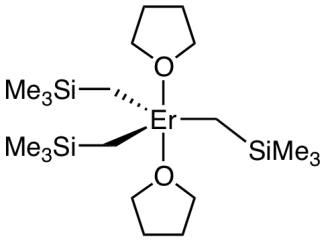

under vacuum to give an oily pink residue. The product was extracted into toluene (10 mL) and then filtered through a bed of Celite on a fine porosity frit. The frit was then washed with toluene (5 × 1 mL). The solvent was removed from the clear pink filtrate under reduced pressure to leave a pink waxy solid. Yield: 3.27 g (81.8%). ^{1}H NMR (benzene-d_6): δ 208.7 (OCH_2CH$_2$), 99.2 (OCH$_2$CH_2), −39.0 (Si(CH_3)$_3$), −255.3 (CH_2).

Synthesis of 4-isopropylphenyl azide

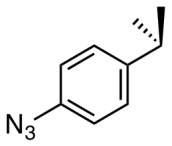

Aqueous 5 M HCl (125 mL) was added dropwise under air to a clear dark red solution of 4-isopropylaniline (10.0 g, 74.2 mmol) in THF (100 mL) at 0 °C. The red-brown solution was stirred for 15 min, following which, a solution of $NaNO_2$ (5.63 g, 81.6 mmol) in H_2O (65 mL) was added dropwise over 20 min. Urea (0.708 g, 11.8 mmol) was added as a solid to remove excess nitrous acid. A solution of NaN_3 (5.65 g, 87.0 mmol) in H_2O (50 mL) was added very slowly at 0 °C, after which the solution was stirred at this temperature for a further 2 h. The product was extracted into Et_2O (3 x 100 mL) and the organic layer was washed with 1 × 100 mL 1 M HCl, dried over $MgSO_4$ and concentrated in vacuo to give a dark red liquid. The product was purified by filtration through a silica column (20 cm), eluting with hexane. The hexane was removed from the eluent by rotary evaporation, leaving PippN_3 as a canary yellow liquid. Yield: 10.4 g (86.7%). ^{1}H NMR (chloroform-*d*): δ 7.21 (d, 2H, $^{3}J_{HH}$ = 8.4 Hz, aromatic C*H*), 6.96 (d, 2H, $^{3}J_{HH}$ = 8.4 Hz, aromatic C*H*), 2.90 (sp, 1H, $^{3}J_{HH}$ = 6.9 Hz, C*H*(CH$_3$)$_2$), 1.24 (d, 6H, $^{3}J_{HH}$ = 6.9 Hz, CH(CH_3)$_2$). ^{13}C{^{1}H} NMR (chloroform-*d*): δ 145.9 (aromatic *C*), 137.5 (aromatic *C*), 127.9 (aromatic *C*), 119.1 (aromatic *C*), 33.7 (*C*H(CH$_3$)$_2$), 24.2 (CH(*C*H$_3$)$_2$). IR (neat): 2960 (m), 2128 (s), 2092 (s), 1506 (s), 1292 (s),

828 (s), 756 (m), 728 (m), 619 (m), 539 (s) cm^{-1}. The spectroscopic analysis of this compound agrees with previously published data for the fully characterized product.

Synthesis of 2-azidopyrimidine

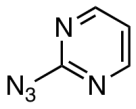

Diethyl ether (50 mL) was added to a 2-neck round bottomed flask charged with 2-iodopyrimidine (0.549 g, 2.66 mmol) to give a clear yellow solution. An aliquot of 1.7 M *t*-BuLi in pentane (3.1 mL, 5.33 mmol) was added dropwise over 15 min at −78 °C resulting in a cloudy orange reaction mixture. The solution was stirred at −78 °C for 5.25 h and gradually acquired a cloudy yellow appearance. At this temperature, tosyl azide (0.523 g, 2.66 mmol) was added by syringe. Following the addition, the flask was allowed to slowly warm to ambient temperature with stirring over 14 h. A saturated NaCl solution (75 mL) was added to the reaction mixture and the organic layer was then separated. The aqueous fraction was washed with 2 × 50 mL of diethyl ether. All organic fractions were combined, dried over $MgSO_4$ and filtered. The solvent was removed by rotary evaporation, leaving an oily yellow residue. A small amount of cold diethyl ether (5 mL) was used to wash the residue, leaving a yellow solid. Yield: 0.210 g (65.1%). The product can exist as a tautomeric mixture of 2-azidopyrimidine and tetrazolo[1,5-a]pyrimidine in solution, depending on the solvent used. Previous literature reported the detection of only one tautomer (2-azidopyrimidine) in chloroform-*d* solution.[239] In this work, a tautomeric mixture of 2-azidopyrimidine and tetrazolo[1,5-a]pyrimidine with a 1:2 ratio was observed in chloroform-*d* solution. ^{1}H NMR (chloroform-*d*, 2-azidopyrimidine): δ 8.60 (d, $^3J_{HH}$ = 4.8 Hz, 2H, 4,6-C*H*), 7.06 (t, $^3J_{HH}$ = 4.8 Hz, 1H, 5-C*H*). ^{1}H NMR (chloroform-*d*, tetrazolo[1,5-a]pyrimidine): δ 9.13

(dd, $^{3}J_{HH}$ = 6.9 Hz, $^{4}J_{HH}$ = 1.7 Hz 1H, C*H*), 9.07 (dd, $^{3}J_{HH}$ = 4.0 Hz, $^{4}J_{HH}$ = 1.8 Hz 1H, C*H*), 7.34 (dd, $^{3}J_{HH}$ = 6.9 Hz, $^{3}J_{HH}$ = 4.0 Hz 1H, C*H*).

Synthesis of phenyl azide-d_5

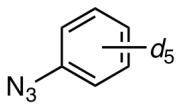

Aqueous 8 M HCl (30 mL) was added dropwise under air to a clear yellow solution of $C_6D_5NH_2$ (2.52 g, 25.7 mmol) in THF (100 mL) at 0 °C. The pale yellow solution was stirred for 15 min, following which, a solution of $NaNO_2$ (1.95 g, 28.3 mmol) in H_2O (16.5 mL) was added dropwise over 10 min. Urea (0.253 g, 4.21 mmol) was added as a solid to remove excess nitrous acid. A solution of NaN_3 (1.85 g, 28.4 mmol) in H_2O (15 mL) was added over 30 min at 0 °C, after which the cloudy white solution was stirred at this temperature for a further 1.75 h. The product was extracted into hexanes (3 × 50 mL) and the combined organic layers were washed with 1 × 50 mL of 1 M HCl, dried over $MgSO_4$ and concentrated in vacuo to give a yellow liquid. The product was purified by filtration through a silica column (20 cm), eluting with hexanes. The solvent was removed from the eluent by rotary evaporation, leaving the product as a canary yellow liquid. Yield: 2.66 g (83.5%). Deuterium content on the ring was found to be ~98% and approximately 2% of the material existed as proteo phenyl azide. ^{13}C NMR (chloroform-*d*): δ 140.0 (s), 129.4 (t, $^{1}J_{CD}$ = 24.5 Hz), 124.5 (t, $^{1}J_{CD}$ = 24.4 Hz), 118.7 (t, $^{1}J_{CD}$ = 24.3 Hz). IR: ν (cm^{-1}): 2276 (vw), 2109 (s), 2094 (s), 2034 (w), 1560 (m), 1409 (vw), 1370 (s), 1302 (vw), 1260 (s), 1098 (w), 1068 (vw), 1040 (vw), 958 (vw), 876 (vw), 841 (vw), 818 (w), 775 (vw), 753 (w), 650 (m), 625 (m), 590 (vw), 547 (s), 530 (m), 425 (s). The spectroscopic analysis of this compound agrees with previously published data for phenyl azide-d_5.[240]

8.2 Experimental Procedures Pertaining to Chapter 2

8.2.1 Synthesis of Compounds

Synthesis of 1,8,9N-Tris(diphenylphosphino)-3,6-dimethylcarbazole (1)

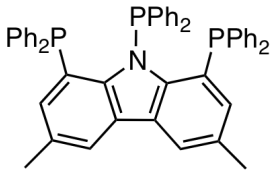

A hexane solution (1.6 M) of *n*-BuLi (0.38 mL, 0.608 mmol) was added dropwise to a solution of 1,8-dibromo-3,6-dimethylcarbazole (0.210 g, 0.595 mmol) in diethyl ether at 0 °C. The yellow reaction mixture was stirred at 0 °C for 1 h, following which, an aliquot of trimethylsilyl chloride (83 μL, 0.652 mmol) was added by microsyringe. The solution was warmed to ambient temperature and stirred for 1 h to give a cloudy yellow mixture. The flask was cooled to −78 °C and a pentane solution (1.7 M) of *t*-BuLi (1.5 mL, 2.55 mmol) was added dropwise via syringe. The solution stirred at −78 °C for 1 h, followed by 3 h at ambient temperature and over this time, acquired a very cloudy yellow appearance with the formation of a thick precipitate. The flask was cooled back to −78 °C and chlorodiphenylphosphine (3.2 mL, 1.78 mmol) was slowly added to generate an intense orange-red coloured solution. The reaction mixture was allowed to slowly warm to ambient temperature as it stirred overnight for 12.5 h and over this time acquired a cloudy yellow appearance. The solution was filtered through a fine porosity frit to remove insoluble byproducts and the frit was then washed with diethyl ether (2 × 20 mL) until the washings were colourless. All volatile components were removed from the clear, dark yellow filtrate under reduced pressure to afford a yellow residue. The residue was washed with heptane (25 mL), collected on a fine porosity frit and dried thoroughly under vacuum. Yield: 0.224 g (50.4%). ^{1}H NMR (chloroform-*d*): δ 7.96 (s, 2H, Cz 4,5-C*H*),

7.42–7.28 (ov m, 10H, aromatic C*H*), 7.24–7.10 (ov m, 12H, aromatic C*H*), 6.96–6.90 (ov m, 10H, aromatic C*H*), 2.43 (s, 6H, CH_3). $^{13}C\{^1H\}$ NMR (chloroform-*d*): δ 139.2 (d, J_{CP} = 5.9 Hz, aromatic *ipso*-*C*), 139.0 (d, J_{CP} = 5.9 Hz, aromatic *ipso*-*C*), 137.0 (dd, J_{CP} = 6.9 Hz, J_{CP} = 6.9 Hz, aromatic *ipso*-*C*), 136.8 (dd, J_{CP} = 6.9 Hz, J_{CP} = 6.9 Hz, aromatic *ipso*-*C*), 136.6 (s, aromatic *C*H), 133.2 (d, J_{CP} = 18.7 Hz, aromatic *C*H), 131.2 (s, aromatic *ipso*-*C*), 130.5 (dt, J_{CP} = 18.7 Hz, J_{CP} = 3.1 Hz, aromatic *C*H), 127.8 (s, aromatic *C*H), 127.7 (s, aromatic *C*H), 127.7 (d, J_{CP} = 26.1 Hz, aromatic *C*H), 127.3 (s, aromatic *C*H), 122.6 (dd, J_{CP} = 20.1 Hz, J_{CP} = 3.1 Hz, aromatic *ipso*-*C*), 121.0 (s, Cz, 4,5-*C*H), 21.2 (s, *C*H_3). $^{31}P\{^1H\}$ NMR (chloroform-*d*): δ 53.3 (t, J_{PP} = 69.5 Hz, 1P), 17.2 (d, J_{PP} = 69.5 Hz, 2P). Anal. Calcd. (%) for $C_{50}H_{40}NP_3$: 80.31; H, 5.39; N, 1.87. Found: C, 80.36; H, 6.14; N, 1.83.

Synthesis of 1,8-Dibromo-3,6-dimethyl-9-BOC-carbazole (3)

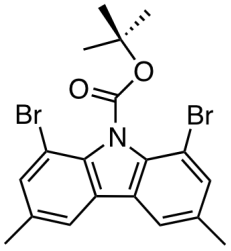

An intimate mixture of 1,8-dibromo-3,6-dimethylcarbazole (0.468 g, 1.33 mmol) and dimethylaminopyridine (0.171 g, 1.40 mmol) was dissolved in 30 mL of dichloromethane to give a clear yellow solution. An excess of di-*tert*-butyl dicarbonate (0.479 g, 2.19 mmol) was added via syringe at ambient temperature. The clear red reaction mixture was stirred for 18 h, generating a yellow solution. The reaction was quenched by addition of 50 mL of 1 M HCl. The layers were separated and the acidic layer was extracted with a further 2 × 50 mL of methylene chloride. The combined fractions were then washed with 3 × 50 mL of 1 M $NaHCO_3$ followed by 2 × 50 mL of 3 M NaCl. The organic layer was dried over $MgSO_4$, filtered and the solvent was removed under vacuum, giving the *N*-

protected product as an off-white solid. Yield: 0.506 g (84.2%). ^{1}H NMR (chloroform-*d*): δ 7.62 (s, 2H, C*H*), 7.43 (s, 2H, C*H*), 2.44 (s, 6H, CH_3), 1.68 (s, 9H, OC(CH_3)$_3$). ^{13}C{^{1}H} NMR (chloroform-*d*): δ 151.5 (*C*=O), 137.0, 133.3, 133.1, 127.5, 119.3, 106.2 (Ar–*C*s), 86.5 (O*C*(CH$_3$)$_3$), 28.1 (OC(*C*H$_3$)$_3$), 20.9 (*C*H$_3$). IR (neat, ATR): 2978 (w), 2922 (w), 2860 (w), 1749 (m, ν C=O), 1557 (w), 1478 (m), 1419 (w), 1368 (m), 1309 (m), 1230 (m), 1177 (m), 1127 (s), 1064 (m), 836 (s) cm^{-1}. Anal. Calcd. (%) for $C_{19}H_{19}Br_2NO_2$: C, 50.36; H, 4.23; N, 3.09. Found: C, 49.83; H, 4.17; N, 3.16.

Synthesis of 1,8-Bis(diphenylphosphino)-3,6-dimethyl-9-BOC-carbazole (4)

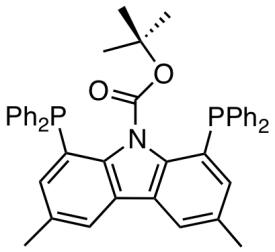

A pentane solution of *t*-BuLi (1.40 mL, 2.38 mmol) was added dropwise to a solution of **3** (0.506 g, 1.12 mmol) in 50 mL of diethyl ether at −78 °C resulting in a cloudy white suspension. The reaction mixture was stirred at −78 °C for 3.5 h, after which an aliquot of chlorodiphenylphosphine (0.425 mL, 2.37 mmol) was added slowly at −78 °C producing a red-orange colour. The solution was allowed to slowly warm to ambient temperature as it was stirred for 16 h, generating a cloudy yellow suspension. The reaction mixture was filtered through a fine porosity frit to remove insoluble byproducts and the frit was then washed with diethyl ether (2 × 20 mL) until the washings were colourless. The solvent was removed from the filtrate under reduced pressure to yield a gold coloured solid. Recrystallization from a toluene solution layered with pentane at −35 °C gave **4** as an off-white solid. Yield: 0.713 g (96.0%) ^{1}H NMR (benzene-d_6): δ 7.54 (m, 8H, phenyl C*H*), 7.46 (s, 2H, Cz 4,5-C*H*), 7.70 (d, $^{3}J_{HP}$ = 4.4 Hz, 2H, Cz 2,7-C*H*), 7.06 (ov m, 12H, phenyl C*H*), 2.06 (s, 6H, CH_3), 1.40 (s, 9H,

OC(CH_3)$_3$). ^{13}C{^{1}H} NMR (chloroform-*d*): δ 152.6 (s, *C*=O), 144.2 (d, J_{CP} = 20.9 Hz, aromatic *ipso*-*C*), 139.0 (d, J_{CP} = 14.8 Hz, aromatic *ipso*-*C*), 135.3 (s, aromatic *C*H), 133.8 (d, J_{CP} = 20.4 Hz, aromatic *C*H), 133.2 (s, aromatic *ipso*-*C*), 128.3 (s, aromatic *C*H), 128.2 (s, aromatic *C*H), 127.8 (d, J_{CP} = 5.5 Hz, aromatic *ipso*-*C*), 126.2 (d, J_{CP} = 22.2 Hz, aromatic *ipso*-*C*), 120.5 (s, aromatic *C*H), 85.5 (s, O*C*(CH$_3$)$_3$), 28.2 (t, J_{CP} = 2.6 Hz, OC(*C*H$_3$)$_3$), 21.3, (s, Cz *C*H$_3$). ^{31}P{^{1}H} NMR (benzene-d_6): δ −12.0. IR (neat): 3060 (w), 2982 (w), 1724 (s, ν C=O), 1557 (w), 1474 (m), 1434 (m), 1388 (m), 1398 (m), 1277 (m), 1246 (m), 1139 (s), 1090 (m), 1023 (w), 856 (m), 829 (m), 741 (s), 694 (s) cm^{-1}. Anal. Calcd. (%) for $C_{43}H_{39}NO_2P_2$: C, 77.81; H, 5.92; N, 2.11. Found: C, 78.24; H, 6.02; N, 2.39.

Synthesis of 1,8-Bis(diphenylphosphino)-3,6-dimethyl-9H-carbazole (2)

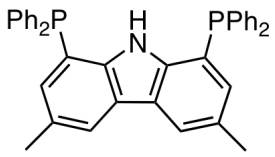

Toluene (50 mL) was added to a 100 mL bomb charged with **4** (9.33 g, 14.1 mmol) to give a cloudy brown suspension. The bomb was heated to 160 °C for 4.5 h under static vacuum, generating a clear red solution. The product was cannula transferred to a 100 mL round bottomed flask where the solvent was removed under vacuum to yield an orange solid. Recrystallization from a toluene solution layered with pentane at −35 °C gave **2** as an analytically pure pale yellow solid. Yield: 7.43 g (93.8%) ^{1}H NMR (benzene-d_6): δ 8.36 (s, 1H, N*H*), 7.81 (s, 2H, aromatic C*H*) 7.37–7.31 (ov m, 10H, aromatic C*H* + phenyl C*H*), 6.98–6.96 (ov m, 12H, phenyl C*H*), 2.26 (s, 6H, CH_3). ^{13}C{^{1}H} NMR (chloroform-*d*): δ 140.8 (d, J_{CP} = 12.9 Hz, aromatic *ipso*-*C*), 135.7 (d, J_{CP} = 9.7 Hz, aromatic *ipso*-*C*), 133.3 (d, J_{CP} = 19.1 Hz, aromatic *C*H), 133.2 (d, J_{CP} = 16.1 Hz, aromatic *C*H), 129.0 (d,

J_{CP} = 6.2 Hz, aromatic *ipso*-*C*), 128.9–128.7 (ov m, 2 aromatic *C*Hs), 122.9 (m, aromatic *ipso*-*C*), 121.8 (aromatic *C*H), 117.0 (d, J_{CP} = 12.7 Hz, aromatic *ipso*-*C*), 21.5 (*C*H_3). $^{31}P\{^1H\}$ NMR (benzene-d_6): δ −15.4. Anal. Calcd. (%) for $C_{38}H_{31}NP_2$: C, 80.98; H, 5.54; N, 2.49. Found: C, 81.19; H, 5.60; N, 2.77.

Synthesis of HL_A^{Mes} (5)

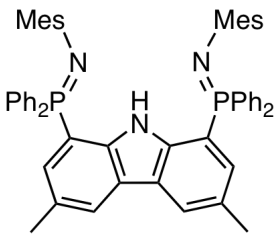

Toluene (40 mL) was added to a flask charged with **2** (1.324 g, 2.35 mmol) to give a yellow solution. An aliquot of mesityl azide (0.798 g, 4.95 mmol) was added via syringe at ambient temperature. Upon addition, a reaction was evident by the evolution of nitrogen gas. The reaction mixture was stirred for 22 h under an argon atmosphere and the solvent was removed under vacuum to afford a yellow solid. In a glovebox, the residue was reconstituted in hot toluene (5 mL), allowed to slowly cool to ambient temperature and then left at −35 °C to crystallize. The mother liquor was decanted to allow for collection of pale yellow crystals of $H\mathbf{L}_{\mathbf{A}}^{\mathbf{Mes}}$, which were washed with pentane (5 × 1 mL) and dried thoroughly under reduced pressure. Yield: 1.33 g (68.1%). ^1H NMR (benzene-d_6): δ 12.18 (s, 1H, N*H*), 7.78 (m, 10H, phenyl C*H* + Cz 4,5-C*H*), 7.29 (d, $^3J_{HP}$ = 13.9 Hz, 2H, Cz 2,7-C*H*), 6.95–6.85 (m, 12H, aromatic C*H*), 6.81 (s, 4H, mesityl C*H*), 2.27 (d, J_{HP} = 2.6 Hz, 6H, mesityl CH_3), 2.22 (s, 6H, Cz CH_3), 1.95 (d, J_{HP} = 1.6 Hz, 12H, mesityl CH_3). $^{13}C\{^1H\}$ NMR (benzene-d_6): δ 145.3 (d, J_{CP} = 3.2 Hz, aromatic *ipso*-*C*), 141.2 (d, J_{CP} = 3.4 Hz, aromatic *ipso*-*C*), 132.8 (s, aromatic *ipso*-*C*), 132.5 (d, J_{CP} = 9.6 Hz, aromatic *C*H), 131.5 (s, aromatic *ipso*-*C*), 131.2 (d, J_{CP} = 2.6 Hz, aromatic *C*H), 129.9 (d, J_{CP} = 8.8 Hz, aromatic *C*H), 128.9 (d, J_{CP} = 3.8 Hz,

aromatic *C*H), 128.6 (d, J_{CP} = 12.0 Hz, aromatic *C*H), 127.6 (s, aromatic *ipso*-*C*), 127.4 (d, J_{CP} = 4.1 Hz, aromatic *ipso*-*C*), 124.0 (d, J_{CP} = 2.2 Hz, aromatic *C*H), 123.9 (d, J_{CP} = 8.4 Hz, aromatic *ipso*-*C*), 117.1 (d, J_{CP} = 106.2 Hz, aromatic *ipso*-*C*), 21.4 (s, *C*H_3), 21.0 (ov s, *C*H_3), 21.0 (ov s, *C*H_3). $^{31}P\{^1H\}$ NMR (benzene-d_6): δ −6.5. Anal. Calcd. (%) for $C_{56}H_{53}N_3P_2$: C, 81.04; H, 6.44; N, 5.06. Found: C, 81.24; H, 6.30; N, 4.73.

Synthesis of (L_A^{Mes}-κ³*N*,κ²*C*$^{P\text{-}Ph}$)Y(THF) (7)

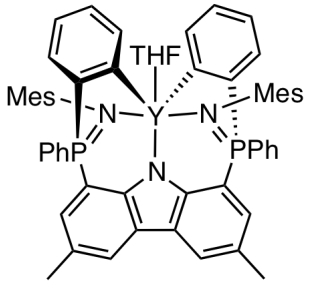

In a glovebox, toluene (2 mL) was added to a 25 mL Erlenmeyer flask charged with **5** (0.134 g, 0.161 mmol) and $Y(CH_2SiMe_3)_3(THF)_2$ (0.0795 g, 0.161 mmol) to give a clear yellow solution. The reaction mixture was stirred at ambient temperature for 17.5 h and gradually acquired a red colour. The solution was filtered through a bed of Celite and the Celite was washed with a further 2 mL of toluene. The clear red filtrate was concentrated to 1 mL under vacuum and then left at −35 ºC to crystallize. The mother liquor was decanted off, leaving a yellow microcrystalline solid that was washed with cold pentane and dried under reduced pressure. Yield: 0.110 g, 69.4%). ^1H NMR (benzene-d_6): δ 7.77 (br ov m, 6H, 4,5-Cz C*H* + phenyl C*H*), 7.71 (dd, $^3J_{HP}$ = 7.6 Hz, $^3J_{HH}$ = 8.7 Hz, 2H, phenyl C*H*), 7.56 (d, $^3J_{HH}$ = 6.7 Hz, 2H, phenyl C*H*), 7.38 (dd, $^3J_{HP}$ = 14.2 Hz, $^4J_{HH}$ = 1.3 Hz, 2H, 2,7-Cz C*H*), 7.18 (m, obscured by solvent, 2H, phenyl C*H*), 7.11–6.90 (ov m, 8H, phenyl C*H*), 6.72 (s, 2H, mesityl *m*-C*H*), 6.65 (s, 2H, mesityl *m*-C*H*), 4.23 (m, 2H, OCH_2CH$_2$), 3.88 (m, 2H, OCH_2CH$_2$), 2.32 (s, 6H, Cz CH_3), 2.10 (s, 6H, mesityl CH_3), 1.97 (s, 6H, mesityl CH_3), 1.74 (s, 6H, mesityl CH_3), 1.22 (m, 4H, OCH$_2$CH_2). $^{13}C\{^1H\}$ NMR (benzene-d_6): δ 198.1 (dd, $^1J_{CY}$ = 42.5 Hz, $^2J_{CP}$ =

38.8 Hz, *C*–Y), 150.6 (d, J_{CP} = 4.9 Hz, aromatic *ipso*-*C*), 142.3 (d, J_{CP} = 8.0 Hz, aromatic *ipso*-*C*), 139.9 (d, J_{CP} = 123.4 Hz, aromatic *ipso*-*C*), 139.1 (d, J_{CP} = 25.9 Hz, phenyl *C*H), 137.7 (d, J_{CP} = 5.6 Hz, aromatic *ipso*-*C*), 134.8 (d, J_{CP} = 5.8 Hz, aromatic *ipso*-*C*), 134.3 (d, J_{CP} = 8.6 Hz, phenyl *C*H), 132.2 (d, J_{CP} = 2.0 Hz, phenyl *C*H), 131.4 (d, J_{CP} = 3.9 Hz, aromatic *ipso*-*C*), 129.7 (s, Mes *m*-*C*H), 129.6 (d, J_{CP} = 2.9 Hz, phenyl *C*H), 128.2 (s, mesityl *m*-*C*H), 128.1 (d, J_{CP} = 6.2 Hz, phenyl *C*H), 127.4 (d, J_{CP} = 3.5 Hz, phenyl *C*H), 127.3 (d, J_{CP} = 10.0 Hz, Cz 2,7-*C*H), 126.6 (d, J_{CP} = 9.2 Hz, aromatic *ipso*-*C*), 125.9 (d, J_{CP} = 0.8 Hz, aromatic *ipso*-*C*), 124.8 (d, J_{CP} = 14.5 Hz, phenyl *C*H), 124.2 (d, J_{CP} = 12.0 Hz, aromatic *ipso*-*C*), 123.8 (d, J_{CP} = 1.5 Hz, Cz 4,5-*C*H), 118.1 (d, J_{CP} = 94.0 Hz, aromatic *ipso*-*C*), 71.8 (s, OCH_2CH_2), 25.9 (s, OCH_2CH_2), 21.5 (s, Cz CH_3), 21.0 (s, Mes CH_3), 20.4 (s, Mes CH_3), 20.3 (d, J_{CP} = 1.2 Hz, Mes CH_3). $^{31}P\{^1H\}$ NMR (benzene-d_6): δ 24.1 (d, $^2J_{PY}$ = 6.2 Hz). Anal. Calcd. (%) for $C_{60}H_{58}N_3OP_2Y$: C, 72.94; H, 5.92; N, 4.25. Found: C, 67.82; H, 6.39; N, 4.32. Low carbon values were obtained for this compound despite repeated analysis attempts.

Synthesis of (L_A^{Mes}-κ³N)Li (8)

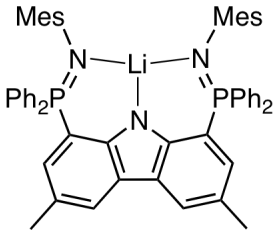

A hexane solution of *n*-BuLi (15.2 mL, 24.4 mmol) was added dropwise over 10 minutes to a vigorously stirred solution of **5** (10.2 g, 24.4 mmol) in heptane (200 mL) at −78 °C. The cloudy white suspension was stirred at −78 °C for 2.5 hours and then allowed to gradually warm to 0 °C where it was stirred for a further 40 minutes with the formation of a clear yellow solution and the evolution of butane gas. The reaction mixture was allowed to warm to ambient temperature where it was stirred for 1 hour to

ensure complete reaction. The solvent was removed *in vacuo* leaving pure lithiated ligand as an orange solid in nearly quantitative yield (10.2 g, 98.3%). ^{1}H NMR (benzene-d_6): δ 8.19 (s, 2H, Cz 4,5-C*H*), 7.64 (m, 8H, phenyl C*H*), 7.13 (d, partially obscured by solvent, 2H, Cz 2,7-C*H*), 6.97–6.81 (ov m, 12H, phenyl C*H*), 6.63 (s, 4H, mesityl C*H*), 2.42 (s, 6H, CH_3), 2.15 (s, 6H, CH_3), 2.01 (s, 12H, CH_3). ^{13}C{^{1}H} NMR (benzene-d_6): δ 153.7 (d, J_{CP} = 4.2 Hz, aromatic *ipso*-*C*), 144.1 (d, J_{CP} = 7.1 Hz, aromatic *ipso*-*C*), 133.9 (d, J_{CP} = 7.4 Hz, aromatic *ipso*-*C*), 132.7 (d, J_{CP} = 9.3 Hz, aromatic *C*H), 132.7 (s, aromatic *ipso*-*C*), 131.4 (d, J_{CP} = 2.9 Hz, aromatic *C*H), 129.4 (d, J_{CP} = 2.6 Hz, aromatic *C*H), 129.3 (d, J_{CP} = 4.0 Hz, aromatic *ipso*-*C*), 128.6 (s, obscured by solvent, aromatic *C*H), 128.4 (s, obscured by solvent, aromatic *C*H), 127.2 (s, aromatic *ipso*-*C*), 125.4 (d, J_{CP} = 3.3 Hz, aromatic *C*H), 122.4 (d, J_{CP} = 12.6 Hz, aromatic *ipso*-*C*), 115.2 (d, J_{CP} = 99.3 Hz, aromatic *ipso*-*C*), 21.9 (s, *C*H$_3$), 21.0 (s, *C*H$_3$), 20.9 (s, *C*H$_3$). ^{31}P{^{1}H} NMR (benzene-d_6): δ 11.0. Anal. Calcd. (%) for $C_{56}H_{52}LiN_3P_2$: C, 80.46; H, 6.27; N, 5.03. Found: C, 80.39; H, 6.76; N, 4.26.

*Synthesis of (L_A^{Mes}-κ^3*N*)ScCl$_2$ (9)*

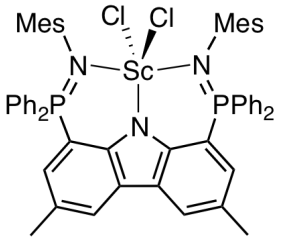

Toluene (25 mL) was added to a bomb charged with **8** (0.389 g, 0.466 mmol) and $ScCl_3(THF)_3$ (0.183 g, 0.499 mmol) to give an orange suspension. The reaction mixture was heated to 100 °C for 17 h resulting in a light orange solution with a white precipitate. The solution was brought into a glovebox where it was filtered through a fine porosity frit to remove LiCl. The filtrate was concentrated under reduced pressure and left at −35 °C to crystallize. Yellow crystals of ($\mathbf{L}_\mathbf{A}^{\mathbf{Mes}}$-κ^3*N*)$ScCl_2$ were collected by

filtration, washed with pentane and dried under vacuum. Yield: 0.367 g (83.3%). ^{1}H NMR (chloroform-*d*): δ 8.17 (s, 2H, Cz 4,5-C*H*), 7.47 (m, 20H, phenyl C*H*), 6.85 (d, $^{3}J_{HP}$ = 15.2 Hz, 2H, Cz 2,7-C*H*), 6.55 (s, 4H, mesityl C*H*), 2.44 (s, 6H, CH_3), 2.05 (s, 6H, CH_3), 1.53 (s, 12H, CH_3). ^{13}C NMR (chloroform-*d*): δ 151.0 (d, J_{CP} = 4.1 Hz, aromatic *ipso*-*C*), 141.4 (d, J_{CP} = 9.1 Hz, aromatic *ipso*-*C*), 137.0 (d, J_{CP} = 6.0 Hz, aromatic *ipso*-*C*), 134.4 (d, J_{CP} = 9.7 Hz, aromatic *C*H), 133.2 (d, J_{CP} = 4.2 Hz, aromatic *ipso*-*C*), 132.4 (d, J_{CP} = 2.6 Hz, aromatic *C*H), 131.2 (d, J_{CP} = 10.5 Hz, aromatic *C*H), 129.2 (d, J_{CP} = 3.5 Hz, aromatic *C*H), 128.1 (d, J_{CP} = 12.1 Hz, aromatic *C*H), 127.8 (d, J_{CP} = 96.2 Hz, aromatic *ipso*-*C*), 126.2 (d, J_{CP} = 13.1 Hz, aromatic *ipso*-*C*), 125.8 (d, J_{CP} = 9.0 Hz, aromatic *ipso*-*C*), 125.0 (s, aromatic *C*H), 109.3 (d, J_{CP} = 106.5 Hz, aromatic *ipso*-*C*), 21.3 (s, *C*H_3), 20.8 (s, *C*H_3), 20.3 (s, *C*H_3). ^{31}P{^{1}H} NMR (benzene-d_6): δ 26.4. Anal. Calcd. (%) for $C_{56}H_{52}Cl_2N_3P_2Sc$: C, 71.19; H, 5.55; N, 4.45. Found: C, 69.21; H, 5.59; N, 4.32. Low carbon values were obtained for this compound despite repeated analysis attempts.

*Synthesis of (L_A^{Mes}-κ^3*N*)YCl$_2$ (10)*

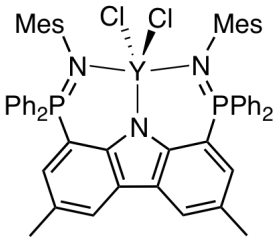

Toluene (50 mL) was added to a bomb charged with **8** (0.401 g, 0.481 mmol) and $YCl_3(THF)_{3.5}$ (0.226 g, 0.504 mmol) to give a red-orange suspension. The reaction mixture was heated to 60 °C for 95 h resulting in a light orange solution with a white precipitate. The solution was brought into a glovebox where it was filtered through a fine porosity frit to remove LiCl. The filtrate was concentrated under reduced pressure and left at −35 °C to crystallize. Yellow crystals of ($\mathbf{L}_{\mathbf{A}}^{\mathbf{Mes}}$-κ^3*N*)$YCl_2$ were collected by

filtration, washed with pentane and dried under vacuum. Yield: 0.343 g (72.1%). ^{1}H NMR (chloroform-*d*): δ 8.26 (s, 2H, Cz 4,5-C*H*), 7.42 (m, 20H, phenyl C*H*), 6.80 (d, $^{3}J_{HP}$ = 15.0 Hz, 2H, Cz 2,7-C*H*), 6.49 (s, 4H, mesityl C*H*), 2.41 (s, 6H, CH_3), 2.10 (s, 6H, CH_3), 1.48 (s, 12H, CH_3). ^{13}C NMR (chloroform-*d*): δ 151.1 (s, aromatic *ipso*-*C*), 138.7 (d, J_{CP} = 8.4 Hz, aromatic *ipso*-*C*), 136.9 (d, J_{CP} = 6.5 Hz, aromatic *ipso*-*C*), 134.0 (d, J_{CP} = 9.5 Hz, aromatic *C*H), 133.4 (d, J_{CP} = 4.0 Hz, aromatic *ipso*-*C*), 132.5 (s, aromatic *C*H), 132.0 (d, J_{CP} = 11.1 Hz, aromatic *C*H), 129.4 (s, aromatic *C*H), 128.3 (d, J_{CP} = 12.0 Hz, aromatic *C*H), 128.0 (d, J_{CP} = 96.1 Hz, aromatic *ipso*-*C*), 126.4 (d, J_{CP} = 8.8 Hz, aromatic *ipso*-*C*), 125.7 (d, J_{CP} = 12.6 Hz, aromatic *ipso*-*C*), 125.2 (s, aromatic *C*H), 109.3 (d, J_{CP} = 107.7 Hz, aromatic *ipso*-*C*), 21.2 (s, *C*H_3), 20.8 (s, *C*H_3), 20.0 (s, *C*H_3). ^{31}P{^{1}H} NMR (benzene-d_6): δ 25.2 (d, $^{2}J_{PY}$ = 2.3 Hz). Anal. Calcd. (%) for $C_{56}H_{52}Cl_2N_3P_2Y$: C, 68.02; H, 5.30; N, 4.25. Found: C, 65.60; H, 5.28; N, 4.24. Low carbon values were obtained for this compound despite repeated analysis attempts.

8.3 Experimental Procedures Pertaining to Chapter 3

8.3.1 Synthesis of Compounds

Synthesis of HL_A^{Ph} (11)

Benzene (150 mL) was added to a flask charged with **2** (4.73 g, 8.39 mmol) to give a yellow solution. An aliquot of phenyl azide (2.07 g, 17.4 mmol) was added via syringe at ambient temperature. Upon addition, a red product rapidly precipitated out of solution along with concurrent evolution of nitrogen gas. The dark red suspension was

stirred under an argon atmosphere for 21 h, following which, the solvent was removed under vacuum and the residue brought into a glovebox. The product was washed with 5 × 2 mL of pentane to remove excess azide and dried thoroughly under reduced pressure to afford crude $H\mathbf{L}_{\mathbf{A}}^{\mathbf{Ph}}$ as a pale red solid. Recrystallization from a hot benzene solution (20 mL) layered with pentane (15 mL) at ambient temperature generated **11** as analytically pure pale yellow prisms. Yield: 6.03 g (96.4%). ^{1}H NMR (chloroform-*d*): δ 11.81 (s, 1H, N*H*), 8.01 (s, 2H, Cz 4,5-C*H*), 7.69 (m, 8H, *P*-phenyl *o*-C*H*), 7.46 (t, *J* = 6.9 Hz, 4H, *P*-phenyl *p*-C*H*), 7.34 (m, 8H, *P*-phenyl *m*-C*H*), 7.20 (d, $^{3}J_{HP}$ = 14.5 Hz, 2H, Cz 2,7-C*H*), 6.85 (m, 4H, *N*-phenyl *m*-C*H*), 6.68 (d, *J* = 8.0 Hz, 4H, *N*-phenyl *o*-C*H*), 6.58 (t, *J* = 14.5 Hz, 2H, *N*-phenyl *p*-C*H*), 2.44 (s, 6H, CH_3). ^{13}C{^{1}H} NMR (chloroform-*d*): δ 151.0 (d, J_{CP} = 3.5 Hz, aromatic *ipso*-*C*), 140.6 (d, J_{CP} = 2.9 Hz, aromatic *ipso*-*C*), 132.9 (d, J_{CP} = 9.8 Hz, aromatic *C*H), 131.7 (d, J_{CP} = 2.6 Hz, aromatic *C*H), 131.3 (d, J_{CP} = 10.5 Hz, aromatic *C*H), 130.8 (d, J_{CP} = 89.5 Hz, aromatic *ipso*-*C*), 128.7 (d, J_{CP} = 11.8 Hz, aromatic *C*H), 128.3 (s, aromatic *C*H), 128.0 (d, J_{CP} = 12.7 Hz, aromatic *ipso*-*C*), 124.2 (d, J_{CP} = 2.5 Hz, aromatic *C*H), 123.8 (d, J_{CP} = 18.0 Hz, aromatic *C*H), 123.6 (d, J_{CP} = 8.5 Hz, aromatic *ipso*-*C*), 117.3 (s, aromatic *C*H), 111.6 (d, J_{CP} = 118.8 Hz, aromatic *ipso*-*C*), 21.6 (s, CH_3). ^{31}P{^{1}H} NMR (benzene-d_6): δ 6.2. Anal. Calcd. (%) for $C_{50}H_{41}NP_2$: C, 80.52; H, 5.54; N, 5.63. Found: C, 80.60; H, 5.93; N, 5.37.

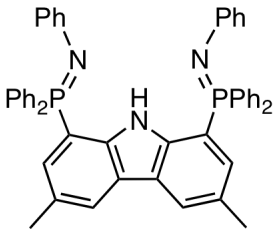

Synthesis of HL_A^{Pipp} (12)

Benzene (75 mL) was added to a flask charged with **2** (2.09 g, 3.71 mmol) to give a light yellow solution. An aliquot of 4-isopropylphenyl azide (1.25 g, 7.72 mmol) was

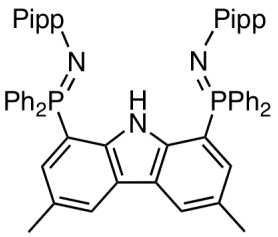

added via syringe at ambient temperature. Upon addition, the solution gradually became a red-orange colour with concurrent evolution of nitrogen gas. The solution was stirred under an argon atmosphere for 20 h, following which, the solvent was removed under vacuum and the residue brought into a glovebox. The product was recrystallized from hot benzene (15 mL) layered with pentane (5 mL) at ambient temperature. Pale yellow crystals of **12** formed over 24 h and were collected by filtration, washed with 2 × 1 mL of pentane and dried thoroughly under reduced pressure. Yield: 2.17 g (70.4%). ^{1}H NMR (chloroform-*d*): δ 11.72 (s, 1H, N*H*), 8.00 (s, 2H, Cz 4,5-C*H*), 7.71 (m, 8H, phenyl C*H*), 7.46 (t, J = 7.4 Hz, 4H, phenyl C*H*), 7.33 (m, 8H, phenyl C*H*), 7.23 (d, $^{3}J_{HP}$ = 14.6 Hz, 2H, Cz 2,7 C*H*), 6.74 (d, $^{3}J_{HH}$ = 8.2 Hz, 4H, Pipp C*H*), 6.64 (d, $^{3}J_{HH}$ = 8.3 Hz, 4H, Pipp C*H*), 2.74 (sp, $^{3}J_{HH}$ = 6.9 Hz, 2H, C*H*(CH$_3$)$_2$), 2.45 (s, 6H, C*H*$_3$), 1.17 (d, $^{3}J_{HH}$ = 6.9 Hz, 12H, CH(C*H*$_3$)$_2$). ^{13}C{^{1}H} NMR (chloroform-*d*): δ 148.3 (s, aromatic *ipso*-*C*), 140.5 (d, J_{CP} = 2.9 Hz, aromatic *ipso*-*C*), 137.5 (s, aromatic *ipso*-*C*), 133.0 (d, J_{CP} = 9.8 Hz, aromatic *C*H), 131.6 (d, J_{CP} = 2.5 Hz, aromatic *C*H), 131.3 (d, J_{CP} = 10.9 Hz, aromatic *C*H), 130.9 (d, J_{CP} = 87.2 Hz, aromatic *ipso*-*C*), 128.6 (d, J_{CP} = 11.7 Hz, aromatic *C*H), 127.9 (d, J_{CP} = 12.8 Hz, aromatic *ipso*-*C*), 126.2 (s, aromatic *C*H), 124.1 (d, J_{CP} = 2.6 Hz, aromatic *C*H), 123.5 (d, J_{CP} = 17.6 Hz, aromatic *ipso*-*C*), 123.5 (d, J_{CP} = 9.0 Hz, aromatic *C*H), 111.9 (d, J_{CP} = 120.2 Hz, aromatic *ipso*-*C*), 33.2 (s, *C*H(CH$_3$)$_2$), 24.4 (s, CH(*C*H$_3$)$_2$), 21.6 (s, *C*H$_3$). ^{31}P{^{1}H} NMR (benzene-d_6): δ 5.5. Anal. Calcd. (%) for $C_{56}H_{53}N_3P_2$: C, 81.04; H, 6.44; N, 5.06. Found: C, 80.21; H, 6.50; N, 4.98.

Synthesis of HL_A^{Pym} (13)

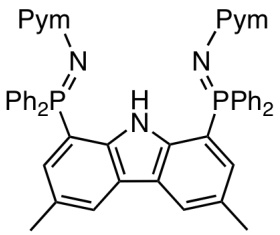

Toluene (50 mL) was added to a flask charged with **2** (0.814 g, 1.44 mmol) and 2-azidopyrimidine (0.351 g, 2.90 mmol) to give a dark yellow solution. The reaction mixture was stirred at ambient temperature under an argon atmosphere for 5 days to give a cloudy orange solution. All volatile components were removed under vacuum and the yellow residue was brought into a glovebox. The product was reconstituted in hot toluene (5 mL) and filtered through a fine porosity frit. The filtrate was cooled slowly to ambient temperature and left overnight to crystallize. Yellow crystals of the product were collected by filtration, washed with pentane (2 × 1 mL) and dried thoroughly under reduced pressure. Yield: 1.05 g (97.3%). ^{1}H NMR (chloroform-*d*): δ 10.77 (s, 1H, N*H*), 8.10 (d, $^{3}J_{HH}$ = 7.4 Hz, 4H, pyrimidine *m*-C*H*), 8.00 (s, 2H, Cz 4,5-C*H*), 7.88 (m, 8H, phenyl C*H*), 7.55 (dd, $^{3}J_{HP}$ = 14.2 Hz, $^{4}J_{HH}$ = 1.2 Hz, 2H, Cz 2,7 C*H*), 7.35 (m, 4H, phenyl C*H*), 7.28–7.20 (m, partially obscured by solvent, 8H, phenyl C*H*), 6.36 (t, $^{3}J_{HH}$ = 4.7 Hz, 2H, pyrimidine *p*-C*H*), 2.44 (s, 6H, CH_3). ^{13}C{^{1}H} NMR (chloroform-*d*): δ 166.8 (s, aromatic *ipso*-*C*), 157.5 (d, J_{CP} = 4.0 Hz, aromatic *C*H), 139.8 (d, J_{CP} = 4.2 Hz, aromatic *ipso*-*C*), 133.6 (d, J_{CP} = 10.3 Hz, aromatic *C*H), 132.1 (d, J_{CP} = 8.9 Hz, aromatic *C*H), 131.6 (d, J_{CP} = 2.8 Hz, aromatic *C*H), 128.5 (d, J_{CP} = 11.9 Hz, aromatic *ipso*-*C*), 128.2 (d, J_{CP} = 12.5 Hz, aromatic *C*H), 127.8 (s, aromatic *ipso*-*C*), 124.3 (d, J_{CP} = 2.9 Hz, aromatic *C*H), 123.4 (d, J_{CP} = 8.8 Hz, aromatic *ipso*-*C*), 110.1 (s, aromatic *C*H), 110.1 (d, J_{CP} = 116.4 Hz, aromatic *ipso*-*C*), 21.4 (s, *C*H_3). ^{31}P{^{1}H} NMR (benzene-d_6): δ 18.5.

Synthesis of (L_A^{Ph}-κ³N)Lu(CH_2SiMe_3)$_2$ (14)

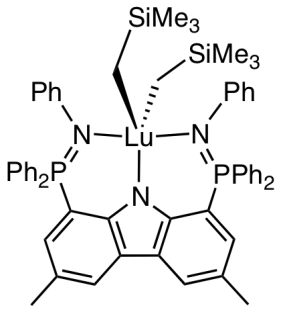

An NMR tube was charged with **11** (0.0400 g, 0.0536 mmol) and Lu(CH_2SiMe_3)$_3$(THF)$_2$ (0.0312 g, 0.0537 mmol) and sealed with a rubber septum and parafilm. The tube was cooled to −78 °C and an aliquot of toluene-d_8 (0.5 mL) was added via syringe. The tube was removed from the cold bath, shaken briefly to mix the reagents and then immediately inserted into a pre-cooled (271.3 K) NMR probe. The dialkyl complex (**14**) was characterized by multinuclear NMR spectroscopy *in situ*. No decomposition was observed over the course of characterization (2 h). ^{1}H NMR (toluene-d_8, 271.3 K): 8.12 (s, 2H, Cz 4,5-C*H*), 7.47 (m, 8H, *P*-phenyl C*H*), 6.93–6.75 (ov m, 24H, aromatic C*H*), 2.29 (s, 6H, CH_3), −0.06 (s, 18H, Si(CH_3)$_3$), −0.79 (s, 4H, CH_2). ^{13}C{^{1}H} NMR (toluene-d_8; 271.3 K): δ 152.5 (d, J_{CP} = 3.6 Hz, aromatic *ipso*-*C*), 147.4 (d, J_{CP} = 7.4 Hz, aromatic *ipso*-*C*), 137.1 (s, aromatic *ipso*-*C*), 134.1 (d, J_{CP} = 9.4 Hz, aromatic *C*H), 132.3 (d, J_{CP} = 2.2 Hz, aromatic *C*H), 130.9 (d, J_{CP} = 11.4 Hz, aromatic *C*H), 129.4 (d, J_{CP} = 7.9 Hz, aromatic *C*H), 129.1 (d, J_{CP} = 2.4 Hz, aromatic *C*H), 128.6 (d, J_{CP} = 11.8 Hz, aromatic *C*H), 127.3 (d, J_{CP} = 9.3 Hz, aromatic *ipso*-*C*), 126.0 (d, J_{CP} = 2.2 Hz, aromatic *C*H), 125.2 (s, aromatic *ipso*-*C*), 123.2 (d, J_{CP} = 2.8 Hz, aromatic *C*H), 108.9 (d, J_{CP} = 111.2 Hz, aromatic *ipso*-*C*), 40.4 (s, *C*H_2), 21.3 (s, *C*H_3), 4.63 (s, Si(*C*H_3)$_3$). ^{31}P{^{1}H} NMR (toluene-d_8; 271.3 K): δ 29.6.

Synthesis of (L_A^{Pipp}-κ³N)Lu(CH_2SiMe_3)$_2$ (15)

An NMR tube was charged with **12** (0.0216 g, 0.0260 mmol) and Lu(CH_2SiMe_3)$_3$(THF)$_2$ (0.0152 g, 0.0262 mmol) and sealed with a rubber septum and

parafilm. The tube was cooled to −78 °C and an aliquot of toluene-d_8 (0.5 mL) was added via syringe. The tube was removed from the cold bath, shaken briefly to mix the reagents and then immediately inserted into a pre-cooled (249.1 K) NMR probe. The dialkyl complex (**15**) was characterized by multinuclear NMR spectroscopy *in situ*. No decomposition was observed over the course of characterization (3 h). ^{1}H NMR (toluene-d_8; 249.1 K): δ 8.11 (s, 2H, Cz 4,5 C*H*), 7.49 (m, 8H phenyl C*H*), 7.11–7.10 (ov m, 4H, aromatic C*H*), 6.96–6.79 (ov m, 18H, aromatic C*H*), 2.63 (sp, $^3J_{HH}$ = 6.6 Hz, 2H, C*H*(CH$_3$)$_2$), 2.29 (s, 6H, CH_3), 1.13 (d, $^3J_{HH}$ = 6.6 Hz, 12H, CH(CH_3)$_2$), −0.01 (s, 18H, Si(CH_3)$_3$), −0.72 (s, 4H, CH_2). ^{13}C{^{1}H} NMR (toluene-d_8; 249.1 K): δ 152.5 (d, J_{CP} = 3.5 Hz, aromatic *ipso*-*C*), 144.8 (d, J_{CP} = 7.5 Hz, aromatic *ipso*-*C*), 143.4 (d, J_{CP} = 3.6 Hz, aromatic *ipso*-*C*), 137.0 (s, aromatic *ipso*-*C*), 134.1 (d, J_{CP} = 9.6 Hz, aromatic *C*H), 132.2 (s, aromatic *C*H), 130.9 (d, J_{CP} = 11.6 Hz, aromatic *C*H), 129.2 (s, aromatic *C*H), 128.5 (d, J_{CP} = 11.7 Hz, aromatic *C*H), 127.3 (d, J_{CP} = 9.3 Hz, aromatic *ipso*-*C*), 127.0 (s, aromatic *C*H), 126.0 (s, aromatic *C*H), 125.0 (s, aromatic *ipso*-*C*), 108.9 (d, J_{CP} = 110.6 Hz, aromatic *ipso*-*C*), 40.0 (s, *C*H$_2$), 33.9 (s, *C*H(CH$_3$)$_2$), 24.5 (s, CH(*C*H$_3$)$_2$), 21.3 (s, *C*H$_3$), 4.71 (s, Si(*C*H$_3$)$_3$). ^{31}P{^{1}H} NMR (toluene-d_8; 249.1 K): δ 29.4.

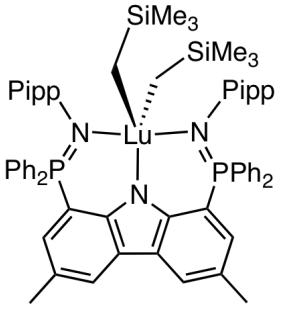

Synthesis of (L_A^{Pym}-κ^{5}N)Lu(CH$_2$SiMe$_3$)$_2$ (16)

An NMR tube was charged with **13** (0.0346 g, 0.0462 mmol) and Lu(CH$_2$SiMe$_3$)$_3$(THF)$_2$ (0.0268 g, 0.0462 mmol) and sealed with a rubber septum and parafilm. The tube was cooled to −78 °C and an aliquot of toluene-d_8 (0.5 mL) was added

via syringe. The tube was removed from the cold bath, shaken briefly to mix the reagents and then immediately inserted into a pre-cooled (263.2 K) NMR probe. The dialkyl complex (**16**) was characterized by multinuclear NMR spectroscopy *in situ*. No decomposition was observed over the course of characterization. ^{1}H NMR (toluene-d_8; 263.2 K): δ 8.28 (br m, 2H, pyrimidine C*H*), 8.10 (s, 2H, Cz 4,5-C*H*), 8.00 (m, 8H, phenyl C*H*), 7.74 (m, 2H, pyrimidine C*H*), 7.23 (d, $^{3}J_{HP}$ = 17.5 Hz, 2H, Cz 2,7-C*H*), 7.05–6.90 (m, 12H, phenyl C*H*), 6.08 (dd, $^{3}J_{HH}$ = 4.9 Hz, $^{3}J_{HH}$ = 4.9 Hz, 2H, pyrimidine C*H*), 2.20 (s, 6H, CH_3), −0.33 (s, 18H, Si(CH_3)$_3$), −1.22 (s, 4H, CH_2). ^{13}C{^{1}H} NMR (toluene-d_8; 263.2 K): δ 165.0 (d, J_{CP} = 2.1 Hz, aromatic *ipso*-*C*), 158.0 (s, aromatic *C*H), 155.6 (d, J_{CP} = 4.7 Hz, aromatic *C*H), 152.3 (d, J_{CP} = 2.8 Hz, aromatic *ipso*-*C*), 137.1 (s, aromatic *ipso*-*C*), 134.1 (d, J_{CP} = 10.5 Hz, aromatic *C*H), 133.8 (d, J_{CP} = 16.0 Hz, aromatic *C*H), 132.4 (d, J_{CP} = 1.9 Hz, aromatic *C*H), 129.8 (s, aromatic *ipso*-*C*), 128.7 (d, J_{CP} = 12.8 Hz, aromatic *C*H), 125.4 (s, aromatic *C*H), 124.3 (d, J_{CP} = 15.3 Hz, aromatic *ipso*-*C*), 111.9 (s, aromatic *C*H), 106.5 (d, J_{CP} = 122.8 Hz, aromatic *ipso*-*C*), 21.0 (s, *C*H_3), 19.6 (s, *C*H_2), 4.8 (s, Si(*C*H_3)$_3$). ^{31}P{^{1}H} NMR (toluene-d_8; 263.2 K): δ 27.2.

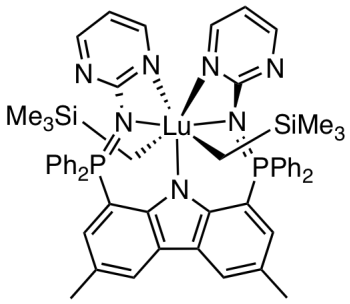

Synthesis of (L_A^{Ph}-κ^{3}N,κ^{2}C$^{P\text{-}Ph}$)Lu(THF) (19)

In a glovebox, a small Erlenmeyer flask was charged with **11** (0.193 g, 0.259 mmol) and Lu(CH_2SiMe_3)$_3$(THF)$_2$ (0.147 g, 0.252 mmol). Benzene (5 mL) was added to this solid mixture at ambient temperature to give a clear dark red solution. The reaction mixture was stirred for 18 h, following which, the volatile components were removed to

afford a yellow powder. The product was recrystallized from a 9 : 1 benzene / THF solution (10 mL) layered with pentane (10 mL). The crystals were collected by filtration, washed with pentane (2 mL) and dried under vacuum. Yield: 0.201 g (80.5%).

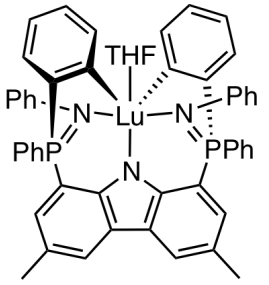

^{1}H NMR (benzene-d_6): δ 8.08 (s, 2H, Cz 4,5-C*H*), 7.97 (m, 4H, *P*-phenyl C*H*), 7.71 (m, 2H, *P*-phenyl C*H*), 7.56 (d, $^{3}J_{HP}$ = 13.4 Hz, 2H, Cz 2,7-C*H*), 7.11–6.97 (ov m, 12H, *P*-phenyl C*H*), 6.77 (ov m, 10H, *N*-phenyl C*H*), 4.00 (s, 4H, OCH_2CH_2), 2.34 (s, 6H, CH_3), 1.15 (s, 4H, OCH$_2$CH_2). ^{13}C{^{1}H} NMR (benzene-d_6): δ 204.6 (dd, $^{2}J_{CP}$ = 41.2 Hz, $^{4}J_{CP}$ = 1.1 Hz, Lu–*C*), 151.5 (d, J_{CP} = 5.7 Hz, aromatic *ipso*-*C*), 147.5 (d, J_{CP} = 7.3 Hz, aromatic *ipso*-*C*), 140.0 (d, J_{CP} = 25.6 Hz, aromatic *C*H), 138.5 (d, J_{CP} = 126.7 Hz, aromatic *ipso*-*C*), 134.2 (d, J_{CP} = 8.5 Hz, aromatic *C*H), 132.2 (d, J_{CP} = 1.7 Hz, aromatic *C*H), 129.6 (d, J_{CP} = 8.7 Hz, aromatic *C*H), 129.1 (d, J_{CP} = 2.1 Hz, aromatic *C*H), 128.7 (s, aromatic *C*H), 128.6 (d, J_{CP} = 7.2 Hz, aromatic *C*H), 128.2 (s, aromatic *C*H), 127.8 (d, J_{CP} = 3.7 Hz, aromatic *C*H), 127.0 (d, J_{CP} = 9.8 Hz, aromatic *ipso*-*C*), 126.3 (d, J_{CP} = 81.5 Hz, aromatic *ipso*-*C*), 124.9 (d, J_{CP} = 11.3 Hz, aromatic *ipso*-*C*), 124.6 (d, J_{CP} = 14.7 Hz, aromatic *C*H), 124.2 (d, J_{CP} = 2.3 Hz, aromatic *C*H), 122.6 (d, J_{CP} = 3.2 Hz, aromatic *C*H), 115.0 (d, J_{CP} = 87.0 Hz, aromatic *ipso*-*C*), 71.3 (s, O*C*H$_2$CH$_2$), 25.3 (s, OCH$_2$*C*H$_2$), 21.5 (s, *C*H$_3$). ^{31}P{^{1}H} NMR (benzene-d_6): δ 25.9. Anal. Calcd. (%) for $C_{54}H_{46}LuN_3OP_2$: C, 65.52; H, 4.68; N, 4.24. Found: C, 64.47; H, 5.02; N, 3.99.

Synthesis of (L_A^{Pipp}-κ^{3}N,κ^{2}C$^{P\text{-}Ph}$)Lu(THF) (20)

In a glovebox, a small Erlenmeyer flask was charged with **12** (0.506 g, 0.609 mmol) and Lu(CH$_2$SiMe$_3$)$_3$(THF)$_2$ (0.354 g, 0.610 mmol). Benzene (5 mL) was added to

this solid mixture at ambient temperature to give a clear dark red solution. The reaction mixture was stirred for 18 h, giving a dark red solution and a small quantity of an orange solid. An aliquot of THF (0.5 mL) was added to redissolve all material and the clear red solution was then layered with pentane (10 mL) and left at ambient temperature to crystallize. Fine needles developed after 48 h, which were collected by filtration, washed with pentane (2 mL) and dried under vacuum. Yield: 0.252 g (38.5%).

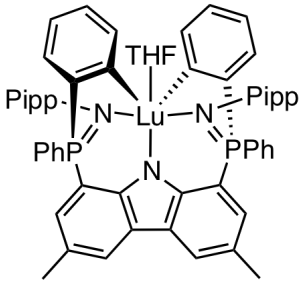

^{1}H NMR (benzene-d_6): δ 8.14 (s, 2H, Cz 4,5-C*H*), 8.00 (m, 4H, phenyl C*H*), 7.72 (m, 2H, phenyl C*H*), 7.57 (d, $^{3}J_{HP}$ = 13.4 Hz, 2H, Cz 2,7-C*H*), 7.13–6.98 (ov m, 12H, phenyl C*H*), 6.69 (dd, $^{3}J_{HH}$ = 8.3 Hz, $^{4}J_{HP}$ = 2.2 Hz, 4H, Pipp C*H*), 6.60 (d, $^{3}J_{HH}$ = 8.3 Hz, 4H, Pipp C*H*), 2.63 (sp, $^{3}J_{HH}$ = 6.9 Hz, 2H, C*H*(CH$_3$)$_2$), 2.37 (s, 6H, C*H*$_3$), 1.14 (d, $^{3}J_{HH}$ = 6.9 Hz, 6H, CH(C*H*$_3$)(CH$_3$)′), 1.12 (d, $^{3}J_{HH}$ = 6.9 Hz, 6H, CH(CH$_3$)(C*H*$_3$)′). ^{13}C{^{1}H} NMR (benzene-d_6): δ 204.7 (dd, $^{2}J_{CP}$ = 40.9 Hz, $^{4}J_{CP}$ = 1.2 Hz, Lu–*C*), 151.6 (d, J_{CP} = 5.7 Hz, aromatic *ipso*-*C*), 144.6 (d, J_{CP} = 7.3 Hz, aromatic *ipso*-*C*), 142.8 (d, J_{CP} = 3.5 Hz, aromatic *ipso*-*C*), 140.0 (d, J_{CP} = 25.3 Hz, aromatic *C*H), 138.5 (d, J_{CP} = 127.3 Hz, aromatic *ipso*-*C*), 134.2 (d, J_{CP} = 8.5 Hz, aromatic *C*H), 132.0 (d, J_{CP} = 2.2 Hz, aromatic *C*H), 129.7 (d, J_{CP} = 8.6 Hz, aromatic *C*H), 128.8 (d, J_{CP} = 24.7 Hz, aromatic *C*H), 128.3 (d, J_{CP} = 4.8 Hz, aromatic *C*H), 128.1 (s, aromatic *C*H), 127.6 (d, J_{CP} = 3.9 Hz, aromatic *C*H), 127.1 (d, J_{CP} = 2.5 Hz, aromatic *C*H), 126.9 (d, J_{CP} = 0.96 Hz, aromatic *ipso*-*C*), 126.7 (d, J_{CP} = 81.3 Hz, aromatic *ipso*-*C*), 124.9 (d, J_{CP} = 11.3 Hz, aromatic *ipso*-*C*), 124.5 (d, J_{CP} = 14.8 Hz, aromatic *C*H), 124.1 (d, J_{CP} = 2.0 Hz, aromatic *C*H), 115.4 (d, J_{CP} = 86.2 Hz, aromatic *ipso*-*C*), 71.2 (s, O*C*H$_2$CH$_2$), 33.9 (s, *C*H(CH$_3$)$_2$), 25.4 (s, OCH$_2$*C*H$_2$), 24.5 (s, CH(*C*H$_3$)(CH$_3$)′), 24.5 (s, CH(CH$_3$)(*C*H$_3$)′), 21.5 (s, *C*H$_3$). ^{31}P{^{1}H}

NMR (benzene-d_6): δ 25.0. Anal. Calcd. (%) for $C_{60}H_{58}LuN_3OP_2$: C, 67.10; H, 5.44; N, 3.91. Found: C, 67.07; H, 6.02; N, 3.64.

Synthesis of [(L_A^{Pym*}-κ^{5}N)Lu]$_2$(THF) (21)

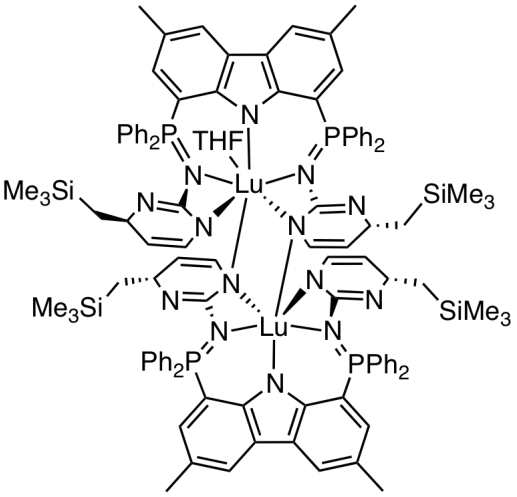

In a glovebox, a small Erlenmeyer flask was charged with **13** (0.256 g, 0.342 mmol) and $Lu(CH_2SiMe_3)_3(THF)_2$ (0.201 g, 0.346 mmol). Toluene (2 mL) and THF (1 mL) were added to this solid mixture at ambient temperature to give a cloudy red solution. The reaction mixture was stirred for 18 h, resulting in a clear dark red solution, which was then filtered through a bed of Celite. All volatile components were removed from the filtrate under reduced pressure to afford an orange-brown powder. The product was recrystallized from a concentrated toluene solution layered with pentane. Yellow crystals were collected by filtration, washed with pentane (2 × 1 mL) and dried thoroughly under reduced pressure. Yield: 0.364 g (94.0%). Acceptable ^{1}H and ^{13}C{^{1}H} NMR spectra could not be obtained for this compound. At ambient temperature in benzene-d_6 solution, the compound exhibited extremely wide line widths and broad spectral features; this may have been due to fluxional solution behaviour occurring on the NMR time scale. Attempts to acquire NMR spectra of the compound at various temperatures in toluene-d_8 (ranging from −60 °C to 90 °C) did not lead to significant spectral improvements. Anal. Calcd. (%) for $C_{112}H_{124}Lu_2N_{14}OP_4Si_4$: C, 59.30; H, 5.51; N, 8.64. Found: C, 58.96; H, 5.23; N, 8.68.

8.3.2 NMR Kinetics

All rate constants were determined by monitoring the $^{31}P\{^{1}H\}$ NMR resonance(s) over the course of the reaction (to at least 3 half lives) at a given temperature.

Typical Experiment

Proteo ligand **11** (0.0400 g, 0.0536 mmol) and $Lu(CH_2SiMe_3)_3(THF)_2$ (0.0312 g, 0.0537 mmol) were added to a Wilmad NMR tube which was then sealed with a rubber septum (Sigma-Aldrich) and parafilm. The tube was cooled to −78 °C and 0.5 mL of toluene-d_8 was injected via syringe. The tube was removed from the cold bath and shaken briefly, generating $(\mathbf{L}_{\mathbf{A}}^{\mathbf{Ph}}\text{-}\kappa^3\text{N})Lu(CH_2SiMe_3)_2$, **14** *in situ*. The tube was then immediately inserted into the NMR probe which was pre-equilibrated to the appropriate temperature. The sample was allowed to equilibrate at the set temperature over the course of shimming the tube in the magnet. $^{31}P\{^{1}H\}$ NMR spectra (16 scans) were recorded at pre-set time intervals until the reaction had progressed to at least 3 half-lives. The extent of reaction at each time interval was determined by integration of the peak intensity of the starting material relative to that of the intermediate and product. An appropriately long delay ($5 \times T_1$) between scans was utilized to ensure that integration was quantitative and not affected by the T_1 relaxation times of the reacting species. A summary of the observed rate constants and half-lives is listed in Table 3.3.

8.4 Experimental Procedures Pertaining to Chapter 4

8.4.1 Synthesis of Compounds

Synthesis of (L_A^{Pipp}-κ³N)LuI₂(THF) (22)

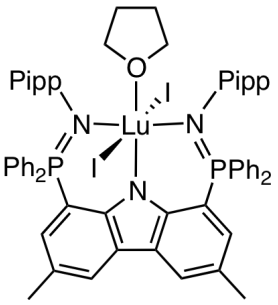

Methylene chloride (5 mL) was added to a flask containing **20** (1.70 g 1.59 mmol) and [Et_3NH]I (0.728 g, 3.18 mmol). The reaction mixture was stirred at ambient temperature for 1 h, and the solution rapidly became cloudy as the product precipitated as a solid. All volatile components were removed under vacuum to give a yellow residue. The sparingly soluble solid was suspended in a mixture of toluene (2 mL) and pentane (10 mL) and collected by filtration. The yellow product was then washed with pentane (4 × 5 mL) and dried thoroughly *in vacuo*. Yield: 1.92 g (91.1%). ^{1}H NMR (chloroform-*d*): δ 8.01 (s, 2H, 4,5-Cz C*H*), 7.90 (m, 8H, phenyl *o*-C*H*), 7.50 (m, 4H, phenyl *p*-C*H*), 7.40 (m, 8H, phenyl *m*-C*H*), 7.10–7.00 (ov m, 6H, Cz 2,7-C*H* + Pipp C*H*), 6.75 (d, $^3J_{HH}$ = 8.0 Hz, 4H, Pipp C*H*), 3.29 (br m, 4H, OCH_2CH_2), 2.67 (sp, $^3J_{HH}$ = 6.9 Hz, 2H, C*H*(CH_3)$_2$), 2.28 (s, 6H, Cz CH_3), 1.05 (d, $^3J_{HH}$ = 6.9 Hz, 12H, CH(CH_3)$_2$), 0.67 (br m, 4H, OCH$_2$CH_2). ^{13}C{^{1}H} NMR (chloroform-*d*): δ 149.2 (d, J_{CP} = 2.6 Hz, aromatic *ipso*-*C*), 144.2 (d, J_{CP} = 4.5 Hz, aromatic *ipso*-*C*), 141.0 (d, J_{CP} = 8.7 Hz, aromatic *ipso*-*C*), 134.9 (d, J_{CP} = 9.3 Hz, aromatic *C*H), 133.2 (d, J_{CP} = 13.9 Hz, aromatic *C*H), 131.8 (d, J_{CP} = 3.0 Hz, aromatic *C*H), 131.4 (d, J_{CP} = 6.1 Hz, aromatic *C*H), 129.3 (d, J_{CP} = 94.7 Hz, aromatic *ipso*-*C*), 128.0 (d, J_{CP} = 12.0 Hz, aromatic *C*H), 126.7 (d, J_{CP} = 10.3 Hz, aromatic *ipso*-*C*), 125.9 (d, J_{CP} = 3.7 Hz, aromatic *C*H), 125.1 (d, J_{CP} = 14.2 Hz, aromatic *ipso*-*C*), 124.2 (s, aromatic *C*H), 106.7 (d, J_{CP} = 113.9 Hz,

aromatic *ipso*-*C*), 73.1 (s, O*C*H$_2$CH$_2$), 33.4 (s, *C*H(CH$_3$)$_2$), 24.1 (s, OCH$_2$*C*H$_2$), 24.0 (s, CH(*C*H$_3$)$_2$), 21.0 (s, Cz *C*H$_3$). ^{31}P{^{1}H} NMR (chloroform-*d*): δ 34.9. Anal. Calcd (%) for $C_{60}H_{60}I_2LuN_3OP_2$: C, 54.19; H, 4.55; N, 3.16. Found: C, 54.30; H, 4.29; N, 3.40.

Synthesis of (L^{Ph}_A-κ^{3}N)Lu(NHMes)$_2$ (23)

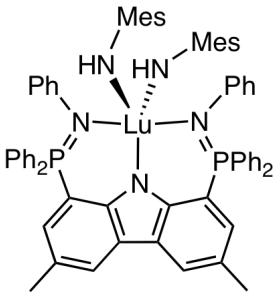

MesNH$_2$ (0.151 mL, 1.07 mmol) was added to a solution of **19** (0.531 g 0.537 mmol) in toluene (20 mL) at ambient temperature. The resulting orange solution was stirred for 1 h, following which, all volatile components were removed under reduced pressure. In a glovebox, the oily residue was washed with pentane (2 × 2 mL) and then dried under vacuum. The solid was taken up in hot benzene, filtered, and allowed to cool to ambient temperature where it was left to crystallize. After two days the mother liquor was decanted off leaving a yellow crystalline solid that was washed with pentane (5 mL) and thoroughly dried *in vacuo*. Yield: 0.376 g (59.0%). ^{1}H NMR (benzene-d_6): δ 8.12 (s, 2H, 4,5-Cz C*H*), 7.71 (dd, $^3J_{HP}$ = 11.1 Hz, $^3J_{HH}$ = 7.3 Hz, 8H, *P*-phenyl *o*-C*H*), 7.42 (d, *J* = 17.1 Hz, 2H, 2,7-Cz C*H*), 6.94–6.82 (m, 20H, aromatic C*H*), 6.70 (m, 6H, aromatic C*H*), 3.97 (s, 2H, N*H*), 2.37 (s, 6H, mesityl *p*-C*H*$_3$), 2.22 (s, 6H, Cz C*H*$_3$), 2.20 (s, 12H, mesityl *o*-C*H*$_3$). ^{13}C{^{1}H} NMR (benzene-d_6): δ 154.2 (s, aromatic *ipso*-*C*), 151.0 (d, J_{CP} = 3.3 Hz, aromatic *ipso*-*C*), 145.9 (d, J_{CP} = 8.2 Hz, aromatic *ipso*-*C*), 134.2 (d, J_{CP} = 9.4 Hz, *P*-phenyl *o*-*C*H), 133.3 (d, J_{CP} = 13.2 Hz, 2,7-Cz *C*H), 132.1 (d, J_{CP} = 2.5 Hz, aromatic *C*H), 131.6 (d, J_{CP} = 6.5 Hz, aromatic *C*H), 131.1 (s, *ipso*-*C*), 129.8 (s, *ipso*-*C*), 129.2 (s, aromatic *C*H), 128.6 (d, partially obscured by solvent, J_{CP} = 11.9 Hz, aromatic *C*H), 127.7 (d, obscured by

solvent, J_{CP} = 3.5 Hz, aromatic *C*H), 125.5 (d, J_{CP} = 13.9 Hz, aromatic *ipso*-*C*), 125.0 (d, J_{CP} = 2.1 Hz, 4,5-Cz *C*H), 123.4 (d, J_{CP} = 3.8 Hz, aromatic *C*H), 121.4 (s, aromatic *ipso*-*C*), 120.0 (s, aromatic *ipso*-*C*), 109.2 (d, J_{CP} = 115.7 Hz, aromatic *ipso*-*C*), 21.1 (s, mesityl *p*-*C*H_3), 21.0 (s, mesityl *o*-*C*H_3), 20.3 (s, Cz *C*H_3). $^{31}P\{^1H\}$ NMR (benzene-d_6): δ 30.6. Anal. Calcd (%) for $C_{68}H_{64}LuN_5P_2$: C, 68.74; H, 5.43; N, 5.89. Found: C, 68.35; H, 5.41; N, 5.40.

Synthesis of (L_A^{Pipp}-κ³N)Lu(NHTrip)₂ (24)

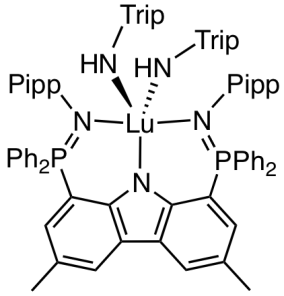

$TripNH_2$ (0.214 g 0.974 mmol) was added via syringe to a solution of **20** (0.502 g 0.467 mmol) in toluene at ambient temperature. The orange solution was stirred for 30 min, after which all volatile components were removed under reduced pressure. In a glovebox, the residue was washed with pentane (2 × 2 mL) and then dried under vacuum. The solid was reconstituted in toluene (2 mL), layered with pentane and left at −35 °C for 16 h to crystallize. The crystalline material was collected by filtration, washed with pentane and thoroughly dried *in vacuo*. Yield: 0.295 g (43.9%). ^1H NMR (benzene-d_6): δ 8.13 (s, 2H, 4,5-Cz C*H*), 7.52 (dd, $^3J_{HP}$ = 11.2 Hz, $^3J_{HH}$ = 7.1 Hz, 8H, phenyl *o*-C*H*), 7.44 (d, $^3J_{HP}$ = 17.7 Hz, 2H, 2,7-Cz C*H*), 7.11 (s, 4H, Trip *m*-C*H*), 6.97 (ov m, $^3J_{HH}$ = 7.2 Hz, 4H, phenyl *p*-C*H*), 6.89 (ov m, 12H, phenyl *m*-C*H* + Pipp *o*-C*H*), 6.56 (d, $^3J_{HH}$ = 7.2 Hz, 4H, Pipp *m*-C*H*), 3.97 (s, 2H, N*H*), 3.26 (br sp, 4H, Trip *o*-C*H*$(CH_3)_2$), 3.01 (sp, $^3J_{HH}$ = 6.9 Hz, 2H, Trip *p*-C*H*$(CH_3)_2$), 2.54 (sp, $^3J_{HH}$ = 6.9 Hz, 2H, Pipp *p*-C*H*$(CH_3)_2$), 2.20 (s, 6H, Cz CH_3), 1.43 (d, $^3J_{HH}$ = 6.9 Hz, 12H, Trip *p*-CH(C$H_3)_2$), 1.11 (d, $^3J_{HH}$ = 6.6 Hz, 24H, Trip *o*-CH(C$H_3)_2$), 1.02 (d, $^3J_{HH}$ = 6.9 Hz,

12H, Pipp *p*-CH(CH_3)$_2$). ^{13}C{^{1}H} NMR (benzene-d_6): δ 152.7 (s, aromatic *ipso*-*C*), 151.5 (d, J_{CP} = 3.3 Hz, aromatic *ipso*-*C*), 143.5 (d, J_{CP} = 4.3 Hz, aromatic *ipso*-*C*), 143.1 (d, J_{CP} = 8.7 Hz, aromatic *ipso*-*C*), 134.9 (d, J_{CP} = 9.5 Hz, phenyl *o*-*C*H), 134.3 (d, J_{CP} = 13.1 Hz, 2,7-Cz *C*H), 132.6 (s, aromatic *ipso*-*C*), 132.3 (s, aromatic *ipso*-*C*), 131.9 (s, phenyl *p*-*C*H), 131.9 (d, J_{CP} = 10.4 Hz, Pipp *o*-*C*H), 130.7 (d, J_{CP} = 92.0 Hz, aromatic *ipso*-*C*), 128.1 (d, J_{CP} = 11.7 Hz, phenyl *m*-*C*H), 125.9 (d, J_{CP} = 3.6 Hz, Pipp *m*-*C*H), 125.4 (d, J_{CP} = 14.1 Hz, aromatic *ipso*-*C*), 125.1 (d, J_{CP} = 3.7 Hz, 4,5-Cz *C*H), 120.6 (s, Trip *m*-*C*H), 120.5 (s, aromatic *ipso*-*C*), 107.6 (d, J_{CP} = 115.6 Hz, aromatic *ipso*-*C*), 34.7 (s, Trip *p*-*C*H(CH$_3$)$_2$), 33.5 (s, Pipp *p*-*C*H(CH$_3$)$_2$), 30.2 (br s, Trip *o*-*C*H(CH$_3$)$_2$), 25.4 (s, Trip *p*-CH(*C*H$_3$)$_2$), 24.3 (s, Trip *o*-CH(*C*H$_3$)$_2$), 24.1 (s, Pipp *p*-CH(*C*H$_3$)$_2$), 21.0 (s, Cz *C*H$_3$). ^{31}P{^{1}H} NMR (benzene-d_6): δ 30.6. Anal. Calcd (%) for $C_{91}H_{112}LuN_5P_2$ (**24**·pentane): C, 72.25; H, 7.46; N, 4.63. Found: C, 72.33; H, 7.82; N, 4.85.

*Synthesis of (L_A^{Pipp}-κ^3*N*,κ*C*$^{N–Pipp}$)Lu(NHMes*) (26)*

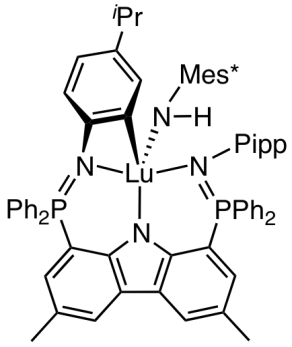

Toluene (40 mL) was added to a bomb charged with an intimate mixture of **20** (0.787 g, 0.733 mmol) and Mes*NH$_2$ (0.192 g, 0.736 mmol) to give an orange solution. The reaction mixture was heated to 100 °C for 3 h, following which, it was cooled to ambient temperature and the volume concentrated under vacuum to ~5 mL. Upon standing for 5 min the product crystallized out of solution as a solid orange mass. In a glovebox, the crystals were redissolved in 5 mL of hot toluene to give a dark red solution. After cooling to ambient temperature, the toluene solution was layered with pentane (5 mL) and left for 16 h to crystallize. Matted needles

of the product were collected by filtration, washed with pentane (2 × 2 mL) and thoroughly dried under reduced pressure. Yield: 0.716 g (77.3%). $^{1}H\{^{31}P\}$ NMR (benzene-d_6): δ 8.02 (s, 1H, 4-Cz C*H*), 7.96 (ov d, $^{3}J_{HH}$ = 8.1 Hz, 2H, phenyl *o*-C*H*), 7.94 (ov s, 1H, 5-Cz C*H*), 7.84 (d, $^{3}J_{HH}$ = 7.4 Hz, 2H, phenyl *o*-C*H*), 7.81–7.78 (m, 2H, aromatic C*H*), 7.56 (d, $^{3}J_{HH}$ = 8.2 Hz, 2H, phenyl *o*-C*H*), 7.84 (d, $^{3}J_{HH}$ = 8.3 Hz, 2H, phenyl *o*-C*H*), 7.39 (s, 2H, Mes* *m*-C*H*), 7.20 (s, 1H, 2-Cz C*H*), 7.14 (s, obscured by solvent, 1H, 7-Cz C*H*), 7.09–7.06 (m, 2H, aromatic C*H*), 7.02–7.00 (m, 4H, aromatic C*H*), 6.94–6.82 (m, 5H, aromatic C*H*), 6.73 (d, 2H, aromatic C*H*), 6.69 (d, 2H, aromatic C*H*), 6.53 (m, 2H, phenyl *m*-C*H*), 4.88 (s, 1H, N*H*), 2.83 (sp, $^{3}J_{HH}$ = 7.0 Hz, 1H, Pipp′ C*H*$(CH_3)_2$), 2.67 (sp, $^{3}J_{HH}$ = 6.8 Hz, 1H, Pipp C*H*$(CH_3)_2$), 2.31 (s, 3H, 3-Cz CH_3), 2.17 (s, 3H, 6-Cz CH_3), 1.40 (s, 9H, *p*-^{t}Bu), 1.36 (s, 18H, *o*-^{t}Bu), 1.30 (d, $^{3}J_{HH}$ = 7.0 Hz, 3H, Pipp′ CH(CH_3)$(CH_3)'$), 1.27 (d, $^{3}J_{HH}$ = 7.0 Hz, 3H, Pipp′ CH(CH_3)(C$H_3)'$), 1.18 (d, $^{3}J_{HH}$ = 6.8 Hz, 3H, Pipp CH(CH_3)$(CH_3)'$), 1.16 (d, $^{3}J_{HH}$ = 6.8 Hz, 3H, Pipp CH(CH_3)(C$H_3)'$). $^{13}C\{^{1}H\}$ NMR (benzene-d_6): δ 182.8 (d, J_{CP} = 21.7 Hz, *C*–Lu), 154.1 (s, aromatic *ipso*-*C*), 151.6 (d, J_{CP} = 2.6 Hz, aromatic *ipso*-*C*), 151.0 (d, J_{CP} = 6.9 Hz, aromatic *ipso*-*C*), 150.5 (d, J_{CP} = 3.6 Hz, aromatic *ipso*-*C*), 143.0 (d, J_{CP} = 6.2 Hz, aromatic *ipso*-*C*), 142.6 (d, J_{CP} = 1.9 Hz, aromatic *ipso*-*C*), 140.0 (s, aromatic *ipso*-*C*), 136.5 (d, J_{CP} = 4.2 Hz, aromatic *C*H), 134.5 (d, J_{CP} = 9.1 Hz, aromatic *C*H), 134.2 (d, J_{CP} = 10.1 Hz, aromatic *C*H), 133.8 (s, aromatic *ipso*-*C*), 133.7 (s, aromatic *ipso*-*C*), 133.2 (s, aromatic *C*H), 133.1 (s, aromatic *C*H), 133.0 (s, aromatic *C*H), 132.9 (s, aromatic *C*H), 132.6 (d, J_{CP} = 2.9 Hz, aromatic *C*H), 131.7 (d, J_{CP} = 2.8 Hz, aromatic *C*H), 131.2 (d, J_{CP} = 8.6 Hz, aromatic *C*H), 131.1 (s, aromatic *C*H), 130.4 (s, aromatic *ipso*-*C*), 130.1 (d, J_{CP} = 34.9 Hz, aromatic *ipso*-*C*), 129.1 (d, J_{CP} = 10.3 Hz, aromatic *C*H), 129.0 (d, J_{CP} = 10.7 Hz,

aromatic *C*H), 128.6 (d, J_{CP} = 12.3 Hz, aromatic *C*H), 128.4 (s, aromatic *C*H), 127.9 (s, aromatic *ipso*-*C*), 127.6 (s, aromatic *C*H), 127.5 (d, J_{CP} = 1.1 Hz, aromatic *ipso*-*C*), 127.4 (d, J_{CP} = 1.1 Hz, aromatic *ipso*-*C*), 126.8 (d, J_{CP} = 11.3 Hz, aromatic *C*H), 126.1 (d, J_{CP} = 47.9 Hz, aromatic *ipso*-*C*), 125.9 (d, J_{CP} = 47.1 Hz, aromatic *ipso*-*C*), 125.6 (d, J_{CP} = 2.5 Hz, aromatic *C*H), 125.4 (d, J_{CP} = 2.6 Hz, aromatic *C*H), 124.8 (s, aromatic *C*H), 124.6 (d, J_{CP} = 90.7 Hz, aromatic *ipso*-*C*), 121.3 (s, Mes* *m*-C*H*), 115.9 (d, J_{CP} = 5.4 Hz, aromatic *C*H), 113.2 (d, J_{CP} = 104.4 Hz, aromatic *ipso*-*C*), 111.6 (d, J_{CP} = 112.3 Hz, aromatic *ipso*-*C*), 35.0 (s, Mes* *C*$(CH_3)_3$), 34.7 (s, Pipp′ *C*H$(CH_3)_2$), 34.5 (s, Mes* *C*$(CH_3)_3$), 33.7 (s, Pipp *C*H$(CH_3)_2$), 32.4 (s, Mes* *p*-C(*C*$H_3)_3$), 30.2 (s, Mes* *o*-C(*C*$H_3)_3$), 25.3 (s, Pipp′ CH(*C*H_3)(CH$_3$)′), 24.8 (s, Pipp′ CH(CH$_3$)(*C*H_3)′), 24.4 (s, Pipp CH(*C*H_3)(CH$_3$)′), 24.3 (s, Pipp CH(CH$_3$)(*C*H_3)′), 21.4 (s, Cz *C*H_3). 21.3 (s, Cz *C*H_3). $^{31}P\{^1H\}$ NMR (benzene-d_6): δ 30.0 (s, 1P, PippN=PPh$_2$), 11.85 (s, 1P, Pipp′N=PPh$_2$). Anal. Calcd (%) for $C_{74}H_{81}LuN_4P_2$: C, 70.35; H, 6.46; N, 4.43. Found: C, 70.17; H, 7.12; N, 4.43.

Synthesis of HL_A^{Ph}-d_{10} (11-d_{10})

This compound was prepared in an identical manner to that described for H$\mathbf{L}_{\mathbf{A}}^{\mathbf{Ph}}$ (**11**) with the exception that phenyl azide-d_5 was used in place of phenyl azide. The ^1H and $^{31}P\{^1H\}$ NMR spectra matched that previously described with the exception that no resonances were observed for the deuterated *N*-aryl groups.

Synthesis of (L_A^{Ph}-$\kappa^3N,\kappa^2C^{P\text{-}Ph}$)Lu(THF)-$d_{10}$ (19-ring-d_{10})

This compound was prepared in an identical manner to that described for **19**, with the exception that $H\mathbf{L}_{\mathbf{A}}^{\mathbf{Ph}}$-$d_{10}$ was used in place of $H\mathbf{L}_{\mathbf{A}}^{\mathbf{Ph}}$. The ^1H and $^{31}P\{^1H\}$ NMR spectra matched that of **19** with the exception that no signals were observed for the deuterated *N*-aryl groups.

Synthesis of Lu(CH_2SiMe_3)$_2$(NHMes*)(THF)$_2$ (27)

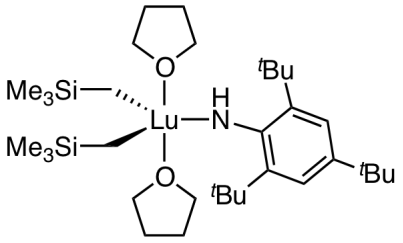

In a glovebox, anhydrous $LuCl_3$ (0.988 g, 3.51 mmol) was slurried for 5 min in THF (3 mL). The slurry was diluted with toluene (10 mL) and then cooled to −35 °C. In a separate flask, a solution of $LiCH_2SiMe_3$ (0.662 g, 7.02 mmol) and KHNMes* (1.05 g, 3.51 mmol) was prepared in THF (5 mL) and cooled to −35 °C. The latter solution was added dropwise over 30 min to the slurry of $LuCl_3$ while keeping the reaction cold. Following the addition, the cloudy mixture was stirred at ambient temperature for 40 min and then centrifuged. The clear brown supernatant was decanted off and all volatile components were removed from the supernatant under vacuum, to afford a crude off-white solid. The product was reconstituted in a minimal amount of toluene and left at −35 °C to crystallize. The mother liquor was decanted of, leaving off-white crystals that were washed with cold pentane (2 × 1 mL) and dried thoroughly under reduced pressure. Yield: 2.22 g (84.0%). ^1H NMR (benzene-d_6): δ 7.50 (s, 2H, aromatic C*H*), 3.85 (s, 1H, N*H*), 3.81 (br m, 8H, OCH_2CH_2), 1.64 (s, 18H, *o*-C(CH_3)$_3$) 1.43 (s, 9H, *p*-C(CH_3)$_3$), 1.18 (m, 8H, OCH$_2$CH_2), 0.362 (s, 18H, CH$_2$Si(CH_3)$_3$), −0.750 (s, 4H, CH_2Si(CH$_3$)$_3$). $^{13}C\{^1H\}$ NMR (benzene-d_6): δ 153.7,

134.7, 133.9, 122.0, 71.6, 39.0, 35.3, 34.5, 32.3, 31.2, 25.2, 4.87. Anal. Calcd. (%) for $C_{34}H_{68}LuNO_2Si_2$: C, 54.16; H, 9.09; N, 1.86. Found: C, 54.19; H, 8.42; N, 2.12.

8.4.2 NMR Kinetics

Rate constants were determined by monitoring the $^{31}P\{^1H\}$ NMR resonance(s) over the course of the reaction (to at least 3 half-lives) at a given temperature.

Typical Experiment

Complex **20** (0.0163 g, 0.0152 mmol) and 2,4,6-tri-*tert*-butylaniline (0.0040 g, 0.0152 mmol) were added to a Wilmad NMR tube that was then sealed with a rubber septum (Sigma-Aldrich) and parafilm. The tube was cooled to 0 °C and 0.5 mL of toluene-d_8 was injected via syringe. The tube was removed from the cold bath and shaken briefly to mix the reagents. The tube was then immediately inserted into the NMR probe which was pre-equilibrated to the appropriate temperature. The sample was allowed to equilibrate at the set temperature over the course of shimming the tube in the magnet. $^{31}P\{^1H\}$ NMR spectra were recorded at pre-set time intervals until the reaction had progressed to at least 3 half-lives. The extent of reaction at each time interval was determined by integration of the peak intensity of the starting material relative to that of the intermediate and final product. An appropriately long delay ($5 \times T_1$) between scans was utilized to ensure that integration was quantitative and not affected by the T_1 relaxation times of the reacting species.

The transformation of **20** to **25** followed the second order rate law d[**20**]/dt = $-k_1$[**20**][Mes*NH_2]. The observed rate constant ($k_{1(obs)}$) for this elementary reaction at various temperatures (from 296.9 K to 349.1 K) was obtained from linear plots of 1/[**20**] versus time. Due to the complexity of the rate law for the transformation of **25** to **26**, the corresponding rate constant ($k_{2(obs)}$) could not be determined algebraically based on a rate law.

As a secondary method, the rate constants $k_{1(calc)}$ and $k_{2(calc)}$ were calculated using the program COPASI 4.5.[180] Based on Equation 4.1, the following rate laws were applied: d[**20**]/dt = $-k_1$[**20**][Mes*NH_2]; d[**25**]/dt = k_1[**20**][Mes*NH_2] − k_2[**25**]; d[**26**]/dt = k_2[**25**]. Parameter values were assigned based on the transient concentrations of **20**, **25** and **26** measured experimentally by $^{31}P\{^1H\}$ NMR spectroscopy over the course of the reaction. The transient concentration of Mes*NH_2 was assumed to be equal to that of **20**. The transient concentrations of **20**, Mes*NH_2, **25** and **26** were weighted using the mean square method in the Parameter Estimation module of COPASI. Start values for determining the calculated rate constants were arbitrarily chosen within the range of 2×10^{-3} $M^{-1}\cdot s^{-1}$ and 2×10^{-1} $M^{-1}\cdot s^{-1}$ for $k_{1(calc)}$, and 6×10^{-5} s^{-1} and 5×10^{-3} s^{-1} for $k_{2(calc)}$, depending on the experimental temperature (296.9 K to 349.1 K), and subsequently refined. A summary of the observed and calculated rate constants and half-lives are listed in Table 4.4 and Table 4.5 for k_1 and k_2, respectively.

8.5 Experimental Procedures Pertaining to Chapter 5

8.5.1 Synthesis of Compounds

Synthesis of (BOC)ONO (29)

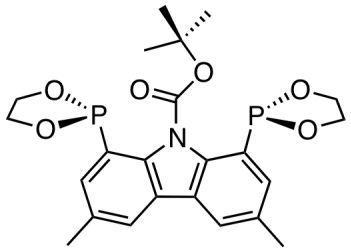

A 2-neck round-bottomed flask was charged with **3** (3.06 g, 6.76 mmol, 1 equiv) and 60 mL of diethyl ether to give a pale yellow-beige coloured suspension. The flask was cooled to −78 °C and a pentane solution (1.63 M) of *t*-BuLi (17.0 mL, 27.7 mmol, 4.1 equiv) was added dropwise. Following the addition, the reaction mixture was stirred at −78 °C for 3.5 h over which time, its appearance became a cloudy yellow-green colour. While maintaining the temperature at −78 °C, 2-chloro-1,3,2-dioxaphospholane (1.32 mL, 14.9 mmol, 2.2 equiv) was added dropwise by syringe to generate a cloudy brown coloured solution. The mixture was allowed to slowly warm to ambient temperature with stirring over 21.5 h, over which time it acquired a cloudy yellow appearance. Following this point, all procedures do not require the use of dry solvent, but the solvent must be thoroughly degassed prior to use and inert atmosphere conditions must be maintained. The reaction mixture was diluted with Et_2O (250 mL), quenched with degassed water (100 mL) and vigorously mixed. The aqueous layer was removed by cannula and the organic layer was dried over $MgSO_4$. The solution was filtered and all volatile components were removed from the flask under reduced pressure to yield **29** as a yellow solid residue. Yield: 2.94 g (91.5%). ^{1}H NMR (benzene-d_6): δ 7.54 (s, 2H, Cz C*H*), 7.42 (s, 2H, Cz C*H*), 3.49 (m, 4H $PO_2(CH_2)_2$), 3.16 (m, 4H m, 4H $PO_2(CH_2)_2$), 2.24 (s, 6H, Cz CH_3), 1.60 (s, 9H, $OC(CH_3)_3$). $^{13}C\{^1H\}$ NMR (chloroform-

d): δ 152.8 (s, OC=O), 138.7 (d, J_{CP} = 5.6 Hz, Cz *ipso*-*C*), 133.6 (s, Cz *ipso*-*C*), 132.1 (d, J_{CP} = 63.1 Hz, Cz 1,8-*C*), 129.3 (d, J_{CP} = 16.3 Hz, Cz 2,7-*C*H), 126.7 (s, Cz *ipso*-*C*), 120.9 (s, Cz 4,5-*C*H), 87.2 (s, O*C*$(CH_3)_3$), 64.3 (d, J_{CP} = 9.5 Hz, $PO_2(CH_2)_2$), 28.6 (t, J_{CP} = 3.3 Hz, OC$(CH_3)_3$), 21.3 (s, Cz CH_3). $^{31}P\{^1H\}$ NMR (benzene-d_6): δ 148.7. Anal. Calcd. (%) for $C_{23}H_{27}NO_6P_2$: C, 58.11; H, 5.72; N, 2.95. Found: C, 57.99; H, 5.53; N, 3.10.

Synthesis of H(ONO) (30)

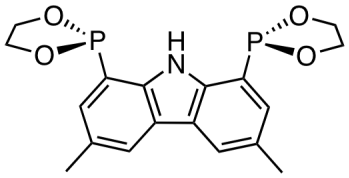

A 250 mL bomb was charged with a suspension of **29** (2.94 g, 6.18 mmol) in toluene (50 mL) and placed under static vacuum. The cloudy orange suspension was heated to 160 °C for 1.5 h, over which time the colour changed to pale orange-yellow. While still hot, the mixture was transferred by cannula to a 100 mL round bottomed flask and the volatile components were removed under vacuum to afford a yellow residue. In a glovebox, the product was suspended in 3 mL of toluene, heated to dissolve all material and then very slowly cooled back to ambient temperature to recrystallize. Pure pale yellow crystals of **30** were collected by filtration, washed with a minimal amount of cold pentane and thoroughly dried under reduced pressure. Yield: 1.56 g (67.3%). ^1H NMR (benzene-d_6): δ 9.95 (br s, 1H, N*H*), 7.76 (s, 2H, 4,5-Cz C*H*), 7.35 (d, $^3J_{HP}$ = 7.0 Hz, 2H, 2,7-Cz C*H*), 3.45 (m, 8H, $PO_2(CH_2)_2$), 2.34 (s, 6H, 3,6-Cz CH_3). $^{13}C\{^1H\}$ NMR (chloroform-*d*): δ 137.6 (d, J_{CP} = 7.0 Hz, Cz *ipso*-*C*), 128.8 (d, J_{CP} = 3.9 Hz, Cz *ipso*-*C*), 127.5 (d, J_{CP} = 20.5 Hz, Cz 2,7-*C*H), 123.9 (d, J_{CP} = 48.4 Hz, Cz 1,8-*C*), 122.8 (s, Cz *ipso*-*C*), 122.2 (s, Cz 4,5-*C*H), 65.0 (d, J_{CP} = 9.0 Hz, $PO_2(CH_2)_2$), 21.4 (s, Cz CH_3).

$^{31}P\{^{1}H\}$ NMR (benzene-d_6): δ 167.9. Anal. Calcd. (%) for $C_{18}H_{19}NO_4P_2$: C, 57.61; H, 5.10; N, 3.73. Found: C, 58.01; H, 5.16; N, 3.67.

Synthesis of HL_B^{Pipp} (31)

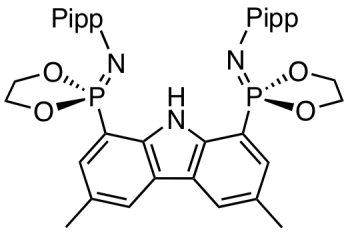

A 100 mL round bottomed flask was charged with **30** (1.05 g, 2.80 mmol, 1 equiv) and 40 mL of toluene to give a yellow suspension. At ambient temperature, *para*-isopropylphenyl azide (0.904 g, 5.61 mmol, 2 equiv) was added dropwise by syringe and the mixture was stirred at ambient temperature for 2 h. As the reaction progressed, the slow evolution of N_2 gas occurred with bubbling and the reaction mixture gradually clarified to give a clear yellow solution. All volatile components were removed under reduced pressure to afford a yellow solid residue. The product was taken up in boiling toluene (10 mL) and cooled very slowly to ambient temperature to recrystallize. Yellow crystals of the product were collected by filtration, washed with cold pentane and thoroughly dried under reduced pressure. Yield: 1.32 g (73.4%). ^{1}H NMR (benzene-d_6): δ 12.0 (br s, 1H, N*H*), 7.76 (s, 2H, 4,5-Cz C*H*), 7.69 (d, $^{3}J_{HP}$ = 16.2 Hz, 2H, 2,7-Cz C*H*), 7.41 (dd, $^{3}J_{HH}$ = 8.4 Hz, $^{4}J_{HP}$ = 2.5 Hz, 2H, 2,6-Pipp C*H*), 7.11 (dd, $^{3}J_{HH}$ = 8.2 Hz, $^{5}J_{HP}$ = 1.5 Hz, 2H, 3,5-Pipp C*H*), 3.56 (m, 8H, $PO_2(CH_2)_2$), 2.84 (sp, $^{3}J_{HH}$ = 6.9 Hz, 2H, Pipp C*H*$(CH_3)_2$), 2.31 (s, 6H, Cz CH_3), 1.27 (d, $^{3}J_{HH}$ = 6.9 Hz, 12H, Pipp CH(CH_3)$_2$). $^{13}C\{^{1}H\}$ NMR (chloroform-*d*): δ 144.4 (d, J_{CP} = 8.2 Hz, Pipp *ipso*-*C*), 140.5 (d, J_{CP} = 3.2 Hz, Pipp *ipso*-*C*), 139.5 (d, J_{CP} = 5.4 Hz, Cz *ipso*-*C*), 130.5 (d, J_{CP} = 9.0 Hz, Cz 4,5-*C*H), 128.1 (d, J_{CP} = 15.1 Hz, Cz *ipso*-*C*), 126.7 (s, Pipp 3,5-*C*H), 125.1 (d, J_{CP} = 3.2 Hz, Cz 2,7-*C*H), 124.2 (d, J_{CP} = 16.3 Hz, Pipp 2,6-*C*H), 123.5

(d, J_{CP} = 12.6 Hz, Cz *ipso*-*C*), 108.2 (d, J_{CP} = 202.9 Hz, Cz *ipso*-*C*), 66.3 (s, $PO_2(CH_2)_2$), 33.3 (s, Pipp $CH(CH_3)_2$), 24.2 (s, Pipp $CH(CH_3)_2$), 21.3 (s, Cz CH_3). $^{31}P\{^1H\}$ NMR (chloroform-*d*): δ 25.2. Anal. Calcd. (%) for $C_{39}H_{44}N_3O_4P_2$ (**30** · 0.5 benzene): C, 68.81; H, 6.51; N, 6.17. Found: C, 68.87; H, 6.49; N, 6.04.

Synthesis of [(L_B^{Pipp}-κ³N,κ²O)Lu]₂ (33)

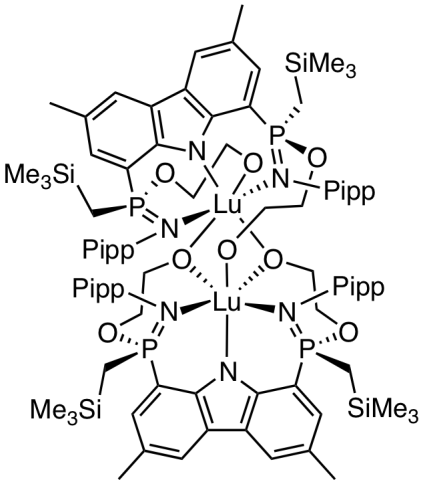

In a glovebox, a 25 mL Erlenmeyer flask was charged with **31** (0.254 g, 0.395 mmol) and $Lu(CH_2SiMe_3)_3(THF)_2$ (0.231 g, 0.397 mmol). Toluene (5 mL) was added to the flask and the orange reaction mixture was stirred at ambient temperature for 18 h. The solution was gently heated and then a hot filtration through bed of Celite was performed. The clear yellow filtrate was concentrated under vacuum to ~1 mL and left at −35 °C to crystallize. Yellow crystals of the product were collected by filtration, washed with a minimal amount of cold pentane and thoroughly dried under reduced pressure. Yield: 0.111 g (28.3%). ^1H NMR (benzene-d_6): δ 8.16 (s, 1H, aromatic C*H*), 8.12 (s, 1H, aromatic C*H*), 8.10 (ov s, 2H, aromatic C*H*), 8.03 (br m, 2H, aromatic C*H*), 7.60–7.20 (ov m, 12H, aromatic C*H*), 7.05 (d, $^3J_{HH}$ = 8.2 Hz, 2H, Pipp C*H*), 6.96 (d, $^3J_{HH}$ = 8.2 Hz, 2H, Pipp C*H*), 5.63 (br s, 2H, aromatic C*H*), 4.69 (m, 2H, CH_2), 4.53 (m, 1H, CH_2), 4.33 (m, 1H, CH_2), 4.03 (m, 1H, CH_2), 3.82 (ov m, 2H, CH_2), 3.50 (ov m, 5H, CH_2), 3.27 (m, 1H, CH_2), 3.16–2.40 (ov m, 7H, CH_2 + Pipp C*H*), 2.59 (s, 6H, Cz CH_3), 2.51 (s, 6H, Cz CH_3), 2.47 (s, 6H, Cz CH_3), 2.42 (s, 6H, Cz CH_3), 1.95–1.42 (ov m, 8H, CH_2), 1.37 (ov

m, 12H, Pipp CH_3), 1.23 (m, 6H, Pipp CH_3), 1.15 (m, 6H, Pipp CH_3), −0.17 (s, 9H, Si(CH_3)$_3$), −0.21 (s, 9H, Si(CH_3)$_3$), −0.40 (s, 9H, Si(CH_3)$_3$), −0.56 (s, 9H, Si(CH_3)$_3$). ^{13}C{^{1}H} NMR (dichloromethane-*d*$_2$): δ 151.9 (d, J_{CP} = 4.3 Hz, aromatic *ipso*-*C*), 150.7 (d, J_{CP} = 5.3 Hz, aromatic *ipso*-*C*), 150.6 (d, J_{CP} = 4.7 Hz, aromatic *ipso*-*C*), 150.4 (d, J_{CP} = 2.4 Hz, aromatic *ipso*-*C*), 147.9 (d, J_{CP} = 7.2 Hz, aromatic *ipso*-*C*), 147.8 (d, J_{CP} = 7.2 Hz, aromatic *ipso*-*C*), 144.4 (d, J_{CP} = 9.4 Hz, aromatic *ipso*-*C*), 143.9 (d, J_{CP} = 7.9 Hz, aromatic *ipso*-*C*), 143.4 (d, J_{CP} = 4.1 Hz, aromatic *ipso*-*C*), 142.4 (ov m, 3 aromatic *ipso*-*C*), 132.1 (d, J_{CP} = 10.4 Hz, aromatic *C*H), 131.3 (br s, aromatic *C*H), 130.2 (d, J_{CP} = 11.6 Hz, aromatic *C*H), 129.8 (d, J_{CP} = 12.5 Hz, aromatic *C*H), 128.9 (br s, aromatic *C*H), 128.8 (br s, aromatic *C*H), 128.4 (d, J_{CP} = 14.2 Hz, aromatic *C*H), 127.6 (d, J_{CP} = 11.2 Hz, aromatic *C*H), 127.4 (d, J_{CP} = 10.3 Hz, aromatic *ipso*-*C*), 126.7 (d, J_{CP} = 9.9 Hz, aromatic *ipso*-*C*), 126.5 (s, aromatic *C*H), 126.1 (d, J_{CP} = 5.4 Hz, aromatic *ipso*-*C*), 126.0 (d, J_{CP} = 6.2 Hz, aromatic *ipso*-*C*), 125.9 (s, aromatic *C*H), 125.8 (s, aromatic *C*H), 125.7 (br s, aromatic *C*H), 125.5 (d, J_{CP} = 13.3 Hz, aromatic *ipso*-*C*), 124.6 (s, aromatic *C*H), 124.5 (s, aromatic *C*H), 124.4 (d, J_{CP} = 3.9 Hz, aromatic *ipso*-*C*), 124.2 (d, J_{CP} = 3.7 Hz, aromatic *ipso*-*C*), 124.2 (d, J_{CP} = 14.8 Hz, aromatic *ipso*-*C*), 124.0 (ov m, 2 aromatic *C*H), 112.7 (d, J_{CP} = 137.3 Hz, aromatic *ipso*-*C*), 112.3 (d, J_{CP} = 136.4 Hz, aromatic *ipso*-*C*), 110.7 (d, J_{CP} = 134.1 Hz, aromatic *ipso*-*C*), 108.9 (d, J_{CP} = 131.7 Hz, aromatic *ipso*-*C*), 77.5 (d, $^2J_{CP}$ = 10.2 Hz, PO*C*H$_2$CH$_2$O), 76.8 (d, $^2J_{CP}$ = 9.2 Hz, PO*C*H$_2$CH$_2$O), 75.9 (d, $^2J_{CP}$ = 6.7 Hz, PO*C*H$_2$CH$_2$O), 74.0 (d, $^2J_{CP}$ = 7.2 Hz, PO*C*H$_2$CH$_2$O), 67.5 (s, POCH$_2$*C*H$_2$O), 66.7 (s, POCH$_2$*C*H$_2$O), 65.3 (s, POCH$_2$*C*H$_2$O), 64.0 (d, $^3J_{CP}$ = 5.0 Hz, POCH$_2$*C*H$_2$O), 34.0 (m, Pipp *C*H(CH$_3$)$_2$ + Pipp *C*H(CH$_3$)$_2$′ + Pipp *C*H(CH$_3$)$_2$″), 33.6 (s, Pipp *C*H(CH$_3$)$_2$‴), 25.0 (s, Pipp CH(*C*H$_3$)(CH$_3$)‴), 24.7 (s, Pipp CH(*C*H$_3$)(CH$_3$)′), 24.6–

24.5 (m, Pipp CH(CH_3)$_2$) + Pipp CH(CH_3)$_2$″), 24.4 (s, Pipp CH(CH_3)(CH_3)′), 23.3 (s, Pipp CH(CH_3)(CH_3)‴), 21.5 (s, Cz CH_3), 21.4 (s, Cz CH_3), 21.2 (s, Cz CH_3), 21.1 (s, Cz CH_3), 18.3 (d, $^1J_{CP}$ = 92.8 Hz, PCH_2Si(CH_3)$_3$), 14.7 (d, $^1J_{CP}$ = 90.7 Hz, PCH_2Si(CH_3)$_3$), 13.6 (d, $^1J_{CP}$ = 92.1 Hz, PCH_2Si(CH_3)$_3$), 11.0 (d, $^1J_{CP}$ = 84.4 Hz, PCH_2Si(CH_3)$_3$), 0.1 (d, $^3J_{CP}$ = 3.2 Hz, PCH$_2$Si(CH_3)$_3$), 0.0 (d, $^3J_{CP}$ = 3.1 Hz, PCH$_2$Si(CH_3)$_3$), −0.4 (d, $^3J_{CP}$ = 3.4 Hz, PCH$_2$Si(CH_3)$_3$), −0.5 (d, $^3J_{CP}$ = 3.6 Hz, PCH$_2$Si(CH_3)$_3$). $^{31}P\{^1H\}$ NMR: δ 55.8 (s, 1P), 54.4 (s, 1P), 48.5 (s, 1P), 48.0 (s, 1P). Anal. Calcd. (%) for $C_{93}H_{136}Lu_2N_6O_8P_4Si_4$ (**33**·pentane): C, 54.43; H, 6.68; N, 4.09. Found: C, 54.26; H, 6.32; N, 4.29.

Synthesis of 1,8-bis(dimethylphosphino)-3,6-dimethyl-9H-carbazole (34)

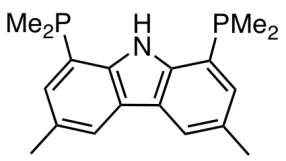

A mixture of toluene and THF (10:1, 20 mL) was added to a 100 mL bomb containing **30** (0.316 g, 0.843 mmol, 1 equiv) and MeLi (95.9 mg, 4.36 mmol, 5.2 equiv) at ambient temperature. Initial NH deprotonation occurred immediately at this temperature as evidenced by a rapid colour change from yellow to orange and evolution of methane gas. The vessel was then heated to 100 °C for 2.5 h to promote derivatization at phosphorus. Upon sitting for 10 min and cooling to ambient temperature, a red immiscible ethylene glycoxide layer was evident at the bottom of the vessel. The reaction mixture was transferred by cannula to a 2-neck round bottomed flask containing degassed H_2O (20 mL) at 0 °C, and mixed vigorously. The aqueous layer was removed by cannula, and the clear yellow organic layer was diluted by addition of 50 mL of degassed diethyl ether. The organic layer was dried by addition of $MgSO_4$, and a cannula filtration was performed. All volatile components were removed from the clear yellow solution under

reduced pressure to afford a yellow solid. Yield: 0.216 g (81.4%). ^{1}H NMR (benzene-d_6): δ 9.28 (br s, 1H, N*H*), 7.83 (s, 2H, Cz 4,5-C*H*), 7.35 (dd, $^{3}J_{HP}$ = 5.6 Hz, $^{4}J_{HH}$ = 1.3 Hz, 2H, Cz 2,7-C*H*), 2.46 (s, 6H, Cz CH_3), 1.15 (d, $^{2}J_{HP}$ = 2.9 Hz, 12H, P(CH_3)$_2$). ^{13}C{^{1}H} NMR (benzene-d_6): δ 141.8 (d, J_{CP} = 22.6 Hz, Cz *ipso*-*C*), 128.8 (d, J_{CP} = 0.8 Hz, Cz *ipso*-*C*), 127.5 (d, $^{2}J_{CP}$ = 2.0 Hz, Cz 2,7-*C*H), 123.1 (dd, J_{CP} = 5.0 Hz, J_{CP} = 2.7 Hz, Cz *ipso*-*C*), 121.7 (d, J_{CP} = 14.3 Hz, Cz *ipso*-*C*), 121.4 (s, Cz 4,5-*C*H), 21.4 (s, Cz *C*H$_3$), 13.4 (d, $^{1}J_{CP}$ = 11.7 Hz, P(*C*H$_3$)$_2$). ^{31}P{^{1}H} NMR (benzene-d_6): δ −64.1. Anal. Calcd. (%) for $C_{18}H_{23}NP_2$: C, 68.56; H, 7.35; N, 4.44. Found: C, 68.79; H, 7.50; N, 4.48.

Synthesis of HL$^{Pipp}_{C}$ (35)

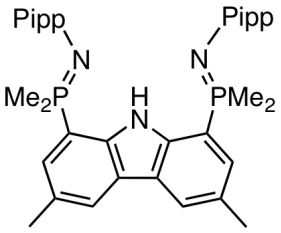

An aliquot of para-isopropylphenyl azide (0.195 g, 1.21 mmol, 2.1 equiv) was added by syringe to a clear yellow solution of **34** (0.184 g, 0.584 mmol, 1 equiv) in 10 mL of toluene at ambient temperature. Upon addition, the solution rapidly became turbid with the precipitation of product along with concurrent evolution of nitrogen gas. The yellow suspension was stirred under an argon atmosphere for 3 h, following which the solvent was removed under vacuum and the residue brought into a glovebox. The product was reconstituted in 2 mL of hot toluene and slowly cooled to ambient temperature to recrystallize. Analytically pure pale yellow prisms of **35** were collected by filtration, washed with a minimal amount of cold pentane and dried thoroughly under reduced pressure. Yield: 0.225 g (66.1%). ^{1}H NMR (benzene-d_6): δ 12.47 (br s, 1H, N*H*), 7.80 (s, 2H, Cz 4,5-C*H*), 7.23 (d, $^{3}J_{HH}$ = 8.2 Hz, 4H, Pipp C*H*), 7.11 (d, $^{3}J_{HP}$ = 13.7 Hz, 2H, Cz 2,7-C*H*), 7.06 (d, J_{HH} = 7.9 Hz, 4H, Pipp C*H*), 2.77 (sp, $^{3}J_{HH}$ = 6.9 Hz, 2H,

C*H*$(CH_3)_2$), 2.36 (s, 6H, Cz C*H*$_3$), 1.38 (d, $^2J_{HP}$ = 12.6 Hz, 12H, P(C*H*$_3)_2$), 1.20 (d, $^3J_{HH}$ = 6.9 Hz, 12H, CH(C*H*$_3)_2$). $^{13}C\{^1H\}$ NMR (chloroform-*d*): δ 149.0 (d, J_{CP} = 4.7 Hz, aromatic *ipso*-*C*), 139.5 (d, J_{CP} = 4.2 Hz, aromatic *ipso*-*C*), 137.3 (s, aromatic *ipso*-*C*), 128.8 (d, J_{CP} = 7.8 Hz, Cz 2,7-*C*H), 128.5 (d, J_{CP} = 10.4 Hz, aromatic *ipso*-*C*), 126.7 (d, J_{CP} = 1.5 Hz, Pipp *C*H), 123.9 (d, J_{CP} = 2.5 Hz, Cz 4,5-*C*H), 123.0 (d, J_{CP} = 7.7 Hz, aromatic *ipso*-*C*), 122.1 (d, J_{CP} = 20.4 Hz, Pipp *C*H), 113.5 (d, J_{CP} = 83.4 Hz, aromatic *ipso*-*C*), 33.0 (s, Pipp *C*H$(CH_3)_2$), 24.2 (s, Pipp CH(*C*H$_3)_2$), 21.4 (s, Cz *C*H$_3$), 15.6 (d, $^1J_{CP}$ = 72.1 Hz, P(*C*H$_3)_2$). $^{31}P\{^1H\}$ NMR (benzene-d_6): δ 5.4. Anal. Calcd. (%) for $C_{36}H_{45}N_3P_2$: C, 74.33; H, 7.80; N, 7.22. Found: C, 74.47; H, 7.73; N, 7.15.

Synthesis of Lu(CH$_2$SiMe$_3$)$_3$(DMAP)$_2$ (36)

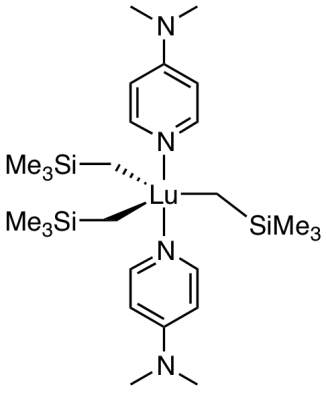

In a glovebox, toluene (3 mL) was added to an intimate mixture of Lu$(CH_2SiMe_3)_3(THF)_2$ (0.270 g, 0.465 mmol) and 4-dimethylaminopyridine (0.115 g, 0.929 mmol) in a small Erlenmeyer flask. The colourless solution was stirred at ambient temperature for 20 min, following which all volatile components were removed under vacuum to yield Lu$(CH_2SiMe_3)_3(DMAP)_2$ as a white solid. Yield: 0.292 g (92.2%). ^1H NMR (benzene-d_6): δ 8.74 (d, $^3J_{HH}$ = 5.9 Hz, 4H, DMAP C*H*), 6.00 (d, $^3J_{HH}$ = 6.4 Hz, 4H, DMAP C*H*), 2.05 (s, 12H, DMAP N(C*H*$_3)_2$), 0.418 (s, 27H, $CH_2Si(CH_3)_3$), −0.240 (s, 6H, C*H*$_2$Si$(CH_3)_3$). $^{13}C\{^1H\}$ NMR (benzene-d_6): δ 154.6 (DMAP *ipso*-*C*), 149.5 (DMAP *C*H), 106.5 (DMAP *C*H), 42.7 (*C*H$_2$Si$(CH_3)_3$), 38.2 (DMAP N(*C*H$_3)_2$), 5.1 (CH$_2$Si(*C*H$_3)_3$). Anal. Calcd. (%) for $C_{26}H_{53}LuN_4Si_3$: C, 45.86; H, 7.85; N, 8.23. Found:

C, 43.51; H, 7.52; N, 8.23. Low carbon values were obtained for this compound despite repeated analysis attempts, possibly as a result of incomplete combustion due to metal-catalyzed silicon carbide formation.

Synthesis of (L_C^{Pipp}-κ^3N,κ^2C)Lu(DMAP)$_2$ (37)

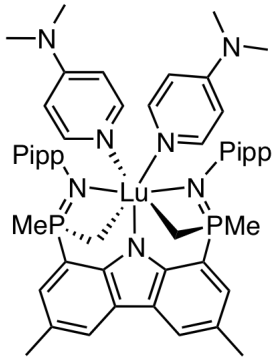

In a glovebox, a 25 mL Erlenmeyer flask was charged with **35** (0.0225 g, 0.0387 mmol) and **36** (0.0265 g, 0.0389 mmol). Benzene (2 mL) was added to the flask and the reaction mixture was stirred at ambient temperature for 1.5 h. The solution was filtered through a bed of Celite, concentrated under reduced pressure to 0.5 mL, and left at ambient temperature to crystallize. The mother liquor was decanted off leaving small yellow crystals that were washed with a minimal amount of cold pentane and dried under vacuum. Yield: 0.0154 g (39.9%). ^{1}H NMR (benzene-d_6): δ 8.54 (d, $^3J_{HH}$ = 6.4 Hz, 4H, DMAP C*H*), 8.23 (s, 2H, Cz 4,5-C*H*), 7.43 (d, $^3J_{HP}$ = 10.5 Hz, 2H, Cz 2,7-C*H*), 6.88 (d, $^3J_{HH}$ = 8.2 Hz, 4H, Pipp C*H*), 6.74 (d, $^3J_{HH}$ = 8.2 Hz, 4H, Pipp C*H*), 5.84 (d, $^3J_{HH}$ = 6.4 Hz, 4H, DMAP C*H*), 2.66 (s, 6H, Cz CH_3), 2.57 (sp, $^3J_{HH}$ = 6.7 Hz, 2H, C*H*(CH_3)$_2$), 2.09 (s, 12H, DMAP N(CH_3)$_2$), 1.99 (d, $^2J_{HP}$ = 12.4 Hz, 6H, PCH_3), 1.03 (d, $^3J_{HH}$ = 6.7 Hz, 12H, CH(CH_3)$_2$), 0.58 (m, 4H, PCH_2Lu). ^{13}C{^{1}H} NMR: δ 154.2 (s, aromatic *ipso*-*C*), 151.9 (d, J_{CP} = 4.1 Hz, aromatic *ipso*-*C*), 151.3 (d, J_{CP} = 6.4 Hz, aromatic *ipso*-*C*), 149.9 (s, DMAP *C*H), 137.8 (s, aromatic *ipso*-*C*), 126.1 (s, Pipp *C*H), 126.0 (d, J_{CP} = 8.9 Hz, Cz 2,7-*C*H), 125.2 (d, J_{CP} = 7.6 Hz, aromatic *ipso*-*C*), 124.4 (d, J_{CP} = 12.9 Hz, Pipp *C*H), 123.7 (d, J_{CP} = 10.4 Hz, aromatic *ipso*-*C*), 123.4 (s, Cz 4,5-*C*H), 121.0 (d, J_{CP} = 82.1 Hz, aromatic *ipso*-*C*), 106.5 (s, DMAP *C*H), 38.2 (s, DMAP

N(CH_3)$_2$), 33.6 (s, Pipp $CH(CH_3)_2$), 24.6 (s, Pipp CH(CH_3)$_2$), 22.2 (s, Cz CH_3), 18.2 (d, $^1J_{CP}$ = 69.9 Hz, PCH_2Lu), 17.2 (d, $^1J_{CP}$ = 39.5 Hz, PCH_3). $^{31}P\{^1H\}$ NMR: δ 23.6. Due to the small amount of product obtained, combustion analysis was not performed on this compound.

8.6 Experimental Procedures Pertaining to Chapter 6

8.6.1 Synthesis of Compounds

Synthesis of 2,5-Bis(diphenylphosphino)-N-(tert-butoxycarbonyl)pyrrole (38)

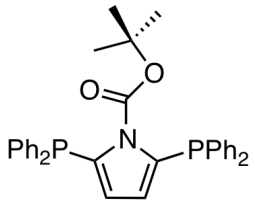

A 2-neck round bottomed flask was charged with *N*-(*tert*-butoxycarbonyl)-2,5-dibromopyrrole (5.0 g, 15.4 mmol) and 200 mL of THF to give a pale yellow-beige coloured suspension. The flask was cooled to −78 °C and a hexane solution (1.6 M) of *n*-BuLi (19.2 mL, 30.8 mmol) was added dropwise. The deep red solution was stirred at −78 °C for 1 h, after which chlorodiphenylphosphine (5.53 mL, 30.8 mmol) was added slowly by syringe. The mixture was allowed to slowly warm to ambient temperature with stirring over 18 h. The THF was removed under reduced pressure to afford a brown foamy residue. The residue was reconstituted in toluene and passed through a column of silica to remove insoluble impurities. After removal of the solvent under vacuum, a red oil remained. The oil was triturated with pentane to liberate the product as a white solid. The solid was collected by filtration and dried thoroughly under vacuum. Yield: 5.46 g (66.2%). ^{1}H NMR (benzene-d_6): δ 7.45 (m, 8H, phenyl C*H*), 7.04 (ov m, 12H, phenyl C*H*), 5.70 (s, 2H, pyrrole C*H*),

1.07 (s, 9H, OC(CH_3)$_3$). $^{13}C\{^1H\}$ NMR (chloroform-*d*): δ 149.8 (s, *C*=O), 138.3 (d, $^1J_{CP}$ = 10.6 Hz, aromatic *ipso*-*C*), 136.2 (d, $^1J_{CP}$ = 17.5 Hz, aromatic *ipso*-*C*), 133.7 (d, J_{CP} = 20.8 Hz, phenyl *C*H), 128.6 (d, J_{CP} = 24.8 Hz, phenyl *C*H), 128.4 (s, phenyl *C*H), 122.7 (s, pyrrole *C*H), 86.4 (s, O*C*(CH_3)$_3$), 27.6 (s, OC(*C*H_3)$_3$). $^{31}P\{^1H\}$ NMR (benzene-d_6): δ −14.5. Anal. Calcd. (%) for $C_{33}H_{31}NO_2P_2$: C, 74.01; H, 5.83; N, 2.62. Found: C, 74.02; H, 5.81; N, 2.62.

Synthesis of 2,5-Bis(diphenylphosphino)pyrrole (39)

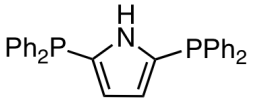

Toluene (50 mL) was added to a 500 mL bomb charged with **38** (3.34 g, 6.24 mmol) and the solution was heated to 155 ºC for 18 h. The solution was transferred by cannula to a round bottomed flask, and the solvent was then removed under vacuum leaving a yellow solid. The residue was reconstituted in a minimal amount of toluene and left at −35 ºC to crystallize. White crystals of the product were collected by filtration, washed with cold pentane and dried thoroughly under reduced pressure. Yield: 2.51 g (92.4%). ^1H NMR (benzene-d_6): δ 7.91 (br s, 1H, N*H*), 7.28 (m, 8H, phenyl C*H*), 6.98 (m, 12H, phenyl C*H*), 6.61 (dd, $^3J_{HP}$ = 4.1 Hz, $^4J_{HP}$ = 2.0 Hz, 2H, pyrrole C*H*). $^{13}C\{^1H\}$ NMR (benzene-d_6): δ 137.9 (d, $^1J_{CP}$ = 9.4 Hz, phenyl *ipso*-*C*) 133.3 (d, $^2J_{CP}$ = 19.2 Hz, phenyl *C*H), 130.1 (dd, $^1J_{CP}$ = 14.8 Hz, $^3J_{CP}$ = 1.3 Hz, pyrrole *ipso*-*C*), 128.9 (s, phenyl *C*H), 128.8 (s, phenyl *C*H), 120.8 (dd, $^2J_{CP}$ = 20.9 Hz, $^3J_{CP}$ = 6.0 Hz, pyrrole *C*H). $^{31}P\{^1H\}$ NMR (benzene-d_6): δ −25.0. Anal. Calcd. (%) for $C_{28}H_{23}NP_2$: C, 77.23; H, 5.32; N, 3.22. Found: C, 77.09; H, 5.36; N, 3.49.

Synthesis of H(L_D^{Pipp}) (40)

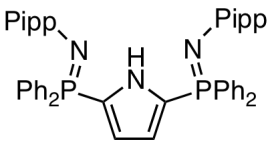

Toluene (40 mL) was added to a 100 mL round bottomed flask charged with **39** (1.50 g, 3.44 mmol) to give a pale yellow solution. An aliquot of *para*-isopropylphenyl azide (1.11 g, 6.89 mmol) was added to the flask *via* syringe at ambient temperature. Upon addition of the azide, the solution immediately began to bubble with the evolution of nitrogen gas. The reaction mixture was stirred for 1 h, after which all volatile components were removed *in vacuo* to liberate an off-white solid. Yield: 2.38 g (98.6%). ^{1}H NMR (benzene-d_6): δ 10.47 (br s, 1H, N*H*), 7.74 (m, 8H, phenyl C*H*), 7.13 (ov d, 4H, Pipp C*H*), 7.06−6.88 (ov m, 16H, phenyl C*H* + Pipp C*H*), 6.52 (m, 2H pyrrole C*H*), 2.77 (sp, $^{3}J_{HH}$ = 6.9 Hz, 2H, C*H*(CH$_3$)$_2$), 1.20 (d, $^{3}J_{HH}$ = 6.9 Hz, 12H, CH(C*H*$_3$)$_2$). ^{13}C{^{1}H} NMR (benzene-d_6): δ 148.9 (s, Pipp *ipso*-*C*), 138.1 (s, Pipp *ipso*-*C*), 132.0 (d, J_{CP} = 110.9 Hz, aromatic *ipso*-*C*), 132.6 (d, J_{CP} = 10.5 Hz, aromatic *C*H), 131.8 (d, J_{CP} = 2.2 Hz, aromatic *C*H), 128.8 (d, J_{CP} = 12.5 Hz, aromatic *C*H), 127.3 (s, aromatic *C*H), 126.8 (d, J_{CP} = 6.2 Hz, aromatic *ipso*-*C*), 123.6 (d, J_{CP} = 18.5 Hz, aromatic *C*H), 119.4 (dd, $^{2}J_{CP}$ = 13.3 Hz, $^{3}J_{CP}$ = 13.2 Hz, pyrrole C*H*), 33.8 (s, *C*H(CH$_3$)$_2$), 24.7 (s, CH(*C*H$_3$)$_2$). ^{31}P{^{1}H} NMR (benzene-d_6): δ −8.1. Anal. Calcd. (%) for $C_{46}H_{45}N_3P_2$: C, 78.72; H, 6.46; N, 5.99. Found: C, 78.68; H, 6.37; N, 5.76.

Synthesis of (L_D^{Pipp}-κ^{3}N)Er(CH$_2$SiMe$_3$)$_2$ (41)

In a glovebox, toluene (1 mL) was added to a 25 mL Erlenmeyer flask charged with **40** (0.261 g, 0.372 mmol) and Er(CH$_2$SiMe$_3$)$_3$(THF)$_2$ (0.213 g, 0.372 mmol) to give a cloudy orange-pink solution. The reaction mixture was stirred at ambient temperature

for 30 min and rapidly clarified as the reaction progressed. The solution was filtered through a bed of Celite and the Celite was washed with a further 1 mL of toluene. The clear orange-pink filtrate was concentrated to 0.5 mL under vacuum and then left at −35 ºC to crystallize. Pale pink crystals of **41** were collected by filtration, washed with cold pentane, and dried under reduced pressure. Yield: 0.314 g (81.0%). ^{1}H NMR (benzene-d_6): δ 86.32 ($\Delta\nu_{1/2}$ = 571 Hz), 29.75 ($\Delta\nu_{1/2}$ = 55 Hz), 17.31 ($\Delta\nu_{1/2}$ = 123 Hz), 14.64 ($\Delta\nu_{1/2}$ = 31 Hz), 9.95 ($\Delta\nu_{1/2}$ = 20 Hz), 8.57 ($\Delta\nu_{1/2}$ = 22 Hz), 8.15 ($\Delta\nu_{1/2}$ = 24 Hz), 7.55 ($\Delta\nu_{1/2}$ = 66 Hz), −23.06 ($\Delta\nu_{1/2}$ = 108 Hz), −184.58 ($\Delta\nu_{1/2}$ = 2000 Hz). ^{31}P{^{1}H} NMR (benzene-d_6): δ −0.29. Anal. Calcd. (%) for $C_{54}H_{66}ErN_3P_2Si_2$: C, 62.21; H, 6.38; N, 4.03. Found: C, 62.42; H, 6.23; N, 4.17.

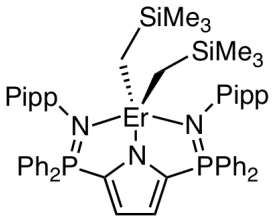

Synthesis of (L_D^{Pipp}-κ^{3}N)Lu(CH_2SiMe_3)$_2$ (42)

In a glovebox, toluene (2 mL) was added to a 25 mL Erlenmeyer flask charged with **40** (0.604 g, 0.861 mmol) and Lu(CH_2SiMe_3)$_3$(THF)$_2$ (0.502 g, 0.864 mmol) to give a cloudy colourless solution. The reaction mixture was stirred at ambient temperature for 30 min and rapidly clarified as the reaction progressed to generate a clear pale yellow appearance. The solution was filtered through a bed of Celite and the Celite was washed with a further 1 mL of toluene. The clear yellow filtrate was concentrated to 1 mL under vacuum and then left at −35 ºC to crystallize. Colourless crystals of **42** were collected by filtration, washed with cold pentane, and dried under reduced pressure. Yield: 0.745 g (82.4%). ^{1}H NMR (benzene-d_6): δ 7.71 (ddd, $^{3}J_{HP}$ = 12.3 Hz, $^{3}J_{HH}$ = 7.9

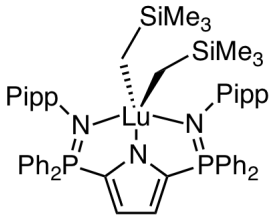

Hz, $^4J_{HH}$ = 1.5 Hz, 8H, phenyl *o*-C*H*) 7.36 (dd, $^3J_{HH}$ = 8.4 Hz, $^4J_{HP}$ = 2.1 Hz, 4H, Pipp *o*-C*H*), 7.05 (d, $^3J_{HH}$ = 8.3 Hz, 4H, Pipp *m*-C*H*), 7.03–6.90 (ov m, 12H, phenyl *m*-C*H* + *p*-C*H*), 6.62 (dd, $^3J_{HP}$ = 2.3 Hz, $^4J_{HP}$ = 1.2 Hz, 2H, pyrrole C*H*), 2.66 (sp, $^3J_{HH}$ = 6.9 Hz, 2H, C*H*$(CH_3)_2$), 1.10 (d, $^3J_{HH}$ = 6.9 Hz, 12H, CH$(CH_3)_2$), 0.18 (s, 18H, Si$(CH_3)_3$), −0.20 (s, 4H, CH_2). $^{13}C\{^1H\}$ NMR (benzene-d_6): δ 144.0 (m, aromatic *ipso*-*C*), 142.6 (d, J_{CP} = 5.7 Hz, aromatic *ipso*-*C*), 133.3 (d, J_{CP} = 10.3 Hz, aromatic *C*H), 132.4 (s, aromatic *C*H), 131.4 (s, aromatic *ipso*-*C*), 130.2 (s, aromatic *ipso*-*C*), 128.7 (d, J_{CP} = 12.3 Hz, aromatic *C*H), 128.6 (d, J_{CP} = 7.7 Hz, aromatic *C*H), 127.5 (d, J_{CP} = 1.0 Hz, aromatic *C*H), 119.3 (dd, $^2J_{CP}$ = 28.0 Hz, $^3J_{CP}$ = 10.7 Hz, pyrrole *C*H), 41.3 (s, *C*H_2), 33.8, (s, *C*H$(CH_3)_2$), 24.2 (s, CH$(CH_3)_2$), 4.9 (s, Si$(CH_3)_3$). $^{31}P\{^1H\}$ NMR (benzene-d_6): δ 25.0. Anal. Calcd. (%) for $C_{54}H_{66}LuN_3P_2Si_2$: C, 61.76; H, 6.33; N, 4.00. Found: C, 61.56; H, 5.98; N, 4.08.

Synthesis of (L_D^{Pipp}-κ³N)Sc(CH₂SiMe₃)₂ (43)

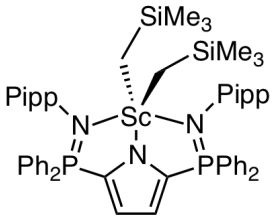

In a glovebox, toluene (2 mL) was added to a flask charged with **40** (0.377 g, 0.537 mmol) and $Sc(CH_2SiMe_3)_3(THF)_2$ (0.242 g, 0.537 mmol). The solution was stirred at ambient temperature for 30 min and rapidly clarified as the reaction progressed to generate a clear yellow appearance. The solution was filtered through a bed of Celite and the Celite was washed with a further 1 mL of toluene. All volatile components were removed from the filtrate under reduced pressure to afford a yellow residue. The product was reconstituted in toluene (0.5 mL) and layered with pentane (0.5 mL) at ambient temperature to recrystallize. After 1 h, the vessel was cooled to −35 ºC for 17 h to promote further crystal growth. Yellow crystals of **43** were collected

by filtration, washed with cold pentane, and dried under reduced pressure. Yield: 0.400 g (80.9%). ^{1}H NMR (benzene-d_6): δ 7.73 (ddd, $^{3}J_{HP}$ = 12.3 Hz, $^{3}J_{HH}$ = 7.9 Hz, $^{4}J_{HH}$ = 1.5 Hz, 8H, phenyl *o*-C*H*) 7.41 (dd, $^{3}J_{HH}$ = 8.5 Hz, $^{4}J_{HP}$ = 2.2 Hz, 4H, Pipp *o*-C*H*), 7.06 (d, $^{3}J_{HH}$ = 8.0 Hz, 4H, Pipp *m*-C*H*), 7.03–6.90 (ov m, 12H, phenyl *m*-C*H* + *p*-C*H*), 6.61 (dd, $^{3}J_{HP}$ = 2.2 Hz, $^{4}J_{HP}$ = 1.2 Hz, 2H, pyrrole C*H*), 2.68 (sp, $^{3}J_{HH}$ = 6.9 Hz, 2H, C*H*(CH$_3$)$_2$), 1.12 (d, $^{3}J_{HH}$ = 6.9 Hz, 12H, CH(C*H*$_3$)$_2$), 0.55 (s, 4H, C*H*$_2$), 0.11 (s, 18H, Si(C*H*$_3$)$_3$). ^{13}C{^{1}H} NMR (benzene-d_6): δ 144.0 (m, aromatic *ipso*-*C*), 143.7 (d, J_{CP} = 6.1 Hz, aromatic *ipso*-*C*), 133.4 (d, J_{CP} = 10.6 Hz, aromatic *C*H), 132.3 (d, J_{CP} = 1.1 Hz, aromatic *C*H), 131.2 (s, aromatic *ipso*-*C*), 130.0 (s, aromatic *ipso*-*C*), 129.6 (d, J_{CP} = 7.5 Hz, aromatic *C*H), 128.7 (d, J_{CP} = 12.4 Hz, aromatic *C*H), 127.3 (dd, J_{CP} = 1.2 Hz, J_{CP} = 1.1 Hz, aromatic *C*H), 118.6 (dd, J_{CP} = 26.7 Hz, J_{CP} = 10.8 Hz, pyrrole *C*H), 40.5 (br s, *C*H$_2$), 33.9, (s, *C*H(CH$_3$)$_2$), 24.2 (s, CH(*C*H$_3$)$_2$), 4.4 (s, Si(*C*H$_3$)$_3$). ^{31}P{^{1}H} NMR (benzene-d_6): δ 23.8. Anal. Calcd. (%) for $C_{54}H_{66}N_3P_2ScSi_2$: C, 70.48; H, 7.23; N, 4.57. Found: C, 70.45; H, 7.18; N, 4.68.

Synthesis of [(L_C^{Pipp}-κ^{3}N)Lu(CH$_2$SiMe$_3$)(OEt$_2$)$_2$][B(C$_6$F$_5$)$_4$] (44)

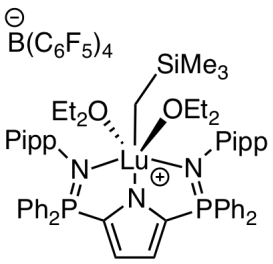

An NMR tube was charged with **42** (0.0110 g, 0.0105 mmol) and [H(OEt$_2$)$_2$]$^+$[B(C$_6$F$_5$)$_4$]$^-$ (0.0089 g, 0.0110 mmol). Benzene-d_6 (0.5 mL) was added to the tube at ambient temperature to give a clear pale yellow solution. Monitoring the reaction by ^{1}H NMR spectroscopy indicated slow conversion to product with concomitant formation of tetramethylsilane. Full conversion to **44** was complete after 4.5 h at ambient temperature. ^{1}H NMR (benzene-d_6): δ 7.46 (br m, 8H, phenyl C*H*), 7.04 (br

m, 12H, phenyl C*H*), 6.95 (d, $^{3}J_{HH}$ = 8.4 Hz, 4H, Pipp C*H*), 6.88 (d, $^{3}J_{HH}$ = 8.4 Hz, 4H, Pipp C*H*), 6.57 (m, 2H, pyrrole C*H*), 3.14 (br m, 8H, OCH_2CH$_3$), 2.62 (sp, $^{3}J_{HH}$ = 6.9 Hz, 2H, C*H*(CH$_3$)$_2$), 1.05 (d, $^{3}J_{HH}$ = 6.9 Hz, 12H, CH(CH_3)$_2$), 0.96 (br m, 12H, OCH$_2$CH_3), −0.02 (s, 9H, Si(CH_3)$_3$), −0.18 (s, 2H, CH_2). ^{31}P{^{1}H} NMR: δ 27.8. ^{11}B NMR: δ −15.2. ^{19}F NMR: δ −132.7 (d, 2F, *o*-C$_6$F$_5$), −163.5 (t, 1F, *p*-C$_6$F$_5$), −167.3 (t, 2F, *m*-C$_6$F$_5$).

Synthesis of [(L_C^{Pipp}-κ^{3}N)Lu(CH$_2$SiMe$_3$)(NHMes*)(DMAP) (45)

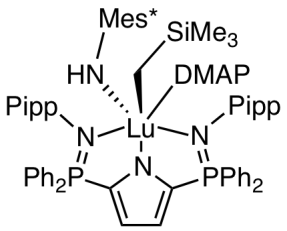

A J-Young NMR tube was charged with **42** (0.0127 g, 0.0121 mmol), Mes*NH$_2$ (0.0032 g, 0.0122 mmol) and DMAP (0.0015 g, 0.0123 mmol). Benzene-d_6 (0.5 mL) was added to the tube at ambient temperature to give a clear pale yellow solution. The tube was heated to 100 ºC for 1.5 h resulting in a green-brown coloured solution of complex **45**. ^{1}H NMR (benzene-d_6): δ 8.47 (d, $^{3}J_{HH}$ = 5.0 Hz, 2H, DMAP C*H*), 7.71 (m, 8H, phenyl C*H*), 7.47 (m, 2H, Mes* *m*-C*H*), 7.19 (dd, $^{3}J_{HH}$ = 8.4 Hz, $^{4}J_{HP}$ = 2.0 Hz, 4H, Pipp C*H*), 7.10–6.92 (ov m, 12H, phenyl C*H*), 6.88 (d, $^{3}J_{HH}$ = 8.4 Hz, 4H, Pipp C*H*), 6.68 (m, 2H, pyrrole C*H*), 6.09 (d, $^{3}J_{HH}$ = 5.0 Hz, 2H, DMAP C*H*), 4.64 (s, 1H, N*H*), 2.62 (sp, $^{3}J_{HH}$ = 6.9 Hz, 2H, C*H*(CH$_3$)$_2$), 2.22 (s, 6H, N(CH_3)$_2$), 1.57 (s, 9H, Mes* *p*-C(CH_3)$_3$), 1.51 (s, 18H, Mes* *o*-C(CH_3)$_3$), 1.09 (d, $^{3}J_{HH}$ = 6.9 Hz, 6H, CH(CH_3)(CH$_3$)′), 1.08 (d, $^{3}J_{HH}$ = 6.9 Hz, 6H, CH(CH$_3$)(CH_3)′), 0.23 (s, 9H, Si(CH_3)$_3$), −0.43 (s, 2H, CH_2). ^{31}P{^{1}H} NMR: δ 22.8.

8.7 X-ray Crystallography

The typical procedure for structure determination by single-crystal X-ray diffraction is outlined in the General Procedure section. This method was used for the structure determination of all compounds except complex **18**, which required special treatment and is discussed separately.

General Procedure

In a glovebox, crystals of a given compound were coated in degassed Paratone oil. A suitable crystal was then selected and mounted onto a glass fibre. Data were collected at 173K using a Bruker SMART APEX II diffractometer (Mo Kα radiation, λ = 0.71073 Å) outfitted with a CCD area-detector and a KRYO-FLEX liquid nitrogen vapour cooling device. A data collection strategy using ω and φ scans at 0.5° steps yielded full hemispherical data with excellent intensity statistics and a final resolution between 0.78 and 0.84 Å. Unit cell parameters were determined and refined on all observed reflections using APEX2 software.[241] Data reduction and correction for Lorentz polarization were performed using SAINT-Plus software.[242] Absorption corrections were applied using SADABS.[243] The structures were solved by either direct or Patterson methods and refined by the least squares method on F^2 using the SHELXTL software suite.[244,245] All non-hydrogen atoms were typically refined anisotropically. However, in certain cases (*i.e.* disorder), non-hydrogen atoms were held isotropic. Hydrogen atom positions were calculated and isotropically refined as riding models to their parent atoms. General crystallographic data collection and refinement parameters for all compounds are listed in Tables 8.1 – 8.9. For full details, including atomic coordinates, bond lengths and

bond angles, please refer to the crystal data in CIF format, which is included on the attached compact disc. Alternatively, the crystal data can be accessed via the Internet at people.uleth.ca/~kevin.johnson/thesis/.

Disorder

Many of the crystal structures contained positional disorder. The disordered regions were typically modeled as isotropic mixtures over two sites and some restraints were applied in order to obtain reasonable bond distances and angles. Occasionally, the disordered regions were modeled anisotropically if permitted by the quality of the data. The following is a listing of the modeled disordered regions and corresponding occupancies over two sites. One representative atom number is used to describe each disordered moiety (*i.e.* for a disordered phenyl ring, only the *ipso* carbon will be listed to represent the entire ring). Compound **5**: one toluene molecule (C1c, 54% / C1d, 46%). Complex **8**: one toluene molecule (C1s, 73% / C1r, 27%). Compound **12**: one isopropyl group (C54, 54% / C54d, 46%). Compound **13**: one chloroform molecule (C1b, 62% / C1c, 38%). Complex **20**: one isopropyl group (C54, 44% / C54z, 56%), two THF rings (O1a, 40% / O1z, 60%; O1, 40% / O1y, 60%) and two benzene molecules (C1d, 38% / C1w, 62%; C1b, 37% / C1v, 63%). Complex **21**: multiple pyrimidine-alkyl moieties (N6, 53% / N6b, 47%; C100, 62% / C200, 38%; C108, 54% / C208, 46%), three phenyl rings (C79, 49% / C79b, 51%; C73, 54% / C73b, 46%; C27, 55% / C27b, 45%) and a THF ligand (O1, 67% / O1b, 33%). Complex **22**: two isopropyl groups (C54, 43% / C54b, 57%; C45, 61% / C45b, 39%). Complex **24**: two isopropyl groups (C82a, 27% / C82b, 73%; C55a, 43% / C55b, 57%). Complex **26**: two *tert*-butyl groups (C66a, 44% / C66b,

56%; C68a, 72% / C68b, 28%) and two isopropyl groups (C47a, 69%; / C47b, 31%; C56a, 46% / C56b, 54%). Complex **33**: multiple *para*-isopropylphenyl rings (C59, 53% / C59b 47%; C24, 61% / C24b, 39%; C68, 51% / C68b, 49%), one trimethylsilyl group (Si2, 46% / Si2b, 54%) and a pentane solvent molecule (C1s, 56% / C1ss, 44%). Complex **37**: one *para*-isopropylphenyl group (C28, 52% / C28b, 48%). Compound **40**: one *para*-isopropylphenyl group (C38a, 50% / C38b, 50%) and two phenyl rings (11a, 50% / 11b, 50%; C5a, 60%, C5b, 40%). Complex **41**: one phenyl ring (C23, 38% / C23b, 62%), one *para*-isopropylphenyl ring (C38, 51% / C38b, 49%) and one trimethylsilyl group (Si1, 61% / Si1b, 39%). Complex **42**: one phenyl ring (C5, 62% / C5b, 38%), one *para*-isopropylphenyl ring (C29, 49% / C29b, 51%) and one trimethylsilyl group (Si2, 57% / Si2b, 43%).

Some crystal structures contained severely disordered solvent molecules, for which no suitable model could be found. The electron density associated with the disordered regions was removed from the reflection file using the SQUEEZE subroutine of PLATON.[246,247] Reduced residuals were observed in the final SQUEEZED structures confirming that the uncertainty in the model was a result of the disordered solvent.[248] Basic details relating to these structures can be found in Tables 8.2, 8.4, 8.5 and 8.8. Full details regarding the SQUEEZE treatment of each structure can be found in the CIF file.

Specific Crystallographic Refinement Details for 18

A solution of **15** was prepared in cold (238 K) toluene/THF *in situ* and left at 238 K for 1 week. Small prisms of **18** crystallized out of the solution as **15** very slowly decomposed. Under these dynamic and highly variable conditions the single crystallinity

of the isolated intermediate was of lowered quality, and repeated attempts to grow higher quality crystals of **18** were unsuccessful. Despite the challenges encountered with crystal quality, a reliable set of low intensity single-crystal data were obtained with a final resolution of 1 Å. Following unit cell determination and refinement, the data could be integrated to give a statistically valid set of structure factors (*F*obs) from which the structure was solved using direct methods. Following application of direct methods the positions of Lu and its immediate coordination sphere was readily resolved; subsequent refinement cycles resolved the remaining components of the structure. Unfortunately too few data were available to wholly refine the structure anisotropically, thus Lu, P, and Si atoms were refined anisotropically, while all C, H, N, and O atoms were refined isotropically with hydrogen atoms inserted as riding spheres with thermal parameters 1.2-1.5 those of their parent atoms. Consequently the final refined model presents elevated residual factors and higher than normally reported estimated standard deviations. Residual electron density in the structure is associated with the heavy Lu atom and left unassigned, thus the sum of peak/hole electron density is >1. Absorption correction did not ameliorate the quality of the data. Nonetheless, the final refined structure obtained from these data unambiguously supports the composition and establishes the connectivity of the crystallized Lu complex.

Table 8.1 Summary of crystallography data collection and structure refinement for compounds **1**, **5** and **8**

	1[a]	**5**[b]	**8**[a]
Formula	$C_{57}H_{48}NP_3$	$C_{126}H_{122}N_6P_4$	$C_{63}H_{60}LiN_3P$
FW /g·mol^{-1}	839.87	1844.18	928.02
Crystal system	Orthorhombic	Triclinic	Triclinic
Space group	$Pna2_1$	$P\bar{1}$	$P\bar{1}$
a /Å	17.4632(10)	13.702(2)	13.695(3)
b /Å	23.0658(13)	18.851(3)	14.183(3)
c /Å	11.4011(6)	20.642(3)	14.978(3)
α /°	90	81.694(2)	113.836(2)
β /°	90	79.290(2)	102.657(2)
γ /°	90	83.504(2)	92.431(2)
Volume /Å^3	4592.4(4)	5163.5(13)	2568.4(8)
Z	4	2	2
D_{calc} /g·cm^{-3}	1.215	1.186	1.200
μ /mm^{-1}	0.169	0.127	0.128
Crystal size /mm^3	0.29 × 0.19 × 0.17	0.24 × 0.12 × 0.07	0.40 × 0.22 × 0.19
θ range /°	1.77 to 27.10	1.52 to 27.10	1.59 to 26.45
N	50663	74246	27644
N_{ind}	10146	22697	10519
Data/restraints/parameters	10146 / 1 / 553	22697 / 0 / 1213	10519 / 232 / 684
GoF on F^2	1.036	0.973	1.003
R_1 (I>2σ(I))[c]	0.0433	0.0753	0.0592
wR_2 (I>2σ(I))[d]	0.1067	0.1360	0.1449
R_1 (all data)[c]	0.0559	0.1915	0.1065
wR_2 (all data)[d]	0.1149	0.1754	0.1706
$\Delta\rho_{max}$ and $\Delta\rho_{min}$ /e·Å^{-3}	0.427 and −0.282	1.064 and −0.396	1.153 and −0.432

Notes: [a]Crystallized with one molecule of toluene in the asymmetric unit. [b]Crystallized with two independent molecules of **5** and two molecules of toluene in the asymmetric unit. [c]$R_1 = \Sigma||F_o| - |F_c||/\Sigma|F_o|$. [d]$wR_2 = \{\Sigma[w(F_o^2 - F_c^2)^2]/\Sigma[w(F_o^2)^2]\}^{1/2}$.

Table 8.2 Summary of crystallography data collection and structure refinement for compounds **9**, **10** and **11**

	9[a]	**10**[a]	**11**[b]
Formula	$C_{63}H_{60}Cl_2N_3P_2Sc$	$C_{63}H_{60}Cl_2N_3P_2Y$	$C_{56}H_{47}N_3P_2$
FW /g·mol^{-1}	1036.94	1080.89	823.91
Crystal system	Rhombohedral	Rhombohedral	Triclinic
Space group	$R\bar{3}$	$R\bar{3}$	$P\bar{1}$
a /Å	23.6675(10)	23.7063(8)	9.018(3)
b /Å	23.6675(10)	23.7063(8)	14.813(4)
c /Å	23.6675(10)	23.7063(8)	19.162(6)
α /°	107.38	107.28	103.236(4)
β /°	107.38	107.28	99.522(4)
γ /°	107.38	107.28	106.150(4)
Volume /Å^3	10923.1(8)	11008.1(6)	2320.5(12)
Z	6	6	2
D_{calc} /g·cm^{-3}	0.946	0.978	1.179
μ /mm^{-1}	0.250	0.943	0.134
Crystal size /mm^3	0.32 × 0.23 × 0.07	0.39 × 0.35 × 0.23	0.24 × 0.13 × 0.08
θ range /°	1.68 to 27.10	1.85 to 27.10	1.59 to 26.37
N	122009	123788	31432
N_{ind}	16076	16199	9473
Data/restraints/parameters	16076 / 44 / 637	16199 / 0 / 649	9473 / 0 / 553
GoF on F^2	0.876	1.074	0.809
R_1 (I>2σ(I)) [c]	0.0728	0.0479	0.0763
wR_2 (I>2σ(I)) [d]	0.1646	0.1455	0.1221
R_1 (all data) [c]	0.2047	0.0738	0.2336
wR_2 (all data) [d]	0.2012	0.1561	0.1658
$\Delta\rho_{max}$ and $\Delta\rho_{min}$ /e·Å^{-3}	0.887 and −0.495	0.547 and −0.411	0.259 and −0.260

Notes: [a]The structure contained two toluene molecules in the asymmetric unit, one of which was severely disordered. In addition, a void existed in the unit cell that contained highly disordered and unidentifiable solvent. The electron density associated with the disordered solvent regions was removed from the reflection file using the SQUEEZE subroutine of PLATON. [b]Crystallized with one molecule of benzene and one severely disordered and unidentifiable solvent molecule in the asymmetric unit. The electron density associated with the disordered solvent was removed from the reflection file using the SQUEEZE subroutine of PLATON. [c]$R_1 = \Sigma||F_o| - |F_c||/\Sigma|F_o|$. [d]$wR_2 = \{\Sigma[w(F_o^2 - F_c^2)^2]/\Sigma[w(F_o^2)^2]\}^{1/2}$.

Table 8.3 Summary of crystallography data collection and structure refinement for compounds **12**, **13** and **18**

	12[a]	**13**[b]	**18**
Formula	$C_{68}H_{65}N_3P_2$	$C_{48}H_{39}Cl_6N_7P_2$	$C_{64}H_{70}LuN_3OP_2Si$
FW /g·mol^{-1}	986.17	988.50	1162.23
Crystal system	Triclinic	Monoclinic	Monoclinic
Space group	$P\bar{1}$	$P2_1/c$	$P2_1/n$
a /Å	8.9413(6)	13.4383(16)	10.7680(13)
b /Å	16.6229(12)	14.7457(18)	21.278(3)
c /Å	19.4273(14)	23.194(3)	26.917(3)
α /°	77.5770(10)	90	90
β /°	80.3780(10)	90.801(3)	99.461(2)
γ /°	78.8940(10)	90	90
Volume /Å^3	2743.2(3)	4595.5(9)	6083.3(13)
Z	2	4	4
D_{calc} /g·cm^{-3}	1.194	1.429	1.269
μ /mm^{-1}	0.124	0.488	1.736
Crystal size /mm^3	0.25 × 0.14 × 0.055	0.26 × 0.09 × 0.05	0.19 × 0.17 × 0.07
θ range /°	1.82 to 25.03	1.64 to 26.37	2.14 to 20.82
N	33540	32559	68237
N_{ind}	9677	9367	6349
Data/restraints/parameters	9677 / 2 / 664	9367 / 30 / 607	6349 / 4 / 318
GoF on F^2	1.033	0.960	1.060
R_1 (I>2σ(I))[c]	0.0518	0.0630	0.0994
wR_2 (I>2σ(I))[d]	0.1232	0.1189	0.2487
R_1 (all data)[c]	0.0764	0.1660	0.1316
wR_2 (all data)[d]	0.1381	0.1556	0.2665
$\Delta\rho_{max}$ and $\Delta\rho_{min}$ /e·Å^{-3}	0.470 and −0.411	0.680 and −0.378	5.600 and −2.051

Notes: [a]Crystallized with two molecules of benzene in the asymmetric unit. [b]Crystallized with two molecules of chloroform in the asymmetric unit. [c]$R_1 = \Sigma||F_o| - |F_c||/\Sigma|F_o|$. [d]$wR_2 = \{\Sigma[w(F_o^2 - F_c^2)^2]/\Sigma[w(F_o^2)^2]\}^{1/2}$.

Table 8.4 Summary of crystallography data collection and structure refinement for compounds **20**, **21** and **22**

	20[a]	**21**[b]	**22**[c]
Formula	$C_{138}H_{134}Lu_2N_6O_2P_4$	$C_{112}H_{124}Lu_2N_{14}OP_4Si_4$	$C_{66}H_{66}I_2LuN_3OP_2$
FW /g·mol^{-1}	2382.33	2268.43	1407.93
Crystal system	Monoclinic	Triclinic	Monoclinic
Space group	$P2_1/n$	$P\bar{1}$	$P2_1/n$
a /Å	10.9319(9)	16.935(2)	13.9268(6)
b /Å	44.979(4)	18.699(2)	20.6789(9)
c /Å	24.495(2)	20.754(3)	20.4645(9)
α /°	90	95.886(2)	90
β /°	99.5860(10)	103.004(2)	91.1610(10)
γ /°	90	95.355(2)	90
Volume /Å^3	11876.1(17)	6323.7(14)	5892.4(4)
Z	4	2	4
D_{calc} /g·cm^{-3}	1.332	1.191	1.587
μ /mm^{-1}	1.761	1.687	2.822
Crystal size /mm^3	0.38 × 0.08 × 0.04	0.36 × 0.17 × 0.14	0.12 × 0.11 × 0.10
θ range /°	1.69 to 26.37	1.56 to 27.10	1.75 to 27.10
N	158092	89676	83135
N_{ind}	24286	27765	12989
Data/restraints/parameters	24286 / 40 / 1295	27765 / 38 / 1118	12989 / 16 / 667
GoF on F^2	1.112	1.012	1.032
R_1 (I>2σ(I))[d]	0.0789	0.0670	0.0307
wR_2 (I>2σ(I))[e]	0.1396	0.1812	0.0653
R_1 (all data)[d]	0.1172	0.1097	0.0455
wR_2 (all data)[e]	0.1530	0.1988	0.0717
$\Delta\rho_{max}$ and $\Delta\rho_{min}$ /e·Å^{-3}	2.562 and −2.028	3.124 and −0.938	1.108 and −1.132

Notes: [a]Crystallized with two independent molecules of **20**, three molecules of benzene and one disordered molecule of pentane in the asymmetric unit. The pentane molecule was removed from the reflection file using the SQUEEZE subroutine of PLATON. [b]Crystallized with a severely disordered and unidentifiable solvent molecule in the asymmetric unit, which was removed from the reflection file using the SQUEEZE subroutine of PLATON. [c]Crystallized with one molecule of benzene in the asymmetric unit. [d]$R_1 = \Sigma||F_o| - |F_c||/\Sigma|F_o|$. [e]$wR_2 = \{\Sigma[w(F_o^2 - F_c^2)^2]/\Sigma[w(F_o^2)^2]\}^{1/2}$.

Table 8.5 Summary of crystallography data collection and structure refinement for compounds **23**, **24** and **26**

	23[a]	**24**[b]	**26**[c]
Formula	$C_{74}H_{70}LuN_5P_2$	$C_{91}H_{112}LuN_5P_2$	$C_{74}H_{81}LuN_4P_2$
FW /g·mol^{-1}	1266.26	1512.77	1263.34
Crystal system	Triclinic	Triclinic	Monoclinic
Space group	$P\bar{1}$	$P\bar{1}$	$C2/c$
a /Å	12.6755(9)	14.357(2)	32.990(3)
b /Å	13.9958(10)	16.959(3)	23.689(2)
c /Å	17.6268(13)	17.593(3)	23.446(2)
α /°	98.9330(10)	85.737(2)	90
β /°	98.6410(10)	74.590(2)	104.0580(10)
γ /°	90.7270(10)	77.178(2)	90
Volume /Å^3	3052.0(4)	4026.1(11)	17774(3)
Z	2	2	8
D_{calc} /g·cm^{-3}	1.378	1.248	0.944
μ /mm^{-1}	1.718	1.313	1.179
Crystal size /mm^3	0.34 × 0.29 × 0.09	0.25 × 0.21 × 0.17	0.38 × 0.13 × 0.07
θ range /°	1.63 to 27.10	1.73 to 25.03	1.79 to 27.10
N	43225	47761	123715
N_{ind}	13380	14118	19565
Data/restraints/parameters	13380 / 0 / 755	14118 / 0 / 910	19565 / 1 / 745
GoF on F^2	1.046	0.948	0.942
R_1 (I>2σ(I))[d]	0.0219	0.0731	0.0449
wR_2 (I>2σ(I))[e]	0.0523	0.1486	0.1119
R_1 (all data)[d]	0.0267	0.1609	0.0776
wR_2 (all data)[e]	0.0546	0.1795	0.1224
$\Delta\rho_{max}$ and $\Delta\rho_{min}$ /e·Å^{-3}	0.947 and −0.363	4.515 and −1.416	2.391 and −0.668

Notes: [a]Crystallized with one molecule of benzene in the asymmetric unit. [b]Crystallized with one molecule of pentane in the asymmetric unit. [c]Crystallized with two highly disordered molecules of pentane in the asymmetric unit, which were removed from the reflection file using the SQUEEZE subroutine of PLATON. [d]$R_1 = \Sigma||F_o| - |F_c||/\Sigma|F_o|$. [e]$wR_2 = \{\Sigma[w(F_o^2 - F_c^2)^2]/\Sigma[w(F_o^2)^2]\}^{1/2}$.

Table 8.6 Summary of crystallography data collection and structure refinement for compounds **27**, **30** and **31**

	27	**30**	**31**[a]
Formula	$C_{34}H_{66}LuNO_2Si_2$	$C_{18}H_{19}NO_4P_2$	$C_{39}H_{44}N_3O_4P_2$
FW /g·mol^{-1}	752.03	375.28	680.71
Crystal system	Triclinic	Triclinic	Orthorhombic
Space group	$P\bar{1}$	$P\bar{1}$	*Pbca*
a /Å	10.1629(17)	8.3969(9)	10.3386(7)
b /Å	13.870(2)	10.2686(10)	20.4403(13)
c /Å	14.739(2)	10.6756(11)	32.986(2)
α /°	94.611(2)	93.7620(10)	90
β /°	107.296(2)	111.3110(10)	90
γ /°	94.683(2)	93.6660(10)	90
Volume /Å^3	1964.9(6)	851.88(15)	6970.8(8)
Z	2	2	8
D_{calc} /g·cm^{-3}	1.271	1.463	1.297
μ /mm^{-1}	2.599	0.279	0.170
Crystal size /mm^3	0.31 × 0.18 × 0.08	0.17 × 0.17 × 0.03	0.47 × 0.42 × 0.08
θ range /°	1.96 to 25.03	2.00 to 27.10	1.99 to 27.10
N	18541	11666	75247
N_{ind}	6908	3735	7693
Data/restraints/parameters	6908 / 0 / 380	3735 / 0 / 228	7693 / 0 / 439
GoF on F^2	1.022	1.021	1.055
R_1 (I>2σ(I))[b]	0.0239	0.0374	0.0399
wR_2 (I>2σ(I))[c]	0.0610	0.0905	0.1030
R_1 (all data)[b]	0.0267	0.0523	0.0492
wR_2 (all data)[c]	0.0631	0.0980	0.1102
$\Delta\rho_{max}$ and $\Delta\rho_{min}$ /e·Å^{-3}	1.702 and −1.243	0.360 and −0.311	0.398 and −0.409

Notes: [a]Crystallized with one molecule of benzene in the asymmetric unit. [b]$R_1 = \Sigma||F_o| - |F_c||/\Sigma|F_o|$. [c]$wR_2 = \{\Sigma[w(F_o^2 - F_c^2)^2]/\Sigma[w(F_o^2)^2]\}^{1/2}$.

Table 8.7 Summary of crystallography data collection and structure refinement for compounds **33**, **35** and **36**

	33[a]	**35**[b]	**36**
Formula	$C_{93}H_{136}Lu_2N_6O_8P_4Si_4$	$C_{43}H_{53}N_3P_2$	$C_{26}H_{53}LuN_4Si_3$
FW /g·mol^{-1}	2052.26	673.82	680.96
Crystal system	Triclinic	Triclinic	Triclinic
Space group	$P\bar{1}$	$P\bar{1}$	$P\bar{1}$
a /Å	14.763(5)	12.3309(10)	9.7431(11)
b /Å	18.123(6)	12.8921(10)	10.3882(12)
c /Å	19.174(6)	14.3479(12)	17.970(2)
α /°	80.777(4)	72.7090(10)	89.9710(10)
β /°	84.329(4)	65.0130(10)	75.7880(10)
γ /°	83.766(4)	72.3270(10)	80.2470(10)
Volume /Å^3	5016(3)	1931.8(3)	1736.1(3)
Z	2	2	2
D_{calc} /g·cm^{-3}	1.359	1.158	1.303
μ /mm^{-1}	2.122	0.146	2.965
Crystal size /mm^3	0.20 × 0.06 × 0.03	0.57 × 0.26 × 0.18	0.28 × 0.11 × 0.06
θ range /°	1.69 to 26.37	1.60 to 27.10	1.99 to 27.10
N	54488	27321	19635
N_{ind}	20429	8478	7597
Data/restraints/parameters	20429 / 19 / 990	8478 / 0 / 423	7597 / 0 / 320
GoF on F^2	0.971	1.036	1.018
R_1 (I>2σ(I))[c]	0.0477	0.0556	0.0306
wR_2 (I>2σ(I))[d]	0.0923	0.1503	0.0588
R_1 (all data)[c]	0.0910	0.0679	0.0419
wR_2 (all data)[d]	0.1084	0.1615	0.0624
$\Delta\rho_{max}$ and $\Delta\rho_{min}$ /e·Å^{-3}	0.717 and −0.851	0.952 and −0.633	0.728 and −1.149

Notes: [a]Crystallized with one molecule of pentane in the asymmetric unit. [b]Crystallized with one molecule of toluene in the asymmetric unit. [c]$R_1 = \Sigma||F_o| - |F_c||/\Sigma|F_o|$. [d]$wR_2 = \{\Sigma[w(F_o^2 - F_c^2)^2]/\Sigma[w(F_o^2)^2]\}^{1/2}$.

Table 8.8 Summary of crystallography data collection and structure refinement for compounds **37** and **40**

	37[a]	**40**[b]
Formula	$C_{62}H_{74}LuN_7P_2$	$C_{46}H_{45}N_3P_2$
FW /g·mol^{-1}	1154.19	701.79
Crystal system	Monoclinic	Triclinic
Space group	$P2_1/c$	$P\bar{1}$
a /Å	11.6505(9)	12.9263(2)
b /Å	21.5593(17)	14.5326(2)
c /Å	23.1631(18)	14.8331(3)
α /°	90	112.5870(10)
β /°	91.0050(10)	103.5210(10)
γ /°	90	108.7700(10)
Volume /Å^3	5817.1(8)	2223.03(8)
Z	4	2
D_{calc} /g·cm^{-3}	1.318	1.048
μ /mm^{-1}	1.796	0.129
Crystal size /mm^3	0.54 × 0.31 × 0.21	0.30 × 0.30 × 0.10
θ range /°	1.75 to 27.10	1.63 to 27.54
N	64976	36845
N_{ind}	12830	10171
Data/restraints/parameters	12830 / 0 / 655	10171 / 42 / 439
GoF on F^2	1.041	1.045
R_1 (I>2σ(I)) [c]	0.0228	0.0709
wR_2 (I>2σ(I)) [d]	0.0539	0.1723
R_1 (all data) [c]	0.0272	0.0950
wR_2 (all data) [d]	0.0566	0.1821
$\Delta\rho_{max}$ and $\Delta\rho_{min}$ /e·Å^{-3}	1.516 and −0.984	0.491 and −0.431

Notes: [a]Crystallized with two molecules of benzene in the asymmetric unit. [b]A highly disordered solvent molecule was removed from the reflection file using the SQUEEZE subroutine of PLATON. [c]$R_1 = \Sigma||F_o| - |F_c||/\Sigma|F_o|$. [d]$wR_2 = \{\Sigma[w(F_o^2 - F_c^2)^2]/\Sigma[w(F_o^2)^2]\}^{1/2}$.

Table 8.9 Summary of crystallography data collection and structure refinement for compounds **41** and **42**

	41	**42**
Formula	$C_{54}H_{66}ErN_3P_2Si_2$	$C_{54}H_{66}LuN_3P_2Si_2$
FW /g·mol^{-1}	1042.48	1050.19
Crystal system	Triclinic	Triclinic
Space group	$P\bar{1}$	$P\bar{1}$
a /Å	9.729(5)	9.7163(6)
b /Å	12.188(6)	12.1266(7)
c /Å	24.287(11)	24.2569(14)
α /°	84.796(5)	84.9530(10)
β /°	78.920(5)	78.9220(10)
γ /°	69.550(5)	69.4640(10)
Volume /Å^3	2647(2)	2625.9(3)
Z	2	2
D_{calc} /g·cm^{-3}	1.308	1.328
μ /mm^{-1}	1.727	2.023
Crystal size /mm^3	0.47 × 0.09 × 0.07	0.31 × 0.22 × 0.13
θ range /°	1.71 to 26.37	1.79 to 27.10
N	34897	37480
N_{ind}	10778	11526
Data/restraints/parameters	10778 / 0 / 548	11526 / 0 / 548
GoF on F^2	1.022	1.023
R_1 (I>2σ(I)) [a]	0.0365	0.0300
wR_2 (I>2σ(I)) [b]	0.0818	0.0721
R_1 (all data) [a]	0.0484	0.0346
wR_2 (all data) [b]	0.0868	0.0746
$\Delta\rho_{max}$ and $\Delta\rho_{min}$ /e·Å^{-3}	0.827 and −0.814	1.124 and −0.853

Notes: [a] $R_1 = \Sigma||F_o| - |F_c||/\Sigma|F_o|$. [b] $wR_2 = \{\Sigma[w(F_o^2 - F_c^2)^2]/\Sigma[w(F_o^2)^2]\}^{1/2}$.

References

1. Schumann, H.; Meese-Marktscheffel, J. A.; Esser, L. *Chem. Rev.* **1995**, *95*, 865–986.
2. Birmingham, J. M.; Wilkinson, G. *J. Am. Chem. Soc.* **1956**, *78*, 42–44.
3. Wilkinson, G.; Birmingham, J. M. *J. Am. Chem. Soc.* **1954**, *76*, 6210.
4. Bochkarev, M. N.; Fedushkin, I. L.; Dechert, S.; Fagin, A. A.; Schumann, H. *Angew. Chem., Int. Ed.* **2001**, *40*, 3176–3178.
5. Clentsmith, G. K. B.; Cloke, F. G. N.; Green, J. C.; Hanks, J.; Hitchcock, P. B.; Nixon, J. F. *Angew. Chem., Int. Ed.* **2003**, *42*, 1038–1041.
6. Cloke, F. G. N. *Chem. Soc. Rev.* **1993**, *22*, 17–24.
7. Cloke, F. G. N.; Khan, K.; Perutz, R. N. *J. Chem. Soc., Chem. Commun.* **1991**, 1372–1373.
8. Evans, W. J. *Inorg. Chem.* **2007**, *46*, 3435–3449.
9. Hitchcock, P. B.; Lappert, M. F.; Maron, L.; Protchenko, A. V. *Angew. Chem., Int. Ed.* **2008**, *47*, 1488–1491.
10. Neculai, A. M.; Neculai, D.; Roesky, H. W.; Magull, J.; Baldus, M.; Andronesi, O.; Jansen, M. *Organometallics* **2002**, *21*, 2590–2592.
11. Evans, W. J. *Polyhedron* **1987**, *6*, 803–835.
12. Atwood, J. L.; Hunter, W. E.; Rogers, R. D.; Holton, J.; McMeeking, J.; Pearce, R.; Lappert, M. F. *J. Chem. Soc., Chem. Commun.* **1978**, 140–142.
13. Lappert, M. F.; Pearce, R. *J. Chem. Soc., Chem. Commun.* **1973**, 126.
14. Bambirra, S.; Meetsma, A.; Hessen, B. *Organometallics* **2006**, *25*, 3454–3462.
15. Meyer, N.; Roesky, P. W.; Bambirra, S.; Meetsma, A.; Hessen, B.; Saliu, K.; Takats, J. *Organometallics* **2008**, *27*, 1501–1505.
16. Wooles, A. J.; Mills, D. P.; Lewis, W.; Blake, A. J.; Liddle, S. T. *Dalton Trans.* **2010**, *39*, 500–510.
17. Bradley, D. C.; Ghotra, J. S.; Hart, F. A. *J. Chem. Soc., Chem. Commun.* **1972**, 349–350.
18. Bradley, D. C.; Ghotra, J. S.; Hart, F. A. *J. Chem. Soc., Dalton Trans.* **1977**, 1021–1023.
19. Ghotra, J. S.; Hursthouse, M. B.; Welch, A. J. *J. Chem. Soc., Chem. Commun.* **1973**, 669–670.
20. Abicht, H.-P.; Issleib, K. *Z. Chem.* **1977**, *17*, 1–9.
21. Dehand, J.; Pfeffer, M. *Coord. Chem. Rev.* **1976**, *18*, 327–352.
22. Evans, D. W.; Baker, G. R.; Newkome, G. R. *Coord. Chem. Rev.* **1989**, *93*, 155–183.
23. Newkome, G. R.; Puckett, W. E.; Gupta, V. K.; Kiefer, G. E. *Chem. Rev.* **1986**, *86*, 451–489.
24. Bruce, M. I. *Angew. Chem., Int. Ed.* **1977**, *16*, 73–86.
25. Rothwell, I. P. *Polyhedron* **1985**, *4*, 177–200.
26. Dias, A. R.; Salema, M. S.; Martinho Simões, J. A.; Pattiasina, J. W.; Teuben, J. H. *J. Organomet. Chem.* **1989**, *364*, 97–103.
27. Evans, W. J.; Davis, B. L. *Chem. Rev.* **2002**, *102*, 2119–2136.

28. Brunner, H.; Wachter, J.; Gehart, G.; Leblanc, J.-C.; Moïse, C. *Organometallics* **1996**, *15*, 1327–1330.
29. Fischer, J. M.; Piers, W. E.; Young, V. G., Jr. *Organometallics* **1996**, *15*, 2410–2412.
30. McDade, C.; Green, J. C.; Bercaw, J. E. *Organometallics* **1982**, *1*, 1629–1634.
31. Schock, L. E.; Brock, C. P.; Marks, T. J. *Organometallics* **1987**, *6*, 232–241.
32. Evans, W. J.; Miller, K. A.; DiPasquale, A. G.; Rheingold, A. L.; Stewart, T. J.; Bau, R. *Angew. Chem., Int. Ed.* **2008**, *47*, 5075–5078.
33. Watson, P. L. *J. Am. Chem. Soc.* **1983**, *105*, 6491–6493.
34. Thompson, M. E.; Baxter, S. M.; Bulls, A. R.; Burger, B. J.; Nolan, M. C.; Santarsiero, B. D.; Schaefer, W. P.; Bercaw, J. E. *J. Am. Chem. Soc.* **1987**, *109*, 203–219.
35. Thompson, M. E.; Bercaw, J. E. *Pure Appl. Chem.* **1984**, *56*, 1–11.
36. Hajela, S.; Schaefer, W. P.; Bercaw, J. E. *Acta Crystallogr., Sect. C: Cryst. Struct. Commun.* **1992**, *48*, 1771–1773.
37. Sadow, A. D.; Tilley, T. D. *J. Am. Chem. Soc.* **2003**, *125*, 7971–7977.
38. Booij, M.; Deelman, B.-J.; Duchateau, R.; Postma, D. S.; Meetsma, A.; Teuben, J. H. *Organometallics* **1993**, *12*, 3531–3540.
39. den Haan, K. H.; Teuben, J. H. *J. Chem. Soc., Chem. Commun.* **1986**, 682–683.
40. Evans, W. J.; Champagne, T. M.; Ziller, J. W. *J. Am. Chem. Soc.* **2006**, *128*, 14270–14271.
41. Evans, W. J.; Ulibarri, T. A.; Ziller, J. W. *Organometallics* **1991**, *10*, 134–142.
42. Evans, W. J.; Perotti, J. M.; Ziller, J. W. *Inorg. Chem.* **2005**, *44*, 5820–5825.
43. Booij, M.; Meetsma, A.; Teuben, J. H. *Organometallics* **1991**, *10*, 3246–3252.
44. Evans, W. J.; Perotti, J. M.; Ziller, J. W. *J. Am. Chem. Soc.* **2005**, *127*, 3894–3909.
45. Sun, J.; Berg, D. J.; Twamley, B. *Organometallics* **2008**, *27*, 683–690.
46. Evans, W. J.; Kozimor, S. A.; Ziller, J. W. *Inorg. Chem.* **2005**, *44*, 7960–7969.
47. Beetstra, D. J.; Meetsma, A.; Hessen, B.; Teuben, J. H. *Organometallics* **2003**, *22*, 4372–4374.
48. Evans, W. J.; Allen, N. T.; Ziller, J. W. *J. Am. Chem. Soc.* **2001**, *123*, 7927–7928.
49. Evans, W. J.; Allen, N. T.; Ziller, J. W. *Angew. Chem., Int. Ed.* **2002**, *41*, 359–361.
50. Jaroschik, F.; Nief, F.; Le Goff, X.-F.; Ricard, L. *Organometallics* **2007**, *26*, 1123–1125.
51. Jaroschik, F.; Nief, F.; Le Goff, X.-F.; Ricard, L. *Organometallics* **2007**, *26*, 3552–3558.
52. Jaroschik, F.; Momin, A.; Nief, F.; Le Goff, X.-F.; Deacon, G. B.; Junk, P. C. *Angew. Chem., Int. Ed.* **2009**, *48*, 1117–1121.
53. Meyer, G. *Angew. Chem., Int. Ed.* **2008**, *47*, 4962–4964.
54. Deacon, G. B.; Forsyth, C. M.; Jaroschik, F.; Junk, P. C.; Kay, D. L.; Maschmeyer, T.; Masters, A. F.; Wang, J.; Field, L. D. *Organometallics* **2008**, *27*, 4772–4778.
55. Ruspic, C.; Moss, J. R.; Schürmann, M.; Harder, S. *Angew. Chem., Int. Ed.* **2008**, *47*, 2121–2126.

56. Edelmann, F. T.; Freckmann, D. M. M.; Schumann, H. *Chem. Rev.* **2002**, *102*, 1851–1896.
57. Mountford, P.; Ward, B. D. *Chem. Commun.* **2003**, 1797–1803.
58. Piers, W. E.; Emslie, D. J. H. *Coord. Chem. Rev.* **2002**, *233-234*, 131–155.
59. Nagendran, S.; Roesky, H. W. *Organometallics* **2008**, *27*, 457–492.
60. Deacon, G. B.; Forsyth, C. M. *Chem. Commun.* **2002**, 2522–2523.
61. Deacon, G. B.; Forsyth, C. M.; Junk, P. C.; Wang, J. *Inorg. Chem.* **2007**, *46*, 10022–10030.
62. Karl, M.; Harms, K.; Seybert, G.; Massa, W.; Fau, S.; Frenking, G.; Dehnicke, K. *Z. Anorg. Allg. Chem.* **1999**, *625*, 2055–2063.
63. Niemeyer, M. *Inorg. Chem.* **2006**, *45*, 9085–9095.
64. Fang, M.; Bates, J. E.; Lorenz, S. E.; Lee, D. S.; Rego, D. B.; Ziller, J. W.; Furche, F.; Evans, W. J. *Inorg. Chem.* **2011**, *50*, 1459–1469.
65. Bennett, C. R.; Bradley, D. C. *J. Chem. Soc., Chem. Commun.* **1974**, 29–30.
66. Berno, P.; Gambarotta, S. *Organometallics* **1994**, *13*, 2569–2571.
67. Berno, P.; Minhas, R.; Hao, S.; Gambarotta, S. *Organometallics* **1994**, *13*, 1052–1054.
68. Cai, H.; Yu, X.; Chen, T.; Chen, X.-T.; You, X.-Z.; Xue, Z. *Can. J. Chem.* **2003**, *81*, 1398–1405.
69. Messere, R.; Spirlet, M.-R.; Jan, D.; Demonceau, A.; Noels, Alfred F. *Eur. J. Inorg. Chem.* **2000**, 1151–1153.
70. Simpson, S. J.; Andersen, R. A. *Inorg. Chem.* **1981**, *20*, 3627–3629.
71. Yu, X.; Bi, S.; Guzei, I. A.; Lin, Z.; Xue, Z.-L. *Inorg. Chem.* **2004**, *43*, 7111–7119.
72. Dormond, A.; El Bouadili, A. A.; Moïse, C. *J. Chem. Soc., Chem. Commun.* **1985**, 914–916.
73. Korobkov, I.; Gambarotta, S. *Inorg. Chem.* **2010**, *49*, 3409–3418.
74. Simpson, S. J.; Turner, H. W.; Andersen, R. A. *Inorg. Chem.* **1981**, *20*, 2991–2995.
75. Fryzuk, M. D. *Can. J. Chem.* **1992**, *70*, 2839–2845.
76. Fryzuk, M. D.; Haddad, T. S.; Rettig, S. J. *Organometallics* **1991**, *10*, 2026–2036.
77. Bourget-Merle, L.; Lappert, M. F.; Severn, J. R. *Chem. Rev.* **2002**, *102*, 3031–3066.
78. Johnson, K. R. D.; Côté, A. P.; Hayes, P. G. *J. Organomet. Chem.* **2010**, *695*, 2747–2755.
79. Hayes, P. G.; Piers, W. E.; Lee, L. W. M.; Knight, L. K.; Parvez, M.; Elsegood, M. R. J.; Clegg, W. *Organometallics* **2001**, *20*, 2533–2544.
80. Hayes, P. G.; Piers, W. E.; Parvez, M. *Organometallics* **2005**, *24*, 1173–1183.
81. Liu, B.; Cui, D.; Ma, J.; Chen, X.; Jing, X. *Chem.—Eur. J.* **2007**, *13*, 834–845.
82. Liu, B.; Liu, X.; Cui, D.; Liu, L. *Organometallics* **2009**, *28*, 1453–1460.
83. Conroy, K. D.; Piers, W. E.; Parvez, M. *J. Organomet. Chem.* **2008**, *693*, 834–846.
84. Bambirra, S.; Boot, S. J.; van Leusen, D.; Meetsma, A.; Hessen, B. *Organometallics* **2004**, *23*, 1891–1898.
85. Tazelaar, C. G. J.; Bambirra, S.; van Leusen, D.; Meetsma, A.; Hessen, B.; Teuben, J. H. *Organometallics* **2004**, *23*, 936–939.

86. Fegler, W.; Spaniol, T. P.; Okuda, J. *Dalton Trans*. **2010**, *39*, 6774–6779.
87. Diaconescu, P. L. *Curr. Org. Chem*. **2008**, *12*, 1388–1405.
88. Watson, P. L. *J. Chem. Soc., Chem. Commun*. **1983**, 276–277.
89. Jantunen, K. C.; Scott, B. L.; Gordon, J. C.; Kiplinger, J. L. *Organometallics* **2007**, *26*, 2777–2781.
90. Arndt, S.; Elvidge, B. R.; Zeimentz, P. M.; Spaniol, T. P.; Okuda, J. *Organometallics* **2006**, *25*, 793–795.
91. Scott, J.; Basuli, F.; Fout, A. R.; Huffman, J. C.; Mindiola, D. J. *Angew. Chem., Int. Ed*. **2008**, *47*, 8502–8505.
92. Lu, E.; Li, Y.; Chen, Y. *Chem. Commun*. **2010**, *46*, 4469–4471.
93. Buchard, A.; Platel, R. H.; Auffrant, A.; Le Goff, X. F.; Le Floch, P.; Williams, C. K. *Organometallics* **2010**, *29*, 2892–2900.
94. Cao, T.-P.-A.; Buchard, A.; Le Goff, X. F.; Auffrant, A.; Williams, C. K. *Inorg. Chem*. **2012**, *51*, 2157–2169.
95. Gamer, M. T.; Dehnen, S.; Roesky, P. W. *Organometallics* **2001**, *20*, 4230–4236.
96. Gamer, M. T.; Rastätter, M.; Roesky, P. W.; Steffens, A.; Glanz, M. *Chem.—Eur. J*. **2005**, *11*, 3165–3172.
97. Gamer, M. T.; Roesky, P. W. *J. Organomet. Chem*. **2002**, *647*, 123–127.
98. Gamer, M. T.; Roesky, P. W.; Palard, I.; Le Hellaye, M.; Guillaume, S. M. *Organometallics* **2007**, *26*, 651–657.
99. Hill, M. S.; Hitchcock, P. B. *Dalton Trans*. **2003**, 4570–4571.
100. Li, D.; Li, S.; Cui, D.; Zhang, X. *J. Organomet. Chem*. **2010**, *695*, 2781–2788.
101. Li, D.; Li, S.; Cui, D.; Zhang, X.; Trifonov, A. A. *Dalton Trans*. **2011**, *40*, 2151–2153.
102. Panda, T. K.; Zulys, A.; Gamer, M. T.; Roesky, P. W. *Organometallics* **2005**, *24*, 2197–2202.
103. Rastätter, M.; Zulys, A.; Roesky, P. W. *Chem. Commun*. **2006**, 874–876.
104. Rastätter, M.; Zulys, A.; Roesky, P. W. *Chem.—Eur. J*. **2007**, *13*, 3606–3616.
105. Wiecko, M.; Roesky, P. W.; Burlakov, V. V.; Spannenberg, A. *Eur. J. Inorg. Chem*. **2007**, 876–881.
106. Wiecko, M.; Roesky, P. W. *Organometallics* **2009**, *28*, 1266–1269.
107. Zulys, A.; Panda, T. K.; Gamer, M. T.; Roesky, P. W. *Chem. Commun*. **2004**, 2584–2585.
108. Ong, C. M.; McKarns, P.; Stephan, D. W. *Organometallics* **1999**, *18*, 4197–4204.
109. Panda, T. K.; Zulys, A.; Gamer, M. T.; Roesky, P. W. *J. Organomet. Chem*. **2005**, *690*, 5078–5089.
110. Welch, G. C.; Piers, W. E.; Parvez, M.; McDonald, R. *Organometallics* **2004**, *23*, 1811–1818.
111. Wooles, A. J.; Gregson, M.; Cooper, O. J.; Middleton-Gear, A.; Mills, D. P.; Lewis, W.; Blake, A. J.; Liddle, S. T. *Organometallics* **2011**, *30*, 5314–5325.
112. Kamalesh Babu, R. P.; Aparna, K.; McDonald, R.; Cavell, R. G. *Organometallics* **2001**, *20*, 1451–1455.
113. Cooper, O. J.; McMaster, J.; Lewis, W.; Blake, A. J.; Liddle, S. T. *Dalton Trans*. **2010**, *39*, 5074–5076.
114. Ma, G.; Ferguson, M. J.; McDonald, R.; Cavell, R. G. *Inorg. Chem*. **2011**, *50*, 6500–6508.

115. Alhomaidan, O.; Beddie, C.; Bai, G.; Stephan, D. W. *Dalton Trans*. **2009**, 1991–1998.
116. Kamalesh Babu, R. P.; Mcdonald, R.; Cavell, R. G. *Chem. Commun*. **2000**, 481–482.
117. Ramos, A.; Stephan, D. W. *Dalton Trans*. **2010**, *39*, 1328–1338.
118. Sarsfield, M. J.; Said, M.; Thornton-Pett, M.; Gerrard, L. A.; Bochmann, M. *J. Chem. Soc., Dalton Trans*. **2001**, 822–827.
119. Cavell, R. G.; Kamalesh Babu, R. P.; Kasani, A.; McDonald, R. *J. Am. Chem. Soc*. **1999**, *121*, 5805–5806.
120. Kamalesh Babu, R. P.; McDonald, R.; Cavell, R. G. *Organometallics* **2000**, *19*, 3462–3465.
121. Brown, C. C.; Glotzbach, C.; Stephan, D. W. *Dalton Trans*. **2010**, *39*, 9626–9632.
122. Cariou, R.; Graham, T. W.; Dahcheh, F.; Stephan, D. W. *Dalton Trans*. **2011**, *40*, 5419–5422.
123. Masuda, J. D.; Wei, P.; Stephan, D. W. *Dalton Trans*. **2003**, 3500–3505.
124. Aparna, K.; Ferguson, M.; Cavell, R. G. *J. Am. Chem. Soc*. **2000**, *122*, 726–727.
125. Buchard, A.; Auffrant, A.; Ricard, L.; Le Goff, X. F.; Platel, R. H.; Williams, C. K.; Le Floch, P. *Dalton Trans*. **2009**, 10219–10222.
126. Liddle, S. T.; McMaster, J.; Green, J. C.; Arnold, P. L. *Chem. Commun*. **2008**, 1747–1749.
127. Mills, D. P.; Cooper, O. J.; McMaster, J.; Lewis, W.; Liddle, S. T. *Dalton Trans*. **2009**, 4547–4555.
128. Mills, D. P.; Wooles, A. J.; McMaster, J.; Lewis, W.; Blake, A. J.; Liddle, S. T. *Organometallics* **2009**, *28*, 6771–6776.
129. Wooles, A. J.; Cooper, O. J.; McMaster, J.; Lewis, W.; Blake, A. J.; Liddle, S. T. *Organometallics* **2010**, *29*, 2315–2321.
130. Zhu, D.; Budzelaar, P. H. M. *Organometallics* **2008**, *27*, 2699–2705.
131. Staudinger, H.; Meyer, J. *Helv. Chim. Acta* **1919**, *2*, 635–646.
132. Basuli, F.; Bailey, B. C.; Tomaszewski, J.; Huffman, J. C.; Mindiola, D. J. *J. Am. Chem. Soc*. **2003**, *125*, 6052–6053.
133. Tsurugi, H.; Matsuo, Y.; Yamagata, T.; Mashima, K. *Organometallics* **2004**, *23*, 2797–2805.
134. Galler, J. L.; Goodchild, S.; Gould, J.; McDonald, R.; Sella, A. *Polyhedron* **2004**, *23*, 253–262.
135. Shao, P.; Berg, D. J.; Bushnell, G. W. *Inorg. Chem*. **1994**, *33*, 6334–6339.
136. Gibson, V. C.; Spitzmesser, S. K.; White, A. J. P.; Williams, D. J. *Dalton Trans*. **2003**, 2718–2727.
137. Mudadu, M. S.; Singh, A. N.; Thummel, R. P. *J. Org. Chem*. **2008**, *73*, 6513–6520.
138. Inoue, M.; Suzuki, T.; Nakada, M. *J. Am. Chem. Soc*. **2003**, *125*, 1140–1141.
139. Chang, Y. M.; Lee, S. H.; Cho, M. Y.; Yoo, B. W.; Rhee, H. J.; Lee, S. H.; Yoon, C. M. *Synth. Commun*. **2005**, *35*, 1851–1857.
140. Kuroki, M.; Tsunashima, Y. *J. Heterocycl. Chem*. **1981**, *18*, 709–714.
141. Wentrup, C.; Gauǵaz, M. *Helv. Chim. Acta* **1971**, *54*, 2108–2111.
142. Smith, K.; James, D. M.; Mistry, A. G.; Bye, M. R.; Faulkner, D. J. *Tetrahedron* **1992**, *48*, 7479–7488.

143. Britovsek, G. J. P.; Gibson, V. C.; Hoarau, O. D.; Spitzmesser, S. K.; White, A. J. P.; Williams, D. J. *Inorg. Chem.* **2003**, *42*, 3454–3465.
144. Silvestru, C.; Drake, J. E. *Coord. Chem. Rev.* **2001**, *223*, 117–216.
145. Katritzky, A. R.; Rewcastle, G. W.; Vazquez de Miguel, L. M. *J. Org. Chem.* **1988**, *53*, 794–799.
146. Zeimentz, P. M.; Okuda, J. *Organometallics* **2007**, *26*, 6388–6396.
147. Wayda, A. L.; Atwood, J. L.; Hunter, W. E. *Organometallics* **1984**, *3*, 939–941.
148. Conroy, K. D.; Hayes, P. G.; Piers, W. E.; Parvez, M. *Organometallics* **2007**, *26*, 4464–4470.
149. Gao, W.; Cui, D. *J. Am. Chem. Soc.* **2008**, *130*, 4984–4991.
150. Hogerheide, M. P.; Grove, D. M.; Boersma, J.; Jastrzebski, J. T. B. H.; Kooijman, H.; Spek, A. L.; van Koten, G. *Chem.—Eur. J.* **1995**, *1*, 343–350.
151. Protchenko, A. V.; Almazova, O. G.; Zakharov, L. N.; Fukin, G. K.; Struchkov, Y. T.; Bochkarev, M. N. *J. Organomet. Chem.* **1997**, *536-537*, 457–463.
152. Rabe, G. W.; Zhang-Preße, M.; Riederer, F. A.; Incarvito, C. D.; Golen, J. A.; Rheingold, A. L. *Acta Crystallogr., Sect. E: Struct. Rep. Online* **2004**, *60*, m1389–m1390.
153. Rufanov, K. A.; Müller, B. H.; Spannenberg, A.; Rosenthal, U. *New J. Chem.* **2006**, *30*, 29–31.
154. Wayda, A. L.; Rogers, R. D. *Organometallics* **1985**, *4*, 1440–1444.
155. Fryzuk, M. D.; Carter, A.; Rettig, S. J. *Organometallics* **1992**, *11*, 469–472.
156. Jantunen, K. C.; Scott, B. L.; Hay, P. J.; Gordon, J. C.; Kiplinger, J. L. *J. Am. Chem. Soc.* **2006**, *128*, 6322–6323.
157. Masuda, J. D.; Jantunen, K. C.; Scott, B. L.; Kiplinger, J. L. *Organometallics* **2008**, *27*, 803–806.
158. Schrock, R. R.; Bonitatebus, P. J., Jr.; Schrodi, Y. *Organometallics* **2001**, *20*, 1056–1058.
159. Schrodi, Y.; Schrock, R. R.; Bonitatebus, P. J., Jr. *Organometallics* **2001**, *20*, 3560**–**3573.
160. Roering, A. J.; Davidson, J. J.; MacMillan, S. N.; Tanski, J. M.; Waterman, R. *Dalton Trans.* **2008**, 4488–4498.
161. Waterman, R. *Organometallics* **2007**, *26*, 2492–2494.
162. Roering, A. J.; Leshinski, S. E.; Chan, S. M.; Shalumova, T.; Macmillan, S. N.; Tanski, J. M.; Waterman, R. *Organometallics* **2010**, *29*, 2557–2565.
163. Mork, B. V.; Tilley, T. D. *J. Am. Chem. Soc.* **2001**, *123*, 9702–9703.
164. Mork, B. V.; Tilley, T. D. *J. Am. Chem. Soc.* **2004**, *126*, 4375–4385.
165. Fedushkin, I. L.; Kurskii, Y. A.; Nevodchikov, V. I.; Bochkarev, M. N.; Müchle, S.; Schumann, H. *Russ. Chem. Bull.* **2002**, *51*, 160–169.
166. Xie, Z.; Liu, Z.; Xue, F.; Zhang, Z.; Mak, T. C. *J. Organomet. Chem.* **1997**, *542*, 285–289.
167. Izod, K.; Liddle, S. T.; Clegg, W. *Inorg. Chem.* **2004**, *43*, 214–218.
168. Taylor, M. D. *Chem. Rev.* **1962**, *62*, 503–511.
169. Collin, J.; Giuseppone, N.; Jaber, N.; Domingos, A.; Maria, L.; Santos, I. *J. Organomet. Chem.* **2001**, *628*, 271–274.
170. Kuehl, C. J.; Simpson, C. K.; John, K. D.; Sattelberger, A. P.; Carlson, C. N.; Hanusa, T. P. *J. Organomet. Chem.* **2003**, *683*, 149–154.

171. Evans, W. J.; Grate, J. W.; Levan, K. R.; Bloom, I.; Peterson, T. T.; Doedens, R. J.; Zhang, H.; Atwood, J. L. *Inorg. Chem.* **1986**, *25*, 3614–3619.
172. Nolan, S. P.; Stern, D.; Marks, T. J. *J. Am. Chem. Soc.* **1989**, *111*, 7844–7853.
173. Watson, P. L.; Whitney, J. F.; Harlow, R. L. *Inorg. Chem.* **1981**, *20*, 3271–3278.
174. Cameron, T. M.; Gordon, J. C.; Scott, B. L. *Organometallics* **2004**, *23*, 2995–3002.
175. Cameron, T. M.; Gordon, J. C.; Scott, B. L.; Tumas, W. *Chem. Commun.* **2004**, 1398–1399.
176. Liu, B.; Cui, D. *Dalton Trans.* **2009**, 550–556.
177. Masuda, J. D.; Jantunen, K. C.; Scott, B. L.; Kiplinger, J. L. *Organometallics* **2008**, *27*, 1299–1304.
178. Basuli, F.; Tomaszewski, J.; Huffman, J. C.; Mindiola, D. J. *Organometallics* **2003**, *22*, 4705–4714.
179. Knight, L. K.; Piers, W. E.; Fleurat-Lessard, P.; Parvez, M.; McDonald, R. *Organometallics* **2004**, *23*, 2087–2094.
180. Hoops, S.; Sahle, S.; Gauges, R.; Lee, C.; Pahle, J.; Simus, N.; Singhal, M.; Xu, L.; Mendes, P.; Kummer, U. *Bioinformatics* **2006**, *22*, 3067–3074.
181. Giesbrecht, G. R.; Gordon, J. C. *Dalton Trans.* **2004**, 2387–2393.
182. Scott, J.; Mindiola, D. J. *Dalton Trans.* **2009**, 8463–8472.
183. Conroy, K. D.; Piers, W. E.; Parvez, M. *Organometallics* **2009**, *28*, 6228–6233.
184. Duncan, A. P.; Bergman, R. G. *Chem. Rec.* **2002**, *2*, 431–445.
185. Fout, A. R.; Kilgore, U. J.; Mindiola, D. J. *Chem.—Eur. J.* **2007**, *13*, 9428–9440.
186. Cámpora, J.; Buchwald, S. L. *Organometallics* **1993**, *12*, 4182–4187.
187. Kamenz, B. L.; Johnson, K. R. D.; Hayes, P. G., unpublished results.
188. Lukešová, L.; Ward, B. D.; Bellemin-Laponnaz, S.; Wadepohl, H.; Gade, L. H. *Organometallics* **2007**, *26*, 4652–4657.
189. Arndt, S.; Zeimentz, P. M.; Spaniol, T. P.; Okuda, J.; Honda, M.; Tatsumi, K. *Dalton Trans.* **2003**, 3622–3627.
190. Rufanov, K. A.; Spannenberg, A. *Mendeleev Commun.* **2008**, *18*, 32–34.
191. Li, T.; Jenter, J.; Roesky, Peter W. *Z. Anorg. Allg. Chem.* **2010**, *636*, 2148–2155.
192. Matsuo, Y.; Mashima, K.; Tani, K. *Organometallics* **2001**, *20*, 3510–3518.
193. Chang, J.-C.; Hung, C.-H.; Huang, J.-H. *Organometallics* **2001**, *20*, 4445–4447.
194. Kuo, P.-C.; Chang, J.-C.; Lee, W.-Y.; Lee, H. M.; Huang, J.-H. *J. Organomet. Chem.* **2005**, *690*, 4168–4174.
195. Kuo, P.-C.; Huang, J.-H.; Hung, C.-H.; Lee, G.-H.; Peng, S.-M. *Eur. J. Inorg. Chem.* **2003**, 1440–1444.
196. Li, Y.; Banerjee, S.; Odom, A. L. *Organometallics* **2005**, *24*, 3272–3278.
197. Mazet, C.; Gade, L. H. *Organometallics* **2001**, *20*, 4144–4146.
198. Mazet, C.; Gade, L. H. *Chem.—Eur. J.* **2003**, *9*, 1759–1767.
199. Huang, W.-Y.; Chuang, S.-J.; Chunag, N.-T.; Hsiao, C.-S.; Datta, A.; Chen, S.-J.; Hu, C.-H.; Huang, J.-H.; Lee, T.-Y.; Lin, C.-H. *Dalton Trans.* **2011**, *40*, 7423–7433.
200. Lien, Y.-L.; Chang, Y.-C.; Chuang, N.-T.; Datta, A.; Chen, S.-J.; Hu, C.-H.; Huang, W.-Y.; Lin, C.-H.; Huang, J.-H. *Inorg. Chem.* **2010**, *49*, 136–143.
201. Groenendaal, L.; Peerlings, H. W. I.; van Dongen, J. L. J.; Havinga, E. E.; Vekemans, J. A. J. M.; Meijer, E. W. *Macromolecules* **1995**, *28*, 116–123.

202. Chen, W.; Cava, M. P. *Tetrahedron Lett.* **1987**, *28*, 6025–6026.
203. Johnson, K. R. D.; Hayes, P. G. *Organometallics* **2009**, *28*, 6352–6361.
204. Zou, J.; Berg, D. J.; Stuart, D.; McDonald, R.; Twamley, B. *Organometallics* **2011**, *30*, 4958–4967.
205. Jutzi, P.; Müller, C.; Stammler, A.; Stammler, H.-G. *Organometallics* **2000**, *19*, 1442–1444.
206. Jeske, G.; Lauke, H.; Mauermann, H.; Schumann, H.; Marks, T. J. *J. Am. Chem. Soc.* **1985**, *107*, 8111–8118.
207. Döring, C.; Kretschmer, W. P.; Kempe, R. *Eur. J. Inorg. Chem.* **2010**, 2853–2860.
208. Huang, K.; Sun, C.-L.; Shi, Z.-J. *Chem. Soc. Rev.* **2011**, *40*, 2435–2452.
209. Sakakura, T.; Choi, J.-C.; Yasuda, H. *Chem. Rev.* **2007**, *107*, 2365–2387.
210. Yin, X.; Moss, J. R. *Coord. Chem. Rev.* **1999**, *181*, 27–59.
211. Seyferth, D.; Rochow, E. G. *J. Am. Chem. Soc.* **1955**, *77*, 907–908.
212. Bruno, J. W.; Marks, T. J.; Day, V. W. *J. Am. Chem. Soc.* **1982**, *104*, 7357–7360.
213. Fendrick, C. M.; Marks, T. J. *J. Am. Chem. Soc.* **1984**, *106*, 2214–2216.
214. Dimitrov, I.; Jankova, K.; Hvilsted, S. *J. Polym. Sci., Part A: Polym. Chem.* **2010**, *48*, 2044–2052.
215. Jung, S.-H.; Song, H.-Y.; Lee, Y.; Jeong, H. M.; Lee, H.-i. *Macromolecules* **2011**, *44*, 1628–1634.
216. Dyall, L. K.; L'Abbé, G.; Dehaen, W. *J. Chem. Soc., Perkin Trans. 2* **1997**, 971–975.
217. Kwok, S. W.; Fotsing, J. R.; Fraser, R. J.; Rodionov, V. O.; Fokin, V. V. *Org. Lett.* **2010**, *12*, 4217–4219.
218. Trofimenko, S. *Polyhedron* **2004**, *23*, 197–203.
219. Trofimenko, S. *J. Chem. Educ.* **2005**, *82*, 1715–1720.
220. Cheng, J.; Saliu, K.; Ferguson, M. J.; McDonald, R.; Takats, J. *J. Organomet. Chem.* **2010**, *695*, 2696–2702.
221. Cheng, J.; Saliu, K.; Kiel, G. Y.; Ferguson, M. J.; McDonald, R.; Takats, J. *Angew. Chem., Int. Ed.* **2008**, *47*, 4910–4913.
222. Ferrence, G. M.; McDonald, R.; Takats, J. *Angew. Chem., Int. Ed.* **1999**, *38*, 2233–2237.
223. Long, D. P.; Bianconi, P. A. *J. Am. Chem. Soc.* **1996**, *118*, 12453–12454.
224. Lopes, I.; Lin, G. Y.; Domingos, A.; McDonald, R.; Marques, N.; Takats, J. *J. Am. Chem. Soc.* **1999**, *121*, 8110–8111.
225. Pieters, R. J.; Rebek, J., Jr. *Recl. Trav. Chim. Pays-Bas* **1993**, *112*, 330–334.
226. Kolb, H. C.; Finn, M. G.; Sharpless, K. B. *Angew. Chem., Int. Ed.* **2001**, *40*, 2004–2021.
227. Meldal, M.; Tornøe, C. W. *Chem. Rev.* **2008**, *108*, 2952–3015.
228. Chen, J.-G.; Suryanarayanan, V.; Lee, K.-M.; Ho, K.-C. *Sol. Energy Mater. Sol. Cells* **2007**, *91*, 1432–1437.
229. Murata, S.; Abe, S.; Tomioka, H. *J. Org. Chem.* **1997**, *62*, 3055–3061.
230. Cwiklicki, A.; Rehse, K. *Arch. Pharm. Pharm. Med. Chem.* **2004**, *337*, 156–163.
231. Pollex, A.; Hiersemann, M. *Org. Lett.* **2005**, *7*, 5705–5708.
232. Vlád, G.; Horváth, I. T. *J. Org. Chem.* **2002**, *67*, 6550–6552.
233. Hayes, P. G.; Piers, W. E. *Inorg. Synth.* **2010**, *35*, 20–24.
234. Sobota, P.; Utko, J.; Szafert, S. *Inorg. Chem.* **1994**, *33*, 5203–5206.

235. Hultzsch, K. C.; Voth, P.; Beckerle, K.; Spaniol, T. P.; Okuda, J. *Organometallics* **2000**, *19*, 228–243.
236. Grubert, L.; Jacobi, D.; Buck, K.; Abraham, W.; Mügge, C.; Krause, E. *Eur. J. Org. Chem.* **2001**, 3921–3932.
237. Hou, Z.; Zhang, Y.; Tezuka, H.; Xie, P.; Tardif, O.; Koizumi, T.-a.; Yamazaki, H.; Wakatsuki, Y. *J. Am. Chem. Soc.* **2000**, *122*, 10533–10543.
238. Masuda, J. D.; Jantunen, K. C.; Ozerov, O. V.; Noonan, K. J. T.; Gates, D. P.; Scott, B. L.; Kiplinger, J. L. *J. Am. Chem. Soc.* **2008**, *130*, 2408–2409.
239. Temple, C., Jr.; Montgomery, J. A. *J. Org. Chem.* **1965**, *30*, 826–829.
240. El-Shahawy, A. *Spectrochim. Acta, Part A* **1983**, *39A*, 115–117.
241. *APEX2*, 2.1-4; Bruker AXS: Madison, WI, 2006.
242. *SAINT-Plus*, 7.23a; Bruker AXS: Madison, WI, 2004.
243. Sheldrick, G. M. *SADABS*, 2004/1; Bruker AXS: Madison, WI, 2004.
244. Sheldrick, G. M. *Acta Crystallogr., Sect. A: Found. Crystallogr.* **2007**, *64*, 112–122.
245. Sheldrick, G. M. *SHELXTL*, 6.14; Bruker AXS: Madison, WI, 2003.
246. van der Sluis, P.; Spek, A. L. *Acta Crystallogr., Sect. A: Found. Crystallogr.* **1990**, *46*, 194–201.
247. Spek, A. L. *J. Appl. Cryst.* **2003**, *36*, 7–13.
248. Sudik, A. C.; Millward, A. R.; Ockwig, N. W.; Côté, A. P.; Kim, J.; Yaghi, O. M. *J. Am. Chem. Soc.* **2005**, *127*, 7110–7118.

Appendix 1 – Publications Arising from Thesis

A large component of the research presented in this thesis has been published in the articles listed below. KRDJ was responsible for all material presented in publications 1 and 2. The contents of publication 3 consist of work primarily contributed by KRDJ; however, Dr. Jamie S. Ritch is credited with solving the crystal structure of compound **40** ($H\mathbf{L}_{\mathbf{D}}^{\mathbf{Pipp}}$) and Mr. Matt A. Hannon played a supporting role by performing ligand synthesis.

Publications

1. Johnson, K. R. D.; Hayes, P. G. "Synthesis and Reactivity of Dialkyl Lutetium Complexes Supported by a Novel Bis(phosphinimine)carbazole Ligand" *Organometallics* **2009**, *28*, 6352–6361.
2. Johnson, K. R. D.; Hayes, P. G. "Kinetic and Mechanistic Investigation of Metallacycle Ring Opening in an Ortho-Metalated Lutetium Aryl Complex" *Organometallics* **2011**, *30*, 58–67.
3. Johnson, K. R. D.; Hannon, M. A.; Ritch, J. S.; Hayes, P. G. "Thermally Stable Rare Earth Dialkyl Complexes Supported by a Novel Bis(phosphinimine)pyrrole Ligand" *Dalton Trans*. **2012**, *41*, 7873–7875. *Invited article in the 'New Talent Americas' special issue.